Strongly-coupled QFTs from String Theory



Marieke van Beest
Wolfson College
University of Oxford

A thesis submitted for the degree of
Doctor of Philosophy

Trinity 2022

Strongly-coupled QFTs from String Theory

Marieke van Beest

Wolfson College

University of Oxford

Abstract: Strongly-coupled regimes of quantum field theory (QFT) are notoriously challenging to explore. In this thesis, which is divided into two parts, I address the question from a string theoretic perspective. I will focus on methods to map out the RG-flow, symmetries and phase structure, first taking a holographic point of view, then within the context of geometric engineering and brane-webs.

Holography constitutes a profound and potent way to describe strongly-coupled QFTs, especially when combined with sophisticated geometric techniques, and modern tools from QFT such as generalized global symmetries and their 't Hooft anomalies. In chapter 3 I will present our work on the gravitational dual of $\mathcal{I}/c$-extremization for a 1d/2d $\mathcal{N}=(0,2)$ theory in the presence of a holomorphically varying axio-dilaton. This generalization makes the analysis suitable for F-theory supergravity solutions, and establishes a correspondence of the two extremization principles furnished by M/F-theory duality. In chapter 4 we develop new holographic methods to compute anomalies of discrete higher-form symmetries, and derive the topological field theory (TFT), which matches these anomalies in the infra-red (IR). This interplay of holography and generalized global symmetries shines new light on the topological sector of supergravity theories and its physical implications. We illustrate the approach in a rich non-conformal holographic setting, which flows to confining $\mathcal{N}=1$ $SU(N)$ Super-Yang Mills (SYM) in the IR, focusing on the 1-form symmetry and its mixed 0-/1-form symmetry anomaly, which is closely related to chiral symmetry breaking in gapped confining vacua.

Geometric engineering and brane-webs enable us to realize a vast array of superconformal field theories (SCFTs) whose salient features would otherwise be out of reach. In my research, I have focused on 5d $\mathcal{N}=1$ SCFTs, which are intrinsically non-perturbative. In chapters 6 and 7 we establish a comprehensive description of 5d SCFTs in terms of Generalized Toric Polygons (GTPs) and map out their moduli space. Using the duality with brane-webs and

insights from toric geometry we parametrize the extended Coulomb branch (CB) and determine an algorithm to compute the magnetic quiver (MQ) describing the Higgs branch (HB). We then apply these methods to all 5d SCFTs that flow to single gauge node theories in the IR with anti-symmetric and fundamental matter. Finally, in chapter 8 we identify a correspondence between 5d extended CB deformations and 3d Fayet-Iliopoulos (FI) deformations in the MQ, which elucidates how changes in the geometry of the HB are implemented as we move along the extended CB.

Statement of Originality

This thesis is based on results from the following publications, to which the author contributed substantially:

[1] "$\mathcal{I}$/**c-Extremization in M/F-Duality**,"
M. van Beest, S. Cizel, S. Schafer-Nameki and J. Sparks,
SciPost Phys. **9** (2020) no.3, 029 doi:10.21468/SciPostPhys.9.3.029 [arXiv:2004.04020].

[2] "**(Symplectic) Leaves and (5d Higgs) Branches in the Poly(go)nesian Tropical Rain Forest**,"
M. van Beest, A. Bourget, J. Eckhard and S. Schafer-Nameki,
JHEP **11** (2020), 124 doi:10.1007/JHEP11(2020)124 [arXiv:2008.05577].

[3] "**(5d RG-flow) Trees in the Tropical Rain Forest**,"
M. van Beest, A. Bourget, J. Eckhard and S. Schäfer-Nameki,
JHEP **03** (2021), 241 doi:10.1007/JHEP03(2021)241 [arXiv:2011.07033].

[4] "**Holography, 1-Form Symmetries, and Confinement**,"
F. Apruzzi, M. van Beest, D. S. W. Gould and S. Schäfer-Nameki,
Phys. Rev. D **104** (2021) no.6, 066005 doi:10.1103/PhysRevD.104.066005
[arXiv:2104.12764].

[5] "**Connecting 5d Higgs Branches via Fayet-Iliopoulos Deformations**,"
M. van Beest, S. Giacomelli,
JHEP **12** (2021), 202 doi:10.1007/JHEP12(2021)202 [arXiv:2110.02872].

The first part of this thesis is on holography, and discusses work from [1] in chapter 3, and from [4] in chapter 4. The second part concerns 5d SCFTs, geometric engineering and brane-webs. Chapter 6 and 7 are truncated versions of [2] and [3] respectively, whereas chapter 8 contains results from [5]. Versions of [2, 3] have appeared previously in the DPhil thesis of co-author Julius Eckhard.

Acknowledgements

First and foremost, I would like to thank my supervisor Sakura Schäfer-Nameki for going above and beyond in her role to raise me to become a capable researcher. She has taught me more than I would have ever thought possible 4 years ago, and I thank her sincerely for always giving my input serious consideration, for guiding me in every aspect of research, and for caring as much as she does.

During my DPhil, I have been fortunate to work with a set of extremely talented people, so I would also like to thank Fabio Apruzzi, Antoine Bourget, José Calderón-Infante, Sebastjan Cizel, Julius Eckhard, Simone Giacomelli, Dewi Gould, Delaram Mirfendereski, James Sparks, Irene Valenzuela, and Yi-Nan Wang. A special thanks also to Chris Beem and Amihay Hanany for agreeing to asses this thesis.

I am deeply grateful for my fellow DPhils, who have been a defining feature of my experience and have become some of my closest friends. I am very proud of and thankful for all the mutual support, encouragement, and kindness this group of students show one another.

Finally, I also want to thank my friends at home and my family for making me feel like they were never far away. Thank you, to my husband Peter for his selflessness, his resolute confidence in my abilities, and for looking out for me. That I could pursue my academic aspirations without any wear on the bonds with my loved ones was your ultimate gift to me.

Marieke May 27, 2022

Contents

1 Introduction **1**

1.1 Outline 3

I Holography **7**

2 Background **9**

2.1 Type IIB Supergravity 9

2.2 Holography 10

2.3 F-theory 11

2.4 Generalized Global Symmetries 14

3 $\mathcal{I}/c$-extremization in M/F-theory **19**

3.1 Introduction 19

3.2 Holographic c-extremization in F-theory 22

3.2.1 AdS_3 Backgrounds 22

3.2.2 Supersymmetric Action 25

3.2.3 Flux Quantization 27

3.2.4 The Complex Cone and the Geometric Extremization Problem 28

3.3 M/F-duality and Holographic $\mathcal{I}$-extremization 30

3.3.1 M/F-duality for AdS-geometries 31

3.3.2 Holographic $\mathcal{I}$-extremization 33

3.3.3 M-theory Supersymmetric Action for Elliptic Fibrations 34

3.4 $\mathcal{I}/c$-extremization 36

3.4.1 Geometry 36

3.4.2 Field Theory 40

3.5 Toric Fibrations over a Curve . . . 42
3.5.1 Toric Fibration . . . 42
3.5.2 F-theory c-extremization for Toric Fibrations . . . 43
3.5.3 M-theory $\mathcal{I}$-extremization for Toric Fibrations . . . 46
3.5.4 Universal Twist: Elliptic Surface . . . 49
3.5.5 Baryonic Twist: $Y^{p,q}$ . . . 51
3.6 Universal Twist Solutions: Elliptic Three-fold . . . 53
3.6.1 F-theory . . . 53
3.6.2 M-theory . . . 54
3.7 Conclusions and Outlook . . . 56

4 Holography, 1-form Symmetries, and Confinement 59
4.1 Introduction . . . 59
4.2 Holographic Dual to Confinement . . . 60
4.3 1-form Symmetries from Supergravity . . . 62
4.4 Boundary Conditions and Mutually Local Lines . . . 65
4.5 Mixed Anomaly and χ_{SB} from Holography . . . 67
4.6 Deformed Conifold Dual to the IR of $\mathcal{N} = 1$ $SU(M)$ SYM . . . 68
4.7 4d IR TFT from Holography . . . 69
4.8 Anomalies from Little String Theory . . . 71
4.9 Conclusions and Outlook . . . 72

II Geometric Engineering and Brane-webs 75

5 Background 77
5.1 5d SCFTs and Gauge Theories . . . 77
5.2 Brane-webs and HW transitions . . . 80
5.3 Magnetic Quivers and Hasse Diagrams . . . 84
5.4 Map from Brane-web to Generalized Toric Polygon . . . 86

6 5d Higgs Branches in the Tropical Rain Forest **91**

6.1 Introduction . . . 91

6.2 Strategy: Higgs Branches from GTP . . . 92

6.3 Higgs Branches for 5d SCFTs from Edge Colorings . . . 94

6.3.1 GTPs and Minkowski Sums . . . 95

6.3.2 The s-rule . . . 100

6.3.3 The r-rule . . . 102

6.3.4 Colorings of GTPs . . . 105

6.3.5 Magnetic Quivers from Colored GTPs . . . 109

6.4 Symplectic Leaves and Colorings with Internal Edges . . . 113

6.4.1 Colorings with Internal Edges . . . 113

6.4.2 Hasse Diagram and Symplectic Leaves . . . 115

6.5 Examples: SQCD at strong/weak coupling, and T_4 . . . 117

6.5.1 $SU(3)_1 + 6\mathbf{F}$ UV SCFT . . . 117

6.5.2 $SU(3)_1 + 6\mathbf{F}$ IR Theory . . . 120

6.5.3 T_4 . . . 121

6.6 Derivation from the Tropics . . . 125

6.6.1 Sub-web Decomposition to Colored Polygon . . . 125

6.6.2 Magnetic Quivers . . . 127

6.6.3 Hasse Diagram . . . 129

6.6.4 Example . . . 130

7 5d RG-flow Trees **133**

7.1 Overview of Results . . . 134

7.2 Construction of GTPs and Edge-moves . . . 136

7.2.1 Generalized Toric Polygons and Webs . . . 136

7.2.2 From Non-convex to Convex Polygons: Edge-moves . . . 139

7.3 Decoupling . . . 141

7.3.1 Decoupling Fundamental Matter . . . 141

7.3.2 Decoupling Anti-symmetric Matter . . . 143

7.3.3 Decoupling for IR Magnetic Quivers . . . 145

7.4 UV Magnetic Quivers for $SU(N)$ with AS and F via GTPs 147
7.4.1 $SU(N)_{\frac{1}{2}} + (2N+3)F$ 147
7.4.2 $SU(N)_{\frac{1}{2}} + 1AS + (N+5)F$ 150
7.5 Enhanced Non-simply-laced Flavor Symmetry 154
7.5.1 $\mathfrak{c}_2$ Quiver 156
7.5.2 $\mathfrak{b}_9$ Quiver 157
7.5.3 $\mathfrak{g}_2$ Quiver 158
7.5.4 Hidden $\mathfrak{su}(2)$ Symmetries 159

8 Connecting 5d Higgs branches via 3d Fayet-Iliopoulos Deformations 161
8.1 Introduction 161
8.2 FI Deformations 162
8.2.1 FI Deformations of Unitary Quivers 163
8.2.2 More General FI Deformations 167
8.2.3 FI Deformations of the Higher Rank E-string Theory 169
8.3 Mass Deformations in 5d via 3d FI Deformations 171
8.3.1 Decoupling 171
8.3.2 Weak Coupling 173
8.3.3 General Movement on the Extended Coulomb Branch 175
8.3.4 Magnetic Quivers with Loops 177
8.3.5 Mirror Symmetry and FI Deformations 181
8.4 (D_{N+2}, D_{N+2}) Conformal Matter Descendant Tree 185
8.5 T_N Theory 190
8.5.1 Parent SCFTs 190
8.5.2 IR Descriptions 192
8.5.3 New Lagrangians from FI Deformations 194

Bibliography 198

Chapter 1

Introduction

The main objective of the research submitted in this thesis has been to capture non-perturbative features of quantum field theories (QFTs) by taking a string theoretic perspective and using state-of-the-art QFT tools. A comprehensive understanding of strongly-coupled QFTs presents a formidable challenge in theoretical physics, which has clearly proved to lie well beyond the scope of conventional field theory methods. Therefore, in order to make progress on this problem, we are compelled to pursue fundamentally new approaches.

String theory has provided invaluable avenues to address this question, which has yielded myriad new qualitative and quantitative results on the non-perturbative dynamics of known field theories and, perhaps more strikingly, on the existence of previously undiscovered QFTs. The first of the string theoretic frameworks which underlies the entire first part of this thesis is the *gauge/gravity duality*: a conjecture stating that the physics of a theory of (quantum) gravity in $d+1$ dimensions may equivalently be described in terms of a gauge theory in d dimensions – providing a concrete manifestation of the so-called holographic principle [6, 7]. The duality was first discovered more than two decades ago [8] in the form of type IIB string theory on $\mathrm{AdS}_5 \times S^5$ dual to a 4d $\mathcal{N} = 4$ Super Yang-Mills (SYM), which is a conformal field theory (CFT) living on a stack of D3-branes. Yet original applications of the correspondence continue to emerge and new pages in the dictionary are progressively being turned.

Recently, our concept of *global symmetries* has enjoyed an explosive expansion. Throughout the development of theoretical physics, ordinary global symmetries have been perhaps the strongest device at our disposal for characterizing physical systems, constraining the dynamics at any given energy scale and organising the field content. Moreover, their 't Hooft anomalies extrapolate between the ultra-violet (UV) and infra-red (IR) behaviour of a theory,

and conservation or spontaneous breaking of global symmetries determines the phase structure. Generalizing our notion of global symmetries to correspond in essence to the existence of *topological operators* acting on local and extended operators alike [9, 10], entails a vast expansion of the applicability of this strategy.

In my recent work, I have focused on understanding the role of generalized global symmetries in the context of holography. This has contributed to a broader understanding of topological sectors of supergravity theories in $d+1$ dimensions, the so-called *Symmetry TFTs*, encoding global structures of d dimensional QFTs – including higher-form global symmetries and their 't Hooft anomalies. Within this programme we have developed a compelling interpretation for an entire sector on the gravity side of the holographic duality, and demonstrated how taking the perspective of generalized global symmetries can sharpen predictions and provide new results for the phase structure of holographic QFTs.

The second part of this thesis is set within the context of *geometric engineering* [11,12] in M-theory of superconformal field theories (SCFTs) and their string dual description in terms of *brane-webs* [13] in type IIB string theory. The fundamental idea of geometric engineering is that we can construct d dimensional SCFTs in string or M-theory by compactifying the full theory on $\mathbb{R}^{1,d-1} \times \mathcal{M}$. If the manifold $\mathcal{M}$ has some length scale ℓ associated with it, in the IR, i.e. at energies below ℓ^{-1}, we can take the perspective of an effective theory living on $\mathbb{R}^{1,d-1}$. Furthermore, the strength of the gravitational interaction is set by the inverse volume of $\mathcal{M}$, so that gravity is frozen to a background value if $\mathcal{M}$ has some non-compact direction. This leaves us with an effective non-gravitational SCFT on $\mathbb{R}^{1,d-1}$, the details of which in general depend on $\mathcal{M}$, implying the possibility to systematically map out an immense landscape of SCFTs, which can – at least in principle – be classified and studied via the geometric properties of $\mathcal{M}$.

The dual picture is that of brane-webs in string theory, where stacks of branes of various dimensionality and charges are arranged in supersymmetry and charge preserving configurations. This gives rise to an SCFT living along the infinite directions shared between the world volumes of the branes. The field content, gauge group and phase space of the SCFT can be engineered by the composition of the web in the transverse directions.

A remarkable class of SCFTs that I have chosen to devote a significant part of my DPhil towards are 5 dimensional theories which have $\mathcal{N} = 1$ supersymmetry. But why focus on

these higher-dimensional theories that can clearly have no immediate phenomenological implications? The exciting aspect of higher-dimensional field theories is precisely that *because* they live in $d > 4$, the coupling g in any gauge theory description will have negative mass dimension, so the SCFT fixed point in the UV is intrinsically strongly-coupled. In fact, since 5 dimensional gauge theories are in this way necessarily unrenormalizable, for a long time their UV fixed points were believed to not exist at all as meaningful QFTs (until [14]). Only by constructing them in string and M-theory [15–17] has it been possible to give evidence for their existence and, recently, to provide classifications and characterize salient properties such as their moduli space and global symmetries. Put differently, we would usually be cut off from studying such intrinsically non-perturbative theories by conventional means, however, here we have a set of advanced tools from string theory that allow us to probe this interesting new class of theories, maybe even making this an opportunity to learn something fundamentally new about QFT itself. In addition, taking the point of view of geometric engineering, it is quite natural to consider further dimensional reduction, thus motivating the greater picture wherein all 8 supercharge theories are connected, bringing a beautiful comprehensive description within view.

1.1 Outline

This thesis is divided into two parts; part I *Holography* and part II *Geometric Engineering and Brane-webs*, united by their relevance to strongly-coupled dynamics of QFTs, but distinct in the approach taken.

In part I *Holography*, I will first provide a brief introduction to some central concepts in chapter 2 that will play a role in chapters 3 and/or 4. Chapter 3 concerns the techniques of $\mathcal{I}/c$-extremization, which provide elegant and efficient solutions to the problem of determining bona fide AdS supergravity backgrounds or, equivalently, their dual SCFTs. Rather than having to tackle a set of coupled differential equations, the task boils down to optimizing a single function; respectively the 1d partition function Z_{1d} or central charge c of a 2d SCFT. In [1] we generalized the gravitational dual of c-extremization to account for a non-trivial axio-dilaton profile, characterized by the complex structure of an elliptic fibration, making the extremization principle applicable to F-theory AdS_3 supergravity solutions. M/F-duality implies that these can be T-dualized to AdS_2 solutions in M-theory, from which we established

the corresponding map between holographic c-extremization in F-theory and $\mathcal{I}$-extremization in M-theory.

Chapter 4 explores the role of higher-form symmetries in the context of a non-conformal holographic setup dual to a confining QFT. Generalized global symmetries and their 't Hooft anomalies represent a genuinely new window into the dynamics of QFTs, and enable a more refined characterization of physical properties which can also be tapped into in the context of the AdS/CFT correspondence. In [4] our focus was on holography in a non-conformal setting, where the 1-form symmetry, which acts on line operators, provides a diagnostic of confinement in the IR. Concretely, we studied the gravitational dual to 4d $\mathcal{N} = 1$ $SU(N)$ super Yang-Mills (SYM), realized by the Klebanov-Strassler solution on the deformed conifold in type IIB supergravity. By identifying the topological supergravity couplings near the boundary we determined the $\mathbb{Z}_N$ 1-form symmetry and a mixed 0-/1-form symmetry anomaly related to chiral symmetry breaking in the gapped confining vacua. Moreover, we showed how the 5d supergravity reduction contains the Lagrangian of the 4d topological field theory (TFT) describing the IR physics, providing an independent derivation from first principles of its existence, which agrees with but does not rely on anomaly matching.

Part II *Geometric Engineering and Brane-webs* gives a string theoretic perspective on 5d $\mathcal{N} = 1$ SCFTs which are intrinsically non-perturbative quantum field theories. Like the first part of the thesis, part II starts with a brief introduction in chapter 5 to the key concepts underlying the research presented in the subsequent chapters. The big picture can be summarized as follows. 5d $\mathcal{N} = 1$ SCFTs can be realized in M-theory on non-compact Calabi-Yau 3-fold singularities, or on 5-brane-webs in type IIB string theory. A 5-brane-web has a dual diagrammatic representation as a generalized toric polygon (GTP), where the generalization with respect to toric geometry consists in allowing for "empty" vertices, which account for the effects of Hanany-Witten brane creation. When the dual polygon is toric, it precisely represents the canonical Calabi-Yau singularity in M-theory. In general, however, the geometric interpretation of a GTP is an interesting open problem.

My research centers on the rich moduli space of 5d $\mathcal{N} = 1$ SCFTs composed of the Higgs branch (HB) and Coulomb branch (CB), which are respectively parametrized by the vacuum expectation values (vevs) of the scalars in the hyper- and vector-multiplets. In the brane-web, the moduli space is described by continuous deformations of the branes, with motion in the

plane of the web corresponding to movement on the Coulomb branch, whereas motion in the transverse directions maps out the Higgs branch. In M-theory, the (extended) Coulomb branch is mapped out by resolutions of the Calabi-Yau 3-fold singularity, and the Higgs branch is realized as its deformation space. The Coulomb branch is well-understood from both an M-theory and brane-web perspective. The Higgs branch, on the other hand, is particularly difficult to characterize, because it receives quantum corrections from instantons in 5d. In M-theory on a canonical singularity these are M2-branes, for which a direct computation is beyond current methods in all but a small class of theories.

To address this, the question we pose in chapter 6 is: can we understand the deformation space associated to a generalized toric polygon? Our solution [2] utilizes the duality with the brane-web, where the HB is captured by the associated magnetic quiver (MQ), which represents a 3d $\mathcal{N} = 4$ gauge theory, whose CB is conjecturally identified with the HB of the 5d SCFT. This solves the problem of accounting for instanton contributions, as the 3d CB can be analyzed in detail using the monopole formula.

In chapter 7 we focus on the practical application of the analysis in chapter 6 to a large set of strongly-coupled field theories, making use of the fact that 5d $\mathcal{N} = 1$ SCFTs organize into descendant trees, generated by successive decoupling of matter and RG-flow. In [3] we develop the necessary machinery to construct entire descendant trees of MQs for all 5d SCFTs that flow to single gauge node theories with anti-symmetric and fundamental matter, as well as $SU(2)^m$ quiver gauge theories. Finally, in chapter 8 we demonstrate a correspondence between 5d extended Coulomb branch deformations and 3d Fayet-Iliopoulos deformations in the MQ, first discussed in [5]. Exploring the nature of this correspondence, we refine and deepen our understanding of the 5d Higgs branch, and gain a new perspective on the interconnectedness of 8 supercharge SCFTs.

Part I

Holography

Chapter 2

Background

2.1 Type IIB Supergravity

Our current understanding of the microscopic nature of the universe relies on a description in terms of QFT, and is very well-evidenced by experiments at the energies we can observe. Nonetheless, there are compelling reasons to believe that at higher energies new elements will be involved. Certainly if we could one day probe the Planck scale, quantum gravity effects would become important and infringe on the current framework, since a reconciliation of gravity and QFT is not possible using conventional perturbative methods. On the other hand, if we are willing to give up the notion that the fundamental constituents of nature are point-like and instead consider a theory of fundamental strings we can realize a UV complete theory of quantum gravity. String theory is an elegant and extensive structure encompassing many sectors and with a plethora of applications. In part I of this thesis, we will mainly be interested in its low-energy effective description so we summarize the central aspects below.

By coupling the fundamental string to the massless closed string states and imposing Weyl invariance, one can obtain an effective 10d action for the massless fields. Recall that the NSNS sector consists of the spacetime metric g, the dilaton ϕ, and the Kalb-Ramond 2-form B_2 with field strength $H_3 = dB_2$. In type IIB string theory, the RR sector contains even-form potentials C_{2m}, $m = 0, \ldots, 4$ with field strengths $F_n = dC_{n-1}$ and $F_n = *F_{10-n}$. To write down the (bosonic) type IIB supergravity action it is convenient to define

$$\begin{aligned} \tau &= C_0 + i\mathrm{e}^{-\phi}\,, \qquad G_3 = F_3 - \tau H_3\,, \\ \widetilde{F}_5 &= F_5 - \frac{1}{2} C_2 \wedge H_3 + \frac{1}{2} B_2 \wedge F_3\,. \end{aligned} \tag{2.1}$$

Because of the self-dual field strength $F_5 = *F_5$ there is no manifestly covariant action for type IIB supergravity, however, the equations of motion (EOMs) can be obtained from the

action

$$S_{\rm IIB} = \frac{2\pi}{l_s^8}\int\left[{\rm vol}_g R - \frac{1}{2\tau_2^2}{\rm d}\tau\wedge *{\rm d}\bar{\tau} + \frac{1}{\tau_2}G_3\wedge *\bar{G}_3 + \frac{1}{2}\widetilde{F}_5\wedge *\widetilde{F}_5 + C_4\wedge H_3\wedge F_3\right], \quad (2.2)$$

and the self-duality condition should then be imposed independently on the level of the EOMs. The work presented in chapters 3 and 4 is embedded in this framework in the context where it realizes holography.

2.2 Holography

The AdS/CFT correspondence [8] relates a $p+1$ dimensional conformal field theory (CFT_{p+1}) to string theory on $\text{AdS}_{p+2}\times X$, where X is a compact space which, together with some flux configuration, comprise a vacuum solution of the (quantum) theory. The CFT side of the duality arises by considering the world-volume theory on a stack of p-branes probing the cone $C(X)$, whereas the gravity side describes the backreacted geometry in the presence of the branes. The field theory can be understood as living on the conformal boundary of the AdS space, providing an important realization of the holographic principle. The AdS/CFT duality is extraordinary because it states that a CFT with no notion of the existence of gravity is dynamically equivalent to a UV complete theory of quantum gravity.

The prototypical example is 4d $\mathcal{N}=4$ SYM with gauge group $SU(N)$ and coupling constant $g_{\rm YM}$, which is dual to type IIB string theory with string length l_s and coupling $g_s = \langle e^{\phi}\rangle$ on $\text{AdS}_5\times S^5$ and N units of F_5-flux threading S^5. The free parameters on each side of the duality map as

$$g_{\rm YM}^2 = 2\pi g_s\,, \qquad 2g_{\rm YM}^2 N = L^4/l_s^4\,, \quad (2.3)$$

with L the AdS radius, and we define the 't Hooft coupling $\lambda \equiv g_{\rm YM}^2 N$. In the strongest form of the correspondence, both the free parameters N and λ can take arbitrary fixed values. While this version is very interesting and may inspire new ideas, it is very difficult to perform computations for arbitrary values of the parameters. The more tractable version of the duality is in the supergravity limit where $N\gg 1$ and the string length is very small compared to the radius of AdS, $l_s/L \ll 1$, so the background is weakly curved. On the CFT side this corresponds to a strong-coupling limit since $\lambda \gg 1$. In other words, in this regime we find a strong/weak duality, which we will exploit in the following chapters to derive properties of the

strongly-coupled dual field theory that are both more conceptually clear and computationally tractable from the gravity perspective.

The duality further implies a one-to-one map or *dictionary* between the spectrum of string theory on $\mathrm{AdS}_{p+2}\times X$ and operators in the CFT_d. The field-operator map is built by matching string states and CFT operators in the same representations of the shared symmetry group – since, for the duality to hold, clearly the symmetries on either side must agree. Consider the example of 4d $\mathcal{N}=4$ SYM which preserves the supergroup $PSU(2,2|4)$. The bosonic subgroup is $SU(2,2)\cong SO(4,2)$ and $SU(4)\cong SO(6)$ which are also the isometry groups of AdS_5 and S^5 respectively. By including the fermionic sector it can be shown that the full $PSU(2,2|4)$ symmetry is also present in the string theory picture.

Finally, the holographic duality, also sometimes referred to as the gauge/gravity duality, has been extended in several directions beyond AdS/CFT. One important generalization that will take center stage in chapter 4 breaks conformal invariance by including fractional branes. This setup realizes a dual field theory with a non-trivial RG-flow.

2.3 F-theory

Generic scenarios in type IIB string theory include configurations with 7-branes. The presence of 7-branes gives rise to a spatially varying string coupling which necessarily leaves the perturbative regime somewhere on the compactification space, rendering this class of string vacua genuinely non-perturbative. F-theory [18–20] is an elegant geometric description of this scenario, to which we provide a brief introduction below, following [21, 22]. As of yet there exists no description of F-theory as a fundamental theory, leaving the framework on a very different footing from M-theory, which can in principle be understood as the 11d theory reducing to 11d supergravity in its low-energy limit. As we shall see, a number of problems present themselves when one attempts to construct an analogous 12d theory, whose low-energy description is type IIB supergravity with a varying axio-dilaton. Instead F-theory should be thought of as an intrinsically strongly-coupled theory which, in certain limits, can be reached by string dualities. In particular, the relevant approaches for the work presented in chapter 3 will be type IIB supergravity with a varying axio-dilaton, modelled by an auxiliary elliptic fibration, and duality with M-theory on a vanishing torus.

A conventional approach to analysing brane configurations in string theory is to use a probe approximation and neglect the backreaction of the branes on the background geometry. This is a valid approximation only if the backreaction vanishes asymptotically far away from the brane. Consider a p-brane in 10 dimensions localized in the normal $n = 9 - p$ directions. Heuristically, the p-brane sources a set of background fields, schematically denoted by Φ, giving rise to a Poisson equation for the fields in the directions normal to the brane

$$\Box\Phi(r) \simeq \delta(r) \Rightarrow \Phi(r) \simeq \frac{1}{r^{n-2}}, \quad n > 2\,. \tag{2.4}$$

So for branes with codimension $n > 2$ the profile of the fields is consistent with the backreaction being negligible far away from the brane. The marginal case corresponds to a 7-brane which gives rise to a logarithmic profile for the background fields. As such backreaction effects are an important part of the picture and must be treated carefully when 7-branes are present.

Let us examine this argument closer for the case of a D7-brane, where the field sourced (magnetically) is the axion, which combines with the string coupling to form the axio-dilaton. Take z to be the complexified coordinate orthogonal to the D7-brane, then supersymmetry implies that the axio-dilaton is a holomorphic function, $\tau = \tau(z)$. The equation of motion for C_8 in the presence of a D7-brane at $z = z_0$ is

$$d * F_9 = \delta(z - z_0)\,. \tag{2.5}$$

The integrated version of this gives

$$\oint_{S^1} F_1 = 1\,. \tag{2.6}$$

In the vicinity of the brane, this equation is solved by

$$\tau(z) = \frac{1}{2\pi i}\ln\frac{z - z_0}{\lambda} + \cdots\,, \tag{2.7}$$

where $+\cdots$ denotes any regular terms and λ is an integration constant. Although this simple solution is modified far away from the brane, a branch cut in the direction normal to the D7-brane can already be detected. As one circles a D7-brane the axio-dilaton transforms as

$$\tau \to \tau + 1\,. \tag{2.8}$$

Analysis of the Einstein equations shows [23] that spacetime becomes locally flat far away from the brane, however, the deficit angle persists in the asymptotic region. This behaviour is

in stark constrast with the powerlaw asymptotics of lower-dimensional branes and the branch cut is evidence of backreaction far away from the brane. Furthermore, this expression implies that the string coupling has aquired a non-trivial profile, vanishing at the position of the brane and diverging logarithmically as $|z - z_0| \to |\lambda|$. Hence, the string coupling is only in the perturbative regime close to the brane.

Fortunately, the presence of the branch cut does not lead to an inconsistency in the effective theory because the action S_{IIB} (2.2) (manifestly) enjoys $SL(2,\mathbb{R})$ symmetry:

$$\tau \to \frac{a\tau + b}{c\tau + d}\,, \qquad \begin{pmatrix} H_3 \\ F_3 \end{pmatrix} \to \begin{pmatrix} d & c \\ b & a \end{pmatrix} \begin{pmatrix} H_3 \\ F_3 \end{pmatrix} = M \begin{pmatrix} H_3 \\ F_3 \end{pmatrix}, \qquad \det M = 1\,. \tag{2.9}$$

Quantum corrections from D(-1)-instantons involve a factor $e^{2\pi i\tau}$, breaking this classical symmetry of type IIB supergravity to $SL(2,\mathbb{Z})$. The quantum theory is invariant under transformations

$$M = \begin{pmatrix} 1 & 0 \\ b & 1 \end{pmatrix}, \qquad b \in \mathbb{Z}\,. \tag{2.10}$$

As one circles a D7-brane the background undergoes a monodromy, transforming by this $SL(2,\mathbb{Z})$ action, so the monodromy is a symmetry of the full quantum theory. Considering the transformation properties of τ, the type IIB supergravity action (2.2) looks suspiciously like something that might be obtained by compactifying a 12d theory on a torus with complex structure τ. Then the $SL(2,\mathbb{Z})$ gauge symmetry of type IIB supergravity is inherited from the geometrical reparametrization symmetry of the torus. Moreover, F_3 and H_3 would arise as the components of some 12d field strength $\hat{F}_4$ reduced along each cycle of the torus. However tempting, as alluded to above, there are a number of issues with this interpretation. For one thing, there is no 12d supergravity with metric signature $(1, 11)$. There is also the question of why the volume of the elliptic fibre as well as the 2-, and 4-form field strengths that should arise from reducing $\hat{F}_4$ along the whole torus and a point, respectively, do not appear.

Nonetheless, the idea of employing a geometric description to study F-theory has been key to the advancement of the field. The essential conjecture of F-theory is that the physics of type IIB compactifications with 7-branes can be encoded geometrically in an auxiliary elliptic fibration over the compactification space, where the axio-dilaton is identified with the complex structure of the elliptic fibre. In particular, the loci at which τ diverges correspond to the positions of 7-branes. Divergence of the complex structure of a torus fibration indicates

the collapse of a one-cycle and thus the degeneration of the fibre. Therefore, the 7-branes are located at the degeneration loci of the fibration.

The last essential piece of this story is the fact that there exists a way to access this geometric description of F-theory via duality with M-theory, taken in its low-energy limit as 11d supergravity, where the interpretation of the elliptic fibration is straightforward. Under T-duality to Type IIA and uplift to 11d supergravity, the torus becomes part of the physical spacetime where the question of its nature becomes textbook supergravity material. This duality will be reviewed in chapter 3 as it plays an important part in the work presented there.

2.4 Generalized Global Symmetries

Symmetries might well be the most powerful tool a theoretical physicist has at their disposal. Understanding the symmetries of a problem usually provides incredibly effective shortcuts to pinning down the most salient features of a theory, and can even be applied across energy scales. Therefore, the more symmetries we can discover in a given system, the better a chance we have at describing it precisely. Recently, the very concept of what constitutes a symmetry has been broadening, starting from higher-form – equivalently, higher codimensional – symmetries [10], to higher-group structures [24–28], and even non-invertible symmetries [29–31] have been brought into this framework despite the fact they do not have a group structure at all but rather are based on fusion categories.

In chapter 4 we will see an example of how higher-form symmetries, in particular the existence of a 1-form symmetry with a mixed anomaly with an R-symmetry, can put strong constraints on the dynamics in the IR. Therefore, we will focus on introducing the notion of higher-form symmetries, starting from a conventional continuous symmetry, and leave the story of abstract categorical symmetries for another time.

In a d-dimensional Euclidean QFT with a conserved current $d * J = 0$, we can define the charge operator as

$$Q(M^{d-1}) = \int_{M^{d-1}} *J \,, \tag{2.11}$$

where M^{d-1} is any $(d-1)$-dimensional submanifold. Then the symmetry generator is

$$U_\alpha(M^{d-1}) \equiv \exp\left[i\alpha Q(M^{d-1})\right] \,, \tag{2.12}$$

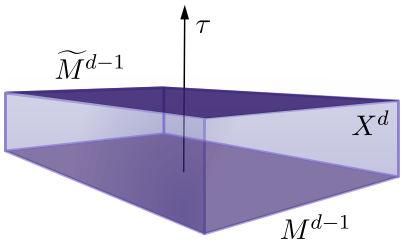


Figure 2.1: Deform a codimension 1 surface M^{d-1} slightly to obtain $\widetilde{M}^{d-1}$ by translating along Euclidean time, tracing out a d dimensional hypersurface X^d.

with α some general group label. The thing to notice is that $U_\alpha(M^{d-1})$ is a *topological* operator in the field theory. Consider deforming M^{d-1} slightly to a new codimension 1 manifold $\widetilde{M}^{d-1}$, tracing out a d dimensional manifold X^d, e.g. we can translate M^{d-1} a little in Euclidean time as shown in figure 2.1. Then

$$\int_{M^{d-1}} *J - \int_{\widetilde{M}^{d-1}} *J = \int_{X^d} d * J = 0\,, \tag{2.13}$$

using Stoke's theorem and the conservation of J.

If we want to generalize our notion of a symmetry to even encompass discrete symmetries, for which there is no conserved current, we have to find a new starting point. We now take the topological nature of the operator to be the defining feature of a symmetry generator. In other words, a global symmetry G is associated to a set of topological operators $U_g(M^{d-1})$ with $g \in G$, satisfying a group multiplication law

$$U_g(M^{d-1})U_{g'}(M^{d-1}) = U_{gg'}(M^{d-1})\,. \tag{2.14}$$

This definition has the further advantage that it is readily generalizable also to higher-form symmetries [10].

A q-form symmetry $G^{(q)}$ is defined by the existence of a codimension $q+1$ topological charge operator $U_g(M^{d-q-1})$. These symmetry generators can link with a q dimensional charged operator $V(M^q)$. The linking results in an action of $U_g(M^{d-q-1})$ on $V(M^q)$ by a group transformation

$$U_g(M^{d-q-1})V_i(M^q) = R_i^j(g)V_j(M^q)\,, \tag{2.15}$$

with $R_i^j(g)$ some representation of the group element $g \in G$. A field theory endowed with a global q-form symmetry can be coupled to a flat non-dynamical $(q+1)$-form gauge field A_{q+1}. The holonomy of this gauge field is measured on $q+1$ dimensional manifolds. Then

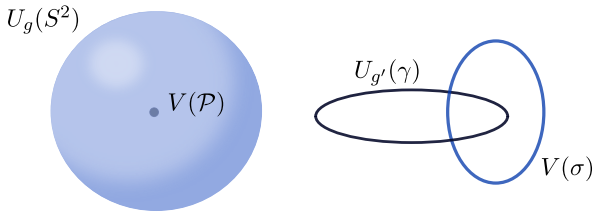


Figure 2.2: Operators associated to a 0-form symmetry $\Gamma^{(0)}$ and 1-form symmetry $\Gamma^{(1)}$ in 3d. The 0-form symmetry is generated by the surface operator $U_g(S^2)$ with $g \in \Gamma^{(0)}$ defined on a 2-sphere. It surrounds a charged particle $V(\mathcal{P})$ situated at the point $\mathcal{P}$. The 1-form symmetry is generated by a topological line operator $U_{g'}(\gamma)$ with $g' \in \Gamma^{(1)}$ defined on the line γ. It links the charged operator $V(\sigma)$ supported on the line σ.

the topological charge operator $U_g(M^{d-q-1})$ is described as generating a holonomy g in A_{q+1} for every $q+1$ dimensional manifold that crosses M^{d-q-1}.

For example in 3d a conventional global 0-form symmetry $\Gamma^{(0)}$ is generated by a set of topological surface operators that may surround a charged point particle. On the other hand, a 1-form symmetry $\Gamma^{(1)}$ in 3d is generated by a set of topological lines operators while the (possibly overlapping) set of charged states are also line operators. Both are shown in figure 2.2. The scenario we are interested in in chapter 4 is a 1-form symmetry in 4d which is generated by surface operators acting on charged lines.

Like ordinary global symmetries, the generalized versions and their 't Hooft anomalies can strongly constrain the dynamics of gauge theories. It was pointed out in [9] that the spectrum of local operators does not see the global form of the gauge group. Rather, the distinction between different global forms is reflected by the set of mutually local line operators present in the theory, which in turn is determines the 1-form symmetry $\Gamma^{(1)}$. One of the most important physical implications of this connection is that the 1-form symmetry provides a diagnostic of confinement in the IR. The order parameter of the 1-form symmetry is the vacuum expectation value (vev) of the Wilson line, which obeys an area law in a confining vacuum. As such, a vacuum that breaks the 1-form symmetry is non-confining, whereas a confining vacuum will conserve the 1-form symmetry.

As a simple example, consider 4d $\mathcal{N} = 1$ $\mathfrak{su}(2)$ SYM. It can be shown that this theory has two vacua with either a monopole (m) or dyon (d) condensate [9]. Because of charge conservation, 't Hooft lines can end on the monopole operators, whereas dyonic lines may end on the dyonic particles. When a charged line can end, the 1-form symmetry generators

Line ops.	Gauge group	vac_m	vac_d
W	$SU(2)$	$\mathbb{Z}_2^{(1)}$	$\mathbb{Z}_2^{(1)}$
H	$SO(3)_+$	$\emptyset$	$\mathbb{Z}_2^{(1)}$
$W+H$	$SO(3)_-$	$\mathbb{Z}_2^{(1)}$	$\emptyset$

Table 2.1: The distinct sets of mutually local line operators for 4d $\mathcal{N}=1$ $\mathfrak{su}(2)$ SYM are either Wilson lines W, 't Hooft lines H, or dyonic lines $W+H$. They give rise to three different theories denoted $SU(2)$ and $SO(3)_\pm$. The last two columns give the conserved 1-form symmetries in respectively the monopole condensate vacuum vac_m, and dyon vacuum vac_d.

act trivially on it since the linking can be undone by a continuous deformation, so the 1-form symmetry is (at least, partially) broken in such a vacuum. In table 2.1 we give the 1-form symmetry in the two vacua for the three possible sets of line operators, as well as the corresponding global form of the gauge group.

Finally, the work presented in chapter 4 develops methods to study higher-form symmetries in the context of holography. To briefly sketch the most important features, global higher-form symmetries in the field theory are associated to p-form gauge fields in the bulk, from which we can construct operators that may link non-trivially in the bulk. Imposing conditions on these operators as we near the conformal boundary ∂AdS then picks out a maximal set of mutually local charged operators in the field theory. That is, for one set of operators we may specify a background value to which they tend as $r \to \infty$, ending them at the conformal boundary so they furnish charged states. A complimentary set of operators can then be allowed to fluctuate all the way to the boundary at infinity, which then gives rise to the symmetry generators in the field theory.

In AdS/CFT, however, conformal symmetry guarantees that the 1-form symmetry is spontaneously broken in the vacuum since the vev of the line operators must vanish. Therefore, we can infer no interesting implications for confinement unless we move to a more general notion of holography. This is precisely what we will do in chapter 4, where we consider the Klebanov-Strassler (KS) solution in Type IIB, which breaks conformal invariance by including fractional D3-branes, giving rise to a field theory describing a Seiberg duality cascade, which flows to $\mathcal{N}=1$ $SU(N)$ SYM in the IR.

Chapter 3

$\mathcal{I}/c$-extremization in M/F-theory

3.1 Introduction

A type IIB supergravity solution with a holomorphically varying axio-dilaton can be given an F-theory interpretation, whereby the varying axio-dilaton is represented as the complex structure of a singular elliptic fibration over spacetime. The axio-dilaton undergoes $SL(2,\mathbb{Z})$ monodromy around the singularities, which in turn encode the 7-branes in the background. Although such F-theory backgrounds have mainly been studied in the context of Minkowski solutions, recently AdS solutions were developed that have the hallmark of a holomorphically varying axio-dilaton. A class of AdS_3 solutions of F-theory were obtained in [32, 33], generalizing the constant τ solutions in e.g. [34–43]. The dual field theories are obtained by wrapping D3-branes on curves, above which the axio-dilaton varies. From the point of view of the 4d $\mathcal{N}=4$ Super-Yang-Mills (SYM) theory on the D3-branes, this corresponds to a varying complexified coupling, and the 2d SCFT is obtained by a duality-twist [44–47]. Generalizations of these F-theory solutions were obtained in [48–51] and the dual field theories were studied in [52, 53].

The most concrete avenue for accessing the geometric interpretation of F-theory is through its duality with M-theory, taken in its low-energy limit as 11d supergravity. The advantage of the M-theory dual perspective is that the elliptic fibration associated to the varying axio-dilaton appears as part of the physical spacetime geometry, rather than as an auxiliary space. There are two ways of dualizing the F-theory solutions, which in terms of dual field theory realized on D3-branes correspond to either mapping D3-branes to M5-branes or to M2-branes, depending on whether the T-duality is applied transverse to or along the world-volume of the D3-branes, respectively. In the former case, the F-theory solutions of [32] map to AdS_3

solutions in M-theory, which are dual to the MSW-strings [54]. Alternatively, by writing the AdS_3 as a constant-sized circle fibration over AdS_2, one can dualize along the fiber and obtain an AdS_2 solution of M-theory.

Among these AdS_3 solutions, the least well-understood are dual to 2d $\mathcal{N} = (0,2)$ supersymmetry [33], where, unlike for $(0,4)$, a general classification is not known. More importantly, the central charge of the 2d SCFTs for $(0,2)$ supersymmetry have to be determined by an extremization principle. Likewise, the dual M-theory AdS_2 backgrounds are holographic duals to 1d $\mathcal{N} = (0,2)$ SCQMs living on the conformal boundary, whose 1d partition function also requires an extremization. Indeed, in a supersymmetric 2d $(0,2)$ field theory the R-symmetry $U(1)_R$ is in general not uniquely defined. If the theory has other global abelian symmetries, these may mix with the $U(1)_R$ to produce an equally good R-symmetry. On the other hand, if the field theory flows to a superconformal fixed point in the infrared, this singles out a unique superconformal R-symmetry. In [55] an extraordinarily simple method for determining the exact R-symmetry of the fixed point SCFT was obtained, starting from the gauge theory description. The authors of [55] showed that extremizing the central charge c of the field theory over all admissible R-symmetries exactly identifies the superconformal R-symmetry. This so-called c-extremization was further developed for compactifications of D3-branes with constant and varying coupling in [33, 56, 57]. It is closely related to the 4d concept of a-maximization, which was formulated in [58]. A related concept, which will also play a central role in this paper, is $\mathcal{I}$-extremization. This has been proposed in [59] as a method for determining the exact R-symmetry of an SCQM, when this theory arises as a compactification of a 3d $\mathcal{N} = 2$ SCFT on a Riemann surface Σ. Then the topologically twisted index of the 3d theory is expected to yield the 1d partition function [60–62] after extremization.

The AdS/CFT correspondence implies that equivalent geometric extremization principles should exist, realizing the gravitational duals of $\mathcal{I}$- and c-extremization. Indeed such geometric duals were constructed in [63, 64] (as well as [65, 66] for a-maximization) for backgrounds where the axio-dilaton is constant. These papers formulate holographic extremization principles for the geometries in [36, 38, 67] by determining a parametrization of the Killing vector that is the geometric counterpart to the R-symmetry, and the conditions for the optimization problem to be well-defined, as well as the geometric quantity to be extremized. A general

proof of the off-shell holographic correspondence with $\mathcal{I}$- and c-extremization was put forth in [68] and extended in [69]. A complementary approach using gauged supergravity was pursued in [70, 71].

Whether one takes the geometric or field theoretic point of view, the extremization principles generally represent a significant simplification of the problem of determining genuine supergravity backgrounds or, equivalently, their dual SCFTs. Instead of directly having to solve a set of coupled (partial) differential equations, we can take the much more technically tractable approach of optimizing a single function.

In this paper we generalize this approach to include a varying axio-dilaton, which provides a powerful tool for identifying F-theory AdS_3 supergravity solutions that can arise from configurations of D3-branes and 7-branes. Furthermore, from this point of view the duality with M-theory AdS_2 backgrounds not only provides a description where the elliptic fibration associated with the varying axio-dilaton is physically manifest, it also implies that in this specific context holographic $\mathcal{I}$- and c-extremization are dual to each other.

More precisely, we will find that in general the two quantities obtained by extremization in M/F-theory only agree up to leading order in an expansion in terms of the volume of the elliptic fiber. Namely, we find

$$\log Z_{\mathrm{1d}} = \frac{1}{4G_2} = \frac{\Delta\phi}{12} c_{\mathrm{sugra}} + \mathcal{O}(k_0) = \sqrt{\frac{2}{3}} \pi N_0^{1/2} \cdot c_{\mathrm{sugra}}^{1/2} + \mathcal{O}(k_0)\,, \tag{3.1}$$

where k_0 is the volume of the elliptic fiber. Here on the left hand side Z_{1d} is the partition function of the 1d SCQM, which via holography is related to the 2d Newton constant G_2 of the dual M-theory AdS_2 solution. On the right hand side c_{sugra} is the leading order 2d central charge of the F-theory AdS_3 solution, $N_0 \in \mathbb{N}$ is a certain quantized flux number, while $\Delta\phi$ is the size of the circle upon which the 2d SCFT is compactified. The correction terms in (3.1) are $\mathcal{O}(k_0)$. In M-theory, this fiber volume is a physical quantity, whereas in F-theory the elliptic fiber is an auxiliary geometric structure, where only the complex structure has a physical meaning, and the volume is strictly taken to zero. The correction terms then generically arise because the M-theory backgrounds include the full backreaction of the 7-branes on the F-theory side, which in particular break the circle isometry on which we T-dualise.

Let us conclude by making some comments on the physical interpretation of (3.1). The left hand side is the logarithm of the 1d partition function of the SCQM on a circle. On the other hand, the first expression involving $c_{\rm sugra}$ is precisely the *Casimir energy* of the 2d $(0,2)$ theory placed on a torus, as one might have expected on general grounds. The final expression on the right hand side of (3.1) is proportional to $c_{\rm sugra}^{1/2}$, with a proportionality constant that is a fixed number. In particular, this shows that to leading order in k_0 the two extremization principles are dual to each other. We shall see explicit examples, where the $\mathcal{O}(k_0)$ correction terms are either zero or non-zero.

3.2 Holographic c-extremization in F-theory

We develop the holographic dual to c-extremization in the context of AdS_3 geometries in F-theory, i.e. type IIB supergravity with a holomorphically varying axio-dilaton τ, which are holographically dual to 2d $\mathcal{N}=(0,2)$ SCFTs. To begin with we review the class of geometries [33], before generalizing holographic c-extremization in type IIB [63] to encompass these F-theory geometries.

3.2.1 AdS_3 Backgrounds

We consider holographic duals to 2d $(0,2)$ SCFTs realized in type IIB with five-form flux and varying axio-dilaton [33]. The geometry underlying the solutions is $\mathrm{AdS}_3\times Y_7$, and is supported by RR five-form flux

$$\begin{aligned} ds_{10}^2 &= L_{10}^2\,\mathrm{e}^{-B_{10}/2}\left[ds^2(\mathrm{AdS}_3)+ds^2(Y_7)\right]\,,\\ F_5 &= -L_{10}^4\left(\mathrm{vol}_{\mathrm{AdS}_3}\wedge F+*_7F\right)\,. \end{aligned} \tag{3.2}$$

In addition the axio-dilaton τ varies over the space Y_7. Here L_{10} is an overall length scale, and B_{10} and F are a function and a closed two-form on Y_7, respectively. Analysis of the supersymmetry equations reveals that Y_7 admits a nowhere vanishing Killing vector ξ, which is the geometric counterpart to the $U(1)$ R-symmetry of the dual $(0,2)$ SCFT. The Killing vector induces a transversely conformally Kähler foliation $\mathcal{F}_\xi$. This entails that there is a locally defined space transverse to ξ, which we will denote by $\mathcal{M}_6$, admitting a Kähler metric. The geometric picture is most straightforward for the case of a *quasi-regular* Killing vector. By definition this means that the orbits of ξ close and Y_7 is the total space of the circle

fibration

$$\begin{array}{ccc} S^1 & \hookrightarrow & Y_7 \\ & & \downarrow \\ & & \mathcal{M}_6 \end{array} \,, \tag{3.3}$$

where the transverse Kähler space $\mathcal{M}_6$ is a compact Kähler orbifold. The R-symmetry is then globally a $U(1)$ symmetry. When the generic orbits do not close, the Killing vector is said to be *irregular*. For a more detailed description of the general properties of $\mathcal{F}_\xi$ we refer the reader to [63]. The brane configuration corresponding to these geometries consists of N D3-branes on $\mathbb{R}^{1,1} \times C$, where C are curves in $\mathcal{M}_6$, above which the axio-dilaton varies. The auxiliary elliptic fiber degenerates over the loci that are subspaces wrapped by the 7-branes, which in the present case have world-volume $\mathcal{W}_8 = \mathrm{AdS}_3 \times \widetilde{S}$, where $\widetilde{S}$ are five-cycles in Y_7.

The supersymmetry equations of type IIB get modified when the axio-dilaton is varying. The $SL(2,\mathbb{Z})$ self-duality of type IIB induces a so-called $U(1)_D$ symmetry, which acts on the fermions and supercharges by

$$U(1)_D : \qquad \gamma = \left(\begin{smallmatrix} a & b \\ c & d \end{smallmatrix}\right) \in SL(2,\mathbb{Z}) : \qquad \mathrm{e}^{i\alpha_\gamma} = \frac{|c\tau + d|}{c\tau + d} \,. \tag{3.4}$$

The action on the fermions with half-integral charge extends the $SL(2,\mathbb{Z})$ by a $\mathbb{Z}_2$ to the metaplectic group [72]. The duality $U(1)$-symmetry $U(1)_D$ can be gauged, and then defines a line bundle $\mathcal{L}$, with connection

$$Q = -\frac{1}{2\tau_2} d\tau_1 \,, \tag{3.5}$$

where $\tau = \tau_1 + i\tau_2$. Furthermore, it is convenient to define the one-form

$$\mathcal{P} = \frac{i}{2\tau_2} d\tau \,. \tag{3.6}$$

Supersymmetry implies that τ is preserved by ξ (i.e. $\mathcal{L}_\xi \tau = 0$) and that it varies holomorphically over the transverse Kähler space. The bundle $\mathcal{L}$ is then transversely holomorphic with the curvature given by

$$i\, d\mathcal{P} = dQ = -i\mathcal{P} \wedge \bar{\mathcal{P}} \,. \tag{3.7}$$

Next we consider how the geometry of Y_7 itself is constrained by supersymmetry. Let η be the one-form dual to ξ. Choosing a local coordinate z so that $\xi = 2\partial_z$, the local expression for η is given by $\eta = \frac{1}{2}(dz + P)$. The derivative of the local one-form P then satisfies

$$dP = \rho_6 - i\mathcal{P} \wedge \bar{\mathcal{P}} \,, \tag{3.8}$$

where ρ_6 is the transverse Ricci form. Finally, there is a relation between the scalar curvature R_6 of the transverse Kähler space and the warp factor B_{10}

$$\mathrm{e}^{B_{10}} = \frac{1}{8}\left(R_6 - 2|\mathcal{P}|^2\right) . \tag{3.9}$$

Before proceeding let us summarize all the expressions for 10d fields after having imposed the supersymmetry equations:

$$\begin{aligned}
ds_{10}^2 &= L_{10}^2\, \mathrm{e}^{-B_{10}/2}\left[ds^2\left(\mathrm{AdS}_3\right) + \frac{1}{4}\left(dz + P\right)^2 + \mathrm{e}^{B_{10}} ds^2\left(\mathcal{M}_6\right)\right] , \\
F_5 &= -L_{10}^4\left(\mathrm{vol}_{\mathrm{AdS}_3} \wedge F + *_7 F\right) , \\
F &= -2J_6 + \frac{1}{2} d\left[e^{-B_{10}}\left(dz + P\right)\right] , \\
dP &= \rho_6 - i\mathcal{P} \wedge \bar{\mathcal{P}} , \\
\mathrm{e}^{B_{10}} &= \frac{1}{8}\left(R_6 - 2|\mathcal{P}|^2\right) .
\end{aligned} \tag{3.10}$$

Here J_6 is the Kähler form on $\mathcal{M}_6$. Notice that all of the 10d fields are completely determined by the transverse Kähler metric together with the line bundle $\mathcal{L}$. We refer to Y_7 satisfying the supersymmetry equations, and therefore having all the properties outlined above, as a *supersymmetric geometry*. For constant axio-dilaton $\mathcal{P} = 0$, and the above reduce to the type IIB equations in [36].

All of the above results hold off-shell, by which we mean that we merely impose supersymmetry, without imposing the equations of motion. For supersymmetric geometries the equations of motion reduce to a PDE on the transverse Kähler space involving the metric and the connection on the line bundle $\mathcal{L}$. This is the so-called *master equation*, given by

$$\Box_6(R_6 - 2|\mathcal{P}|^2) = \frac{1}{2}R_6^2 - (R_6)_{\mu\nu}(R_6)^{\mu\nu} + 2|\mathcal{P}|^2 R_6 - 4(R_6)_{\mu\nu}\mathcal{P}^\mu\bar{\mathcal{P}}^\nu . \tag{3.11}$$

Geometries satisfying this equation will be called *on-shell*, and are solutions of the type IIB supergravity equations with varying axio-dilaton, provided that the five-form flux is appropriately quantized. We will return to the flux quantization conditions in a later section.

The F-theory perspective amounts to giving the varying axio-dilaton a geometric interpretation in terms of an auxiliary elliptic fibration

$$\begin{array}{ccc} \mathbb{E}_\tau & \hookrightarrow & \mathcal{M}_8^\tau \\ & & \downarrow \\ & & \mathcal{M}_6 \end{array} . \tag{3.12}$$

The total space $\mathcal{M}_8^\tau$ is Kähler but not Calabi-Yau[1]. Locally, away from the singular fibers, the metric on the total space is

$$ds^2(\mathcal{M}_8^\tau) = \frac{1}{\tau_2}\left[(d\psi + \tau_1 d\phi)^2 + \tau_2^2 d\phi^2\right] + ds^2(\mathcal{M}_6)\,. \tag{3.13}$$

The master equation can then be interpreted as a curvature condition on the total space $\mathcal{M}_8^\tau$. Taking this view, the master equation is

$$\Box_8(R_8) = \frac{1}{2}R_8^2 - (R_8)_{\mu\nu}(R_8)^{\mu\nu}\,, \tag{3.14}$$

which is precisely the form of the equation for constant axio-dilaton, just in two dimensions higher.

3.2.2 Supersymmetric Action

A key step in constructing the geometric dual of c-extremization for type IIB AdS_3 geometries with 2d $(0,2)$ duals and *constant* axio-dilaton was deriving a certain geometric function called the *supersymmetric action*. Solutions to the master equation are extrema of this action, and the corresponding extremal value can be used to compute the central charge of the dual SCFT. In this section, we generalize this action to backgrounds with varying axio-dilaton.

The type IIB supergravity equations including varying τ are

$$R_{\mu\nu} = 2\mathcal{P}_{(\mu}\bar{\mathcal{P}}_{\nu)} + \frac{1}{96}(F_5)_{\mu\sigma_1\cdots\sigma_4}(F_5)_\nu{}^{\sigma_1\cdots\sigma_4}\,, \qquad d*F_5 = 0\,, \tag{3.15}$$

where $\mu,\nu = 0,1,...,9$. Writing out the components of the Einstein equations along the internal space Y_7 we obtain

$$\begin{aligned} 0 = {} & R_{7ab} - 2\mathcal{P}_{(a}\bar{\mathcal{P}}_{b)} + \frac{1}{2}\nabla_a B_{10}\nabla_b B_{10} + 2\nabla_{ab}B_{10} + \frac{1}{4}\nabla^2 B_{10} g_{7ab} - \frac{1}{2}\left(dB_{10}\right)^2 g_{7ab} \\ & + \frac{1}{2}\mathrm{e}^{2B_{10}}F_{ac}F_b{}^d - \frac{1}{8}\mathrm{e}^{2B_{10}}F^2 g_{7ab}\,, \end{aligned} \tag{3.16}$$

where $a,b = 1,2,...,7$. This arises by extremizing the following action functional

$$S_F = \int_{Y_7}\mathrm{e}^{-2B_{10}}\left[R_7 - 2|\mathcal{P}|^2 - 6 + \frac{9}{2}\left(dB_{10}\right)^2 + \frac{1}{4}\mathrm{e}^{2B_{10}}F^2\right]\mathrm{vol}_{Y_7}\,, \tag{3.17}$$

with respect to the 7d metric, and generalizes the action functional for constant τ in [38]. Varying the other fields in this action gives rise to the remaining type IIB equations of motion.

[1]We will denote spaces which enjoy an elliptic fibration with a superscript τ, indicating the complex structure of the elliptic fiber.

We now specialize to the case where Y_7 is supersymmetric. Using the notation introduced in the previous subsection, the metric on Y_7 can be written as

$$ds^2(Y_7) = \eta^2 + \mathrm{e}^{B_{10}} ds^2(\mathcal{M}_6) \,, \tag{3.18}$$

where $ds^2(\mathcal{M}_6)$ is the transverse Kähler metric. Writing out the Ricci scalar we obtain (up to total derivatives)

$$R_7 = \mathrm{e}^{-B_{10}} R_6 - 5\mathrm{e}^{-B_{10}} (dB_{10})^2 - \frac{1}{16}\mathrm{e}^{-2B_{10}} (dP)^2 \,. \tag{3.19}$$

Furthermore, the flux term in the action is

$$\frac{1}{4}\mathrm{e}^{2B_{10}} F^2 = 6 - \frac{1}{2}\mathrm{e}^{-B_{10}} \left(R_6 - 2|\mathcal{P}|^2\right) + \frac{1}{16}\mathrm{e}^{-2B_{10}} (dP)^2 + \frac{1}{2}\mathrm{e}^{-B_{10}} (dB_{10})^2 \,. \tag{3.20}$$

Combining these, we find that the action evaluated on supersymmetric geometries is given by

$$\begin{aligned} S_F =& \frac{1}{2}\int_{Y_7} \mathrm{e}^{-3B_{10}} \left(R_6 - 2|\mathcal{P}|^2\right) \mathrm{vol}_{Y_7} \\ =& \int_{Y_7} \eta \wedge \left(\rho_6 - i\mathcal{P}\wedge\bar{\mathcal{P}}\right) \wedge \frac{J_6^2}{2} \,. \end{aligned} \tag{3.21}$$

We may rewrite this in a slightly nicer way as follows. Notice that $i\mathcal{P}\wedge\bar{\mathcal{P}}$ is the curvature of the connection (3.5) and hence is a representative of $2\pi c_1(\mathcal{L})$. The action only depends on the cohomology class and not the particular representative, so we can rewrite it in terms of $c_1(\mathcal{L})$ as

$$S_F = \int_{Y_7} \eta \wedge (\rho_6 - 2\pi c_1(\mathcal{L})) \wedge \frac{J_6^2}{2} \,. \tag{3.22}$$

For fixed R-symmetry vector ξ this function depends only on the transverse Kähler class of the Kähler form J_6, and here also the first Chern class of the line bundle $\mathcal{L}$.

The central charge of the dual 2d (0,2) SCFT is computed from the Brown-Henneaux formula [73]

$$c_{\mathrm{sugra}} = \frac{3L_{10}}{2G_3} \,, \tag{3.23}$$

where

$$\frac{1}{G_3} = \frac{L_{10}^7}{G_{10}} \int_{Y_7} \mathrm{e}^{-2B_{10}} \mathrm{vol}_{Y_7} \tag{3.24}$$

is the effective 3d Newton constant, and G_{10} is the 10d Newton constant. For an off-shell supersymmetric geometry the trial central charge is

$$c_{\mathrm{trial}} = \frac{12(2\pi)^2}{\nu_3^2} S_F \,, \tag{3.25}$$

where

$$\nu_3 = \frac{2(2\pi l_s)^4}{L_{10}^4}\,. \tag{3.26}$$

An F-theory solution necessarily extremizes c_{trial} over the class of off-shell geometries, and the central charge of the holographic dual SCFT is determined by

$$c_{\text{sugra}} = \frac{12(2\pi)^2}{\nu_3^2} S_F\Big|_{\text{on-shell}}\,. \tag{3.27}$$

3.2.3 Flux Quantization

To have a genuine solution of string theory, the five-form flux must be appropriately quantized. We now describe how to quantize the flux for off-shell supersymmetric geometries, which is essential for completing the setup of the extremization problem.

The type IIB flux quantization conditions are

$$\frac{1}{(2\pi l_s)^4}\int_{S_\alpha} F_5 = N_\alpha^F \in \mathbb{Z}\,, \tag{3.28}$$

with five-cycles $S_\alpha \in H_5(Y_7,\mathbb{Z})$, and the restriction of the five-form flux to Y_7 is given by [33]

$$F_5|_{Y_7} = \frac{L_{10}^4}{4}\left[(dz+P)\wedge\left(\rho_6 - i\mathcal{P}\wedge\bar{\mathcal{P}}\right)\wedge J_6 + \frac{1}{2}*_6 d\left(R_6 - 2|\mathcal{P}|^2\right)\right]\,. \tag{3.29}$$

They can also be expressed as

$$\nu_3 N_\alpha^F = \int_{S_\alpha} \eta\wedge(\rho_6 - 2\pi c_1(\mathcal{L}))\wedge J_6\,. \tag{3.30}$$

For the flux quantization conditions to be well-defined we have to ensure that the integrals in (3.28) do not depend on the representatives of the cycles S_α. This is automatic for on-shell geometries since the master equation is equivalent to F_5 being closed. For off-shell geometries the setup requires some additional care.

To make the flux quantization conditions well-defined we will impose two topological assumptions. Firstly, we require that

$$H^2(Y_7,\mathbb{R}) \cong H_B^2(\mathcal{F}_\xi)/\left[\rho_6 - 2\pi c_1(\mathcal{L})\right]\,. \tag{3.31}$$

We have introduced the basic cohomology groups H_B^* of the foliation $\mathcal{F}_\xi$ that are formed by restricting the exterior derivative to ξ-invariant differential forms. Note that $[\rho_6 - 2\pi c_1(\mathcal{L})]$ is a closed basic class that is exact in $H^2(Y_7,\mathbb{R})$ due to (3.8). This condition is most transparent

in the quasi-regular case, where it implies that every cycle in $H_5(Y_7,\mathbb{Z})$ admits a representative which is a circle-bundle over a four-cycle in $\mathcal{M}_6$.

This condition by itself is not sufficient for the flux quantization conditions to be well-defined. The issue resides in the fact that even if we choose representatives S_α and S_β in the same homology class and both tangent to ξ, the flux integrals can still be different. To see this explicitly note that, by the first assumption, any two cycles that differ by the Poincaré dual (PD) cycle $\alpha[\rho_6 - 2\pi c_1(\mathcal{L})]_{\rm PD}$ are homologous. However, for such cycles

$$\int_{S_\alpha} \eta\wedge(\rho_6 - 2\pi c_1(\mathcal{L}))\wedge J_6 - \int_{S_\beta} \eta\wedge(\rho_6 - 2\pi c_1(\mathcal{L}))\wedge J_6 = \alpha\int_{Y_7} \eta\wedge(\rho_6 - 2\pi c_1(\mathcal{L}))^2\wedge J_6\,. \quad (3.32)$$

Therefore the second condition we impose is the vanishing of the integral on the right side, i.e.

$$\int_{Y_7} \eta\wedge(\rho_6 - 2\pi c_1(\mathcal{L}))^2\wedge J_6 = 0\,. \quad (3.33)$$

Imposing these two conditions on the off-shell geometries ensures that the flux quantization is indeed well-defined. Furthermore, (3.33) is identified as the integral of the master equation, which follows by writing the latter as

$$\Box_6\left(R_6 - 2|\mathcal{P}|^2\right) = (J_6\wedge J_6)\lrcorner\left[\left(\rho_6 - i\mathcal{P}\wedge\bar{\mathcal{P}}\right)\wedge\left(\rho_6 - i\mathcal{P}\wedge\bar{\mathcal{P}}\right)\right]\,. \quad (3.34)$$

Integrating this equation over Y_7, the left hand side vanishes using Stokes' theorem. Using the identity

$$[(J_6\wedge J_6)\lrcorner(a\wedge a)]\,\frac{J_6^3}{3!} = 2a^2\wedge J_6\,, \quad (3.35)$$

we obtain precisely (3.33).

3.2.4 The Complex Cone and the Geometric Extremization Problem

Having set up the abstract extremization problem, we now turn to the question of how to parametrize the class of off-shell supersymmetric geometries over which we extremize the action, by constructing a complex cone associated to Y_7 that allows us to parametrize the space of R-symmetry vectors on Y_7.

Consider the cone $C(Y_7)$ with metric

$$ds^2(C(Y_7)) = dr^2 + r^2 ds^2(Y_7)\,, \quad (3.36)$$

where $r \in \mathbb{R}_{>0}$. As for the constant axio-dilaton case, we can consider the natural, locally defined $(4,0)$-form on the cone that is given by

$$\Omega_{(4,0)} = \mathrm{e}^{iz}\mathrm{e}^{3B_{10}/2} r^3 \left[dr - \frac{ir}{2}\left(dz + P\right)\right] \wedge \Omega_6 \,. \tag{3.37}$$

However, this form does not extend to a global form unless the duality bundle $\mathcal{L}$ is trivial, i.e. the axio-dilaton is constant. To see this note that (3.8) implies that e^{iz} transforms as a local section[2] of $K_{\mathcal{M}_6}^{-1} \otimes \mathcal{L}^{-1}$, whereas Ω_6 is a local section of $K_{\mathcal{M}_6}$. The object $\Omega_{(4,0)}$ therefore transforms as a local section of $\mathcal{L}^{-1}$. Since $\mathcal{L}$ admits a global holomorphic section its dual does not, unless $\mathcal{L}$ is trivial. In particular, $\Omega_{(4,0)}$ is not globally defined as a form, when the axio-dilaton varies.

To circumvent this issue we use the auxiliary elliptic fibration introduced in (3.12), where the complex structure of the elliptic fiber encodes the axio-dilaton. Moreover, we assume that this fibration has a holomorphic section $\sigma : \mathcal{M}_6 \to \mathcal{M}_8^\tau$. Since τ is preserved by the Killing vector we can construct an elliptic fibration over Y_7 by letting the elliptic fiber be constant along the orbits of ξ. This gives a 9d space, which we denote by Y_9^τ, endowed with the metric

$$ds^2(Y_9^\tau) = ds^2(Y_7) + \mathrm{e}^{B_{10}} ds^2(\mathbb{E}_\tau) = \eta^2 + \mathrm{e}^{B_{10}} ds^2\left(\mathcal{M}_8^\tau\right) \,. \tag{3.38}$$

One can think of Y_9^τ as an elliptic fibration over Y_7, with the elliptic fibers being invariant along the Killing vector direction $\xi = 2\partial_z$. The differential forms pull back from Y_7 to Y_9^τ, and as usual we conflate the forms with their lifts to avoid notational clutter. We can now define the cone over Y_9^τ as

$$ds^2(C(Y_9^\tau)) = dr^2 + r^2 ds^2(Y_9^\tau) \,. \tag{3.39}$$

This cone admits a natural $SU(5)$ structure, with the $(5,0)$-form locally given by

$$\Omega_{(5,0)} = \mathrm{e}^{iz}\mathrm{e}^{2B_{10}} r^4 \left[dr - \frac{ir}{2}\left(dz + P\right)\right] \wedge \Omega_8 \,. \tag{3.40}$$

The fundamental two-form is exactly the same as in [63] and is not relevant for our purposes. The local holomorphic volume form on $\mathcal{M}_8^\tau$ is

$$\Omega_8 = \mathcal{P} \wedge \Omega_6 \,, \tag{3.41}$$

[2]We are suppressing the pullbacks in the notation for various bundles.

which satisfies

$$d\Omega_8 = iP \wedge \Omega_8 \,. \tag{3.42}$$

The local holomorphic volume form $\Omega_{(5,0)}$ now does extend to a global form, as Ω_8 is a section of $K_{\mathcal{M}_6} \otimes \mathcal{L}$ and the extra $\mathcal{L}$ now cancels with the $\mathcal{L}^{-1}$. In addition, by using (3.42) we can show that the holomorphic volume form is conformally closed

$$d\Psi = 0 \,, \qquad \Psi \equiv \mathrm{e}^{-2B_{10}} r^{-7} \Omega_{(5,0)} \,, \tag{3.43}$$

i.e. $C(Y_9^7)$ has vanishing first Chern class. We find that Ψ is charged under the R-symmetry vector field

$$\mathcal{L}_\xi \Psi = 2i\Psi \,. \tag{3.44}$$

This implies that ξ is a holomorphic vector field, which is paired with the radial vector field under the complex structure $\mathcal{I}(\xi) = -r\partial_r$.

Suppose now that $C(Y_9^7)$ admits a holomorphic $U(1)^s$ action, generated by a set of holomorphic vector fields ∂_{φ_i}, $i = 1, 2, ..., s$. We parametrize the general R-symmetry vector in terms of these holomorphic vector fields

$$\xi = \sum_{i=1}^{s} b_i \partial_{\varphi_i} \,, \tag{3.45}$$

and choose a basis where Ψ has charge 1 under ∂_{φ_1} and charge 0 under the remaining generators. This fixes $b_1 = 2$, and leaves the remaining b_i, $i = 2, 3, ..., s$ as free variables to be extremized over in S_F.

We can now summarize the extremization principle in F-theory: The supersymmetic action S_F in (3.22) is a function of the R-symmetry vector ξ defined in (3.45) and the basic Kähler class $[J_6]$ of $\mathcal{M}_6$. Imposing the flux quantization conditions (3.30) and the associated topological constraints (3.31) and (3.33) relate the R-symmetry parameters (b_i above) and the transverse Kähler class parameters. A putative solution extremizes the supersymmetric action over the remaining free variables. The central charge of the dual SCFT is then computed using (3.27). We shall exemplify this procedure in section 3.5.

3.3 M/F-duality and Holographic $\mathcal{I}$-extremization

The axio-dilaton in F-theory can at times be somewhat obscure, as it is not part of the geometry of the spacetime. To clarify the role of the elliptic fibration, it is often useful to

consider a dual M-theory background. For AdS_3 solutions, this could either be a dual AdS_3 or AdS_2 solution of M-theory. In the current framework we will dualize to the latter, which in the field theory corresponds to the circle-reduction to a 1d SCQM. The associated geometric extremization principle, holographic $\mathcal{I}$-extremization, was studied in [63]. In this section we will apply this formalism to the class of geometries that are dual to the F-theory backgrounds and study the extremization principle.

3.3.1 M/F-duality for AdS-geometries

Any M-theory geometry with an elliptic fibration can be dualized to obtain a corresponding F-theory geometry with varying axio-dilaton, by first reducing to Type IIA along one cycle of the elliptic fibration and subsequently T-dualizing along the second cycle. This approach is valid away from singular fibers, where locally the geometry of the elliptic fiber is

$$ds^2\left(\mathbb{E}_\tau\right) = \frac{L_{11}^2}{\tau_2}\left((dx+\tau_1 dy)^2+\tau_2^2 dy^2\right) . \tag{3.46}$$

We have introduced an overall M-theory length scale L_{11} and the periodic coordinates $x \sim x + 2\pi\Delta x$ and $y \sim y + 2\pi\Delta y$, where we set $\Delta x = \Delta y$. The M-theory background can be dimensionally reduced on a circle to yield a Type IIA background. Specifically, the two metrics are related as

$$ds_{11}^2 = L_{11}^2\left(\frac{l_s}{l_p}\right)^4 \mathrm{e}^{4\phi_{\rm IIA}/3}(dx+C_1)^2 + \left(\frac{l_p}{l_s}\right)^2 \mathrm{e}^{-2\phi_{\rm IIA}/3} ds_{\rm IIA}^2 \,, \tag{3.47}$$

where l_s and l_p are the string and 11d Planck lengths, and $ds_{\rm IIA}^2$, $\mathrm{e}^{\phi_{\rm IIA}}$ and C_1 are respectively the metric, the fluctuating dilaton and the RR one-form potential of Type IIA. Comparison with (3.46) allows us to immediately identify

$$C_1 = \tau_1 dy \,, \qquad \mathrm{e}^{4\phi_{\rm IIA}/3} = \left(\frac{l_p}{l_s}\right)^4 \frac{1}{\tau_2} \,, \qquad ds_{\rm IIA}^2 = L_{11}^2\left(\frac{l_s}{l_p}\right)^2 \mathrm{e}^{2\phi_{\rm IIA}/3}\tau_2 dy^2 + ds_9^2 \,, \tag{3.48}$$

where ds_9^2 is the metric on the 9d space of the Type IIA geometry orthogonal to the y circle. Dimensionally reducing the M-theory action to that of Type IIA (here it is sufficient to consider the Ricci scalar term) fixes the period of the circle to be

$$L_{11}\Delta x = \frac{l_p^3}{l_s^2} \,, \tag{3.49}$$

where we have used $16\pi G_{11} = (2\pi)^8 l_p^9$ and $16\pi G_{10} = (2\pi)^7 l_s^8$ for the 11d and 10d Newton constants, respectively. Hence, we can express the volume of the elliptic fiber in terms of

fundamental length scales as

$$\mathrm{vol}\left(\mathbb{E}_\tau\right) = (2\pi\Delta x)^2 = \frac{(2\pi)^2 l_p^6}{L_{11}^2 l_s^4}\,. \tag{3.50}$$

Carrying out T-duality along the y circle results in

$$R_{\rm IIB} = \frac{l_s^2}{L_{11}\Delta y} = \frac{l_s^4}{l_p^3}\,, \qquad C_0 = (C_1)_y = \tau_1\,, \qquad \mathrm{e}^{\phi_{\rm IIB}} = \frac{l_s}{\frac{l_s}{l_p}L_{11}\Delta y\,\mathrm{e}^{\phi_{\rm IIA}/3}\sqrt{\tau_2}}\mathrm{e}^{\phi_{\rm IIA}} = \frac{1}{\tau_2}\,. \tag{3.51}$$

This then identifies $\tau = \tau_1 + i\tau_2 = C_0 + i\,\mathrm{e}^{-\phi_{\rm IIB}}$.

Applied to the AdS_3 F-theory geometries of section 3.2, the key observation is that we dualize along the AdS direction by first writing AdS_3 as a circle fibration over AdS_2 [74]

$$ds^2\left(\mathrm{AdS}_3\right) = \frac{1}{4}\left(-r^2dt^2 + \frac{dr^2}{r^2} + (d\phi + a_1)^2\right) = \frac{1}{4}ds^2\left(\mathrm{AdS}_2\right) + \frac{1}{4}(d\phi + a_1)^2\,, \tag{3.52}$$

where $\phi \sim \phi + \Delta\phi$ is the circle coordinate and $a_1 = rdt$ so that $da_1 = \mathrm{vol}_{\mathrm{AdS}_2}$. The F-theory metric can then be written as

$$ds_{10}^2 = L_{11}^2\mathrm{e}^{-B_{11}/2}\left[ds^2\left(\mathrm{AdS}_2\right) + (d\phi + a_1)^2 + (dz + P)^2 + \mathrm{e}^{B_{11}}ds^2\left(\mathcal{M}_6\right)\right]\,, \tag{3.53}$$

where we have taken the M/F-theory length scales and warp factors to be related by

$$L_{10} = \sqrt{2}L_{11}\,, \qquad \mathrm{e}^{B_{10}} = \frac{1}{4}\mathrm{e}^{B_{11}}\,. \tag{3.54}$$

T-duality along the ϕ direction results in

$$\begin{aligned}
ds_{\rm IIA}^2 &= L_{11}^2\sqrt{\tau_2}\,\mathrm{e}^{B_{11}/2}d\phi^2 + L_{11}^2\frac{\mathrm{e}^{-B_{11}/2}}{\sqrt{\tau_2}}\left[ds^2\left(\mathrm{AdS}_2\right) + (dz + P)^2 + \mathrm{e}^{B_{11}}ds^2\left(\mathcal{M}_6\right)\right]\,,\\
\mathrm{e}^{-2\phi_{\rm IIA}} &= \frac{l_p^6}{l_s^6}\tau_2^{3/2}\mathrm{e}^{-B_{11}/2}\,,\\
H &= L_{11}^2 d\phi \wedge \mathrm{vol}_{\mathrm{AdS}_2}\,,\\
F_2 &= L_{11}d\tau_1 \wedge d\phi\,,\\
F_4 &= \frac{1}{2}L_{11}^3\mathrm{vol}_{\mathrm{AdS}_2} \wedge F\,.
\end{aligned} \tag{3.55}$$

Finally, we uplift to M-theory using the metric in (3.47). We find that the M-theory geometries dual to the AdS_3 F-theory geometries in (3.10) are

$$\begin{aligned}
ds_{11}^2 &= L_{11}^2\mathrm{e}^{-2B_{11}/3}\left[ds^2\left(\mathrm{AdS}_2\right) + (dz + P)^2 + \mathrm{e}^{B_{11}}ds^2\left(\mathcal{M}_8^\tau\right)\right]\,,\\
G_4 &= L_{11}^3\mathrm{vol}_{\mathrm{AdS}_2} \wedge \left[-J_8 + d\left(\mathrm{e}^{-B_{11}}\left(dz + P\right)\right)\right]\,,\\
dP &= \rho_8\,,\\
\mathrm{e}^{B_{11}} &= \frac{1}{2}R_8\,,
\end{aligned} \tag{3.56}$$

where J_8, ρ_8 and R_8 denote the Kähler form, Ricci form, and Ricci scalar of the Kähler four-fold $\mathcal{M}_8^\tau$. This is exactly the space introduced in (3.12) with metric (3.13), which in M-theory forms part of the physical spacetime. Its Ricci form and scalar are related to the corresponding $\mathcal{M}_6$ quantities as

$$\rho_8 = \rho_6 - i\mathcal{P}\wedge\bar{\mathcal{P}}\,, \qquad R_8 = R_6 - 2|\mathcal{P}|^2\,. \tag{3.57}$$

Notice that the duality determines the period of the ϕ circle in terms of fundamental length scales to be

$$\frac{L_{11}\Delta\phi}{2\pi} = \frac{l_s^4}{l_p^3}\,. \tag{3.58}$$

3.3.2 Holographic $\mathcal{I}$-extremization

In this section we will briefly summarize the central aspects of the general version of holographic $\mathcal{I}$-extremization, before specializing to elliptically fibered M-theory geometries. The extremization principle applies to any supersymmetric M-theory AdS_2 geometry with electric four-form flux

$$\begin{aligned} ds_{11}^2 &= L_{11}^2 \mathrm{e}^{-2B_{11}/3}\left[ds^2\left(\mathrm{AdS}_2\right) + ds^2\left(Y_9^\tau\right)\right]\,, \\ G_4 &= L_{11}^3 \mathrm{vol}_{\mathrm{AdS}_2}\wedge F\,, \end{aligned} \tag{3.59}$$

where the compact internal space Y_9^τ admits a natural unit length Killing vector ξ. The leaf spaces of the transverse foliation $\mathcal{F}_\xi$ admit a Kähler structure. Following the notation in section 3.3.1 we denote that transverse space by $\mathcal{M}_8^\tau$[3]. The warp factor B_{11} and closed two-form F are defined on the internal space Y_9^τ. These supersymmetric geometries can be put on-shell by imposing the condition

$$\Box_8 R_8 = \frac{1}{2}R_8^2 - (R_8)_{\mu\nu}(R_8)^{\mu\nu} \tag{3.60}$$

on the transverse space. Clearly, the M-theory duals derived in the previous section belong to this class of theories. The geometric dual of $\mathcal{I}$-extremization is formulated as follows. For an M-theory supergravity background to be consistent, the G_4-flux has to be quantized before extremizing, which is well-defined if we impose the topological restriction

$$H^2(Y_9^\tau,\mathbb{R}) = H_B^2(\mathcal{F}_\xi)/[\rho_8] \tag{3.61}$$

[3]Note that this internal space differs from the F-theory compact space with the auxiliary elliptic fibration by the normalization of the Killing vector.

and constraint equation

$$\int_{Y_9^\tau} \eta \wedge \rho_8^2 \wedge \frac{J_8^2}{2} = 0\,. \tag{3.62}$$

Then flux quantization over all seven-cycles $\widetilde{S}_I \in H_7(Y_9^\tau, \mathbb{Z})$ is given by

$$\nu_4 N_I^M = \int_{\widetilde{S}_I} \eta \wedge \rho_8 \wedge \frac{J_8^2}{2}\,, \tag{3.63}$$

where we have introduced the positive constant

$$\nu_4 = \frac{(2\pi l_p)^6}{L_{11}^6}\,. \tag{3.64}$$

An analogous cone $C(Y_9^\tau)$ to the one presented in section 3.2.4 can be constructed for the present M-theory geometries. This cone likewise has a globally defined holomorphic $(5,0)$-form, which allows for a parametrization of the M-theory R-symmetry vector in terms of a $U(1)^s$ action on the cone, as in (3.45). Note that the holomorphic $(5,0)$-form on $C(Y_9^\tau)$ has charge 1 under the R-symmetry vector field, so that the first coefficient in the parametrization is $b_1 = 1$ (again, this is due to a factor of 2 difference in the normalization of the R-symmetry vector in M- versus F-theory).

Having fixed a complex cone $C(Y_9^\tau)$ and imposed the constraint equation (3.62) and flux quantization (3.63), the supersymmetric action

$$S_M = \int_{Y_9^\tau} \eta \wedge \rho_8 \wedge \frac{J_8^3}{3!}\,, \tag{3.65}$$

can be extremized with respect to the remaining variables in ξ and $[J_8]$. This is a necessary condition for the geometry Y_9^τ to be on-shell, i.e. to satisfy the master equation (3.60). The effective AdS_2 Newton constant of such an on-shell solution is then

$$\frac{1}{G_2} = \frac{8(2\pi)^2}{\nu_4^{3/2}} S_M \bigg|_{\text{on-shell}}\,. \tag{3.66}$$

3.3.3 M-theory Supersymmetric Action for Elliptic Fibrations

Finally, we specialize the M-theory geometries to those with F-theory duals, i.e. $\mathcal{M}_8^\tau$ is an elliptic fibration over a base $\mathcal{M}_6$ with a section $\sigma : \mathcal{M}_6 \to \mathcal{M}_8^\tau$. We are interested in determining how the flux quantization conditions (3.63) and supersymmetric action (3.65) depend on data of the base $\mathcal{M}_6$. For this purpose we will here focus on on-shell solutions, which allows us to assume a choice of a regular Killing vector. This in turn ensures that

the transverse Kähler space $\mathcal{M}_8^\tau$ is a smooth manifold. We will return to the extremization problem in the subsequent sections.

The Shioda-Tate-Wazir theorem for elliptically fibered Kähler manifolds [75] asserts[4] that we can decompose the (cohomology class of the) Kähler form on $\mathcal{M}_8^\tau$ as

$$J_8 = k_0\omega_0 + \sum_\alpha k_\alpha\omega_\alpha + \sum_i k_i\omega_i \equiv \sum_I k_I\omega_I \,. \tag{3.67}$$

This decomposition corresponds to three divisor classes, which generate the Picard group of $\mathcal{M}_8^\tau$. These are: the divisor corresponding to the section σ with its dual (1,1)-form ω_0, the pullback divisors C_α with dual forms denoted by ω_α, and finally the resolution divisors (also referred to as Cartan divisors) D_i with dual forms ω_i. For a more thorough discussion see [32]. Note that we do not require the Kähler parameters k_I to be integers; rather they are real numbers, which will ultimately be determined by the flux integers. Moreover, the Killing vector is assumed to be regular, implying a smooth $\mathcal{M}_8^\tau$. We assume for simplicity that the elliptic fibration is a smooth Weierstrass model and thus only has Kodaira type I_1 fibers and no resolution divisors.

With the expansion (3.67) the supersymmetric action (3.65) becomes

$$S_M = \sum_{IJK} \frac{k_I k_J k_K}{3!} \int_{Y_9^\tau} \eta \wedge \rho_8 \wedge \omega_I \wedge \omega_J \wedge \omega_K \,. \tag{3.68}$$

The integral in S_M can be pushed down to an intersection on the base using adjunction

$$c_1(\mathcal{M}_8^\tau) = c_1(\mathcal{M}_6) - c_1(\mathcal{L}) \,. \tag{3.69}$$

Furthermore, since the Killing vector is regular, we can integrate out the circle direction, which we take to have period $2\pi\ell$, and write the supersymmetric action as

$$S_M = (2\pi)^2\ell \sum_{IJK} \frac{k_I k_J k_K}{3!} \int_{\mathcal{M}_8^\tau} (c_1(\mathcal{M}_6) - c_1(\mathcal{L})) \wedge \omega_I \wedge \omega_J \wedge \omega_K \,. \tag{3.70}$$

We define the intersection numbers

$$C_{IJK} \equiv (c_1(\mathcal{M}_6) - c_1(\mathcal{L})) \cdot C_I \cdot C_J \cdot C_K = \int_{\mathcal{M}_8^\tau} (c_1(\mathcal{M}_6) - c_1(\mathcal{L})) \wedge \omega_I \wedge \omega_J \wedge \omega_K \,. \tag{3.71}$$

Using the intersection identity

$$\sigma \cdot_{\mathcal{M}_8^\tau} (\sigma + c_1(\mathcal{L})) = 0 \,, \tag{3.72}$$

[4]For this to be true we need to impose some topological restrictions, namely $h^{1,0}(\mathcal{M}_8^\tau) = h^{2,0}(\mathcal{M}_8^\tau) = 0$. Also we assume for simplicity that there are no extra sections, i.e. the Mordell Weil group is trivial. From now on we assume this to hold.

a short computation shows that

$$\begin{aligned} C_{000} &= (c_1(\mathcal{M}_6) - c_1(\mathcal{L})) \cdot c_1(\mathcal{L}) \cdot c_1(\mathcal{L}) \,, \\ C_{00\alpha} &= -\left(c_1(\mathcal{M}_6) - c_1(\mathcal{L})\right) \cdot c_1(\mathcal{L}) \cdot C_\alpha \,, \\ C_{0\alpha\beta} &= (c_1(\mathcal{M}_6) - c_1(\mathcal{L})) \cdot C_\alpha \cdot C_\beta \,, \\ C_{\alpha\beta\gamma} &= 0 \,, \end{aligned} \tag{3.73}$$

which are manifestly intersection numbers on the base $\mathcal{M}_6$. Then the supersymmetric action specialized to elliptic fibrations is given in terms of intersection numbers on the base as

$$S_M = (2\pi)^2 \ell \sum_{IJK} \frac{k_I k_J k_K}{3!} C_{IJK} \,. \tag{3.74}$$

The flux quantization conditions (3.63) specialized to elliptic fibrations become

$$\nu_4 N_I^M = (2\pi)^2 \ell \sum_{JK} \frac{k_J k_K}{2} C_{IJK} \,. \tag{3.75}$$

Finally, observe that the Kähler parameter k_0 of the elliptic fiber is exactly the volume of a (non-singular) fiber

$$\mathrm{vol}(\mathbb{E}_\tau) = \int_{\mathbb{E}_\tau} J_8 = k_0 \int_{\mathbb{E}_\tau} \omega_0 = k_0 \,. \tag{3.76}$$

From the discussion of the M/F-duality, specifically using (3.50), we find that k_0 is expressed in terms of fundamental lengths as

$$k_0 = \frac{(2\pi)^2 l_p^6}{L_{11}^2 l_s^4} \,. \tag{3.77}$$

3.4 $\mathcal{I}/c$-extremization

We will now compare the extremization procedures in M/F-theory. We will first provide the map between the two geometric extremization procedures, and then discuss the dual field theory.

3.4.1 Geometry

What we have argued so far is that an F-theory AdS_3 geometry is characterized by the complex geometry of the internal space $\mathcal{M}_6$ and the axio-dilaton profile. They are conveniently thought of here in terms of the complex cone $C(Y_9^\tau)$, which is a $\mathbb{C}^*$ fibration over an elliptically fibered base $\mathcal{M}_8^\tau$. An on-shell solution is ultimately determined by imposing a topological constraint, as well as a choice of quantized flux numbers $N_\alpha^F \in \mathbb{Z}$, where

$\alpha = 1, \ldots, \dim H_5(Y_7, \mathbb{R})$, as these fix the Kähler class parameters of the internal space geometry. Such a solution is then dual to a 2d $(0,2)$ SCFT living on the conformal boundary of AdS_3, for example as written in the usual Poincaré slicing. The holographic central charge c_{sugra} of this theory is computed using equation (3.27).

Associated to any such F-theory solution is a different global form of AdS_3, which is a circle bundle over AdS_2, as in (3.52). Topologically the circle fibration is trivial, with the fiber coordinate ϕ having period $\Delta\phi$, which *a priori* is arbitrary. Since the size of the ϕ circle in the AdS_3 is bounded it becomes part of the internal space, and the remaining conformal boundary is 1-dimensional. This implies that the associated solutions have an interpretation as holographic duals to 1d SCQM.

T-dualizing along this circle and uplifting to M-theory, the circle becomes part of the internal space of the M-theory geometry and, together with the circle introduced in the uplift from Type IIA to M-theory, it makes up the elliptic fiber $\mathbb{E}_\tau$ with volume k_0. The M-theory AdS_2 geometries obtained in this way are determined by the complex geometry of the internal space $\mathcal{M}_8^\tau$. An analogous cone construction $C(Y_9^\tau)$ exists for the M-theory geometries [63], which provides a parametrization of the R-symmetry vector. Finding on-shell M-theory solutions amounts to imposing a topological constraint and a choice of flux numbers $N_I^M \in \mathbb{Z}$, where $I = 1, \ldots, \dim H_7(Y_9^\tau, \mathbb{R})$, which fix the Kähler class parameters of the internal complex geometry. The effective AdS_2 Newton constant is then computed as in (3.66).

The two supergravity duals each contain a set of parameters that are mapped to each other through the duality. On either side, the flux quantization conditions come with a dimensionless combination of length scales characteristic of each theory, namely ν_3 in F-theory and ν_4 in M-theory. Furthermore, on the F-theory side we have the circle length $\Delta\phi$ as an *a priori* free parameter, and on the M-theory side we have the fiber volume k_0. These parameters are given in terms of fundamental length scales as

$$\text{F-theory/IIB}: \quad \begin{cases} \nu_3 = \dfrac{2(2\pi l_s)^4}{L_{10}^4} \\ \dfrac{\Delta\phi}{2\pi} = \dfrac{\sqrt{2} l_s^4}{L_{10} l_p^3} \end{cases} \qquad \text{M-theory}: \quad \begin{cases} \nu_4 = \dfrac{(2\pi l_p)^6}{L_{11}^6} \\ k_0 = \dfrac{(2\pi)^2 l_p^6}{L_{11}^2 l_s^4} \end{cases} \tag{3.78}$$

With $L_{11} = L_{10}/\sqrt{2}$, we find the following relation

$$\Delta\phi = \frac{\sqrt{\nu_4}}{k_0}\,. \tag{3.79}$$

As T-duality inverts the radius of the circle, $\Delta\phi$ is indeed expected to be inversely related to the volume of the elliptic fiber. Given such an M-theory geometry, we can trace through the duality in the other direction by taking the F-theory limit, corresponding to shrinking the elliptic fiber to zero size, $k_0 \to 0$. This in turn takes $\Delta\phi \to \infty$, decompactifying the ϕ circle.

Any solution to the topological constraint together with some configuration of flux numbers makes for a perfectly consistent and physical M-theory solution. However, in this paper we are not interested in a generic M-theory solution; rather, we wish to find the ones *with F-theory duals*, and the map that takes us from one to the other.

For this purpose, it is instructive to compare Kähler classes on the two sides of the duality, focusing on the k_0 dependence on the M-theory side, since the F-theory limit takes k_0 to zero. In other words, we concentrate on the contributions coming from the volume of the elliptic fibration, which forms part of the physical data in M-theory, and ceases to have a physical interpretation in F-theory. Consider again the decomposition of the 8d Kähler form J_8 in (3.67)

$$J_8 = k_0\omega_0 + \sum_\alpha k_\alpha \omega_\alpha \,. \tag{3.80}$$

Recall that ω_α are pullbacks from the base $\mathcal{M}_6$ and together with ω_0 generate the second integral cohomology of $\mathcal{M}_8^\tau$. Once the M-theory topological constraint is imposed and the fluxes are properly quantized, the parameters k_α depend implicitly on the size of the elliptic fiber k_0. We will see this in examples in later sections. We denote the Kähler parameters of J_6 by k_α such that

$$J_6 = \sum_\alpha \mathsf{k}_\alpha \omega_\alpha \,. \tag{3.81}$$

The requirement for mapping a specific M-theory solution to its F-theory dual is that the Kähler class on $\mathcal{M}_8^\tau$ should match that of $\mathcal{M}_6$ in the F-theory limit, i.e.

$$J_6 = \lim_{k_0\to 0} J_8 = \lim_{k_0\to 0} \sum_\alpha k_\alpha \omega_\alpha \,. \tag{3.82}$$

In geometric terms we are collapsing the elliptic fiber, while keeping the volume of the total space bounded. The metric on $\mathcal{M}_8^\tau$, with Kähler form J_8, then under appropriate convergence conditions tends to a (singular) metric on $\mathcal{M}_6$, with Kähler form J_6. This implies that the 8d and 6d Kähler parameters are related by

$$k_\alpha = \mathsf{k}_\alpha + \mathcal{O}(k_0) \,. \tag{3.83}$$

This ansatz for the decomposition of the 8d Kähler form results in an M-theory topological constraint equation, which can be expanded order by order in k_0 to give

$$k_0 \int_{Y_7} \eta \wedge (c_1(\mathcal{M}_6) - c_1(\mathcal{L}))^2 \wedge J_6 + \mathcal{O}(k_0^2) = 0\,. \tag{3.84}$$

The lowest order term is exactly the constraint equation for the F-theory geometries that was independently derived in section 3.2.3. Since this equation must be satisfied order by order in k_0, the F-theory constraint equation is thus built into its dual M-theory solution by imposing that J_8 satisfy (3.82). Requiring the higher order terms to vanish constrains the form of (3.83).

For every M-theory flux integer $N_\alpha^M \in \mathbb{Z}$ there exists an F-theory flux integer $N_\alpha^F \in \mathbb{Z}$, where the M-theory seven-cycle is exactly the corresponding F-theory five-cycle with the elliptic fibration. The requirement (3.82) ensures that in dual solutions these flux configurations match on the nose, i.e. we have $N_\alpha^M = N_\alpha^F \equiv N_\alpha \in \mathbb{Z}$. In a sense, this condition expresses the fact that every D3-brane is simply converted to an M2-brane.

When determining an on-shell F-theory solution, imposing the N_α flux quantization conditions and the topological constraint determine the complex geometry of Y_7 by fixing the R-symmetry vector and the Kähler parameters of $\mathcal{M}_6$. In M-theory there is an additional distinguished flux integer $N_0^M \equiv N_0$, which has no F-theory analog, as it arises from the section σ of the elliptic fibration, i.e.

$$\nu_4 N_0 = \int_{Y_7} \eta \wedge \rho_8 \wedge \frac{J_8^2}{2}\,. \tag{3.85}$$

The distinguished flux integer does not map to any flux integer present in F-theory; rather, expanding in orders of k_0, we find that its leading contribution is determined by the type IIB ϕ circle length and the central charge as

$$N_0 = \left(\frac{\Delta\phi}{2\pi}\right)^2 \frac{c_{\text{sugra}}}{24} + \mathcal{O}(k_0)\,. \tag{3.86}$$

This additional flux quantization condition is matched by the extra Kähler parameter k_0 in the compact space of the M-theory geometry. In practice, as we shall see in examples, fixing this additional flux number then fixes the period $\Delta\phi$. Hence, imposing the M-theory topological constraint and flux quantization conditions determines the decomposition of J_8 and the internal space geometry Y_9^τ.

The map from holographic $\mathcal{I}$-extremization in M-theory to c-extremization in F-theory is completed by considering the relation between the two actions. *Before* imposing the topological constraint or flux quantization, the dual supersymmetric actions are related as

$$S_M = 2k_0 S_F + \mathcal{O}(k_0^2)\,. \tag{3.87}$$

The on-shell central charge of the 2d SCFT is then formally related to the AdS_2 Newton constant by

$$\frac{1}{G_2} = \frac{\Delta\phi}{3} c_{\text{sugra}} + \mathcal{O}(k_0)\,. \tag{3.88}$$

The reason this should only be read as a formal expression for the AdS_2 Newton constant is that the N_0 flux quantization condition has not been imposed, thus leaving in factors of k_0. Since a Kähler parameter of the internal space still appears explicitly in the equations, it cannot be understood as a physical quantity. From the above, we can thus conclude that *holographic $\mathcal{I}$-extremization in M-theory does not in general equal holographic c-extremization in F-theory.* In other words, extremizing $1/G_2$ does not necessarily correspond to finding an extremum for c_{sugra}.

This result generalizes the relation derived in [76], where the AdS_2 is considered as arising directly in type IIB by writing AdS_3 as the total space of a circle fibration. The effective Newton constants are then related by dimensional reduction on this circle

$$G_3 = \frac{\Delta\phi}{2} G_2\,. \tag{3.89}$$

Equation (3.88) takes into account corrections from the 7-branes and exactly reduces to the supergravity result in (3.89) when the elliptic fibration is trivial.

Interestingly, for many cases that we study later in this paper, the $\mathcal{O}(k_0)$ terms are in fact absent in (3.88), even for a non-trivial elliptic fibration, so that (3.89) holds exactly. This is true for all the toric examples in section 3.5. As a proof of concept, we therefore also consider a known set of solutions, the universal twist solutions with elliptic three-fold factor, in section 3.6, which do have non-zero subleading terms.

3.4.2 Field Theory

Finally, we comment on the physical interpretation of (3.88) in terms of the holographically dual field theories. First recall how the two field theory duals are constructed. On the F-theory side, the dual field theories are realized on D3-branes along $\mathbb{R}^{1,1} \times C$, where C are

curves in F-theory compactifications, above which the axio-dilaton profile is non-trivial. This induces a varying coupling τ of the 4d gauge theory on the D3-branes, and the 2d $(0,2)$ field theory along $\mathbb{R}^{1,1}$ acquires a dependence on the $U(1)_D$ duality line bundle $\mathcal{L}$ [44–47, 52]. T-duality along a circle in the D3-brane world-volume gives rise to a configuration of D2-branes, which uplift in M-theory to M2-branes wrapped on the curves C, i.e. the M2-branes realize a 1d SCQM.

While AdS_2 holography is still very much under development, it is natural to identify minus the logarithm of the partition function of the 1d theory with the renormalized supergravity action. As shown in [63] we may thus identify

$$\log Z_{\mathrm{1d}} = \frac{1}{4G_2}\,. \tag{3.90}$$

If we consider the 1d SCQM as arising directly from a circle reduction of the 2d (0,2) SCFT, or, equivalently, from duality with M-theory on a trivially fibered torus, then we can use (3.89) and the standard Brown-Henneaux relation [73] to deduce that

$$\log Z_{\mathrm{1d}} = \frac{1}{4G_2} = \frac{\Delta\phi}{8G_3} = \frac{\Delta\phi}{12}c_{\mathrm{sugra}}\,. \tag{3.91}$$

Of course this is precisely equation (3.88), without the $\mathcal{O}(k_0)$ correction terms. The partition function on the left hand side of (3.90) is defined by putting the 1d SCQM on a circle. On the other hand, we have also effectively reduced from 2d to 1d on the ϕ circle. Physically one might then anticipate some relation between the 1d partition function and the 2d partition function, where the 2d $(0,2)$ theory is put on a torus T^2. We note that this is indeed precisely the case: putting a 2d CFT on a torus leads to a Casimir energy contribution to the partition function

$$Z_{T^2}(\mathrm{Casimir}) = \exp\left(\frac{r_1}{r_2}\frac{c}{12}\right)\,, \tag{3.92}$$

where r_1, r_2 are the lengths of the circles in the T^2, and c is the central charge. We should then also recall that $\Delta\phi$ is dimensionless, but may be written as

$$\Delta\phi = \frac{2\pi R_{\mathrm{IIB}}}{L_{11}}\,, \tag{3.93}$$

where R_{IIB} is the dimensionful type IIB ϕ circle length and L_{11} is the overall dimensionful length scale in M-theory. The right hand side of (3.91) may then be identified with (the logarithm of) this Casimir contribution to the T^2 partition function. Recall here that in the

M-theory solution $\Delta\phi$ depends on the additional M-theory flux number N_0, while the central charge c_{sugra} depends only on the F-theory data, which does not include N_0. In the above identification, the extra parameter N_0 determines, via $\Delta\phi$, the geometry of the T^2 on which the 2d $(0,2)$ SCFT is placed. Notice then that the 2d $(0,2)$ theory itself does not depend on the integer N_0, while the 1d SCQM that it reduces to does depend on N_0. It would be interesting to understand this in more detail, and in particular whether the integer N_0 has a simple 1d interpretation. In addition, a study of the supersymmetric Casimir energy [77], its S^1-reduction, and the holographic duals, would be of interst and may shed light on subleading corrections.

3.5 Toric Fibrations over a Curve

In this section, we consider a class of toric geometries fibered over a complex curve or an elliptically fibered surface, where we can derive explicit formulas for the off-shell M/F-theory extremization problem. We show that, for these geometries, $\mathcal{I}$- and c-extremization are equivalent without any corrections in k_0, the volume of the elliptic fiber. Moreover, we apply the extremization principle to the cases referred to in the literature as the *universal* and *baryonic twists*.

3.5.1 Toric Fibration

We are interested in geometries where the compact part of the space consists of a toric five-manifold fibered over either, in the case of F-theory, a Riemann surface Σ with genus g or, in M-theory, an elliptic surface

$$\begin{array}{ccc} \mathbb{E}_\tau & \hookrightarrow & B_4^\tau \\ & & \downarrow \\ & & \Sigma \end{array} \,. \tag{3.94}$$

We start with a review of the properties of the toric fiber, which we denote by Y_5. We require that the cone $C(Y_5)$ is complex and Kähler, i.e. that Y_5 is Sasaki, and that $C(Y_5)$ admits a global holomorphic (3,0)-form. Such cones are called Gorenstein and the geometry of such toric Kähler cones has been extensively studied in e.g. [65, 78]. For our purposes, the essential feature of the fibered toric geometries is that all relevant quantities turn out to be expressible in terms of (derivatives of) a *master volume* of the fiber

$$\mathcal{V} \equiv \int_{Y_5} \eta \wedge \frac{\omega^2}{2} \,, \tag{3.95}$$

where ω is the Kähler form on the space transverse to η in Y_5. Moreover, for a fixed Gorenstein toric Kähler cone $C(Y_5)$, there is a simple explicit expression for $\mathcal{V}$ in terms of the toric data. The master volume is a function of the inward pointing primitive normals to the $d \geq 3$ facets of the polyhedral cone $v_a \in \mathbb{Z}^3$, with $a = 1, ..., d$, as well as the transverse Kähler parameters λ_a and trial R-symmetry vector $\vec{b} = (b_1, b_2, b_3)$. The master volume is given by

$$\mathcal{V}(\vec{b}, \{\lambda_a\}, \{\vec{v}_a\}) = \frac{(2\pi)^3}{2} \sum_{a=1}^{d} \lambda_a \frac{\lambda_{a-1}[\vec{v}_a, \vec{v}_{a+1}, \vec{b}] - \lambda_a[\vec{v}_{a-1}, \vec{v}_{a+1}, \vec{b}] + \lambda_{a+1}[\vec{v}_{a-1}, \vec{v}_a, \vec{b}]}{[\vec{v}_{a-1}, \vec{v}_a, \vec{b}][\vec{v}_a, \vec{v}_{a+1}, \vec{b}]} \,. \tag{3.96}$$

Here $[\cdot, \cdot, \cdot]$ denotes a 3×3 determinant, and we cyclically order $\vec{v}_0 = \vec{v}_d$, $\vec{v}_{d+1} = \vec{v}_1$, with similar identifications for the λ_a. Note that two of the Kähler class parameters are redundant, so that $\mathcal{V}$ is effectively only a function of $d - 2$ of the d Kähler class parameters λ_a.

3.5.2 F-theory c-extremization for Toric Fibrations

In this section, we consider the fibration of Y_5 over a Riemann surface Σ, and derive the F-theory c-extremization equations specialized to this class of geometries. The fibration of Y_5 over Σ can be parametrized as follows. The toric manifold is equipped with an isometric $U(1)^3$ action, generated by a set of holomorphic vector fields $\partial_{\varphi_i}, i = 1, 2, 3$. We choose three line bundles $\mathcal{O}(n_i)$ on the Riemann surface so that, topologically, the compactification space is defined to be the total space of the associated bundle

$$Y_7 = \mathcal{O}(\vec{n}) \times_{U(1)^3} Y_5 \,. \tag{3.97}$$

For simplicity we shall assume that the axio-dilaton varies only over the Riemann surface Σ. That is, taking the F-theory perspective, the variation of the axio-dilaton is captured by an auxiliary elliptic fibration as in (3.12), where the total space that we will consider is

$$\begin{array}{ccccc} & & & & Y_9^\tau \\ & & & \swarrow & \downarrow p^*(\pi) \\ \mathbb{E}_\tau & \hookrightarrow & B_4^\tau & & Y_7 \\ & & \sigma \circlearrowleft \downarrow \pi & \swarrow & p \\ & & \Sigma & & \end{array} \,. \tag{3.98}$$

Recall that the manifold Y_9^τ is obtained by pulling back the elliptic fibration π to Y_7 as in section 3.2.4. The existence of a global holomorphic $(5, 0)$-form on $C(Y_9^\tau)$ places certain restrictions on $\vec{n}$. We may construct such a global $(5, 0)$-form by first noting that $C(Y_5)$

admits a global $(3,0)$-form $\Omega_{(3,0)}$. The $(3,0)$-form has an explicit $\mathrm{e}^{i\varphi_1}$ dependence, since it has R-charge 2. On B_4^τ there is a local $(2,0)$-form $\Xi_{(2,0)}$, which is a local section of $K_{B_4^\tau}$. We have

$$K_{B_4^\tau} = K_\Sigma \otimes \mathcal{L} \tag{3.99}$$

where $\mathcal{L}$ is the duality line bundle, whose connection depends on the variation of the axio-dilaton as introduced in section 3.2 and

$$\deg(K_{B_4^\tau}) = 2g - 2 + \deg \mathcal{L}\,. \tag{3.100}$$

The holomorphic volume form on $C(Y_9^\tau)$ is constructed as

$$\Omega_{(5,0)} = \Omega_{(3,0)} \wedge \Xi_{(2,0)}\,, \tag{3.101}$$

where $\Omega_{(3,0)}$ is twisted over Σ as in (3.97). Since $\mathrm{e}^{i\varphi_1}$ is a section of $\mathcal{O}(n_1)$, we can ensure that $\Omega_{(5,0)}$ is a global non-vanishing form by taking

$$n_1 = 2 - 2g - \deg \mathcal{L}\,. \tag{3.102}$$

The twist is implemented at the level of the forms by introducing a connection A_i on each $\mathcal{O}(n_i)$ with curvature $F_i = dA_i$. The curvatures satisfy

$$\int_\Sigma \frac{F_i}{2\pi} = n_i \in \mathbb{Z}\,. \tag{3.103}$$

The fibration in (3.97) amounts to making the replacements

$$\begin{aligned}
\eta &\;\to\; \eta_{\text{twist}} \equiv \eta + 2\sum_{i=1}^{3} w_i A_i\,,\\
\omega &\;\to\; \omega_{\text{twist}} \equiv \omega + \sum_{i=1}^{3} \left(dx_i \wedge A_i + x_i F_i\right)\,,\\
J_6 &\;\to\; J_{6\text{twist}} = \omega_{\text{twist}} + A\text{vol}_\Sigma\,,
\end{aligned} \tag{3.104}$$

where w_i are the moment map coordinates restricted to Y_5 and x_i are global functions on Y_5 invariant under the $U(1)^3$ action (see [78] for further details). Note that the frequently appearing combination

$$[\rho_6 - 2\pi c_1(\mathcal{L})] \;\to\; [\rho_6 - 2\pi c_1(\mathcal{L})]_{\text{twist}} = [b_1 d\eta_{\text{twist}}] \tag{3.105}$$

also obtains an A_i dependence under the twist. With these replacements the supersymmetric action is

$$\begin{aligned} S_F &= \int_{Y_7} \eta_{\text{twist}} \wedge [\rho_6 - 2\pi c_1(\mathcal{L})]_{\text{twist}} \wedge \frac{J_{6\text{twist}}^2}{2!} \\ &= \int_{Y_7} \eta_{\text{twist}} \wedge b_1 d\eta_{\text{twist}} \wedge \frac{(\omega_{\text{twist}} + A\text{vol}_\Sigma)^2}{2!} \\ &= A\int_{Y_5} \eta \wedge \rho_6 \wedge \omega + 2\pi \sum_{i=1}^{3} n_i \int_{Y_5} \eta \wedge \omega \wedge (x_i \rho_6 + b_1 w_i \omega)\,, \end{aligned} \tag{3.106}$$

where we have abused notation and denoted the forms η and ρ_6 and their restrictions to Y_5 by the same symbol. To get the second equality we used the F-theory relation (3.105), which effectively reduces the expression to its constant axio-dilaton counterpart. The action is then identical to the case without the auxiliary elliptic fibration, apart from the fact that n_1, given in (3.102), depends on the degree of the duality line bundle. As mentioned above, the action can be rewritten in terms of derivatives of the master volume (3.96). Since we have shown that the F-theory action reduces to the constant axio-dilaton case, except for the dependence of n_1 on the duality line bundle, we can read off the result from [78]

$$S_F = -A \sum_{a=1}^{d} \frac{\partial \mathcal{V}}{\partial \lambda_a} - 2\pi b_1 \sum_{i=1}^{3} n_i \frac{\partial \mathcal{V}}{\partial b_i}\,. \tag{3.107}$$

Under the twist the constraint equation becomes

$$\begin{aligned} 0 &= \int_{Y_7} \eta_{\text{twist}} \wedge [\rho_6 - 2\pi c_1(\mathcal{L})]_{\text{twist}}^2 \wedge J_{6\text{twist}} \\ &= A\int_{Y_5} \eta \wedge \rho_6^2 + \int_{Y_7} \eta_{\text{twist}} \wedge (b_1 d\eta_{\text{twist}})^2 \wedge \omega_{\text{twist}} \\ &= A\int_{Y_5} \eta \wedge \rho_6^2 + 2\pi \sum_{i=1}^{3} n_i \int_{Y_5} \eta \wedge \rho_6 \wedge (x_i \rho_6 + 4 b_1 w_i \omega)\,. \end{aligned} \tag{3.108}$$

In terms of the master volume the equation is

$$A \sum_{a,b=1}^{d} \frac{\partial^2 \mathcal{V}}{\partial \lambda_a \partial \lambda_b} - 2\pi n_1 \sum_{a=1}^{d} \frac{\partial \mathcal{V}}{\partial \lambda_a} + 2\pi b_1 \sum_{a=1}^{d} \sum_{i=1}^{3} n_i \frac{\partial^2 \mathcal{V}}{\partial \lambda_a \partial b_i} = 0\,. \tag{3.109}$$

Finally, we turn our attention to the flux integers. There are two types of five-cycles in Y_7. The first type are torus invariant three-cycles $S_a \subset Y_5$ fibered over Σ, which schematically will be written as $(S_a \to \Sigma)$. The second is Y_5 itself. The latter does not receive any contributions from the Riemann surface, since the curvatures F_i and $c_1(\mathcal{L})$ integrate to zero on Y_5. We find

$$\nu_3 N = \int_{Y_5} \eta \wedge \rho_6 \wedge \omega = -\sum_{a=1}^{d} \frac{\partial \mathcal{V}}{\partial \lambda_a}\,. \tag{3.110}$$

For the other class of five-cycles, the flux quantization conditions are given by

$$\begin{aligned}\nu_3 M_a &= \int_{(S_a\to\Sigma)} \eta_{\text{twist}} \wedge [\rho_6 - 2\pi c_1(\mathcal{L})]_{\text{twist}} \wedge J_{6\text{twist}} \\ &= \int_{(S_a\to\Sigma)} \eta_{\text{twist}} \wedge b_1 d\eta_{\text{twist}} \wedge (\omega_{\text{twist}} + A\text{vol}_\Sigma) \\ &= A\int_{S_a} \eta\wedge\rho_6 + 2\pi\sum_{i=1}^{3} n_i \int_{S_a} \eta\wedge(2b_1 w_i\omega + x_i\rho_6) \\ &= \frac{A}{2\pi}\sum_{b=1}^{d}\frac{\partial^2\mathcal{V}}{\partial\lambda_a\partial\lambda_b} + b_1\sum_{i=1}^{3} n_i\frac{\partial^2\mathcal{V}}{\partial\lambda_a\partial b_i}\,.\end{aligned} \tag{3.111}$$

The extremization procedure now amounts to explicitly solving the topological constraint (3.109) and flux quantization conditions (3.110) and (3.111) for the Kähler parameters A, λ_a and R-symmetry vector b_i and subsequently extremizing the action (3.107) with respect to the remaining free parameters.

3.5.3 M-theory $\mathcal{I}$-extremization for Toric Fibrations

In this section, we establish the $\mathcal{I}$-extremization procedure dual to the c-extremization for fibered toric geometries set up in the previous section. In the context of M-theory, we are considering the physical compactification space

$$\begin{array}{ccc} & & Y_9^\tau \\ & \swarrow & \\ \mathbb{E}_\tau \hookrightarrow & B_4^\tau & \\ & \sigma\big(\uparrow\big\downarrow\pi & \\ & \Sigma & \end{array}\,. \tag{3.112}$$

Here we view Y_9^τ as the space Y_5 fibered over the elliptic surface B_4^τ. This is achieved in the same way as in (3.97), but the vector bundle $\mathcal{O}(\vec{n})$ is now pulled back from Σ to B_4^τ. The cone $C(Y_9^\tau)$ also admits a non-vanishing holomorphic volume form precisely if

$$n_1 = 2 - 2g - \deg\mathcal{L}\,. \tag{3.113}$$

This geometric setup fits into the framework of [79]. In what follows we will make use of the formulas for toric fibrations over a general complex surface derived in that paper and specialize them to the elliptic surface case. We make the following ansatz for the Kähler form on B_4^τ

$$J_{B_4^\tau} = k_0\omega_0 + \left(A + \frac{k_0\deg\mathcal{L}}{2}\right)\text{vol}_\Sigma\,. \tag{3.114}$$

In other words, we are assuming that the Kähler class on the elliptic surface is just a linear combination of the base and the fiber class. One can also derive similar formulas for a more general ansatz where Cartan divisors are added. The choice of the shift of A by $k_0 \deg \mathcal{L}/2$ is convenient in order to compare to the F-theory parameters at the end of this section. Using the ansatz the volume of the elliptic surface is

$$\mathrm{vol}(B_4^\tau) = \int_{B_4^\tau} \frac{J_{B_4^\tau}^2}{2} = -\frac{k_0^2 \deg \mathcal{L}}{2} + \left(A k_0 + \frac{k_0^2 \deg \mathcal{L}}{2} \right) = A k_0 \,, \tag{3.115}$$

where we used

$$\int_{B_4^\tau} \omega_0^2 = -\deg \mathcal{L} \,, \qquad \int_{B_4^\tau} \omega_0 \wedge \mathrm{vol}_\Sigma = 1 \,. \tag{3.116}$$

Furthermore, the curvature integrals specialize to

$$\int_\Sigma F_i = 2\pi n_i \,, \qquad \int_{\mathbb{E}_\tau} F_i = 0 \,, \tag{3.117}$$

and $F_i \wedge F_j = 0$ for dimensional reasons. With these results the M-theory constraint equation reduces to

$$A \sum_{a,b=1}^{d} \frac{\partial^2 \mathcal{V}}{\partial \lambda_a \partial \lambda_b} - 2\pi n_1 \sum_{a=1}^{d} \frac{\partial \mathcal{V}}{\partial \lambda_a} + 2\pi b_1 \sum_{a=1}^{d} \sum_{i=1}^{3} n_i \frac{\partial^2 \mathcal{V}}{\partial \lambda_a \partial b_i} = 0 \,, \tag{3.118}$$

which is exactly the same as the F-theory constraint given in (3.109). The M-theory supersymmetric action becomes

$$S_M = -A k_0 \sum_{a=1}^{d} \frac{\partial \mathcal{V}}{\partial \lambda_a} - 2\pi k_0 b_1 \sum_{i=1}^{3} n_i \frac{\partial \mathcal{V}}{\partial b_i} \,. \tag{3.119}$$

Let us now focus on the flux quantization conditions. The seven-cycles fall into two classes, where the cycles in the first class are obtained by fibering Y_5 over a two-cycle in the base, and the second class contains three-cycles in Y_5 (associated with toric divisors on the cone) fibered over the entire base. The flux integer corresponding to fixing a point in Σ and quantizing over the cycle $Y_5 \times \mathbb{E}_\tau$ is

$$\nu_4 N = -k_0 \sum_{a=1}^{d} \frac{\partial \mathcal{V}}{\partial \lambda_a} \,. \tag{3.120}$$

The quantization conditions associated to fibrations of toric three-cycles over B_4^τ are

$$\nu_4 M_a = \frac{A k_0}{2\pi} \sum_{b=1}^{d} \frac{\partial^2 \mathcal{V}}{\partial \lambda_a \partial \lambda_b} + k_0 b_1 \sum_{i=1}^{3} n_i \frac{\partial^2 \mathcal{V}}{\partial \lambda_a \partial b_i} \,. \tag{3.121}$$

There is one final cycle we need to consider, arising from the section of the elliptic fibration. Geometrically this is the space Y_5 fibered over Σ and the corresponding flux number is given by

$$\nu_4 N_0 = -\left(A - \frac{k_0 \deg \mathcal{L}}{2}\right) \sum_{a=1}^{d} \frac{\partial \mathcal{V}}{\partial \lambda_a} - 2\pi b_1 \sum_{i=1}^{3} n_i \frac{\partial \mathcal{V}}{\partial b_i} \,. \tag{3.122}$$

Notice that, combining the expressions for the flux numbers, the supersymmetric action can be rewritten as

$$S_M = k_0 \nu_4 \left(N_0 + \frac{1}{2} N \deg \mathcal{L}\right) \,. \tag{3.123}$$

This toric setup provides an instructive example of the M/F-theory relations we have described in section 3.4. In the ansatz for the Kähler class (3.114) we have explicitly included the k_0 corrections to the Kähler class on the base of the elliptic fibration. Indeed, the parameter A is precisely the F-theory Kähler parameter on Σ and the relation

$$\lim_{k_0 \to 0} J_{B_4^\tau} = \lim_{k_0 \to 0} \left(k_0 \omega_0 + J_\Sigma + \frac{k_0 \deg \mathcal{L}}{2} \mathrm{vol}_\Sigma\right) = J_\Sigma \tag{3.124}$$

holds. The way to derive the explicit form of the correction term is to start with a general ansatz for the Kähler form on B_4^τ and impose that the $\mathcal{O}(k_0^2)$ terms in the M-theory constraint equation cancel. In this way the constraint equation reduces just to the linear term, which is precisely the F-theory constraint equation. Moreover, the flux integers M_a and N also match on both sides if we take into account the relation $\nu_3 = \nu_4/2k_0$, as well as the fact that the master volume functions differ by a factor of 2.

An interesting feature of these geometries is that, despite including the full backreaction of the 7-branes in the M-theory background, there are no k_0 corrections in the supersymmetric action, i.e. we find

$$S_M = 2k_0 S_F \,. \tag{3.125}$$

This implies that the resulting on-shell solutions will have

$$\frac{1}{4G_2} = \frac{\Delta\phi}{12} c_{\mathrm{sugra}} \tag{3.126}$$

on the nose, even though we are considering a non-trivial elliptic fibration. This is precisely the relation (3.91). We also see that this relation actually holds off-shell. The upshot of this discussion is that $\mathcal{I}$- and c-extremization are indeed equivalent for toric fibrations over a Riemann surface.

3.5.4 Universal Twist: Elliptic Surface

In this section, we focus on a known class of F-theory supergravity solutions found in [33], the so-called universal twist solution for elliptic surfaces. We apply the holographic $\mathcal{I}/c$-extremization developed in sections 3.2 and 3.3, which allows us to simultaneously re-derive the central charge of the 2d field theory dual to these F-theory solutions and determine $1/G_2$ of their M-theory duals, without ever explicitly solving the master equation.

The universal twist solutions are based on the ansatz

$$\begin{array}{ccc} S^1 & \hookrightarrow & Y_7 \\ & & \downarrow \\ & & \Sigma \times \mathcal{M}_4 \end{array} \tag{3.127}$$

which assumes that the transverse Kähler space $\mathcal{M}_6$ is a product of a complex curve and a Kähler surface. We are interested in the set of universal twist solutions where the elliptic fibration is non-trivial only over the complex curve, so that $\mathcal{M}_8^\tau$ contains an elliptic surface

$$\mathcal{M}_8^\tau = (\mathbb{E}_\tau \to \Sigma) \times \mathcal{M}_4 \,. \tag{3.128}$$

This corresponds to choosing the twist parameters n_i parallel to the R-symmetry vector, i.e. we take

$$n_i = \frac{n_1}{b_1} b_i \,, \tag{3.129}$$

which immediately implies

$$\sum_{a,b=1}^{d} \frac{\partial^2 \mathcal{V}}{\partial\lambda_a \partial\lambda_b} = 8 b_1^2 \mathrm{Vol}(Y_5) \,, \qquad b_1 \sum_{i=1}^{3} n_i \frac{\partial \mathcal{V}}{\partial b_i} = -n_1 \mathcal{V} \,. \tag{3.130}$$

The topological constraint, which must be imposed for either side of the duality, is

$$8A\, b_1^2\, \mathrm{Vol}(Y_5) - 4\pi n_1 \sum_{a=1}^{d} \frac{\partial \mathcal{V}}{\partial \lambda_a} = 0 \,. \tag{3.131}$$

The M/F-theory flux integers are given by

$$\begin{aligned} \nu_3 N &= -\sum_{a=1}^{d} \frac{\partial \mathcal{V}}{\partial \lambda_a} \,, \\ \nu_3 M_a &= \frac{A}{2\pi} \sum_{b=1}^{d} \frac{\partial^2 \mathcal{V}}{\partial\lambda_a \partial\lambda_b} - n_1 \frac{\partial \mathcal{V}}{\partial \lambda_a} \,. \end{aligned} \tag{3.132}$$

Here we have chosen to write the quantization conditions manifestly as F-theory equations. The distinguished M-theory flux integer is N_0, which satisfies

$$\nu_4 N_0 = -\left(A - \frac{k_0 \deg \mathcal{L}}{2}\right) \sum_{a=1}^{d} \frac{\partial \mathcal{V}}{\partial \lambda_a} + 2\pi n_1 \mathcal{V} \,. \tag{3.133}$$

The M/F-theory supersymmetric actions are

$$\begin{aligned} S_F &= A\,\nu_3 N + 2\pi n_1 \mathcal{V}\,, \\ S_M &= A\,\nu_4 N + 2\pi k_0 n_1 \mathcal{V}\,, \end{aligned} \tag{3.134}$$

so that again equation (3.125) holds, on the nose.

With these relations in place, we proceed to impose all common M/F-theory conditions (i.e. all but the N_0 flux quantization) and derive expressions for the supersymmetric actions that take these conditions into account. We start by rewriting the topological constraint in terms of the flux integer N as

$$2A\,b_1^2\,\mathrm{Vol}(Y_5) + \pi n_1 \nu_3 N = 0\,. \tag{3.135}$$

Solving this constraint for A and substituting into the supersymmetric actions yields

$$\begin{aligned} S_F &= -\frac{\pi n_1 \nu_3^2 N^2}{2b_1^2 \mathrm{Vol}(Y_5)} + 2\pi n_1 \mathcal{V}\,, \\ S_M &= -\frac{\pi n_1 \nu_4^2 N^2}{2b_1^2 k_0 \mathrm{Vol}(Y_5)} + 2\pi k_0 n_1 \mathcal{V}\,. \end{aligned} \tag{3.136}$$

We can impose quantization of the M_a by choosing $\lambda_a \equiv \lambda$. This ensures that the M_a are quantized as

$$M_a = -N\,. \tag{3.137}$$

This solution implies that the master volume is

$$\mathcal{V} = 4b_1^2 \lambda^2 \mathrm{Vol}(Y_5)\,, \tag{3.138}$$

and the flux quantization condition for N fixes λ to be

$$\lambda = -\frac{\nu_3 N}{8b_1^2 \mathrm{Vol}(Y_5)}\,. \tag{3.139}$$

The supersymmetric actions can then be written as

$$\begin{aligned} S_F &= -\frac{3\pi n_1 \nu_3^2 N^2}{8b_1^2 \mathrm{Vol}(Y_5)}\,, \\ S_M &= -\frac{3\pi n_1 \nu_4^2 N^2}{8k_0 b_1^2 \mathrm{Vol}(Y_5)}\,. \end{aligned} \tag{3.140}$$

Since $\mathrm{Vol}(Y_5)$ is extremized for a Reeb vector with $r_1 = 3$, we set the M/F-theory R-symmetry vector $\vec{b}_F = \frac{2}{3}\vec{r} = 2\vec{b}_M$. Let $\vec{r}_*$ denote the extremal Reeb vector, corresponding to a Sasaki-Einstein metric on Y_5. We thus find the actions

$$\begin{aligned} S_F(\vec{r}_*) &= -\frac{\pi n_1 \nu_3^2 N^2}{36 \mathrm{Vol}(Y_5)(\vec{r}_*)}\,, \\ S_M(\vec{r}_*) &= -\frac{\pi n_1 \nu_4^2 N^2}{72 k_0 \mathrm{Vol}(Y_5)(\vec{r}_*)}\,. \end{aligned} \tag{3.141}$$

The 2d central charge is then given by (3.27) as

$$c_{\text{sugra}} = \frac{12(2\pi)^2}{\nu_3^2} S_F(\vec{r}_*) = -\frac{(2\pi)^3 n_1 N^2}{6\text{Vol}(Y_5)(\vec{r}_*)}\,. \tag{3.142}$$

The AdS_2 Newton constant is given by (3.66) as

$$\frac{1}{G_2} = \frac{8(2\pi)^2}{\nu_4^{3/2}} S_M(\vec{r}_*) = -\frac{4\pi^3 n_1 \Delta\phi N^2}{9\text{Vol}(Y_5)(\vec{r}_*)} = \Delta\phi \frac{c_{\text{sugra}}}{3}\,, \tag{3.143}$$

as expected. However, this expression for the Newton constant cannot yet be understood to reflect a physical quantity due to the presence of $\Delta\phi$, which is a parameter of the internal space. In order for this to constitute a genuine M-theory solution, we still need to impose the N_0 flux quantization condition

$$N_0 = -\frac{\pi n_1 \nu_4 N^2}{72 k_0^2 \text{Vol}(Y_5)(\vec{r}_*)} - \frac{1}{2} N \deg \mathcal{L}\,. \tag{3.144}$$

This condition fixes the period $\Delta\phi$ in terms of the distinguished flux number. We find

$$\Delta\phi = \pm\frac{6}{N}\sqrt{\frac{\text{Vol}(Y_5)(\vec{r}_*)\,(2N_0 + N\deg\mathcal{L})}{-\pi n_1}}\,. \tag{3.145}$$

The Newton constant of this genuine M-theory solution is then

$$\frac{1}{G_2} = \frac{8\pi^2 N}{3}\sqrt{\frac{-\pi n_1\,(2N_0 + N\deg\mathcal{L})}{\text{Vol}(Y_5)(\vec{r}_*)}}\,. \tag{3.146}$$

3.5.5 Baryonic Twist: $Y^{p,q}$

We now consider the so-called baryonic twist solutions [33, 78]. For simplicity we present the computations for $Y_5 = Y^{p,q}$. The $Y^{p,q}$ metrics first appeared in [80] and their toric data was derived in [81]. The $d = 4$ ordered inward pointing normal vectors are

$$v_1 = (1,0,0), \quad v_2 = (1,1,0), \quad v_3 = (1,p,p), \quad v_4 = (1,p-q-1,p-q)\,. \tag{3.147}$$

The $Y^{p,q}$ metrics have $p > q > 0$ and the polyhedral cone with vectors v_a, $a = 1,\ldots,4$ is convex. We take the free twist parameters to be $n_2 = n_3 \equiv n$ for simplicity. We first discuss the F-theory side. We define rescaled fluxes m_a and twist parameter s as

$$M_a \equiv -n_1 m_a N, \qquad n \equiv -n_1 s\,, \tag{3.148}$$

and immediately rename $m_1 \equiv m$ for notational convenience. The remaining fluxes are

$$m_2 = m_4 = \frac{(1-m)p + s}{p+q}, \qquad m_3 = \frac{(m-1)(p-q) - 2s}{p+q}\,. \tag{3.149}$$

We can then determine the trial central charge, which we do not quote here as the expression is extremely long. Extremizing with respect to b_2, b_3 gives the R-symmetry vector $\vec{b} = (2, b_2, b_2)$ with

$$b_2 = -2p\frac{p^3\left[2(m-1)^2q+(2m-3)s\right]-2p^2\left[(m-1)^2q^2+(2m-1)qs+2s^2\right]+pqs[(2m-3)q-2s]-2q^2s^2}{p^4(2m-1)+2p^3[(2m-1)q+s]+p^2\left[(4m^2-6m+3)q^2+4mqs+4s^2\right]+2pqs[(3-2m)q+2s]+4q^2s^2}\,, \tag{3.150}$$

and on-shell central charge

$$c_{\text{sugra}} = \frac{12N^2n_1p[(m-1)p-s]\left[p^3\left(2m^2-3m+1\right)+p^2\left(\left(-2m^2+3m-1\right)q-4ms+s\right)+pqs(2m-3)-2qs^2\right]}{p^4(2m-1)+2p^3[(2m-1)q+s]+p^2\left[(4m^2-6m+3)q^2+4mqs+4s^2\right]+2pqs[(3-2m)q+2s]+4q^2s^2}\,. \tag{3.151}$$

Note that, for a trivial line bundle with $\deg\mathcal{L} = 0$, we find that b_2 and c_{sugra} reduce to (6.6) and (6.7) in [78].

On the M-theory side we again start by explicitly writing down the master volume $\mathcal{V}$ as a function of λ_a and b_i using (3.147). Having imposed the topological constraint and flux quantization for N and M_1, we reproduce the relations between the fluxes given in (3.149). The trial Newton constant can then be written down; however, the expression is not quoted here as it is very long. Extremizing with respect to b_2, b_3 gives the R-symmetry vector $\vec{b} = (1, b_2, b_2)$ with

$$b_2 = -p\frac{p^3\left[2(m-1)^2q+(2m-3)s\right]-2p^2\left[(m-1)^2q^2+(2m-1)qs+2s^2\right]+pqs[(2m-3)q-2s]-2q^2s^2}{p^4(2m-1)+2p^3[(2m-1)q+s]+p^2\left[(4m^2-6m+3)q^2+4mqs+4s^2\right]+2pqs[(3-2m)q+2s]+4q^2s^2}\,, \tag{3.152}$$

which is exactly half the corresponding R-symmetry component in F-theory, i.e. we have indeed found $\vec{b}_F = 2\vec{b}_M$. The preliminary Newton constant is

$$\frac{1}{G_2} = \frac{4\Delta\phi N^2n_1p(-mp+p+s)\left[p^3\left(2m^2-3m+1\right)+p^2\left(\left(-2m^2+3m-1\right)q-4ms+s\right)+pqs(2m-3)-2qs^2\right]}{p^4(2m-1)+2p^3((2m-1)q+s)+p^2\left((4m^2-6m+3)q^2+4mqs+4s^2\right)+2pqs((3-2m)q+2s)+4q^2s^2} = \Delta\phi\frac{c_{\text{sugra}}}{3}\,. \tag{3.153}$$

In order for this to correspond to a genuine M-theory solution, we must still impose quantization of N_0. Solving the flux quantization condition for N_0 for k_0, the Newton constant in terms of M-theory fluxes is

$$\frac{1}{G_2} = 8\pi N\sqrt{\frac{-pn_1[2N_0+\deg\mathcal{L}N][(m-1)p-s]\left[p^3\left(2m^2-3m+1\right)+p^2\left(\left(-2m^2+3m-1\right)q-4ms+s\right)+pqs(2m-3)-2qs^2\right]}{p^4(2m-1)+2p^3((2m-1)q+s)+p^2\left((4m^2-6m+3)q^2+4mqs+4s^2\right)+2pqs((3-2m)q+2s)+4q^2s^2}}\,. \tag{3.154}$$

This concludes the discussion of solutions where $\mathcal{I}$- and c-extremization agree exactly across M/F-theory duality.

3.6 Universal Twist Solutions: Elliptic Three-fold

We would like to demonstrate that generically $1/G_2$ and c_{sugra} do not match exactly, as in the examples in section 3.5, but rather $1/G_2$ includes higher order corrections in k_0 as argued for in (3.88). These are absent in the F-theory solution, where the volume of the elliptic fiber is strictly zero. To this end, we consider the (on-shell) universal twist elliptic three-fold solutions, which were determined in [33]. We will first give a brief summary of the known F-theory solutions and then provide the corresponding M-theory analysis, and a comparison of the two.

3.6.1 F-theory

The universal twist solutions are based on the product ansatz

$$\begin{array}{ccc} S^1 & \hookrightarrow & Y_7 \\ & & \downarrow \\ & & \Sigma \times \mathcal{M}_4 \end{array} , \tag{3.155}$$

where the transverse $\mathcal{M}_6$ factorizes as a product of a complex curve and a Kähler surface. To $\mathcal{M}_6$ we associate an auxiliary elliptic fibration $\mathcal{M}_8^\tau$, and assume that the fibration is non-trivial only over the $\mathcal{M}_4$ factor, so that the total space is given by

$$\mathcal{M}_8^\tau = \Sigma \times (\mathbb{E}_\tau \to \mathcal{M}_4) \ . \tag{3.156}$$

The metrics on Σ and $\mathcal{M}_4$ satisfy

$$\begin{aligned} \rho_4 + dQ &= 6J_{\mathcal{M}_4} \, , \\ \rho_\Sigma &= -3J_\Sigma \, . \end{aligned} \tag{3.157}$$

Note that we assume that the Killing vector is regular throughout the following, and the period of the circle coordinate z is $2\pi\ell$. The volume of Σ is given by

$$\text{Vol}(\Sigma) = \frac{2\pi}{3}(2g-2) \, , \tag{3.158}$$

which follows from the Gauss-Bonnet theorem. Moreover,

$$[J_{\mathcal{M}_4}] = \frac{\pi}{3}\left(c_1(\mathcal{M}_4) - c_1(\mathcal{L})\right) \ . \tag{3.159}$$

This equation implies that the volume of the circle-fibration over $\mathcal{M}_4$, denoted by $\mathcal{M}_5$, is

$$\text{Vol}(\mathcal{M}_5) = \frac{\pi^3 \ell}{27} \int_{\mathcal{M}_4} \left(c_1(\mathcal{M}_4) - c_1(\mathcal{L})\right)^2 \ . \tag{3.160}$$

There are two classes of flux quantization conditions. The first corresponds to the cycle at fixed coordinates in Σ, which is a copy of $\mathcal{M}_5$. The flux integer is

$$\nu_3 N^F = 18\text{Vol}(\mathcal{M}_5)\,. \tag{3.161}$$

The second class of flux quantization conditions is obtained as a $U(1)$ fibration over the product of Σ with two-cycles C_α in $\mathcal{M}_4$. They are given by

$$\nu_3 M^F_\alpha = 3\pi\ell\text{Vol}(\Sigma)C_\alpha \cdot [J_{\mathcal{M}_4}]\,. \tag{3.162}$$

Finally, the central charge of the 2d $(0,2)$ theory was computed in [33] to be

$$c_{\text{sugra}} = \frac{2\pi^2\text{Vol}(\Sigma)(N^F)^2}{\text{Vol}(\mathcal{M}_5)}\,. \tag{3.163}$$

3.6.2 M-theory

We start with the F-theory metric on $\mathcal{M}_6$ and construct the M-theory solution from it. We will specialize to the case where $\mathcal{M}_4 = \mathbb{CP}^2$. Consider the Kähler class ansatz

$$J_8 = k_0\omega_0 + xJ_\Sigma + yJ_{\mathcal{M}_4}. \tag{3.164}$$

The cruical point is that the form of the metrics on Σ and $\mathcal{M}_4$ are exactly the same as in the previous subsection, and we think of the F-theory solution as a 0-th order solution in a suitable expansion in the volume of the elliptic fiber. We have introduced x and y that parametrize the Kähler cone of $\mathcal{M}_6 = \Sigma \times \mathcal{M}_4$. Given this parametrization we now compute the Kähler class of the M-theory solution.

Note that the Kähler class on $\mathcal{M}_4$ is

$$[J_{\mathcal{M}_4}] = \frac{\pi}{3}(3 - \deg\mathcal{L})[H]\,, \tag{3.165}$$

where $[H]$ is the hyperplane class of $\mathbb{CP}^2$. The line bundle associated to the elliptic fibration lives over $\mathcal{M}_4$ and in particular $c_1(\mathcal{L})^2 \neq 0$. From the M-theory constraint we derive the following equation

$$x = y - \frac{3k_0\deg\mathcal{L}}{2\pi(3-\deg\mathcal{L})}\,, \tag{3.166}$$

where

$$\deg\mathcal{L} = c_1(\mathcal{L})\cdot[H]\,. \tag{3.167}$$

This allows us to eliminate the parameter x from the above ansatz. With this we can then compute the M-theory supersymmetric action

$$S_M = \frac{4\pi^2\ell(g-1)}{3}k_0\left[\pi^2y^2(3-\deg\mathcal{L})^2 - 3\pi y(3-\deg\mathcal{L})\deg\mathcal{L}k_0 + 2\deg\mathcal{L}^2k_0^2\right]. \quad (3.168)$$

The remaining parameters, y and k_0 are fixed by flux quantization in M-theory

$$\begin{aligned}
\nu_4 N_0 &= \frac{4\pi^2\ell(g-1)}{3}\left[\pi^2y^2(3-\deg\mathcal{L})^2 - 4\pi y(3-\deg\mathcal{L})\deg\mathcal{L}k_0 + 3\deg\mathcal{L}^2k_0^2\right], \\
\nu_4 N^M &= \frac{4\pi^3\ell}{3}yk_0(3-\deg\mathcal{L})^2 + 2\pi^2\ell(3-\deg\mathcal{L})\deg\mathcal{L}k_0^2, \\
\nu_4 M^M &= \frac{4\pi^2\ell(g-1)}{3}\left[2\pi(3-\deg\mathcal{L})yk_0 + 3\left(1-\frac{6}{(3-\deg\mathcal{L})\pi}\right)\deg\mathcal{L}k_0^2\right].
\end{aligned} \quad (3.169)$$

Imposing the flux quantization condition for N^M gives

$$y = \frac{3\nu_4N^M}{4\pi^3\ell(3-\deg\mathcal{L})^2k_0} - \frac{3\deg\mathcal{L}}{2\pi(3-\deg\mathcal{L})}k_0. \quad (3.170)$$

Let us briefly digress and examine this expression in more detail. Note that we can substitute N^F into the above to obtain

$$y = \frac{N^M}{N^F} - \frac{3\deg\mathcal{L}}{2\pi(3-\deg\mathcal{L})}k_0. \quad (3.171)$$

From this expression it is apparent that

$$\lim_{k_0\to 0} J_8 = J_\Sigma + J_{\mathcal{M}_4} \quad (3.172)$$

holds if $N^M = N^F \equiv N$ are identified, as expected. Substituting (3.170) into the supersymmetric action results in

$$S_M = \frac{3(g-1)\nu_4^2N^2}{4\pi^2\ell(3-\deg\mathcal{L})^2k_0} - \frac{6\nu_4N(g-1)\deg\mathcal{L}}{3-\deg\mathcal{L}}k_0 + \frac{35\pi^2\ell(g-1)}{3}(\deg\mathcal{L})^2k_0^3. \quad (3.173)$$

Using (3.66), we determine the leading contribution to the preliminary Newton constant to be

$$\frac{1}{G_2} = \frac{24(g-1)\sqrt{\nu_4}N^2}{\ell(3-\deg\mathcal{L})^2k_0} + \mathcal{O}(k_0). \quad (3.174)$$

Comparing this with the expression for c_{sugra} derived in the previous subsection, we indeed find

$$\frac{1}{G_2} = \frac{\Delta\phi}{3}c_{\text{sugra}} + \mathcal{O}(k_0). \quad (3.175)$$

The distinguished flux number N_0 is given by

$$N_0 = \frac{3(g-1)\nu_4}{\pi^2\ell(3-\deg\mathcal{L})^2k_0^2}N^2 - \frac{7(g-1)\deg\mathcal{L}}{3-\deg\mathcal{L}}N + 15\pi^2\ell(g-1)(\deg\mathcal{L})^2\frac{k_0^2}{\nu_4}. \quad (3.176)$$

Substituting in the duality relations we find

$$N_0 = \left(\frac{\Delta\phi}{2\pi}\right)^2 \frac{c_{\rm sugra}}{24} - \frac{7(g-1)\deg\mathcal{L}}{3-\deg\mathcal{L}}N + \frac{15\ell(g-1)(\deg\mathcal{L})^2}{4}\left(\frac{2\pi}{\Delta\phi}\right)^2 . \tag{3.177}$$

In particular, this is an expansion in $\Delta\phi$ where the quadratic term is proportional to $c_{\rm sugra}$, again as expected. Finally, we record that

$$\begin{aligned}\frac{1}{G_2} = \frac{16\pi^2}{81\deg\mathcal{L}}\left[16\pi(3-\deg\mathcal{L})N_0 + 3{\rm Vol}(\Sigma)N\deg\mathcal{L} + \mathbf{V}\right] \\ \times\sqrt{\frac{2(3-\deg\mathcal{L})N_0 - 21{\rm Vol}(\Sigma)N\deg\mathcal{L} + 2\mathbf{V}}{15(3-\deg\mathcal{L}){\rm Vol}(\mathcal{M}_5){\rm Vol}(\Sigma)}}\,,\end{aligned} \tag{3.178}$$

where

$$\mathbf{V} = \sqrt{4\pi^2(3-\deg\mathcal{L})^2N_0^2 + 42\pi{\rm Vol}(\Sigma)N_0N(3-\deg\mathcal{L})\deg\mathcal{L} + 9\left[N{\rm Vol}(\Sigma)\deg\mathcal{L}\right]^2}\,. \tag{3.179}$$

As a check on this expression we may formally expand it around the trivial torus fibration with $\deg\mathcal{L} = 0$

$$\frac{1}{G_2} = 8\pi^2N\sqrt{\frac{N_0{\rm Vol}(\Sigma)}{3{\rm Vol}(\mathcal{M}_5)}} - 5\pi N^2\sqrt{\frac{{\rm Vol}(\Sigma)^3}{3N_0{\rm Vol}(\mathcal{M}_5)}}\deg\mathcal{L} + \mathcal{O}(\deg\mathcal{L}^2)\,. \tag{3.180}$$

The first term should then match (3.146), and using the expression (3.158) for ${\rm Vol}(\Sigma)$ one can see that this is indeed the case.

3.7 Conclusions and Outlook

There has been much progress recently in tests of holography for 2d and 1d SCFTs. With decreasing number of supercharges on either side of the correspondence, the duality becomes more interesting and harder to study. The class of theories we discussed in this paper have the minimal amount of supersymmetry, whilst keeping a non-trivial R-symmetry. The $U(1)$ R-symmetry in 2d and 1d can mix with global $U(1)$ symmetries, and only after applying c- or $\mathcal{I}$-extremization is the true superconformal R-symmetry determined. The main paradigm in this paper was to study this problem holographically in the context of type IIB solutions, where the axio-dilaton has a non-trivial spacetime-dependent profile – i.e. F-theory. We showed that the c-extremization of 2d SCFTs obtained from wrapped D3-branes in F-theory compactifications define a geometric extremization problem in the holographically dual AdS_3 solutions. This allowed us to compute, using an off-shell approach, the central charge of the SCFTs from holography.

As a counterpoint to the 2d SCFTs, we discussed 1d SCQMs obtained by M2-branes wrapped on complex curves, and the dual holographic $\mathcal{I}$-extremization principle in M-theory. By M/F-duality, whereby an elliptic fiber in the M-theory geometry becomes the auxiliary elliptic fibration of F-theory, these two setups can be related. The F-theory result for the central charge is obtained by considering the limit in M-theory where the volume of the elliptic fiber is taken to zero ($k_0 \to 0$). As we showed, there are classes of SCFTs where the resulting identification (3.1) is true without any higher order corrections in k_0 – these were discussed in section 3.5. In contrast, the class of solutions in section 3.6 showed that in general there can indeed be corrections to the F-theory expression of the central charge, in order for this to match the 1d partition function. Whenever both sides agree, the solution has an elliptic fibration that is non-trivial only over a complex curve. We observed that for elliptic fibrations over higher-dimensional base manifolds, there are generically correction terms, which arise from non-trivial higher intersection numbers on the base, e.g. from $c_1(\mathcal{L})^2$. This was exemplified in the elliptic three-folds of section 3.6.

Our analysis was largely focused on the geometric side of holography. Much is known about the wrapped D3-brane theories in F-theory, in terms of central charge computations. However much less understood is the precise relation between the dimensional reduction of such 2d SCFTs with the 1d SCQM that arises from the dual M2-brane configuration, and the associated 1d partition function. Related computations are known for higher (and non-chiral) supersymmetric theories, but for $(0,2)$ this remains an exciting open problem.

Chapter 4

Holography, 1-form Symmetries, and Confinement

4.1 Introduction

Generalized global symmetries and their 't Hooft anomalies can highly constrain the dynamics of gauge theories. A prime example is the role of 1-form symmetries in confinement of $\mathcal{N}=1$ $SU(N)$ SYM or adjoint QCD theories. In this case the 1-form symmetry is $\Gamma^{(1)}=\mathbb{Z}_N$ and corresponds to the center of the gauge group, which acts on line operators [9,10] and provides a diagnostic of confinement. The order parameter for this symmetry is the vev of the Wilson line in the fundamental representation, which obeys an area law in a confining vacuum. This implies the vanishing of the vev of an infinitely extended Wilson line, thus preserving the 1-form symmetry. In addition, $\mathcal{N}=1$ $SU(N)$ SYM also has a 0-form R-symmetry $U(1)_R$. The Adler-Bell-Jackiw (ABJ) or chiral anomaly breaks $U(1)_R$ to $\Gamma^{(0)}=\mathbb{Z}_{2N}$, which by chiral symmetry breaking ($\chi_{\rm SB}$) [82] reduces to $\mathbb{Z}_2$ in the confining phase

$$U(1) \quad \xrightarrow{\text{ABJ}} \quad \mathbb{Z}_{2N} \quad \xrightarrow{\chi_{\rm SB}} \quad \mathbb{Z}_2\,. \tag{4.1}$$

There is a 0-/1-form symmetry mixed 't Hooft anomaly

$$\mathcal{A}[b_2,A]=2\pi\,N^2\int_{X_5} A\,b_2\,b_2\,, \tag{4.2}$$

where b_2 is the background for $\mathbb{Z}_N^{(1)}$ and A for $\Gamma^{(0)}$, which satisfy $\oint b_2\in\frac{\mathbb{Z}}{N}$ and $\oint A\in\frac{\mathbb{Z}}{2N}$. This anomaly constrains the IR strongly-coupled physics [10, 83, 84]. In a confining vacuum the 1-form symmetry is unbroken, and the 0-form background has to satisfy $\oint A\in\frac{\mathbb{Z}}{2}$ and $\Gamma^{(0)}$ is broken to $\Gamma^{(0)}=\mathbb{Z}_2$. This breaking indicates the existence of N distinct confining vacua, modelled by a gapped TFT.

The goal is to develop new methods to compute anomalies of discrete higher-form symmetries and moreover, provide a derivation of the TFT sectors, which match these anomalies – without relying on anomaly matching or a Lagrangian description of the UV. This work provides a proof of concept by successfully implementing this in the context of the confinement of 4d $\mathcal{N}=1$ SYM. What we show is that the dual supergravity theory captures not only the background fields for the higher-form symmetries, and their anomalies, but also provides a derivation of the 4d TFT that governs the IR confining phase of the theory.

Higher-form symmetries in the AdS/CFT correspondence were discussed in [85–90]. Our focus here is on holography in a non-conformal setting, providing a dual to $\mathcal{N}=1$ $SU(N)$ SYM [91–94]. Concretely, we determine the 1-form symmetry and its anomalies in the Klebanov-Strassler (KS) [95–100] solution, and derive the theory in the far IR. The central tool for our analysis is the consistent truncation of supergravity to 5d [101–103].

The main results are as follows: from the 5d topological couplings, we identify the 1-form symmetry and anomalies that will be central to chiral symmetry breaking. Perhaps even more strikingly, we derive the TFT description of the gapped IR confining vacua of $\mathcal{N}=1$ $SU(N)$ SYM. We show how the 5d supergravity reduction remarkably contains the Lagrangian of the 4d TFT describing the IR physics, providing an independent derivation of the existence of this TFT sector, which agrees with but does not rely on anomaly matching.

4.2 Holographic Dual to Confinement

One of the most successful holographic realizations of $\mathcal{N}=1$ $SU(N)$ SYM theory is the KS solution [96]. This construction is realised in 10d type IIB supergravity, and it consists of two main ingredients:

1. N D3-branes probing the conifold $C(T^{1,1})$, which is a conical Calabi-Yau singularity with 5d link $T^{1,1}$ that is topologically $S^2 \times S^3$. The near-horizon of this brane system is $\mathrm{AdS}_5 \times T^{1,1}$ with 5-form flux $\int_{T^{1,1}} F_5 = N$.

2. M D5-branes wrapping the $S^2 \subset T^{1,1}$, known as fractional D3-branes. The D5-branes backreact on the external geometry, modifying the AdS_5 metric.

The KS solution at large r is

$$ds_{10}^2 = ds_{\mathcal{M}_5}^2 + \mathcal{R}^2(r) ds_{T^{1,1}}^2 \,, \quad \mathcal{R}(r) \sim \ln(r/r_s)^{1/4} \,, \tag{4.3}$$

where

$$ds^2_{\mathcal{M}_5} = \frac{r^2}{\mathcal{R}^2(r)} d\vec{x}^2 + \frac{\mathcal{R}^2(r)}{r^2} dr^2 \,, \tag{4.4}$$

and $r_s = r_0 e^{-\frac{2\pi N}{3g_s M^2} - \frac{1}{4}}$ with r_0 the UV scale. At large r, the quantization of fluxes is

$$\begin{aligned} &\int_{S^3} F_3 = M \,, \quad \int_{S^2} B_2 = \mathcal{L}(r) \,, \\ &\int_{T^{1,1}} F_5 = \mathcal{K}(r) = N + M\mathcal{L}(r) \,, \quad \mathcal{L}(r) = \frac{3g_s M}{2\pi} \ln(r/r_0) \,. \end{aligned} \tag{4.5}$$

We refer to this as the UV KS solution, valid for r sufficiently large and $g_s \mathcal{K}(r) \gg 1$. Note that F_5 is no longer quantised: its integral over the internal space acquires a radial dependence as a result of the backreaction from the fractional branes. Furthermore, the solution has a naked singularity at $\mathcal{R}(r_s) = 0$. Therefore, at small radial distances $r \to r_s$, (4.3) is no longer valid but gets replaced by the full warped, deformed conifold solution [96], which will be the relevant regime to study when we discuss the TFT in the IR. We can consider $r_s \to 0$, when $\frac{N}{M^2} \gg 1$.

The dual field theory description is given by an $SU(N+M) \times SU(N)$ gauge theory with bifundamental matter in $(\mathbf{N+M}, \overline{\mathbf{N}}) \oplus (\overline{\mathbf{N+M}}, \mathbf{N})$, where a combination of the two gauge couplings flows strong coupling. In particular, this theory is not conformal and the gauge couplings of the two factors run in opposite directions. E.g. when $SU(N+M)$ with $N_F = 2N$ becomes strongly coupled, we apply Seiberg duality [104], resulting in $SU(N-M)$ with $N_F = 2N$. This process perpetuates with the new gauge couplings flowing in opposite directions, giving rise to a 'duality cascade'. For $N = \kappa M$, $\kappa \in \mathbb{N}$, the endpoint is $\mathcal{N} = 1$ $SU(M)$ SYM at strong coupling (but we keep N an arbitrary large integer for now).

The RG-flow of the gauge theory cascade is mirrored explicitly in the dual gravity background. Moving from large r towards the origin in steps of

$$r \to r e^{-\frac{2\pi}{3g_s M}} \,, \tag{4.6}$$

has the effect of changing $\int_{S^2} B_2$ and $\int_{T^{1,1}} F_5$ by

$$\mathcal{L}(r) \to \mathcal{L}(r) - 1, \qquad \mathcal{K}(r) \to \mathcal{K}(r) - M \,. \tag{4.7}$$

At slices $r = r_k$ with

$$r_k = r_0 e^{-\frac{2\pi k}{3g_s M}} \,, \tag{4.8}$$

the flux integers $\mathcal{L}, \mathcal{K}$ are integer, and the supergravity background is dual to the $SU(N-(k-1)M) \times SU(N-kM)$ gauge theory in the baryonic branch [105]. For $N = \kappa M$ the endpoint is reached at a value r_κ where there are only M units of F_3-flux and no F_5-flux. In this regime, $r \sim r_\kappa$, the solution (4.3) breaks down before reaching the $r \to r_s$ limit, since $g_s\mathcal{K}(r_\kappa) = 0$, and the metric in (4.3) is not smooth. We therefore have the following hierarchy of scales

$$r_0 \gg r_k \gg r_\kappa > r_s \,. \tag{4.9}$$

4.3 1-form Symmetries from Supergravity

The global form of the gauge group, or put differently, the set of mutually local line operators, can be determined in holography by considering boundary conditions of Chern-Simons-like couplings [85–87]. Put in a more modern language, the 2-form backgrounds for 1-form symmetries of the holographic field theory are determined by topological couplings in the bulk and specific b.c.s yield absolute theories (i.e. definite spectra of line operators). On the gauge theory side of the duality cascade, the $\mathbb{Z}_{N+M} \times \mathbb{Z}_N$ center symmetry of $SU(N+M) \times SU(N)$ is broken by the matter to

$$\Gamma^{(1)} = \mathbb{Z}_{\gcd(N,N+M)} = \mathbb{Z}_{\gcd(N,M)} \,. \tag{4.10}$$

This remains invariant along the RG-flow.

In order to derive the 1-form symmetry holographically we study fluctuations around the UV KS solution, when r is sufficiently large and $g_s\mathcal{K}(r) \gg 1$, which describes each step of the cascade until $r \sim r_\kappa$. The latter corresponds to the end of the cascade and the smooth gravity dual is the warped deformed conifold, which we will investigate momentarily. We reduce type IIB supergravity on $T^{1,1}$ and study the topological couplings of 2-form gauge fields. The strings which couple to these fields induce line operators on the r_k slices, which in turn furnish the 1-form symmetry of the boundary theory. In particular the 1-form symmetry is deduced from the bulk couplings by imposing a set of consistent b.c.s in which a subset of the 2-form gauge potentials are fixed in a subgroup of $U(1)$.

We first consider fluctuations of the fluxes around the background on the cohomology of $T^{1,1}$, i.e. F_q expanded along $\omega_p \in H^p(T^{1,1}, \mathbb{Z})$ as

$$F_q = \sum_p f_{q-p} \wedge \omega_p \,, \tag{4.11}$$

and insert these into the type IIB equations

$$\begin{aligned} dH_3 &= 0\,, & d*_{10}H_3 &= -g_s^2 F_5 \wedge F_3\,,\\ dF_3 &= 0\,, & d*_{10}F_3 &= F_5 \wedge H_3\,,\\ dF_5 &= H_3 \wedge F_3\,, & *_{10}F_5 &= F_5\,. \end{aligned} \tag{4.12}$$

The couplings obtained in this way can equally be thought of as embedded into some consistent truncation (e.g. [101]). We work at the level of the equations of motion rather than reducing the type IIB supergravity action itself, to correctly account for contributions from the self-dual F_5. Since we are in the UV regime at large $r \sim r_0$, both cycles $S^2 \times S^3 \subset T^{1,1}$ are non-degenerate, so the non-trivial cohomology elements are the volume forms of the two spheres $\omega_2 \in H^2(T^{1,1},\mathbb{Z})$ and $\omega_3 \in H^3(T^{1,1},\mathbb{Z})$ (see e.g. [98] for conventions and an explicit parametrization). The expansion is

$$\begin{aligned} \delta F_3 &= g_3 + \pi l_s^2 \omega_2 \wedge g_1\,, \qquad \delta H_3 = h_3\,,\\ \delta F_5 &= \pi l_s^2 \omega_2 \wedge f_3 + \frac{2\pi l_s^2}{6}\mathcal{R}\omega_3 \wedge *f_3\,. \end{aligned} \tag{4.13}$$

Here, $h_3, g_{1,3}, f_3$ are all external fields. Self-duality of δF_5 implies a choice of frame: we can fix one expansion component in terms of the other. We use the 3-form piece, since the operators of the boundary 1-form symmetry are manifest in this frame. The Bianchi identities for H_3, F_3 imply that the corresponding 5d fields are closed, so we write

$$h_3 = db_2\,, \qquad g_3 = dc_2\,, \qquad g_1 = dc_0\,. \tag{4.14}$$

We interpret c_0 as an axion, whereas b_2, c_2 couple to F1s and D1s, respectively. The Bianchi identity for δF_5 implies that f_3 is not closed

$$df_3 = d\mathcal{L} \wedge g_3 + h_3 \wedge g_1\,. \tag{4.15}$$

As such, we shift the field to define a new gauge potential

$$da_2 = f_3 - \mathcal{L}dc_2 - b_2 dc_0\,, \tag{4.16}$$

which couples to D3-branes wrapping $S^2 \subset T^{1,1}$. The 5d equations of motion are

$$\begin{aligned} d(\mathcal{R} *_5 f_3) &= \frac{3}{2\pi}M db_2\\ d(\mathcal{R}^5 *_5 db_2) &= -27\pi l_s^4 g_s^2(\mathcal{K}dc_2 - M f_3 + \frac{2\pi}{3}\mathcal{R} *_5 f_3 \wedge dc_0)\\ d(\mathcal{R}^5 *_5 dc_2) &= 27\pi l_s^4(\mathcal{K}db_2 + \frac{2\pi}{3}\mathcal{R} *_5 f_3 \wedge d\mathcal{L})\\ d(\mathcal{R} *_5 dc_0) &= -\mathcal{R} *_5 f_3 \wedge db_2\,. \end{aligned} \tag{4.17}$$

We are interested in studying the theory near a slice defined by $r = r_k$ for some $k \ll \frac{N}{M}$, i.e. a slice which is far away from the IR, where the UV KS solution is valid. Parametrising the radial coordinate as $r = r_k + r'$ where $r' \ll r_k$ we find that the effective D3 charge is

$$\mathcal{K}(r) = N - kM + \mathcal{O}(r'/r_k)\,. \tag{4.18}$$

At long distances the kinetic terms and couplings of higher mass dimension will be suppressed with respect to terms with fewer derivatives. From the equations of motion (4.17) we extract leading topological contributions

$$N db_2 = 0\,, \qquad M db_2 = 0\,, \qquad N dc_2 - M da_2 = 0\,, \tag{4.19}$$

where we ignore c_0, which can be gauged away via a Stückelberg mechanism. These couplings are embedded into the consistent truncation of [101]. One can compare by varying their topological action, changing duality frame and restricting to the relevant fields. We define the (minimal) linear combination

$$\mathcal{C} = q_1 c_2 - q_2 a_2\,, \tag{4.20}$$

with $\gcd(N,M)q_1 = N$, $\gcd(N,M)q_2 = M$. The center-of-mass mode $\mathcal{B}$ defined by

$$(c_2, a_2) = (q_2\mathcal{B}, q_1\mathcal{B})\,, \tag{4.21}$$

corresponding to the 1-form symmetry of the collective motion of the D3-branes, decouples from the action. The leading contributions to the equations of motion can thus be written as the topological equations

$$\gcd(N,M) d\mathcal{C} = 0\,, \qquad \gcd(N,M) db_2 = 0\,. \tag{4.22}$$

These equations imply that b_2 and $\mathcal{C}$ are flat gauge fields. The reduction on the UV KS solution can thus be lifted to the following 5d effective bulk TFT

$$\boxed{S_{\rm BF} = 2\pi\, \gcd(N,M) \int_{\mathcal{M}_5} b_2 \wedge d\mathcal{C}\,.} \tag{4.23}$$

Quantisation of this BF-action implies that the two $U(1)$ gauge fields must in fact take values in $\mathbb{Z}_{\gcd(N,M)}$ [85]. That is, the holonomies of these gauge fields are constrained to lie in

$$\oint_{M_2} b_2 \in \frac{\mathbb{Z}}{\text{gcd(N,M)}}\,, \qquad \oint_{M_2} \mathcal{C} \in \frac{\mathbb{Z}}{\text{gcd(N,M)}}\,, \qquad \partial M_2 = \emptyset\,. \tag{4.24}$$

1-form symmetries are generated by *topological* surface operators [10], which are realized by the bulk operators

$$U_b(M_2) = e^{2\pi i \oint_{M_2} b_2}\,, \qquad U_c(M_2) = e^{2\pi i \oint_{M_2} \mathcal{C}}\,, \qquad \partial M_2 = \emptyset\,. \tag{4.25}$$

Generically, due to non-commutativity of fluxes, these do not commute [85]

$$U_b(M_2)U_c(N_2) = U_c(N_2)U_b(M_2)e^{\frac{2\pi i L(M_2,N_2)}{\gcd(N,M)}}\,, \tag{4.26}$$

where L is the linking of the surfaces. These *charge* operators generate a 1-form symmetry, which acts on *charged* line operators in the 4d field theory. For each slice $\mathcal{M}_5|_{r_k}$ the charged line operators are

$$U_b(\Sigma) = e^{2\pi i \oint_{\Sigma} b_2}\,, \qquad U_c(\Sigma) = e^{2\pi i \oint_{\Sigma} \mathcal{C}}\,, \qquad \partial\Sigma \subset \mathcal{M}_5|_{r_k}\,, \tag{4.27}$$

where Σ is some open surface whose boundary lies in the r_k slice. However only a maximal set of mutually local line operators are allowed, which are encoded in the b.c.s of b_2 and $\mathcal{C}$.

4.4 Boundary Conditions and Mutually Local Lines

A possible choice of b.c. for (4.23) is

$$b_2 \text{ Dirichlet}\,, \qquad \mathcal{C} \text{ Neumann}\,. \tag{4.28}$$

Since $\mathcal{C}$ is free to vary at the boundary, $U_c(M_2)$ with $\partial M_2 = \emptyset$ will correspond to the topological charge operator for the 1-form symmetry. By varying the topological action we find a condition

$$\gcd(N,M)b_2 \wedge \delta\mathcal{C}|_{r_k} = 0\,, \tag{4.29}$$

which forces b_2 to take fixed values at the boundary. This implies that we can define a flat connection b_1 in 4d taking values in $\mathbb{Z}_{\gcd(N,M)}$, i.e. $\gcd(N,M)b_2 = db_1 = 0$ at the slice $r = r_k$. Therefore, U_b restricted to $\partial\Sigma \subset \mathcal{M}_5|_{r_k}$ corresponds to the charged line operators of the field theory. As is well known, the fundamental strings, carrying world-volume b_2, ending on the boundary indeed give rise to Wilson lines in the 4d theory. The screening can equally be seen by considering the analog of the 'baryon vertex' [106] in this setup: integrating the Bianchi identities for D5-branes on $T^{1,1}$ and D3-branes on S^3 yields

$$\begin{aligned} \int_{T^{1,1}} dF_7 &= \int_{T^{1,1}} H_3 \wedge F_5 = (N - kM)H_3 \\ \int_{S^3} dF_5 &= \int_{S^3} H_3 \wedge F_3 = MH_3\,. \end{aligned} \tag{4.30}$$

Thus D5-branes on $T^{1,1}$ screen $N - kM$ F1s, and D3-branes on S^3 screen M F1s. The minimal configuration of screened strings is thus $\gcd(N, M)$.

Clearly an alternative is to exchange the two gauge fields and consider

$$b_2 \text{ Neumann}\,, \qquad \mathcal{C} \text{ Dirichlet}\,. \tag{4.31}$$

Now the topological operator $U_c(\partial\Sigma) = e^{2\pi i \oint_{\partial\Sigma} \mathcal{C}}$ on $\partial\Sigma \subset \mathcal{M}_5|_{r_k}$ gives rise to the charged operators of the field theory, whereas $U_b(M_2)$ for closed M_2 defines the charge operators, and we again find the 1-form symmetry (4.10). Physically, this choice of boundary conditions means that bound states of D1-strings and D3-branes wrapped on S^2 can end on the boundary to form line operators. From the Bianchi identities we find that $\gcd(N, M)$ many of the D1-D3 bound states can end on an NS5-brane wrapping $T^{1,1}$. This provides a screening mechanism for the line operators and is consistent with the 1-form symmetry. This configuration of lines corresponds in the dual field theory to the 't Hooft lines of the SYM theory.

We can consider general boundary conditions on the fields through gauging. Let $\gcd(N, M) = pq$. We can then consider the theory,

$$S_{\text{CS}'} = \frac{1}{2\pi} \int \left(p b_2' \wedge d\mathcal{C}' + q b_2'' \wedge d\mathcal{C}'' + b_2'' \wedge d\mathcal{C}' \right) . \tag{4.32}$$

We can recover the action (4.23) by integrating out b_2'' and $\mathcal{C}'$. Writing it in this way, we see that these backgrounds can be coupled to a 4d theory in a way that exhibits $\mathbb{Z}_p \times \mathbb{Z}_q$ 1-form symmetry, where the line operators are realized in terms of (p, q)-strings, where the D-strings also include wrapped D3-branes.

From a bulk point of view we can see the screening by considering (p, q) 5-branes wrapping $T^{1,1}$. The Bianchi identities for (p, q) 5-branes are

$$\begin{aligned} p \int_{T^{1,1}} dF_7 &= N H_3\,, \\ \frac{q}{(2\pi l_s)^4} \int_{T^{1,1}} dH_7 = \frac{q}{(2\pi l_s)^4} \int_{T^{1,1}} F_3 \wedge F_5 &= (N - kM) F_3 - M da_2\,. \end{aligned} \tag{4.33}$$

Therefore bound states of q F1-strings and p D1-D3 bound states can end on a (p, q) 5-brane. This process is dual to the baryon vertex screening the line operators of the dual theory, which are given by the bound states of q F1-strings and p D1-D3, at constant r_k slices.

The existence of alternative b.c.s will potentially lead in the IR to the strongly-coupled vacua of $\mathcal{N} = 1$ $PSU(M)$ SYM, when N is a multiple of M. Since one of the vacua has a

different (non-confining) behaviour, we believe that this provides evidence for the existence of a new holographic solution in the IR describing this deconfining vacuum, the spontaneous breaking of the 1-form symmetry, and therefore this phase transition.

4.5 Mixed Anomaly and $\chi_{\mathbf{SB}}$ from Holography

All things are now in place to derive holographically the mixed anomaly (4.2). From here onwards, we set $N = \kappa M$, where the bottom of the cascade is a confining phase $SU(M)$ SYM. To do this, we need to study the rest of the topological couplings in the 5d bulk supergravity action. In particular we need to include the R-symmetry of the dual field theory, which is realized in terms of the $U(1)$-isometry (Reeb-vector) of the $T^{1,1}$ solution. This can be described by a $U(1)$ 1-form gauge field A, which enters the metric of $T^{1,1}$ as $d\beta \to d\beta - A$, where β is the coordinate of the Hopf fiber of the S^3. The additional 5d topological terms in the action are

$$S_{5\mathrm{d}} = 2\pi \int \frac{\mathcal{R}}{2} |dc_0 + 2MA|^2 + \frac{M}{2} b_2^2 \, dc_0 + M^2 b_2^2 \, A \,. \tag{4.34}$$

The first term is the kinetic term for the axion. Since it contains two derivatives it is subleading when evaluated on the UV KS solution, when r is large, with respect to the topological terms. On the other hand its effect is important, since it realises the Stückelberg mechanism for the $U(1)_R$ gauge field A. The shift symmetry of the axion, $c_0 \sim c_0 + 2\pi$, is gauged by the $U(1)_R$ symmetry, so that the action is invariant under the non-linear transformation

$$A \to A + d\alpha \,, \qquad c_0 \to c_0 - 2M\alpha \,. \tag{4.35}$$

We can use this symmetry to completely gauge away the axion, leaving only a mass term for the gauge field. Fixing $c_0 = 0$, there is still a residual discrete symmetry generated by

$$\alpha \in \frac{\pi \mathbb{Z}}{M} \,. \tag{4.36}$$

This is the direct way to identify the breaking of

$$U(1)_R \to \mathbb{Z}_{2M}^{(0)} \,, \tag{4.37}$$

as required by the ABJ anomaly.

The second term in (4.34) corresponds to the anomaly between the 0-form background A for $\mathbb{Z}^{(0)}_{2M}$, with fractional periods $\oint A \in \frac{\mathbb{Z}}{2M}$, and b_2 for $\mathbb{Z}^{(1)}_M$, with $\oint b_2 \in \frac{\mathbb{Z}}{M}$

$$\mathcal{A}[b_2, A] = 2\pi M^2 \int_{\mathcal{M}_5} b_2\, b_2\, A\,, \tag{4.38}$$

which is a mixed 0-/1-form symmetry anomaly. As expected it does not depend on the energy scale, and therefore this term will survive in the IR. In the IR we expect the theory to be dual to a confining vacuum of $SU(M)$ SYM, so the $\mathbb{Z}^{(1)}_M$ should be unbroken, and this gapped phase should be described by a 4d TFT. Assuming $\mathcal{M}_5$ is spin, then b_2^2 is even. Since A is a $\mathbb{Z}_{2M}$ background, (4.38) is not integral in general. It was proven in [84] that unless this term is integral there cannot be a 4d TFT with $\Gamma^{(0)} = \mathbb{Z}_{2M}$ and $\Gamma^{(1)} = \mathbb{Z}_M$ symmetries in the IR that saturates all the anomalies of the theory in the UV. On the other hand, integrality of (4.38) and an unbroken $\mathbb{Z}^{(1)}_M$ forces the R-symmetry gauge field to take periods $\oint A \in \frac{\mathbb{Z}}{2}$, implying chiral symmetry breaking in the IR vacuum of $SU(M)$ SYM. The take-away from this analysis is thus that the presence of this topological coupling in the UV KS supergravity solution is already preempting and consistent with the chiral symmetry breaking in the gapped confining vacuum with $\mathbb{Z}^{(0)}_2$ and $\mathbb{Z}^{(1)}_M$ symmetries.

4.6 Deformed Conifold Dual to the IR of $\mathcal{N} = 1$ $SU(M)$ SYM

At small radial distances $r \to r_s$, the KS solution is sensitive to the deformation of the conifold induced by the M D5-branes wrapping $S^2 \subset T^{1,1}$. The non-zero F_3 flux threading the S^3 prevents this cycle from shrinking to zero volume, whereas the S^2 collapses. Here the effective number of D3-branes is zero and the gauge theory dual is the IR regime of pure $\mathcal{N} = 1$ $SU(M)$ SYM. The warped, deformed conifold is parametrised by a new coordinate τ, which, at large τ, is related to r by

$$r^2 = 32^{-5/3}\epsilon^{4/3}e^{2\tau/3}\,. \tag{4.39}$$

Near $\tau \to 0$ the metric is approximately $\mathbb{R}^{3,1}$ times the deformed conifold [96]. We refer to this as the IR KS solution. For the sake of illustration we include the shrinking S^2 in the degenerate metric

$$\begin{aligned} ds^2_{10} &= c_1\epsilon^{-4/3}(g_s M l_s^2)^{-1}d\vec{x}^2 + c_2 g_s M l_s^2 ds^2_6\,, \\ ds^2_6 &= \frac{1}{2}d\tau^2 + \frac{1}{2}(g^5)^2 + (g^3)^2 + (g^4)^2 + \frac{1}{4}\tau^2[(g^1)^2 + (g^2)^2]\,, \end{aligned} \tag{4.40}$$

where $\{g^i\}$ are the standard basis of 1-forms on $T^{1,1}$ [107] and c_i are numerical constants [108]. For $g_s M \gg 1$ the curvatures are small everywhere, even in the far IR, such that the supergravity approximation is always reliable. At $\tau = 0$ the flux background has significant simplifications

$$F_5 = 0\,, \qquad H_3 = 0\,, \qquad F_3 = \frac{l_s^2 M}{2} g^5 \wedge g^3 \wedge g^4\,. \tag{4.41}$$

Since the S^2 shrinks to zero radius as $\tau \to 0$, we modify our expansion (4.13) to ignore any fluctuations over the 2-sphere. This has the immediate consequence of removing all F_5 fluctuations, $\delta F_5 = 0$, as we would otherwise be unable to enforce self-duality. The massless fluctuations around the IR KS background are therefore simply

$$\delta H_3 = h_3\,, \qquad \delta F_3 = g_3\,. \tag{4.42}$$

The Bianchi identities imply that $g_3 = dc_2$, $h_3 = db_2$ are closed and the equations of motion for H_3 and F_3 furnish two kinetic terms

$$d *_5 h_3 = 0\,, \qquad d *_5 g_3 = 0\,. \tag{4.43}$$

Contrary to the UV KS solution, the kinetic terms are not suppressed in this regime. We get a single non-trivial contribution from the F_5 Bianchi identity implying that

$$M db_2 = 0\,. \tag{4.44}$$

We have no freedom in selecting boundary conditions here, the holographic duality picks out a confining vacuum and in particular a global form of the gauge group, namely the $SU(M)$ simply-connected group, with an unbroken electric 1-form symmetry $\mathbb{Z}_M^{(1)}$. From the bulk perspective, F1s can end on the boundary, indicating the presence of Wilson lines in the gauge theory. Furthermore, M fundamental strings are screened by wrapped D5-branes that correspond to the baryon vertex in the 4d theory.

4.7 4d IR TFT from Holography

Finally, we now turn to the derivation of the IR description of the confining vacua. We derive the action of the IR 4d TFT, which matches (4.38), and realises spontaneous chiral symmetry

breaking, $\mathbb{Z}_{2M} \to \mathbb{Z}_2$. Based on a field theoretic anomaly matching argument, a candidate TFT was proposed in [10]

$$S_{\text{TFT}_{4\text{d}}} = \int M\phi \left(dc_3 + \frac{M}{2} b_2^2 \right) = \int M\phi F_4 \,. \tag{4.45}$$

The M vacua, labelled by $\langle e^{i\phi} \rangle = e^{\frac{2\pi i \ell}{M}}$, $\ell = 0, 1, \dots M-1$, are separated by domain walls (DWs) [109], $e^{i \oint c_3}$. We now give a holographic derivation of the IR TFT based on the 5d bulk couplings of the IR KS solution.

The smooth IR gravity dual background is the deformed conifold solution, where $\tau \to 0$. In this regime there is no hierarchy between the 5d bulk kinetic and topological terms, and the former need to be taken into account. Before the S^2 degenerates, the D5-branes source $C_6 = \omega_3 \wedge c_3$, and in addition since $F_7 = *F_3$ we consider

$$dc_3 = \frac{\mathcal{R}}{2} *_5 (dc_0 + 2MA) \,. \tag{4.46}$$

Therefore, in the IR the dynamics of c_0 becomes relevant. Since A corresponds to the true isometry of the IR KS solution, i.e. is a $\mathbb{Z}_2$ gauge field, c_0 does not shift under a gauge transformation of A. In the IR, the topological 5d action is

$$S_{5\text{d}}^{\text{IR}} = 2\pi \int 2MA dc_3 + dc_0 dc_3 + \frac{M}{2} b_2^2 \, dc_0 \,. \tag{4.47}$$

We first notice that the mixed anomaly between $\Gamma^{(0)} = \mathbb{Z}_{2M}$ and $\Gamma^{(1)} = \mathbb{Z}_M$ has disappeared. This is due to an additional topological term $|c^\Omega(r)|^2 b_2^2 A$ [101,110,111], which for the UV KS solution depends on the UV scale r_0, but is constant in the IR $c^\Omega = M$. This is consistent with anomaly matching since the IR theory has $\Gamma^{(0)} = \mathbb{Z}_2$, which is not anomalous on spin manifolds. Varying by c_0 implies $M db_2 = 0$, in agreement with the equations of motion on the deformed conifold. When this condition is satisfied, the last two terms give rise to topological counterterms for the 4d theory living at the boundary. This implies that they are not anomalies, but rather the imprint of the TFT (4.45) in the IR, which is precisely obtained by identifying $c_0 \leftrightarrow M\phi$ and evaluating these terms at the boundary. In particular, c_0 is related to the presence of DWs given by D5-branes wrapping S^3. These source $\int_B F_3$, where B is the Poincaré dual cycle in the deformed conifold with S^2 boundary at infinity. This entails that $\int_B F_3 \sim \int_{S^2} c_0 \omega_2$, and because of the presence of the D5 DWs, $c_0 = \ell$ is quantized and corresponds to the number of D5s. The UV anomaly (4.38) in the IR is realised by the action of $\Gamma^{(0)} = \mathbb{Z}_{2M}$, $\ell \to \ell + 1$, which is however not a symmetry of the IR vacuum.

This IR theory is furthermore invariant under 1-form symmetry transformations

$$b_2 \to b_2 + d\lambda\,, \tag{4.48}$$

which implies that

$$c_3 \to c_3 - M b_2 \lambda - \frac{M}{2}\lambda d\lambda\,. \tag{4.49}$$

The fact that the transformation of the 1-form symmetry enters in the shift of c_3 signals the presence of a 3-group [10, 112]. This can be derived from the D5-brane realization of the DWs: the CS-action of the D5-brane is

$$\mathcal{L}_{CS} = \sum_p C_p \wedge e^{b_2}\,. \tag{4.50}$$

The DWs extend in the 4d spacetime such that

$$F_4 = \int_{S^3} d\mathcal{L}_{CS} = dc_3 + \frac{M}{2} b_2^2\,, \tag{4.51}$$

the 3-group follows from the gauge invariance of the world-volume action of the D5 and is consistent with gauge invariance of (4.47).

4.8 Anomalies from Little String Theory

An alternative large N limit of 4d $\mathcal{N}=1$ SYM is the solution in [113], which is the topologically twisted S^2-reduction of 6d little string theory (LST) on N NS5-branes in Type IIB, which in the IR is 6d $(1,1)$ SYM. We now derive the chiral symmetry breaking in 4d $\mathcal{N}=1$ SYM for gauge group G from a twisted S^2-reduction of LST. The anomaly polynomial of LSTs has a term [28]

$$I_{8,\text{mixed}} \supset 2h_G^\vee c_2(R_{6d}) c_2(F_G)\,, \tag{4.52}$$

where R_{6d}, F_G are the $SU(2)_R$ and gauge bundles, respectively. We consider the decomposition $R_{6d} = (R \otimes K_{S^2}^{1/2}) \oplus (R \otimes K_{S^2}^{1/2})^\vee$, where R is the 4d $U(1)_R$-bundle and K_{S^2} is the canonical bundle on S^2. The twist is realized by

$$c_2(R) = -\left(dA_R + \frac{1}{2}c_1(K_{S^2})\right)^2\,, \tag{4.53}$$

where A_R is associated to the 4d $U(1)_R$. Integrating (4.52) on S^2

$$I_6 = \int_{S^2} I_{8,\text{mixed}} \supset 2h_G^\vee dA_R \wedge c_2(F_G)\,. \tag{4.54}$$

This is the ABJ anomaly of 4d $\mathcal{N}=1$ SYM, and it trivializes on a closed 6-manifold, Y_6, when

$$2h_G^\vee dA_R = 0\,, \tag{4.55}$$

i.e. when A_R is in $\mathbb{Z}_{2h_G^\vee}$. In fact, this corresponds to the breaking of the

$$U(1)_R \to \mathbb{Z}_{2h_G^\vee} \tag{4.56}$$

by the ABJ anomaly.

We now also derive the mixed 0-/1-form 't Hooft anomaly between $\mathbb{Z}_{2h_G^\vee}$ and 1-form symmetry $\Gamma^{(1)} = Z(G)$, where $Z(G)$ is the center of the simply connected G. Let $\mathcal{M}_5 = \partial Y_6$ and consider the anomaly of the 4d theory

$$I_5 \supset 2h_G^\vee A_R \wedge c_2(F_G)\,, \qquad I_6 = dI_5\,. \tag{4.57}$$

Activating a 1-form symmetry background $b_2 \in H^2(\mathcal{M}_4, Z(G))$, makes the instanton density fractional, since it is evaluated in $G/Z(G)$ bundles, and I_5 becomes

$$I_5 \supset 2h_G^\vee \alpha_G A_R \cup \mathfrak{P}(b_2)\,, \tag{4.58}$$

where $\mathfrak{P}(b_2)$ is the Pontryagin square [114] and for $SU(N)$ $\alpha_G = \frac{N-1}{2N}$. In particular, A_R is not a $U(1)_R$ bundle, but rather a $\mathbb{Z}_{2h_G^\vee}$ surviving subbundle, i.e. non-trivial configuration such that $2h_G^\vee dA_R = 0$ on a closed Y_6. Note that due to this, the anomaly does not trivialize anymore when α_G is fractional ($\oint \mathfrak{P}(b_2) \in \mathbb{Z}$). A_R has then periodicity $\oint A_R \in \frac{\mathbb{Z}}{2h_G^\vee}$ and from (4.58) we have recovered the full mixed anomaly between the chiral symmetry and the 1-form symmetry, which we derived holographically in the previous section.

4.9 Conclusions and Outlook

In this work, we have studied confinement in 4d $\mathcal{N}=1$ $SU(M)$ SYM from a holographic point of view, focusing on the 1-form symmetry and its relation to chiral symmetry breaking. In the 5d supergravity dual, obtained by truncation of the KS solution, we identified the topological couplings that determine the 1-form symmetry and its 't Hooft anomalies. One such coupling is a mixed 0-form/1-form symmetry anomaly closely related to chiral symmetry breaking in gapped confining vacua. From the dual gravity description we also derived the 4d TFT that governs the IR from first principles, and which realises chiral symmetry breaking,

confirming the anomaly-based arguments in [10]. Finally, complementing this, we derived the chiral and mixed anomalies from the LST realization of pure SYM.

Our result for $\mathcal{N} = 1$ $SU(M)$ SYM provides an exposition of a more general methodology: utilizing supergravity couplings to determine anomalies and IR sectors of QFTs. It represents a proof of principle that there is a fruitful interplay between holographic methods using gravitational theories and modern QFT methods relying on generalized global symmetries. This connection sheds new light on holography, as it breathes life into numerous often obscure topological couplings in supergravity theories, and fills them with physical relevance. Moreover, it is remarkable that holography can be used to explicitly derive topological sectors describing gapped confining phases beyond standard AdS/CFT, and providing sharp predictions of results which within QFT are often only inferred indirectly.

Applications in many other contexts come to mind: geometric constructions within string theory, e.g. gauge theories obtained from singular Calabi-Yau spaces or G_2 manifolds in M-theory, are perfect grounds where these methods can be applied. More far-reaching phenomenological applications arise in the context of non-supersymmetric deformations where the KS solution has played a central role. Finally, the construction of low dimensional quantum systems in string theory provides another avenue where such topological anomaly matching arguments are well-studied, and our holographic perspective would provide a top-down counter-check to these considerations.

Part II

Geometric Engineering and Brane-webs

Chapter 5

Background

5.1 5d SCFTs and Gauge Theories

This chapter concerns 5d $\mathcal{N} = 1$ SCFTs which admit a weakly coupled gauge theory description. Field theoretically, the best way to understand this is by starting with an SCFT in the UV and turning on a Super Yang-Mills term for a gauge group. This is a relevant operator as the gauge coupling g has negative mass dimension in 5d and thus triggers an RG-flow. We say that two weakly coupled gauge theory descriptions are 'UV dual' if they have the same UV-completion, i.e. they are two deformations of the same SCFT. From the gauge theory perspective we can reach the UV limit by taking the gauge coupling to infinity $g \to \infty$.

Let us consider a specific 5d $\mathcal{N} = 1$ gauge theory with gauge group G of rank r, associated to a Lie algebra $\mathfrak{g}$ with generators T_i, and matter hypermultiplets transforming in some representation $\boldsymbol{R}$ of G. We take G to be simple for now, but will relax this condition to semi-simple later. The vector multiplet contains the gauge field A and a real scalar whose vevs ϕ^i, $i = 1, \ldots, r$ parametrise the Coulomb branch. The Coulomb branch is described by the effective Lagrangian

$$\mathcal{L}_{\text{CB}} = \tau_{ij} \left(\mathrm{d}\phi^i \wedge \star \mathrm{d}\phi^j + \mathrm{d}A^i \wedge \star \mathrm{d}A^j \right) + \frac{c_{ijk}}{24\pi^2} \mathrm{d}A^i \wedge \mathrm{d}A^j \wedge A^k + \ldots \,, \tag{5.1}$$

where τ_{ij} and c_{ijk} are the effective gauge coupling and Chern-Simons level, respectively, and the A^i are the gauge fields for the Cartan subgroup $U(1)^r \subset G$. They can be conveniently obtained from a single function, the prepotential $\mathcal{F}(\phi^i)$

$$\tau_{ij} = \frac{\partial^2 \mathcal{F}}{\partial \phi^i \partial \phi^j} \,, \qquad c_{ijk} = \frac{\partial^3 \mathcal{F}}{\partial \phi^i \partial \phi^j \partial \phi^k} \,. \tag{5.2}$$

The IMS prepotential [16] of a pure 5d $\mathcal{N}=1$ gauge theory with gauge group G is given by

$$\mathcal{F}_{\text{IMS}} = \frac{1}{2g_0^2} h_{ij}\phi^i\phi^j + \frac{k}{6} d_{ijk}\phi^i\phi^j\phi^k + \frac{1}{6}\sum_{\alpha\in\Phi_+} |\alpha\cdot\phi|^3 \,, \tag{5.3}$$

where $h_{ij} = \operatorname{Tr}(T_iT_j)$ and the $\alpha \in \Phi_+$ are the positive roots of $\mathfrak{g}$. For $G = SU(N)$, $N \geq 3$ the symmetric tensor $d_{ijk} = \frac{1}{2}\operatorname{Tr}(T_i\{T_j, T_k\})$ is non-zero and k is the bare Chern-Simons level. We choose a Weyl wedge such that $\alpha\cdot\phi > 0$ for all α. To couple the theory to matter we add the term

$$\mathcal{F}_{\text{matter}} = \sum_{\boldsymbol{R}}\sum_{I=1}^{N_R}\mathcal{F}_{\boldsymbol{R}}\,, \qquad \mathcal{F}_{\boldsymbol{R}} = -\frac{1}{12}\sum_{a=1}^{\dim\boldsymbol{R}} |\lambda^a\cdot\phi - m_I|^3 \,, \tag{5.4}$$

where $\boldsymbol{R}$ runs over the irreducible representations of G and the λ^a are the weights of $\boldsymbol{R}$. The matter content of such a theory consists of N_R hypermultiplets in the representation $\boldsymbol{R}$ with masses m_I. We will mainly be concerned with theories with N_{AS} anti-symmetric matter multiplets and N_F fundamentals. These theories will be denoted

$$G_k + N_{AS}\boldsymbol{AS} + N_F\boldsymbol{F}\,. \tag{5.5}$$

Another class of theories we encounter are quiver gauge theories, consisting of multiple simple gauge groups, coupled by bifundamental matter. The prepotential of a quiver $G_1 - G_2$ with two constituents is given by

$$\mathcal{F} = \mathcal{F}^{(1)}_{\text{IMS}} + \mathcal{F}^{(2)}_{\text{IMS}} - \frac{1}{12}\sum_{a=1}^{\dim\boldsymbol{F}_1}\sum_{b=1}^{\dim\boldsymbol{F}_2}\left|\lambda^a\cdot\phi^{(1)} + \lambda^b\cdot\phi^{(2)} - m_B\right|^3 \,, \tag{5.6}$$

where m_B is the mass of the bifundamental matter field. Of course, this generalises to arbitrary quivers with additional matter.

An important feature of the prepotential is its ability to describe the gauge theory in various phases. We see that the matter contribution (5.4) depends on the relative values of the Coulomb branch parameters ϕ^i and the flavor masses m_I. Together with the bare gauge coupling[1]

$$m_0 = \frac{1}{g_0^2} \tag{5.7}$$

they form the extended Coulomb branch.

The flavor symmetry $\mathfrak{g}_{\text{F,cl}}$ of a weakly coupled gauge theory is easy to determine. Given a theory with a single gauge group G, N_R hypermultiplets in representation $\boldsymbol{R}$ contribute as

$$\boldsymbol{R}\text{ complex }\Rightarrow \mathfrak{u}(N_R)\,, \qquad \boldsymbol{R}\text{ real }\Rightarrow \mathfrak{sp}(N_R)\,, \qquad \boldsymbol{R}\text{ quaternionic }\Rightarrow \mathfrak{so}(2N_R)\,. \tag{5.8}$$

[1] Or multiple gauge couplings in case of a quiver gauge theory.

G	$SU(2)$	$SU(3)$	$SU(4)$	$SU(N \geq 5)$	$Sp(N \geq 2)$
$\mathfrak{g}_{\mathrm{F,cl}}$	$\mathfrak{so}(2N_F)$	$\mathfrak{u}(N_F)$	$\mathfrak{u}(N_F) \oplus \mathfrak{sp}(N_{AS})$	$\mathfrak{u}(N_F) \oplus \mathfrak{u}(N_{AS})$	$\mathfrak{so}(2N_F) \oplus \mathfrak{sp}(N_{AS})$

Table 5.1: Classical flavor symmetry algebras for gauge theories of the form (5.5).

G	$I_2(\boldsymbol{F})$	$I_2(\boldsymbol{AS})$	$I_2(\boldsymbol{Sym})$	$A(\boldsymbol{F})$	$A(\boldsymbol{AS})$	$A(\boldsymbol{Sym})$
$SU(N)$	$\frac{1}{2}$	$\frac{N-2}{2}$	$\frac{N+2}{2}$	1	$N-4$	$N+4$
$Sp(N)$	$\frac{1}{2}$	$N-1$	$N+1$	-	-	-

Table 5.2: Second index and triangle anomaly coefficient for various representations of G.

For the theories in (5.5) the flavor symmetry algebras are given in table 5.1. In a quiver gauge theory each bifundamental contributes an additional $U(1)$ to the classical flavor symmetry.[2] Furthermore, each simple gauge group constituent has a topological flavor symmetry $U(1)_T$ with current

$$J_T = \frac{1}{8\pi^2} \star \mathrm{Tr}\,(\mathrm{d}A \wedge \mathrm{d}A)\ . \tag{5.9}$$

In the strongly coupled limit the flavor symmetry algebra is enhanced

$$\mathfrak{g}_{\mathrm{F,cl}} \oplus \bigoplus_{j=1}^{n} \mathfrak{u}(1)_T^{(j)} \to \mathfrak{g}_{\mathrm{F}}\,, \tag{5.10}$$

where n is the number of simple gauge group constituents.

In this paper we will be interested in explicitly integrating out matter. Consider a theory with a single gauge group and matter in representation $\boldsymbol{R}$ of mass m_I. Taking $m_I \to \pm\infty$[3] corresponds to decoupling the hypermultiplet. In this limit $\mathcal{F}_{\boldsymbol{R}}$ simplifies to

$$\begin{aligned}\lim_{m_I\to\pm\infty} \mathcal{F}_{\boldsymbol{R}} = \pm\frac{1}{12}\Bigg(& -m_I^3\ \dim \boldsymbol{R} + 3m_I^2 \underbrace{\left(\sum_a \lambda_i^a\right)}_{0} \phi^i \\ & -3m_I \underbrace{\left(\sum_a \lambda_i^a \lambda_j^a\right)}_{2I_2(\boldsymbol{R})\ h_{ij}} \phi^i\phi^j + \underbrace{\left(\sum_a \lambda_i^a \lambda_j^a \lambda_k^a\right)}_{A(\boldsymbol{R})\ d_{ijk}} \phi^i\phi^j\phi^k \Bigg)\ .\end{aligned} \tag{5.11}$$

Here, the quantities I_2 and A are the second index and the triangle anomaly coefficient, respectively, and only depend on $\boldsymbol{R}$ and G. For the gauge groups and representations of interest they are summarised in table 5.2. Clearly, $A(\boldsymbol{R})$ is only relevant for $G = SU(N > 2)$ as d_{ijk} otherwise vanishes.

[2] For $SU(2) - SU(2)$ quivers this is instead $SU(2)$.

[3] In fact it is sufficient to choose $|m_I|$ large enough such that all the terms in (5.4) have the same sign.

Additionally, we generally have

$$I_2(\bar{\boldsymbol{R}}) = I_2(\boldsymbol{R})\,, \qquad A(\bar{\boldsymbol{R}}) = -A(\boldsymbol{R})\,. \tag{5.12}$$

By comparison with (5.3) we see that integrating out a matter multiplet by taking its mass to $\pm\infty$ shifts the parameters as

$$m_0 \to m_0 \mp m_I I_2(\boldsymbol{R})\,, \qquad k \to k \pm \frac{1}{2} A(\boldsymbol{R})\,. \tag{5.13}$$

Note that the constant shift in the prepotential is non-physical, whereas we should view the new shifted gauge coupling as physical. The approach we use in this chapter takes as its starting point the set of so-called marginal or KK-theories in 5d, which UV complete in 6d. Decoupling matter from these theories we obtain a descendant tree, each of which describes another SCFT in the UV.

5.2 Brane-webs and HW transitions

5d $\mathcal{N} = 1$ SCFTs can be realized in type IIB string theory in terms of webs of (p, q) 5- and 7-branes [115]. Here, we review the basic features of this description. Consider type IIB string theory with axio-dilaton τ and a web of 5-branes extended along the $(x_0, \ldots, x_4)$-directions and at some angle θ in the (x_5, x_6)-plane. We adopt the convention that a (p, q) 5-brane is a bound state of p D5-branes and q NS5-branes. Rotations in the (x_7, x_8, x_9)-directions realize the $SU(2)_R$ R-symmetry of the 5d theory. Each 5-brane is a $\frac{1}{2}$-BPS object, preserving 16 supercharges. To be precise, a (p, q) 5-brane at an angle θ in the (x_5, x_6)-direction imposes the condition [13]

$$\epsilon_2 = \Gamma_{01234}\,(\cos\theta\ \Gamma_5 + \sin\theta\ \Gamma_6)\,(\sin\beta\ \epsilon_1 + \cos\beta\ \epsilon_2) \tag{5.14}$$

on the supersymmetry parameters $\epsilon_{1,2}$ of type IIB, where

$$\tan\beta = \frac{\Re(p + q\tau)}{\Im(p + q\tau)}\,. \tag{5.15}$$

Additionally, a pure NS5-brane imposes

$$\epsilon_1 = -\Gamma_{01234}\,(\cos\theta\ \Gamma_5 + \sin\theta\ \Gamma_6)\,\epsilon_1\,. \tag{5.16}$$

A general configuration of branes breaks supersymmetry completely. However, one can show that brane configurations satisfying

$$\tan\theta = \tan\beta \tag{5.17}$$

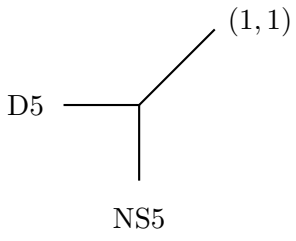
preserve 8 supercharges. This condition implies that the angle of a (p,q) 5-brane in the (x_5, x_6)-direction is completely determined by (p,q) and the choice of τ. In [17] it was shown that τ is a redundant parameter with respect to the low-energy field theory realised on the web. Therefore, it can always be normalised to $\tau = i$, so that

$$\tan\theta = \frac{p}{q}\,. \tag{5.18}$$

All brane configurations related by a global $SL(2,\mathbb{Z})$ transformation are physically equivalent and all pictures are drawn at $\tau = i$. If there are no coincident branes the most general web is engineered out of triple-intersections called junctions. At each junction, charge conservation implies

$$\sum_{i=1}^{3} \pm\,(p_i, q_i) = (0,0)\ , \tag{5.19}$$

where the signs reflect the orientation of each brane with respect to the junction. In other words, any allowed junction is locally $SL(2,\mathbb{Z})$-equivalent to the standard configuration of a D5-, an NS5- and a (1,1)-brane:



(5.20)

A generic brane-web contains both finite (internal) and semi-infinite (external) 5-branes. It is straightforward to read off the ranks of the gauge and flavor group of the 5d theory from the web. We have [17]

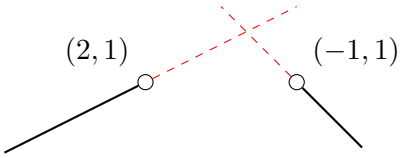
$$\begin{aligned} r &= \#\text{ local deformations}\,, \\ r_F &= \#\text{ global deformations} = \#\text{ external 5-branes} - 3\,. \end{aligned} \tag{5.21}$$

A deformation is a variation of the brane-web that leaves the type and relative position of the 5-branes invariant. Local deformations also leave the position of the external 5-branes

invariant, whereas global deformations change their positions. The position of an external 5-brane is specified by a single coordinate, corresponding to one deformation for each semi-infinite 5-brane. However, there are three unphysical global deformations comprising two global translations in the (x_5, x_6)-plane and the position of one of the external 5-branes, which is fixed by supersymmetry.

Any semi-infinite (p, q) 5-brane can be made finite by letting it end on a corresponding (p, q) 7-brane, extending in the $(x_0, \ldots, x_4, x_7, x_8, x_9)$-directions. A 7-brane will be indicated by a circle and its (p, q) charge will be implied by the angle of the 5-brane ending on it. The branch cut of a given (p, q) 7-brane will be taken to point away from the 5-brane-web, along the direction $\tan\theta = p/q$, so as to not disrupt the 5-brane configuration. Furthermore, a (p, q) 7-brane can be translated along this direction without affecting the 5d theory.

Consider a brane-web with two external 5-branes ending on 7-branes whose branch cuts (shown explicitly here as a dashed red line) intersect, e.g.



(5.22)

Going to the strong coupling point of the 5d theory corresponds to taking the length of the internal 5-branes to zero. If a brane-web contains monodromy cuts that cross, we must exchange the order of the corresponding 7-branes, preserving both the total monodromy and charge, before taking this limit. In the exchange, one 7-brane will change type because it crosses the branch cut of the other, whereas the type of the second 7-brane is preserved but the number of 5-branes that end on it changes to conserve charge. This is known as Hanany-Witten (HW) brane creation [13]. Specifically, the branch cut of a (p, q) 7-brane induces a transformation

$$M_{p,q} = \begin{pmatrix} 1 - pq & p^2 \\ -q^2 & 1 + pq \end{pmatrix} . \tag{5.23}$$

The total monodromy is given by the counter-clockwise product of the $M_{p,q}$. Exchanging two 7-branes while preserving their total monodromy implies

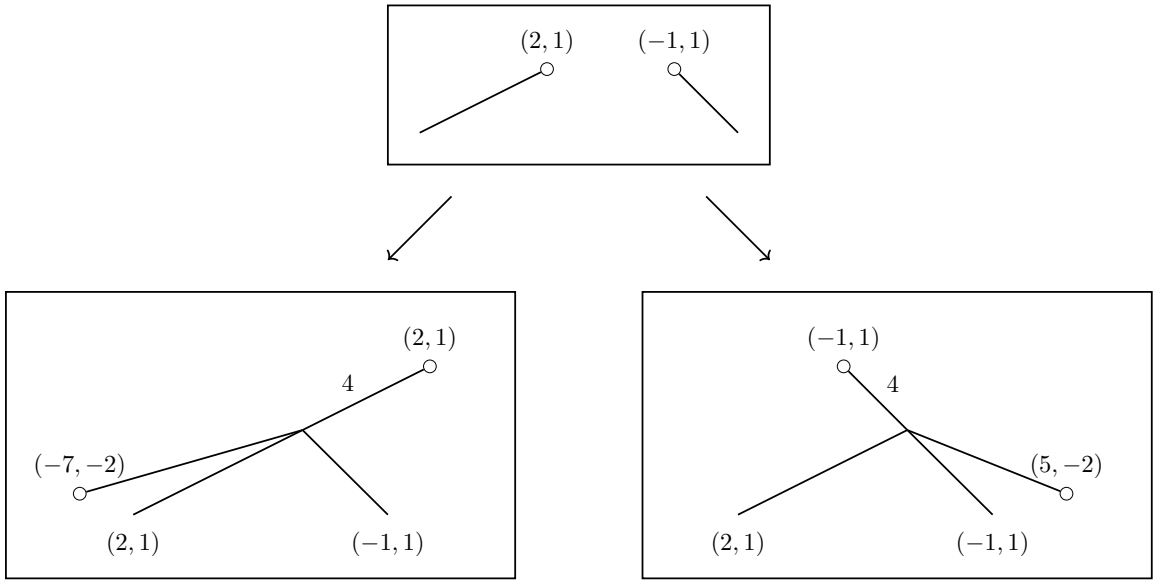
$$M_{p_1,q_1} M_{p_2,q_2} = \begin{cases} M_{p_2,q_2} M_{p_1',q_1'} , & \begin{pmatrix} p_1' \\ q_1' \end{pmatrix} = \begin{pmatrix} p_1 \\ q_1 \end{pmatrix} + (p_1 q_2 - p_2 q_1) \begin{pmatrix} p_2 \\ q_2 \end{pmatrix} \\ M_{p_2',q_2'} M_{p_1,q_1} , & \begin{pmatrix} p_2' \\ q_2' \end{pmatrix} = \begin{pmatrix} p_2 \\ q_2 \end{pmatrix} + (p_1 q_2 - p_2 q_1) \begin{pmatrix} p_1 \\ q_1 \end{pmatrix} \end{cases} . \tag{5.24}$$

In the configuration (5.22) $(p_1, q_1) = (-1, 1)$ and $(p_2, q_2) = (2, 1)$, giving $(p_1', q_1') = (-7, -2)$ and $(p_2', q_2') = (5, -2)$.

Additional 5-branes are created when a 7-brane crosses a stack of 5-branes. The number of new 5-branes created depends on how many 5-branes are in the stack. In particular, exchanging two 7-branes as in the top line of (5.24), with N_1 5-branes ending on the first 7-brane and N_2 on the second, the number of new 5-branes created is

$$\Delta N_2 = |p_1 q_2 - p_2 q_1| \, N_1 \, . \tag{5.25}$$

The number of 5-branes created in the move in the bottom line of (5.24) is obtained by taking $N_1 \leftrightarrow N_2$. For example, the two possible HW moves for the configuration in (5.22) are



(5.26)

Here, and in the following, we only write the number of coincident 5-branes if it is greater than one. As this example illustrates, performing a HW move usually leads to configurations where multiple 5-branes end on the same 7-brane.

In general, the number of 5-branes that can end on a single 7-brane is constrained by the so-called *s-rule*. Given a web that satisfies the s-rule (e.g. one where each 7-brane has a single 5-brane ending on it), performing HW moves conserves this property, i.e. it gives another consistent supersymmetric brane-web. The simplest formulation of the s-rule constrains the number of D5-branes n_{D5} that connect a single D7-brane and a stack of n_{NS5} NS5-branes to be $n_{\text{D5}} \leq n_{\text{NS5}}$. A brane-web is said to obey the s-rule if there exists a full resolution

of the web such that each junction locally obeys the s-rule [116]. The $SL(2,\mathbb{Z})$-invariant generalization of the s-rule for a junction of three branes (p_i, q_i) is

$$\left|\det \begin{pmatrix} p_i & q_i \\ p_j & q_j \end{pmatrix}\right| \geq \gcd(p_k, q_k)^2 \,, \tag{5.27}$$

for every permutation (i, j, k) of $(1, 2, 3)$.

It is possible to add other types of branes to the brane-webs, such as orientifold planes [117–119]. In the case of $O7$-planes, these can be resolved in terms of (p, q) 7-branes, and we will use the resolved webs.

5.3 Magnetic Quivers and Hasse Diagrams

The Higgs branch of a 5d $\mathcal{N} = 1$ theory $\mathcal{T}$ can be characterized in terms of its magnetic quiver (MQ) and Hasse diagram. The MQ is a graph, representing a 3d $\mathcal{N} = 4$ quiver gauge theory, whose Coulomb branch is a symplectic singularity, which is conjecturally identified with the Higgs branch of the 5d theory [120]

$$\mathrm{CB}[\mathrm{MQ}] = \mathrm{HB}[\mathcal{T}] \,. \tag{5.28}$$

In this thesis we focus exclusively on theories where the MQs are unitary gauge group quivers. The Higgs branch of 5d SCFTs has quantum corrections and the advantage of using the detour via MQs is that these instanton corrections in 5d can be understood from the exact Coulomb branch of the 3d $\mathcal{N} = 4$ MQ using the monopole formula (to compute its Hilbert series) [121–125]. The expectation is that the MQ will yield the complete Higgs branch for the 5d SCFTs.

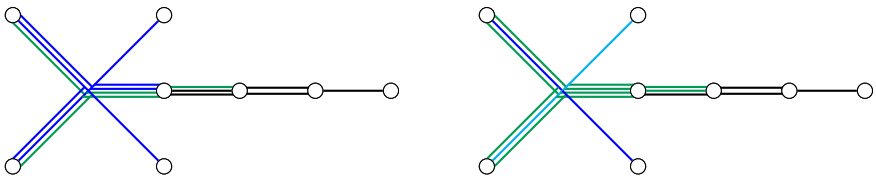
So far the MQs were derived either from the knowledge of the moduli space, or using brane-webs. We proposed a complimentary method in [2] which is the topic of chapter 6. It can be determined also for 5d SCFTs realized as M-theory on canonical three-fold singularities by employing string dualities, and relating this to a 4d SCFT in Type IIB obtained from the same canonical singularity [126]. Further compactifying to 3d and using mirror symmetry, i.e. T-duality, one finds the MQ. At present, this is however limited to hypersurface singularities, where the CB branch spectrum for the 4d SCFT can be computed.

Let us briefly review the derivation of the MQ from the brane-web for the types of theories we will be interested in. The relevant rules were conjectured in [120]. First, divide the 5-branes maximally into sub-webs that can move freely between the 7-branes, i.e. sub-webs

which conserve charge and obey the s-rule. The division is maximal in the sense that no sub-web may be decomposable into a set of (strictly) smaller sub-webs. The decomposition into sub-webs is not necessarily unique. When there is more than a single decomposition, each corresponds to a MQ and the Higgs branch of the 5d theory is given by the union of the Coulomb branches of the set of MQs. For each maximal decomposition, a set of m identical sub-webs corresponds to a gauge node with group $U(m)$ in the MQ. The number of edges k_{IJ} between a pair (I, J) of gauge nodes in the MQ is determined by selecting the two corresponding sub-webs W_I, W_J, and, viewing the 5-branes as curves in tropical geometry, computing their stable intersection $SI(W_I, W_J)$. Furthermore k_{IJ} receives contributions from the 7-branes as follows. For each 7-brane A_i, add the number X_i of combinations of two 5-branes from the respective sub-webs which attach to the 7-brane on *opposite* sides, and subtract the number Y_i of combinations that end on *the same* side. The of edges is thus

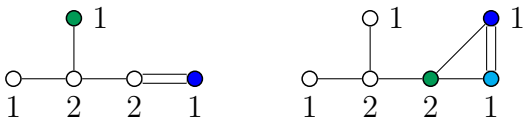
$$k_{IJ} = SI(W_I, W_J) + \sum_i X_i - \sum_i Y_i \,. \tag{5.29}$$

An example that will be used throughout chapter 6 is the brane-web realising the UV fixed point of $SU(4)_4 + 4\boldsymbol{F}$. This has two maximal sub-web decompositions



(5.30)

associated to a set of MQs



. (5.31)

From the magnetic quiver it is possible to compute the flavor symmetry algebra of the 5d SCFT. Given a MQ with nodes m_I, number of edges k_{IJ}, and number of loops ℓ_I (which will be discussed in the following chapter), we define the balance of a node as

$$\beta_I = -2m_I + 2\ell_I(m_I - 1) + \sum_{J \neq I} k_{IJ} m_J \,. \tag{5.32}$$

Naturally, there are three different types of nodes,

$$\begin{array}{lcl} \beta_I = 0 & \text{balanced} & \circ \\ \beta_I > 0 & \text{overbalanced} & \bullet \\ \beta_I < 0 & \text{underbalanced} & \bullet \end{array} \tag{5.33}$$

A MQ with an underbalanced node is said to be "bad" or "ugly", see [127]. This means that there are BPS monopole operators violating or saturating the unitary bound respectively. For ugly quivers, it is known that one can use a Seiberg duality to flow to an SCFT, together with a set of free hypermultiplets. For ugly quivers we will use the following local Seiberg duality to balance the nodes:

$$U(n_I) + (2n_I - |\beta_I|)\boldsymbol{F} \longleftrightarrow U(n_I - |\beta_I|) + (2n_I - |\beta_I|)\boldsymbol{F} + |\beta_I|\,\boldsymbol{H}\,, \tag{5.34}$$

where $\boldsymbol{H}$ indicates free hypermultiplets and $\beta_I < 0$.[4] The process of repeatedly applying this duality always terminates for ugly quivers. We regard the endpoint of this process as the MQ of the theory and do not usually include the free hypermultiplets. Then, the balanced nodes form the Dynkin diagram of a finite Lie algebra. In many cases the balanced nodes directly gives the non-abelian part of the enhanced flavor symmetry of the theory. However, we find examples in which the flavor symmetry is larger than expected from the balanced nodes. To determine the flavor symmetry in general one has to compute the Hilbert series.

The Hasse diagram is a graphical representation of the decomposition (or *foliation*) structure of the Higgs branch, a symplectic singularity. It describes a partially ordered set of symplectic leaves, with each leaf corresponding to a physical phase of the 5d SCFT. The transition from one leaf to another (respecting the partial order) is described by the transverse slice between the two leaves, which again corresponds to a symplectic singularity. The Hasse diagram can be either obtained from the standard quiver subtraction [128–130], or by the method proposed in [2] which will be discussed in the following chapter. To construct the Hasse diagram starting from a MQ representing the entire symplectic singularity, we identify all subgraphs that are elementary slices and iteratively perform quiver subtractions until the process terminates.

5.4 Map from Brane-web to Generalized Toric Polygon

As we have already discussed, 5d $\mathcal{N} = 1$ SCFTs can arise in type IIB string theory as the world-volume theory of a 5-brane-web. Another fruitful realization is by geometric engineering in M-theory compactified on $\mathbb{R}^{1,4} \times \mathrm{CY}_3$ where CY_3 is a non-compact canonical Calabi-Yau

[4] In [127] it was argued that this duality can only be applied for $\beta_I = -1$. However, evidence suggests that in the case of ugly quivers it also holds in general. For bad quivers the duality (5.34) can not be applied. Thus, in principle one first needs to check the dimensions of the monopole operators. It would indeed be interesting to derive the general duality from first principle.

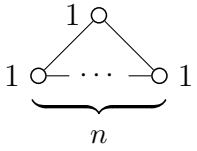
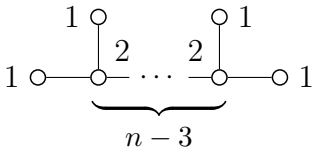
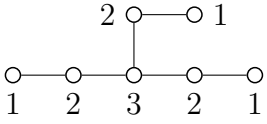
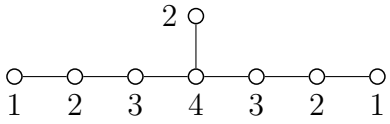
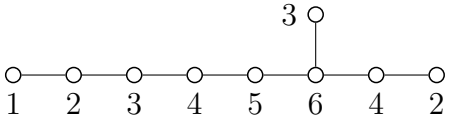
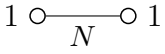
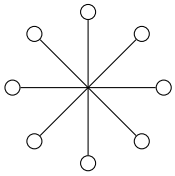
Singularity	Magnetic quiver
$\mathfrak{a}_n$	
$\mathfrak{d}_n$	
$\mathfrak{e}_6$	
$\mathfrak{e}_7$	
$\mathfrak{e}_8$	
A_{N-1}	

Table 5.3: Summary of the elementary transverse slices that can appear in the Hasse diagram of a symplectic variety defined by a unitary and simply laced magnetic quiver. For the first five lines, these are closures of minimal nilpotent orbits of type $\mathfrak{g}$. In the last line are the Kleinian singularities of type A_{N-1}, simply denoted by A_{N-1}. For each transverse slice, the second column gives a magnetic quiver.

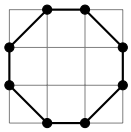
three-fold singularity. In the geometric description the Higgs branch is associated with deformations of the canonical singularity, whereas the (extended) Coulomb branch is parametrized by resolutions, i.e. Kähler deformations, of the singularity. However, while the resolutions of singular Calabi-Yau three-folds have lead to many new results for the CB, it is less clear how one can in practice determine the structure of the HB from geometry. A precise correspondence of the deformation space of the Calabi-Yau singularity and the HB of the associated 5d SCFT has only been achieved for singularities that can be realized as strictly convex toric polygons [131, 132] and, recently, for isolated hyper-surface singularities [126, 133, 134].

For a strictly convex toric Calabi-Yau three-fold singularity however, there is a beautiful and complete picture relating the M-/string theory realizations of 5d SCFTs by a one-to-one map, and where both branches of the moduli space can be determined in general from either perspective. That is, starting e.g. from a 5-brane-web in type IIB such as



(5.35)

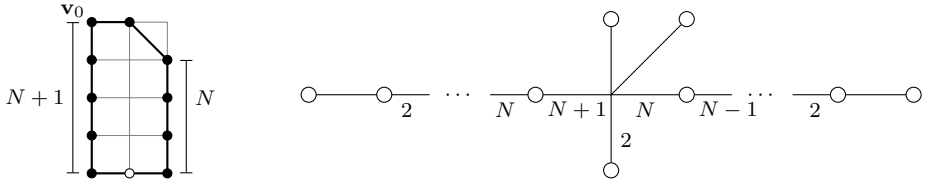
the moduli space of the corresponding 5d theory can be studied in terms of its planar and transverse brane deformations. The brane-web is dual to a strictly convex toric polygon, whose resolutions and deformations are known in general [131, 132] and equivalently map out the moduli space of the 5d theory. In particular, the one-to-one map of the type IIB and M-theory representations associates to each face (compact and non-compact) in the brane-web a vertex in the polygon, and every 5-brane is related to an edge drawn transverse to the brane:



(5.36)

That being said, many 5d SCFTs have brane-web descriptions whose duals do not fall into the class described above or even the class of toric polygons. In general, the brane-web may contain a sector where more than a single 5-brane ends on the same 7-brane, for which the dual diagram is a generalized toric polygon (GTP): a convex polygon, describing an SCFT, that can have lattice points along its edges that are *not* in the set of vertices. In particular, a set of n 5-branes ending on the same 7-brane in the web is represented in the GTP by

n line segments separated by white dots. One such theory is the strong coupling limit of $SU(N)_1 + 2N\mathbf{F}$ whose GTP and brane-web realizations are



(5.37)

where we have drawn the GTP for $N = 3$. The label indicates the length of the edge for general N, if it is greater than 1. Likewise, in the web, we will note the number of individual branes in a stack next to the segment representing it, if it is greater than 1. Notice the empty vertex on the bottom edge of the GTP, dual to the two NS5-branes ending on a single $(0, 1)$-7-brane.

It is not known how or whether one can associate a Calabi-Yau singularity to a generic GTP, and consequently a general geometric analysis of the deformation space remains out of reach. However, the duality with the brane-web extends to the decomposition that determines the magnetic quiver, generalizing the work of [131, 132], as we shall see in chapter 6.

Finally, where a gauge theory description is available, this phase is represented by a non-convex lattice polygon with a ruling, called a pre-GTP. In chapter 7 we demonstrate how to relate it to a GTP by applying a (non-unique) series of monodromy-preserving edge-moves [3], dual to Hanany-Witten brane creation, to cure the non-convexity. We then go to the strong coupling point by removing the ruling, and, in this way, arrive at a GTP.

Chapter 6

5d Higgs Branches in the Tropical Rain Forest

6.1 Introduction

Our understanding of 5d SCFTs [14–16] derives in large part from our ability to construct and study these theories in string theory. 5d $\mathcal{N} = 1$ SCFTs can arise in M-theory by compactification on a (non-compact) canonical Calabi-Yau three-fold singularity [133, 135–166], or in type IIB string theory as the world-volume theory of a 5-brane-web [13, 115, 117, 118, 167–177]. The moduli space of the 5d SCFT comprises the Higgs branch (HB) and (extended) Coulomb branch (CB), mapped out in M-theory respectively by the deformations and resolutions of the canonical singularity. Much progress has been made in the exploration of the CB, using the resolutions of singular Calabi-Yau three-folds, allowing the classification of a vast number of theories. On the contrary the deformations and their relation to the HB have been somewhat less systematically studied.

On the other hand, for many 5d SCFTs, where a 5-brane-web description is available, there has been recent progress towards a comprehensive description of the Higgs branch in terms of the associated magnetic quiver (MQ) and Hasse diagram [120, 128–130, 178–196]. The magnetic quiver represents a 3d $\mathcal{N} = 4$ quiver gauge theory, whose Coulomb branch is conjecturally identified with the Higgs branch of the 5d theory. The 3d CB is well-understood, and can be studied in detail from the representation theoretic point of view by computing its Hilbert series and highest weight generating function [121, 122, 197, 198]. The Hasse diagram, introduced in [129], is a depiction of the partially ordered set corresponding to the foliation of the Higgs branch by symplectic leaves. Any pair of leaves which can be compared in the partial order defines a transverse slice between the two leaves, which is again a symplectic singularity,

and to which one can associate a magnetic quiver. The leaves correspond physically to phases of the SCFT, while the transverse slices are associated to new theories obtained from the original theory by (a generalization of) the Higgs mechanism.

Ideally these insights should have a counterpart in the M-theory construction of said 5d SCFTs. Geometrically, there exists so far no comprehensive analysis. To counteract this, we propose here an approach which capitalizes on the developments in the 5-brane-webs. For any 5d SCFT with a brane-web realization without orientifold-planes there exists a one-to-one map to a dual representation of the theory in terms of a generalized toric polygon (GTP), or dot diagram [17, 116, 199, 200]. In particular, when the dual polygon is a conventional toric diagram, corresponding to a brane-web with a single 5-brane ending on each 7-brane, this polygon precisely represents the canonical Calabi-Yau singularity on which M-theory can be compactified to give rise to the same 5d SCFT. Utilizing the map of 5-brane-webs to generalized toric polygons, we identify the rules for determining the magnetic quiver and Hasse diagrams in terms of the polygons.

This approach provides a first step to generalizing the deformation theory of strictly convex Calabi-Yau singularities. Applied to strictly convex polygons, our approach reproduces precisely the mathematical results of Altmann [131, 132]: the deformations are parametrized in terms of the Minkowski sum decomposition of the polygon. The Altmann algorithm then further maps these to the algebraic deformations of the canonical singularity. This last step requires to first find the map from GTPs to canonical singularities. This is a very interesting question to which we hope to return in the future.

6.2 Strategy: Higgs Branches from GTP

In this paper we consider 5d SCFTs defined by so-called generalized toric polygons (GTP) P (or dot diagrams) introduced in [116]. We denote these theories by $\mathcal{T}_P$. The GTPs are lattice polygons, which generalize the concept of a toric fan for a Calabi-Yau three-fold. They map one-to-one to a 5-brane-web $\mathcal{W}_P$

$$P \quad \longleftrightarrow \quad \mathcal{W}_P \,. \tag{6.1}$$

In the case when P is a toric polygon, we can associate an actual Calabi-Yau three-fold geometry $\mathbf{X}_P$ to it, and the dual web is associated to a tropical geometry [201].

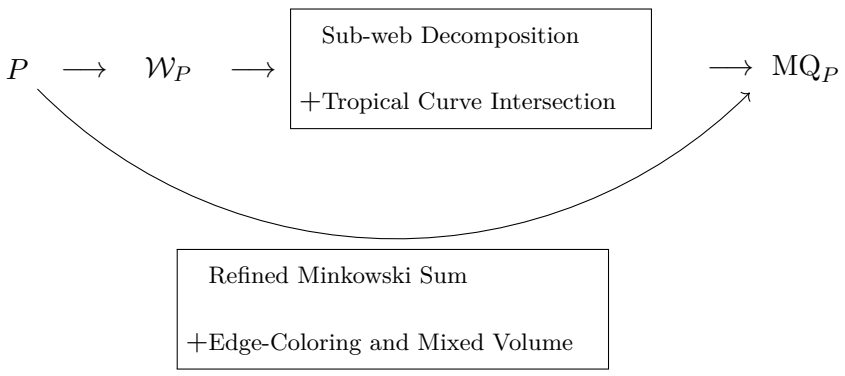
The moduli spaces of such 5d SCFTs are parametrized by the vevs of scalar fields, either in the vector multiplet – the Coulomb branch (CB) – or the hypermultiplet – Higgs branch (HB). One of the challenges has been to compute the Higgs branch from a geometric approach to 5d SCFTs, though recent progress has been made in [126] for hypersurface singularities. Unlike the CB in 5d, the HB receives quantum corrections from instantons – in M-theory on a canonical singularity, these are M2-brane instantons. Computing these directly in 5d is a formidable task.

In the 5-brane-webs, an alternative proposal was made that identifies the HB in 5d with the CB of a magnetic quiver (MQ), which is a 3d $\mathcal{N} = 4$ quiver gauge theory (and in the current context, with $U(N)$ gauge nodes). The conjecture in [120] is that the Coulomb branch of the magnetic quiver MQ_P associated to a GTP P can be identified with the Higgs branch of the 5d SCFT

$$\mathrm{CB}[\mathrm{MQ}_P] = \mathrm{HB}[\mathcal{T}_P]\,. \tag{6.2}$$

Both of these spaces are hyper-Kähler cones, and the isomorphism is as such. The advantage however is that the CB of 3d $\mathcal{N} = 4$ theories is much better under control, using the monopole formula to compute their (refined) Hilbert series [121], and subsequent work [122–125]. The dressed monopole operators in 3d resum the 5d instanton corrections, and conjecturally this yields the correct hyper-Kähler cone for the 5d HB. A derivation using the M-theory geometry makes use of dualities in string theory, relating the 5d SCFT to a 4d SCFT obtained by compactifying Type IIB on the same geometry [126]. Reducing to 3d and applying mirror symmetry, realized as T-duality, identifies the magnetic quiver in certain instances.

The approach taken in this paper makes use of the one-to-one map in (6.1), which allows us to identify in the GTP P each of the steps in the construction of the magnetic quiver in the brane-web: the strategy, which will be expanded in section 6.6, is:



(6.3)

In the following we identify the direct map from P to MQ_P. We use the rules derived from the brane-webs, and translate these into the language of the generalized toric polygons. We find that in the case of strictly convex toric polygons, we make contact with the work of Altmann on versal deformations [131, 132].

In addition we extract the foliation structure of this hyper-Kähler cone in terms of symplectic leaves, which is achieved combinatorially in terms of the quiver subtractions [128]. The partially ordered set of such leaves is the Hasse diagram. The elementary transverse slices of the Hasse diagram of the 5d Higgs branches for the theories we consider here can be closures of minimal nilpotent orbits $\mathfrak{g}$ or Kleinian singularities – see table 5.3, which includes their magnetic quivers [202, 203]. In some other instances, there can also be elementary slices of "rank-0" [129, 186], or of more exotic type (see for instance [204, 205]). However a full classification of possible leaves is unknown. In our discussion of the Hasse diagram, which is distinct from the derivation of the magnetic quiver, we focus on the symplectic leaves that appear in table 5.3.

Although we propose a way to derive the MQ from P directly, a first principle derivation from geometry is of course missing, except for the strictly convex toric case. In fact for P not a toric, but a generalized toric polygon, it is thus far unknown what the associated canonical singularity is. Building this dictionary should now be strongly motivated, given the efficiency of how we can determine the MQs from P, using very simple combinatorial rules – which simplify not only the brane-web based analysis, but also connect to the known geometric constructions in toric geometry.

6.3 Higgs Branches for 5d SCFTs from Edge Colorings

We start our analysis by presenting the direct construction of the MQ_P from the GTP P in (6.3). We review properties of toric polygons and their composition and introduce generalizations that apply to GTPs. Furthermore, we provide criteria for a GTP (or a subpolygon thereof) to satisfy the so-called *s-rule*, which in the dual brane-web ensures that the configuration preserves supersymmetry.

With this background, we then introduce the coloring of a GTP, which amounts to a generalization of a Minkowski sum decomposition for toric polygons. Finally, we give a short

algorithm that associates a tropical quiver (TQ) to each coloring of a given GTP. We conjecture that the tropical quiver can then be identified with the magnetic quiver characterizing the 5d Higgs branch of the SCFT – and in cases when there are multiple cones of the Higgs branch, i.e. multiple colorings, the union of these tropical quivers comprise the full Higgs branch of the 5d SCFT.

6.3.1 GTPs and Minkowski Sums

The concept of a generalized toric polygon was first introduced in [116] as a dual graph to a 5-brane-web with multiple 5-branes ending on a single 7-brane. This generalization was motivated, as such diagrams furnish 5d SCFTs. We define a generalized toric polygon P as a lattice polygon, i.e. in terms of a set of vertices $\boldsymbol{v}_i \in \mathbb{Z}^2$, and edges, E_α, $\alpha = 1, \cdots, n_E$, which connect a subset of the vertices. A toric polygon is a special case of this, where each lattice point on an edge is also a vertex. This is not necessarily the case for a GTP. The absent lattice points are sometimes referred to as 'white dots'. The GTP is the convex hull of the vertices. The set of all vertices and edges will be denoted by

$$V_b = \{\boldsymbol{v}_i \in \mathbb{Z}^2\}\,, \qquad E = \cup_\alpha E_\alpha\,. \tag{6.4}$$

A subset of the edges are the external edges, which are the boundary of the GTP,

$$\partial P = \cup_\alpha E_\alpha^\partial \equiv E^\partial \subset E\,, \tag{6.5}$$

and likewise the complement of these in E are the internal edges, $E \backslash E^\partial \equiv E^{\text{in}}$. For the rest of this section we will assume $E^{\text{in}} = \emptyset$. We will return to the treatment of GTPs with internal edges in section 6.4.1.

The set of vertices is in general a subset of the set of points

$$V_b \subset E \cap \mathbb{Z}^2\,. \tag{6.6}$$

The set of points that are in the complement $(E^\partial \cap \mathbb{Z}^2)\backslash V_b \equiv V_w$, will sometimes be denoted by white dots/vertices, and

$$V = V_b \cup V_w\,, \tag{6.7}$$

denotes the complete set of vertices – black and white. The vertices along an edge E_α, will be labeled by $\boldsymbol{v}_{\alpha,i} \in V_b$, $i = 0, \cdots, b_\alpha + 1$. If a vertex is the boundary of an edge,

$$\partial E_\alpha = \boldsymbol{v}^{\text{ex}}_{\alpha,0} \cup \boldsymbol{v}^{\text{ex}}_{\alpha,b_\alpha+1}\,, \tag{6.8}$$

we refer to it as an extreme vertex, which are always $\boldsymbol{v}_{\alpha,i}$ with $i = 0$ and $i = b_\alpha + 1$. Note that extreme vertices cannot lie in the interior of any other edge and (for now, in the absence of internal edges) must be part of the boundary of two edges.

Given that an edge $E_\alpha = \overline{\boldsymbol{v}^{\text{ex}}_{\alpha,0}\boldsymbol{v}^{\text{ex}}_{\alpha,b_\alpha+1}}$ is a vector in $\mathbb{R}^2$ connecting lattice points, it can be identified with a pair of integers. We call the greatest common divisor of this pair of integers

$$\lambda_\alpha = \text{gcd}(E_\alpha)\,, \tag{6.9}$$

where we note that this is $SL(2,\mathbb{Z})$ invariant. We then define the reduced vector

$$L_\alpha = \frac{E_\alpha}{\lambda_\alpha} \equiv (x_\alpha, y_\alpha)\,. \tag{6.10}$$

Furthermore, we define an orientation of the external edges by

$$\boldsymbol{v}^{\text{ex}}_{\alpha+1,0} = \boldsymbol{v}^{\text{ex}}_{\alpha,b_\alpha+1}\,, \tag{6.11}$$

where we understand the periodicity in the α-indices. Because of closedness of the boundary of P

$$0 = \sum_\alpha \lambda_\alpha L^\partial_\alpha\,, \tag{6.12}$$

where the L^∂_α are the line segments of the external edges and we take the sum with the orientation implied by (6.11). Finally, we define a partition of λ_α in terms of the vertices along an external edge E^∂_α as

$$\lambda_\alpha = \sum_{i=1}^{b_\alpha+1} \mu_{\alpha,i}\,, \qquad \mu_{\alpha,i} L^\partial_\alpha = \overline{\boldsymbol{v}_{\alpha,i}\boldsymbol{v}_{\alpha,i-1}}\,, \tag{6.13}$$

with b_α the number of non-extreme vertices along E^∂_α. Note that for a toric polygon these partitions are always given by $\{1^{b_\alpha+1}\}$. We order the partition in descending magnitude

$$\mu_{\alpha,x} \geq \mu_{\alpha,x+1}\,, \tag{6.14}$$

where the index x is introduced as an ordered version of the index i. This ordered partition will also be referred to as $\{\mu_\alpha\}$.

In the following we will make use of the standard partial order pertaining to a set of integer partitions of an integer $N \geq 1$, called the *dominance ordering*. We therefore review it here for the convenience of the reader:

Definition 1 (Dominance Ordering)**.** *Let ρ and ρ' be two partitions of N, which means that they are sequences of integers satisfying*

$$N = \sum_{1\leq i} \rho_i = \sum_{1\leq i} \rho'_i \qquad \textit{and} \qquad \rho_1 \geq \rho_2 \geq \cdots \geq 0\,, \quad \rho'_1 \geq \rho'_2 \geq \cdots \geq 0\,. \tag{6.15}$$

The dominance order is defined as follow: we say $\{\rho\} \geq \{\rho'\}$, if for all $j \geq 1$, we have

$$\sum_{1\leq i\leq j} \rho_i \geq \sum_{1\leq i\leq j} \rho'_i\,, \tag{6.16}$$

i.e. the smallest partition is given by $\{1^N\}$, whereas the largest partition is $\{N\}$.

Example. In tandem with the general analysis in this section, we go through one example that illustrates all the salient points. The example is the SCFT associated to an IR description given by

$$SU(4)_4 + 4\boldsymbol{F}\,, \tag{6.17}$$

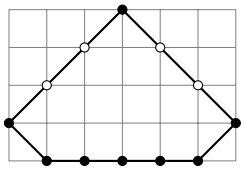
which has vertices

$$V_b = ((0,0),(1,-1),(2,-1),(3,-1),(4,-1),(5,-1),(6,0),(3,3))\,, \tag{6.18}$$

with no internal lines. From this we can read off the white dots

$$V_w = ((5,1),(4,2),(2,2),(1,1))\,, \tag{6.19}$$

which we draw as

$P =$  (6.20)

We label the edges in counter-clockwise order, beginning on the lower left

$$\begin{aligned} E_\alpha &= ((1,-1),(4,0),(1,1),(-3,3),(-3,-3))\,,\\ L_\alpha &= ((1,-1),(1,0),(1,1),(-1,1),(-1,-1))\,,\\ \lambda_\alpha &= (1,4,1,3,3)\,. \end{aligned} \tag{6.21}$$

From the distribution of black and white vertices we can read off

$$b_\alpha = (0,3,0,0,0)\,, \qquad \{\mu_\alpha\} = (\{1\},\{1^4\},\{1\},\{3\},\{3\})\,. \tag{6.22}$$

For a conventional toric polygon there exists a composition rule, the Minkowski sum, which is instrumental in analyzing the deformations of a toric polygon [131, 132]. We give the definition of a Minkowski sum of two polygons below, as well as a generalization that we introduce for GTPs, which we call the *refined Minkowski sum*, from which we define a notion of colored GTPs, that underlie the construction of the magnetic quiver.

Definition 2 (Minkowski Sum)**.** *A Minkowski sum of two polygons P_a and P_b is defined by*

$$P_a + P_b = \{\boldsymbol{v}_a + \boldsymbol{w}_b\} \,, \tag{6.23}$$

where $\boldsymbol{v}_a \in V_{P_a}$ and $\boldsymbol{w}_b \in V_{P_b}$ are the vertices of P_a and P_b.

Note that this definition does not distinguish between black and white vertices. This means that the Minkowski sum is not uniquely defined for a set of GTPs. We will thus introduce a refinement of the Minkowski sum, which can accommodate the presence of white dots in a GTP.

Definition 3 (Refined Minkowski Sum)**.** *Let P_a and P_b be GTPs. We define their refined Minkowski sum (or partition sum) as*

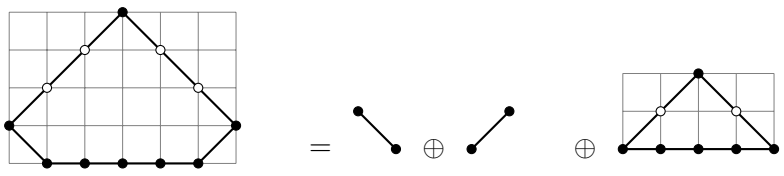
$$P_a \oplus P_b \,, \tag{6.24}$$

such that the edges agree with the ones of $P_a + P_b$, i.e. the ordinary Minkowski sum, and the partitions are

$$\mu_{\alpha,x}^{P_a \oplus P_b} = \mu_{\alpha,x}^{P_a} + \mu_{\alpha,x}^{P_b} \,. \tag{6.25}$$

Contrary to the Minkowski sum, the partition sum uniquely determines the partition of all the edges of the resulting GTP. In other words, it imposes a unique configuration of black and white vertices along the edges (up to an irrelevant reordering) of the resulting GTP.

Example. (Continued) We can write P in (6.20) as a refined Minkowski sum



. (6.26)

Note that the third summand cannot be further decomposed due to the $\{1^4\}$ partition on the lower edge. In terms of the partitions we have

$$\begin{aligned}\{\mu_\alpha^P\} &= \Big(\{1\},\{1^4\},\{1\},\{3\},\{3\}\Big) \\ &= (\{1\},-,-,\{1\},-) + (-,-,\{1\},-,\{1\}) \\ &+ (-,\{1^4\},-,\{2\},\{2\})\,.\end{aligned} \tag{6.27}$$

Finally, we review a well-known concept in tropical geometry, the mixed volume of a set of summands inside a polygon. The mixed volume is defined purely in terms of the edges of the summands and so can readily be computed for any GTP. We will use the mixed volume in the following to construct the magnetic quiver.

Definition 4 (Mixed Volume)**.** *Let P be a d-dimensional (refined) Minkowski sum*

$$P = \sum_{c=1}^{d} S^c\,. \tag{6.28}$$

Consider the object

$$P(\delta^c) = \sum_{c=1}^{d} \delta^c S^c\,, \tag{6.29}$$

where the $\delta^c \in \mathbb{R}$ are scaling parameters. Then, the volume of P is a formal polynomial in the δ^c of degree d, denoted by $vol_P(\delta^c)$. The mixed volume of d Minkowski summands inside P is given by the coefficient

$$MV(S^1,\ldots,S^d) = \left.vol_P(\delta^c)\right|_{\delta^1\ldots\delta^d}\,. \tag{6.30}$$

For the derivation of the magnetic quiver, only the mixed volume of two polygons will be relevant. Let P be a (refined) Minkowski sum as above for $d = 2$, i.e. take $P = S^1 + S^2$ and consequently $P(\delta^1,\delta^2) = \delta^1 S^1 + \delta^2 S^2$. By definition we have, for some constants V^1 and V^2,

$$\mathrm{vol}_P(\delta^1,\delta^2) = \mathrm{V}^1\left(\delta^1\right)^2 + \mathrm{MV}(S^1,S^2)\delta^1\delta^2 + \mathrm{V}^2\left(\delta^2\right)^2\,, \tag{6.31}$$

where the volume is just the Euclidean area. Consider the cases $P(1,0) = S^1$ and $P(0,1) = S^2$. Then, we have

$$\mathrm{Area}(S^1) = \mathrm{V}^1\,, \qquad \mathrm{Area}(S^2) = \mathrm{V}^2\,. \tag{6.32}$$

Furthermore, in the case $P(1,1) = P$ we then have

$$\mathrm{Area}(P) = \mathrm{Area}(S^1) + \mathrm{MV}(S^1,S^2) + \mathrm{Area}(S^2)\,, \tag{6.33}$$

from which it follows that the mixed volume of two Minkowski summands is given by

$$\mathrm{MV}(S^1, S^2) = \mathrm{Area}\left(S^1 + S^2\right) - \mathrm{Area}\left(S^1\right) - \mathrm{Area}\left(S^2\right) , \tag{6.34}$$

where we use the Euclidean metric to compute the areas.

6.3.2 The s-rule

Not all GTPs give rise to a supersymmetric theory in 5d (unlike any convex toric polygon). It is possible for a GTP to have an insufficient distribution of vertices (in a sense, too many white dots). This is the GTP equivalent of a web configuration that is non-supersymmetric because it has too many 5-branes ending on a single 7-brane – this is referred to as a web that does not satisfy the so-called *s-rule*. Determining whether a GTP satisfies the s-rule is a highly non-local problem. In [116] it was argued that a GTP P obeys the s-rule, if there exists a consistent resolution, i.e. a tessellation, of P into tiles. Here we generalize the definition of such a tile and introduce notions of minimality and irreducibility, related to the s-rule.

Definition 5 (Tiles)**.** *A tile T is a GTP such that*

1. *$E_\alpha = (E_1, E_2, E_3, E_4)$, where $L_4 = -L_2$ and $\lambda_2 \geq \lambda_4$ where we allow $\lambda_4 = 0$. Thus, T is either a trapezoid or a triangle.*

2. *The partitions are*

$$\{\mu_\alpha\} = \{\lambda_\alpha\} , \tag{6.35}$$

   i.e. T has no non-extreme vertices.

3. *Define the auxiliary GTP $\widetilde{T}$ with*

$$\widetilde{L}_\alpha = (L_1, L_2, L_3) , \qquad \widetilde{\lambda}_\alpha = (\lambda_1, \lambda_2 - \lambda_4, \lambda_3) , \qquad \{\widetilde{\mu}_\alpha\} = \{\widetilde{\lambda}_\alpha\} , \tag{6.36}$$

   such that T is the refined Minkowski sum of the triangle $\widetilde{T}$ and the line of length λ_4 along E_4. Then,

$$\widetilde{\lambda}_\alpha \widetilde{\lambda}_\beta \left|\det(\widetilde{L}_\alpha, \widetilde{L}_\beta)\right| \geq (\widetilde{\lambda}_\gamma)^2 , \qquad \forall \alpha \neq \beta , \ \alpha \neq \gamma , \ \beta \neq \gamma . \tag{6.37}$$

With this general definition of a tile, we use the requirement of [116, 206] to determine whether a GTP respects the s-rule. We furthermore define concepts of minimality and irreducibility that are related to the s-rule, and which will be essential input for our definition of a coloring.

Definition 6 (s-Rule, Minimality, Irreducibility, and IMPs)**.** *Let P be a GTP with edges E_α of length λ_α and partitions $\{\mu_\alpha\}$.*

1. *P is said to obey the s-rule, if P can, by the inclusion of internal edges, be tessellated by tiles.*

2. *Let $\widetilde{P}$ be a GTP with edges E_α of length λ^α and partitions*

$$\{\widetilde{\mu}_\alpha\} > \{\mu_\alpha\}\,, \tag{6.38}$$

   i.e. $\widetilde{P}$ is obtained from P by removing vertices along the edges. P is said to obey the s-rule minimally (or we say that P itself is minimal) if $\widetilde{P}$ does not obey the s-rule for any choice of $\{\widetilde{\mu}_\alpha\}$.

3. *P is irreducible if there is no decomposition*

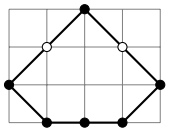
$$P = P_1 \oplus P_2\,, \tag{6.39}$$

   such that P_1 and P_2 obey the s-rule.

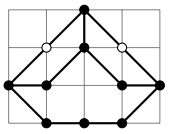
If P is irreducible and obeys the s-rule minimally, we say that P is an IMP, for Irreducible and Minimal Polygon.

The idea is that, given any GTP as a starting point, one can always find a minimal GTP by removing vertices (i.e. converting black vertices into white ones) in the original polygon. The minimal polygon has the largest possible number of white dots, whilst still satisfying the s-rule, i.e. there is no possible way to remove another vertex from the GTP without breaking supersymmetry. On the other hand, a GTP is said to be irreducible if it cannot be further decomposed into a partition sum of two other polygons. It is possible for a GTP to be minimal but not irreducible, or irreducible but not minimal. In the following section, we will require both conditions to be met by the building blocks of the coloring. To avoid notational clutter, an irreducible GTP, that obeys the s-rule minimally is called an irreducible minimal polygon (IMP).

Example. (Continued) Let us return to the example introduced in (6.20). Consider a sub-polygon Q that sits inside P, given by

$Q =$  (6.40)

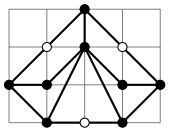
A way to tesselate Q is

$Q \to$  (6.41)

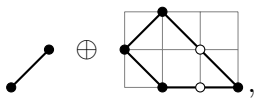
where we have omitted the triangulation of the part of the GTP that is completely surrounded by black vertices, as these can always be triangulated in a standard toric way. We can easily check that the two symmetric trapezoids are tiles. Thus, Q obeys the s-rule. We check whether Q is minimal by defining $\widetilde{Q}$ in which we have removed the only allowed vertex, which sits on the lower edge. In terms of partitions we have

$$\{\widetilde{\mu}_2\} = \{2\} > \{1^2\} = \{\mu_2\}\,, \tag{6.42}$$

satisfying (6.38). We find that $\widetilde{Q}$ still obeys the s-rule, since there exists a valid resolution of $\widetilde{Q}$ given by

$\widetilde{Q} =$  (6.43)

Thus, while Q is not a minimal polygon, $\widetilde{Q}$ is, since there are no more vertices that can be removed in $\widetilde{Q}$. We can also check that $\widetilde{Q}$ is irreducible. For example, we could try to write $\widetilde{Q}$ as a partition sum

 , (6.44)

but then the last summand does not obey the s-rule itself. Thus, $\widetilde{Q}$ is an IMP.

6.3.3 The r-rule

We now turn to the discussion of the rank of a GTP/web. When studying these constructions from a general point of view as we do here, a natural question is whether any web/GTP gives rise to a 5d SCFT. Clearly there are several basic consistency requirements that need to be

satisfied: charge conservation (which is implemented in the GTP by these forming polygons) and supersymmetry, which is implemented in terms of the s-rule. However we argue that these conditions alone still can be insufficient to guarantee that the theory realized on the associated 5-brane system is in fact a 5d SCFT.

We propose that in addition to the charge conservation and s-rule, another condition needs to be satisfied for a GTP/web to give rise to a 5d SCFT, namely that its rank be non-negative. We define the rank of a GTP P as

$$r(P) = r_0 - \frac{1}{2}\sum_{\alpha}\sum_{x=1}^{b_\alpha+1}\mu_{\alpha,x}\left(\mu_{\alpha,x}-1\right)\,, \tag{6.45}$$

where r_0 is the number of internal nodes of P. We can use Pick's theorem [207] to write this as

$$r_0 = \text{Area}(P) + 1 - \frac{1}{2}\sum_{\alpha}\lambda_\alpha\,, \tag{6.46}$$

where $\text{Area}(P)$ is the Euclidean area of P. Putting this together, and using (6.13), this gives

$$r(P) = \text{Area}(P) + 1 - \frac{1}{2}\sum_{\alpha}\sum_{x=1}^{b_\alpha+1}\mu_{\alpha,x}^2\,. \tag{6.47}$$

We conjecture that this coincides with the gauge rank of the 5d gauge theory or SCFT that P represents. This is substantiated by agreement in all examples considered in [2, 3], and by the invariance of (6.47) under edge-moves. Therefore, to make sense of a GTP as associated to a 5d theory, its rank r should be non-negative.

Definition 7 (r-rule)**.** *Let P be a GTP with edges E_α of length λ_α and partitions $\{\mu_\alpha\}$. P is said to obey the r-rule, if*

$$r(P) \geq 0\,. \tag{6.48}$$

It is straight forward to show that the r-rule implies the s-rule for triangle GTP or trinion webs, and is thus strictly stronger. To show this, consider a triangular GTP P with edges $E_\alpha, \alpha = 1, 2, 3$, of length λ_α and partitions $\{\mu_\alpha\} = \{\lambda_\alpha\}$, i.e. P has no non-extreme vertices. The area of P is given by

$$\text{Area}(P) = \frac{1}{2}\lambda_\alpha\lambda_\beta|\det(L_\alpha, L_\beta)|\,, \tag{6.49}$$

for any choice of $\alpha \neq \beta$. Thus, the rank of P is

$$2r = \lambda_1\lambda_2|\det(L_1, L_2)| - \lambda_1^2 - \lambda_2^2 - \lambda_3^2 + 2\,, \tag{6.50}$$

and equivalently for all other permutations of (1,2,3). From the above it immediately follows that

$$\Big(\lambda_1\lambda_2|\det(L_1,L_2)| - \lambda_3^2\Big) = 2r + (\lambda_1^2-1) + (\lambda_2^2-1)\,. \tag{6.51}$$

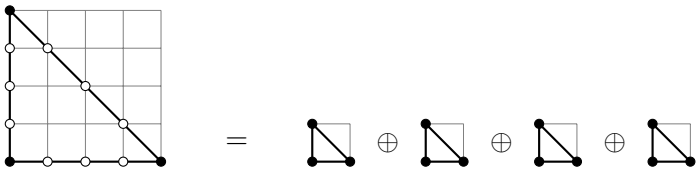
Since $\lambda_\alpha \geq 1$, the r-rule implies

$$\lambda_1\lambda_2|\det(L_1,L_2)| \geq \lambda_3^2\,, \tag{6.52}$$

and similarly for the other permutations, which is precisely the s-rule for a triangular GTP, given in definition 6.

Example. (Continued) Let us illustrate these concepts on the example introduced in (6.20). The number of internal dots is $r_0 = 12$, which can be computed using Pick's theorem (6.46) as $r_0 = 18+1-\frac{1}{2}(1+3+1+3+3+3) = 12$. This would be the rank of the theory if all the vertices on the edges of (6.20) were black. However the presence of white dots reduces the rank to $r = r_0 - \frac{1}{2}(3\cdot 3(3-1)) = 3$. Alternatively, the rank can be computed directly from (6.47) as $r = 18+1-\frac{1}{2}(5\cdot 1^2 + 3\cdot 3^2) = 3$. The conclusion is that the GTP (6.20) satisfies the r-rule.

Example. Let us consider an example of a GTP which satisfies the s-rule but violates the r-rule, i.e. it has negative rank. One such GTP is



(6.53)

with

$$L_\alpha = ((1,0),(-1,1),(0,-1))\,, \qquad \lambda_\alpha = (4,4,4)\,, \qquad \mu_{\alpha,x} = (\{4\},\{4\},\{4\})\,. \tag{6.54}$$

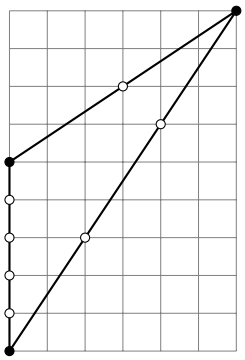
Clearly, this GTP satisfies the s-rule as, according to definition 5, it is itself a resolution tile, given that it satisfies 6.37 as

$$4\cdot 4\cdot 1 \geq 4^2\,. \tag{6.55}$$

The rank r of this GTP is

$$r = \frac{4\cdot 4}{2} + 1 - \frac{3}{2}\cdot 4^2 = -15\,. \tag{6.56}$$

Example. In the previous example, the GTP was a Minkowski multiple of a simpler GTP. We now show that there also exist irreducible GTPs which violate the r-rule while satisfying the s-rule. Consider



(6.57)

for which the data is

$$L_\alpha = ((2,3),(-3,-2),(0,-1))\,, \qquad \lambda_\alpha = (3,2,5)\,, \qquad \mu_{\alpha,x} = (\{3\},\{2\},\{5\})\,. \tag{6.58}$$

Again, this GTP is itself a resolution tile, which satisfies 6.37 for each edge:

$$3\cdot 2\cdot 5 \geq 5^2\,, \qquad 3\cdot 5\cdot 2 \geq 2^2\,, \qquad 2\cdot 5\cdot 3 \geq 3^2\,. \tag{6.59}$$

However the rank r of this GTP is

$$r = \frac{5\cdot 6}{2} + 1 - \frac{1}{2}(3^2+2^2+5^2) = -3\,. \tag{6.60}$$

It would be very interesting to derive this r-rule from first principles. However, we should alert the reader, that even the r-rule can be insufficient to guarantee that the GTP corresponds to a 5d SCFT. There can e.g. be magnetic quivers arising from GTPs that are bad quivers. In such instances we would conjecture that the associated 5d theory is not an SCFT. Of course this precise correspondence between SCFTs and GTPs requires further investigation.

6.3.4 Colorings of GTPs

In this section we define the notion of *coloring* of a GTP, which is the crucial step in determining the magnetic quiver. A coloring of a polygon is dual to a maximal subdivision of the 5-brane-web into consistent, supersymmetric sub-webs. The definition relies on the data of the polygon, as well as the generalized decomposition rule, the refined Minkowski sum, which was introduced in section 6.3.1. Furthermore, an essential feature of the building blocks of the coloring is that they represent minimal supersymmetric configurations. This criterion is

implemented by requiring irreducibility and minimality with respect to the s-rule, see section 6.3.2.

Algorithm 1 (Colored Polygon)**.** *Let P be a GTP (with no internal edges), with edge lengths λ_α. Let $\{\lambda_\alpha^c \in \mathbb{N}\}$ be a partition of the edge lengths, such that*

$$\sum_{c=1}^{n_c} \lambda_\alpha^c = \lambda_\alpha \,, \tag{6.61}$$

where n_c is the number of colors, and along each edge E_α of P, λ_α^c segments L_α are colored by c. A partition defines a colored GTP $(P, \{\lambda_\alpha^c\})$, if the following conditions are met:

1. *For each $c = 1, \cdots, n_c$ the associated line segments form a polygon, i.e.*

$$0 = \sum_\alpha \lambda_\alpha^c L_\alpha \,. \tag{6.62}$$

We denote these color sub-polygons by S^c. [1]

2. *Each S^c is a refined Minkowski sum of m_c times the same IMP T^c,*

$$S^c = \underbrace{T^c \oplus \cdots \oplus T^c}_{m^c} , \tag{6.63}$$

and we require that the IMP T^c satisfies the r-rule

$$r(T^c) \geq 0 \,. \tag{6.64}$$

Furthermore, the IMPs used for different colors must be distinct,

$$T^c \neq T^d \,, \qquad c \neq d \,. \tag{6.65}$$

3. *For each α,*

$$\{\mu_\alpha\} \leq \sum_{c=1}^{n_c} \{\mu_\alpha^c\} \,, \tag{6.66}$$

where we use the dominance partial order of the partitions defined by (6.13) *for P and S^c respectively.*

We then write

$$P \leq \bigoplus_{c=1}^{n_c} S^c \,, \qquad P = S^1 + \cdots + S^{n_c} \,. \tag{6.67}$$

[1] This also include the case of two parallel lines, as e.g. in (6.73).

For strict inequality of the partitions in (6.66) *we also write* $P < \bigoplus_{c=1}^{n_c} S^c$.

In other words, we color the edges of a GTP such that the edges pertaining to a single color form a closed sub-polygon S^c. A closed sub-polygon must be made up of a number m^c of identical IMPs T^c. We require that no two distinct sub-polygons are comprised of the same IMP (in such a situation the two sub-polygons are identified and the resulting multiple of tiles m^c is the sum). The final condition essentially ensures that all the sub-polygons fit simultaneously into the GTP. The above conditions were derived by using the map from brane-web to GTP to identify the dual concept of a maximal subdivision of the web into sub-webs. The details of this map are explained in section 6.6.

Example. (Continued) We discuss the coloring of the example (6.20). We need to determine the colored sub-polygons that are multiples of IMPs. We already know of one IMP, $\widetilde{Q}$ in (6.43), defining a blue sub-polygon S^b with $m^b = 1$. The data of the blue sub-polygon inside P is

$$\lambda^b_\alpha = (1,2,1,2,2)\,, \qquad \{\mu^b_\alpha\} = (\{1\},\{2\},\{1\},\{2\},\{2\})\,. \tag{6.68}$$

We can check that another IMP defines a green sub-polygon S_g with $m_g = 1$ and

$$\lambda^g_\alpha = (0,2,0,1,1)\,, \qquad \{\mu^g_\alpha\} = (-,\{1^2\},-,\{1\},\{1\})\,. \tag{6.69}$$

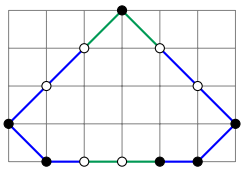
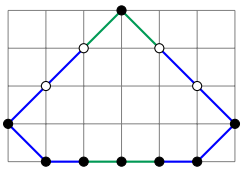
Combining the two colors we obtain

$$\{\mu^b_\alpha\} + \{\mu^g_\alpha\} = (\{1\},\{3,1\},\{1\},\{3\},\{3\}) > (\{1\},\{1^4\},\{1\},\{3\},\{3\}) = \{\mu_\alpha\}\,, \tag{6.70}$$

so indeed

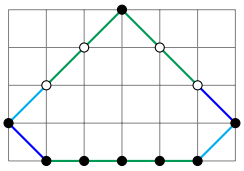
$$P < S^b \oplus S^g\,. \tag{6.71}$$

We can draw this as

$S^b \oplus S^g =$  $>$  $= P$ (6.72)

Note that the two GTPs have the same coloring but different partitions. From now on, we only draw the partitions of the full GTP (in this case P). We can actually check that there

is a second coloring of P, given by

$$S^b \oplus S^g \oplus S^c > \quad \text{} \tag{6.73}$$

In this coloring,

$$S^g = T^g \oplus T^g \,, \tag{6.74}$$

so $m^g = 2$, in other words, the green sub-polygon has multiplicity 2.

In the strictly convex toric case, our definition of a coloring exactly reduces to identifying the decomposition of a given polygon into Minkowski summands, which was shown in [131, 132] to parametrize the deformations of the geometry.

Color-Subdivided GTPs. Before we show how to associate a quiver to a colored GTP, we will explain how to graphically determine the mixed volume of definition 4, between two colored sub-polygons. To this end, we define a *color sub-division* of a colored GTP $(P, \{\lambda^c_\alpha\})$, in terms of uni-colored polygons and bi-colored parallelograms. The sub-division agrees with the coloring of the edges of P on the boundary, and extends this to the interior. The mixed volume of two color sub-polygons is dual to the tropical stable intersection of two sub-webs in the brane-web.

Definition 8 (Color-subdivided GTP.)**.** *A color-subdivision of a GTP is an extension of the coloring $(P, \{\lambda^c_\alpha\})$ to the interior by two types of polygons:*

1. *Parallelograms $G^{c_1 c_2}$, where parallel edges have the same color*

2. *Polygons G^c where all edges have the same color*

such that as a set

$$P = \bigcup_{c_1, c_2} G^{c_1 c_2} \cup \bigcup_{c} G^c \,, \tag{6.75}$$

with the sub-polygons intersecting each other at most in edges. Furthermore, the color sub-division agrees with the edge-coloring, i.e.

$$\partial \left(\bigcup_{c_1, c_2} G^{c_1 c_2} \cup \bigcup_{c} G^c \right) \Big|_{E_\alpha} = \{\lambda^c_\alpha\} \,. \tag{6.76}$$

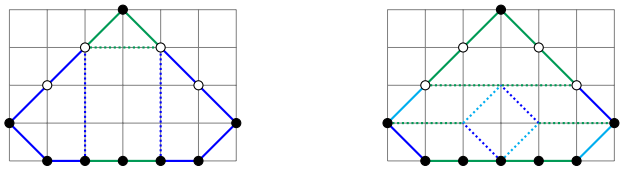
Due to the last requirement, a colored polygon $(P, \{\lambda^c_\alpha\})$ determines a color-subdivision of P, albeit not uniquely. Yet the sum of the area of all parallelograms G^{c_1,c_2} (that are bi-colored in c_1 and c_2) is an invariant, and, as shown in [201] section 4.6, precisely gives the mixed volume of the sub-polygons S^{c_1} and S^{c_2}. For each pair c_1, c_2 we write this invariant

$$A^{c_1,c_2} = \sum \text{Area}(G^{c_1,c_2}) = \text{MV}(S^{c_1}, S^{c_2})\,, \tag{6.77}$$

where the sum is over all parallelograms with colors c_1 and c_2, and we use the standard flat metric in $\mathbb{R}^2$ to compute the area.

Example. Consider the two colorings of P in (6.72) and (6.73). The color sub-division is given by introducing virtual lines, dividing the respective polygons as

Coloring 1: Coloring 2:



(6.78)

such that the respective areas are

$$\begin{aligned} &\text{Coloring 1:} \qquad A^{bg} = 6 \\ &\text{Coloring 2:} \qquad A^{bg} = A^{cg} = 4\,, \qquad A^{bc} = 2\,. \end{aligned} \tag{6.79}$$

6.3.5 Magnetic Quivers from Colored GTPs

Associated to a colored GTP we now define a quiver, which we refer to as the tropical quiver. If the GTP in question allows for more than a single consistent coloring, then each coloring gives rise to its own quiver. The tropical quiver will be identified with the magnetic quiver, i.e. the 3d $\mathcal{N} = 4$ theory, whose Coulomb branch is isomorphic to the Higgs branch of the 5d theory $\mathcal{T}_P$.

Definition 9 (Tropical Quiver)**.** *The tropical quiver $TQ(P, \{\lambda^c_\alpha\})$ of a colored GTP is given by a set of nodes with labels m_I and symmetric intersections k_{IJ}. Given a colored GTP $(P, \{\lambda^c_\alpha\})$ we define it as follows.*

1. *Color nodes: Each color maps to a node in the tropical quiver. The labels of the nodes are the m^c defined in* (6.63)*. In general, this is given by*

$$m^c = \gcd_{\alpha} \left(\lambda^c_\alpha\right) . \tag{6.80}$$

The intersections between the nodes of color c_1 and c_2 are determined from two parts. The first is the mixed volume $MV(S^{c_1}, S^{c_2})$ of definition 4. The second contribution, which is negative, comes from configurations where an edge E_α is colored in both colors, i.e. $\lambda^{c_1}_\alpha, \lambda^{c_2}_\alpha > 0$. Thus,

$$k^{c_1,c_2} = \frac{1}{m^{c_1} m^{c_2}} \left(MV(S^{c_1}, S^{c_2}) - \sum_\alpha \sum_{x=1}^{b_\alpha+1} \mu^{c_1}_{\alpha,x} \mu^{c_2}_{\alpha,x} \right) . \tag{6.81}$$

In particular, the self-intersection of a color node is given by

$$k^{cc} = \frac{1}{(m^c)^2} \left(2Area(S^c) - \sum_\alpha \sum_{x=1}^{b_\alpha+1} (\mu^c_{\alpha,x})^2 \right) , \tag{6.82}$$

where $Area(S^c)$ is the Euclidean area of the c-colored sub-polygon. The self-intersection determines the number of edges beginning and ending on the c-colored node (i.e. loops) as

$$\ell^c = 1 + \frac{k^{cc}}{2} . \tag{6.83}$$

2. *Tails: There are additional nodes in the tropical quiver that are not associated to a color. For each edge E_α, the tropical quiver contains a sequence of nodes of length b_α. The labels of these nodes are given by*

$$m_{\alpha,x} = \sum_{y=1}^{x} \left(-\mu_{\alpha,y} + \sum_{c=1}^{n_c} \mu^c_{\alpha,y} \right) , \tag{6.84}$$

where $x = 1, \ldots b_\alpha$.[2] *Neighboring nodes pertaining to the same edge are connected once, i.e. the number of intersections between the tail nodes is*

$$k_{\alpha,x;\beta,y} = \delta_{\alpha,\beta} \left(\delta_{|x-y|,1} - 2\delta_{x,y} \right) . \tag{6.85}$$

We have introduced a term so that the self-intersections are $k_{\alpha,x;\alpha,x} = -2$. The tail nodes cannot have loops attached to them. The number of edges between color and tail nodes is given by

$$k^c_{\alpha,x} = \frac{1}{m^c} \left(\mu^c_{\alpha,x} - \mu^c_{\alpha,x+1} \right) . \tag{6.86}$$

[2]Note that one can easily show that all $m_{\alpha,x}$ with $x > b_\alpha$ vanish identically.

Since each colored sub-polygon S^c, consisting of m^c IMPs, is dual to a sub-web of multiplicity m^c, we map it to a node in the tropical quiver with label m^c. The two contributions to the edges between color nodes in the tropical quiver correspond to the stable intersection number and 7-brane contribution in the web. We refer the reader to section 6.6 for details on the GTP-to-brane-web map. The tail nodes are not realized in $(P, \{\lambda^c_\alpha\})$ as a colored sub-polygon. The information needed to construct the tails is nonetheless contained in the colored GTP, and is given above in terms of the data defined in the previous subsections.

Self-intersection. The self-intersection k^{cc} of a colored sub-polygon S^c is a measure of the amount of adjoint matter associated to the corresponding node. Specifically, if the self-intersection number differs from -2, the $U(m^c)$ ($m^c \neq 1$) node of the magnetic quiver is associated with ℓ^c adjoint matter multiplets, indicated by a loop attached to this node. Moreover, the self-intersection of a colored sub-polygon is related to the rank of the Higgsed sub-sector of the SCFT that this sub-polygon corresponds to. In particular, we find

$$k^{cc} = 2(r(T^c) - 1)\,, \tag{6.87}$$

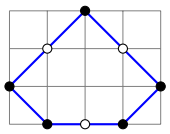
where T^c is the IMP in (6.63). Thus, the self-intersection is bounded from below by -2. The tail nodes have self-intersection $k_{\alpha,x;\alpha,x} = -2$ so they cannot have adjoint matter associated to them. For theories with a high number of flavors the appearance of colored sub-polygons with $k^{cc} \neq -2$ is very rare [3]. It *is* a feature of our main example, in a trivial sense however, as we show below.

Conjecture 1 (Tropical and Magnetic Quivers)**.** *Let P be a GTP, associated to a 5d SCFT $\mathcal{T}_P$. There is a bijection between the inequivalent colorings of P and the cones of the Higgs branch of $\mathcal{T}_P$; moreover, the tropical quiver associated to a coloring is identified with a magnetic quiver for the corresponding cone in the Higgs branch.*

We obtain this conjecture by utilizing the one-to-one map to the brane-webs, that describe the 5d $\mathcal{N} = 1$ theories, in section 6.6.

Example. Now we are in the position to compute the tropical quiver of P in (6.20) using

its colorings. First, consider (6.72). There are two colored sub-polygons

$S^b =$  $S^g =$  (6.88)

with multiplicities $m^b = m^g = 1$. We compute the intersection of the corresponding color nodes explicitly

$$k^{bg} = (6 - 0 - 2 - 0 - 2 - 2) = 0\,, \tag{6.89}$$

where the area was given in (6.79) and the partitions are given in (6.68) and (6.69) respectively. The self-intersection numbers of the two colored sub-polygons are

$$k^{bb} = 2 \cdot 7 - 3 \cdot 2^2 - 1 - 1 = 0\,, \qquad k^{gg} = 2 \cdot 1 - 4 \cdot 1 = -2\,. \tag{6.90}$$

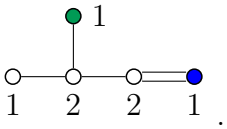
However, given that m^b=1 the adjoint representation is trivial, so we drop the loop in the magnetic quiver. Now, consider the tails. The only edge of P with $b_\alpha \neq 0$ is E_2 with $b_2 = 3$. Thus we can compute

$$m_{2,1} = -1 + 2 + 1 = 2\,, \quad m_{2,2} = -2 + 2 + 2 = 2\,, \quad m_{2,3} = -3 + 2 + 2 = 1\,, \tag{6.91}$$

Finally, the intersections between the color and tail nodes are given by

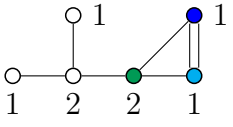
$$k^b_{2,1} = 2\,, \qquad k^g_{2,2} = 1\,, \tag{6.92}$$

with all others vanishing. Thus, the tropical quiver for P with this coloring is



. (6.93)

We can repeat the analysis above for the second coloring of P in (6.73), and find that the tropical quiver associated to this coloring is



. (6.94)

We identify each of these tropical quivers with a magnetic quiver, giving the two cones on the Higgs branch of the 5d SCFT $\mathcal{T}_P$. This theory can be shown to represent the strongly coupled $SU(4)_4 + 4\boldsymbol{F}$ [120].

6.4 Symplectic Leaves and Colorings with Internal Edges

Our discussion so far required the GTP to have no internal lines. In M-theory, such geometries correspond to 5d SCFTs – which are the main focus of our attention. In this section we generalize our approach to include GTPs with internal lines, which in the geometry are partial resolutions, and in 5d language correspond to opening up partial (extended) Coulomb branch directions. The motivation is two-fold: obviously if one would like to study weakly coupled 5d gauge theories, these have rulings, i.e. internal edges. Secondly, and perhaps more importantly for the current endeavor of mapping out the Higgs branch, we require these to construct the Hasse diagram, i.e. the partially ordered set of symplectic leaves that comprise the Higgs branch, as a hyper-Kähler cone. The Higgsing is constructed by successively opening partial Coulomb branch directions.

6.4.1 Colorings with Internal Edges

For a polygon with internal edges $E^{\text{in}} \neq \emptyset$, the edge coloring has to be extended to E^{in}. The first step is to extend our algorithm 1. For polygons with internal edges, the s-rule only has to be obeyed on external edges (it is irrelevant to apply it to internal edges, given that these are dual to internal 5-branes, which do not end on any 7-branes). A colored sub-polygon S^c needs to be divided completely by internal edges, so that all extreme vertices in S^c are part of at least two edges. We argue for this approach in the brane picture in section 6.6.1.

Algorithm 2 (Coloring for Polygons with Internal Edges)**.** *Consider any GTP P and denote the sub-polygons defined by the internal edges by P_A, where $A \subset \alpha = \{1, \cdots, n_E\}$, such that the P_A do themselves not have any internal edges. A coloring for a GTP P with $E^{in} \neq \emptyset$ is a partition*

$$\sum_{c=1}^{n_c} \lambda_\alpha^c = \lambda_\alpha \,. \tag{6.95}$$

For all c, the $\{\lambda_\alpha^c\}$ defines a refined Minkowski summand S^c of $P \leq S^1 \oplus \cdots \oplus S^{n_c}$ obeying the following rules:

1. *The S^c can be divided into sub-polygons*

$$S^c = \bigcup S_A^c \,, \tag{6.96}$$

   without internal lines.

2. *For all c and A*

$$S_A^c = \underbrace{T_A^c \oplus \cdots \oplus T_A^c}_{m_A^c}\,, \tag{6.97}$$

where each T_A^c is irreducible and obeys the s-rule minimally, for all external edges of P. We require that for $c \neq d$

$$T_A^c \neq T_A^d\,, \quad \forall A\,. \tag{6.98}$$

The multiplicity of S^c is given by

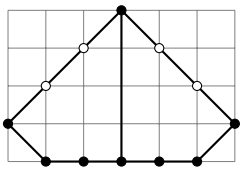
$$m^c = \gcd_A m_A^c\,. \tag{6.99}$$

3. *The partition is maximal, i.e. there is no sub-partition*

$$S^{c_1} \leq S^{c_2} \oplus S^{c_3}\,, \tag{6.100}$$

such that the resulting coloring is valid.

Example. Let us exemplify this by finding the coloring for the weakly coupled $SU(4)$ description of P in (6.20). Turning on the $SU(4)$ gauge coupling corresponds to adding an internal edge, so that the GTP becomes

$P' =$  (6.101)

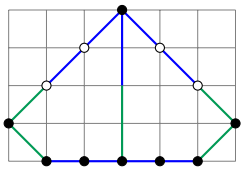
We do not distinguish between black and white vertices along the internal edge. By including the internal edge the GTP data changes to

$$\begin{aligned} &L_\alpha^\partial = ((1,-1),(1,0),(1,0),(1,1),(-1,1),(-1,-1)\,, \qquad L^{\text{in}} = (0,1) \\ &\lambda_\alpha^\partial = (1,2,2,1,3,3)\,, \qquad \{\mu_\alpha\} = (\{1\},\{1^2\},\{1^2\},\{1\},\{3\},\{3\})\,, \qquad \lambda^{\text{in}} = 4\,. \end{aligned} \tag{6.102}$$

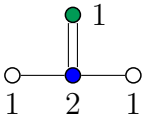
Furthermore, the internal edge splits P into two with the edges divided as

$$A_1 = \{1,2,6,\text{in}\}\,, \qquad A_2 = \{3,4,5,\text{in}\}\,. \tag{6.103}$$

We need to find compatible colorings of P'_{A_1} and P'_{A_2}, i.e. the coloring on the internal edge agrees. The only possible coloring is

 (6.104)

From here, we can again compute the magnetic quiver, noting that the lower line is now divided into two distinct edges. The magnetic quiver turns out to be



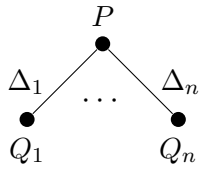
(6.105)

as expected for a weakly coupled $SU(4) + 4\boldsymbol{F}$.

6.4.2 Hasse Diagram and Symplectic Leaves

The Higgs branch of a 5d SCFT or gauge theory, has a foliation in terms of symplectic leaves, as reviewed in section 6.2. Starting from the magnetic quiver associated to the 5d QFT, the Hasse diagram can be obtained by successive quiver subtractions [128, 129, 181]. Here we provide a derivation in terms of the data of the colored polygon $(P, \{\lambda_\alpha^c\})$.

The Hasse diagram is obtained by introducing successive partial resolutions into the GTP. In each step we start with a polygon P and find subtractions Δ_i that result in the next layer Q_i of the Hasse diagram – there can in general be multiple such subtractions:



(6.106)

If at some point the GTPs Q_j along different branches agree, these nodes should be identified, leading to interconnections. This idea was first introduced in [129], where it was argued in the brane picture that the Higgs branch at specific points along the Coulomb branch reproduces the different layers in the Hasse diagram.

Definition 10 (Hasse diagram of a GTP)**.** *Let P be a GTP, characterized by edges E_α with $\lambda_\alpha^{(P)}$ and $\mu_{\alpha,x}^{(P)}$. A transition in the Hasse diagram $P \xrightarrow{\Delta} Q$ is a set of internal edges E_β, which correspond to a partial resolution, with lengths ν_β, such that:*

1. *There is a GTP, Q, characterized by*

$$E^{\partial}_{(Q)} = E^{\partial}_{(P)}\,, \quad E^{in}_{(Q)} = E^{in}_{(P)} \cup E_\beta\,, \quad \lambda_\alpha^{(Q)} = \{\lambda_\alpha^{(P)}, \nu_\beta\}\,, \quad \mu_{\alpha,x}^{(Q)} = \mu_{\alpha,x}^{(P)}\,. \tag{6.107}$$

2. *Q admits a coloring, such that there is a color c^* with*

$$\nu_\beta^{c^*} = \nu_\beta \quad \forall \beta \,, \tag{6.108}$$

with associated $\lambda_\alpha^{c^*}$ and $\mu_{\alpha,x}^{c^*}$.

3. *There is a GTP Δ characterized by*

$$E_{(\Delta)} = \{E_\alpha^{(P)} | \lambda_\alpha^{c^*} \neq 0\} \,, \qquad \lambda_\alpha^{(\Delta)} = \lambda_\alpha^{c^*} \,, \qquad \mu_{\alpha,x}^{(\Delta)} = \mu_{\alpha,x}^{c^*} \,, \tag{6.109}$$

such that the magnetic quiver of Δ is a either the magnetic quiver of a Kleinian singularity or the closure of a minimal nilpotent orbit.

Note that the leaves that we allow here are those discussed in section 6.2. In case that a given GTP has symplectic leaves that go outside of this class, it would interesting to see how these are realized in the GTP in terms of introducing internal lines. We are confident that any effect that occurs in the webs has a counterpart in our formulation in terms of the GTPs, including more general symplectic leaves.

A physical way to understand the transitions in the Hasse diagram is in terms of a Higgsing, or combinatorially in terms of quiver subtractions in the magnetic quiver [128]. Essentially, we replace the affine Dynkin diagram of an ADE algebra (or a Kleinian singularity) by a single $U(1)$ rebalancing node. The idea is that the newly introduced color c^* represents the rebalancing node. Including the ν_β, S^{c^*} has magnetic quiver $U(1)$ but excluding them it would represent an ADE singularity.

In practice we identify Δ by the following procedure. If $P \xrightarrow{\Delta} Q$ is a transition in a Hasse diagram, we can write P as a refined Minkowski sum

$$P \leq \Delta \oplus S \,, \tag{6.110}$$

where S is another GTP, which need not be irreducible and could be empty. Conversely, such a Minkowski sum decomposition induces a transition in the Hasse diagram if

1. The magnetic quiver of Δ is a symplectic singularity

2. There is an extension of Δ by internal lines ν_β to Δ_ν with $\lambda_\alpha^{(\Delta_\nu)} = \{\lambda_\alpha^{(\Delta)}, \nu_\beta\}$ such that the s-rule for Δ_ν is obeyed minimally on each external edge.

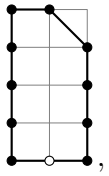
Then, $Q \leq \Delta_\nu \oplus S$ with $\mu^{(Q)}_{\alpha,x} = \mu^{(P)}_{\alpha,x}$. This implies that, should we find a Δ representing a symplectic singularity as a refined Minkowski summand of P, we can subtract the corresponding magnetic quiver, provided that Δ can be condensed to a $U(1)$ by the inclusion of internal lines.

6.5 Examples: SQCD at strong/weak coupling, and T_4

We now provide a small set of additional examples to show the workings of our conjecture. The present section is a truncated version of section 5 in [2] where a large class of diverse examples is presented, including SQCD-like theories with anti-symmetric matter, descendants of T_N that are non-Lagrangian, and isolated toric singularities, which have a direct connection to the work of Altmann [131, 132].

6.5.1 $SU(3)_1 + 6\mathbf{F}$ UV SCFT

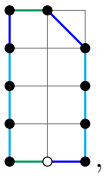
Our first example is the strongly coupled SCFT, with IR description given by $SU(3)_1 + 6\boldsymbol{F}$. The GTP P is given by

$P =$  , (6.111)

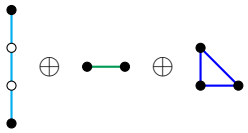
which is characterized by the following data:

$$\begin{aligned} L_\alpha &= ((0,-1),(1,0),(0,1),(-1,1),(-1,0)) \\ \lambda_\alpha &= (4,2,3,1,1)\,, \qquad \mu_{\alpha,x} = (\{1^4\},\{2\},\{1^3\},\{1\},\{1\})\,. \end{aligned} \tag{6.112}$$

As usual, we label the five edges of P in counterclockwise order, starting from the top left edge. The unique consistent coloring (blue, green, cyan) of this diagram is given by

 , (6.113)

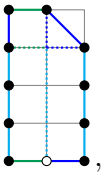
i.e. the refined Minkowski sum decomposition of P is given by

$P <$  (6.114)

with the partitions and multiplicities of these colorings being

$$\begin{aligned}
&\lambda^c_\alpha = (3,0,3,0,0)\,, \quad \mu^c_{\alpha x} = (\{3\},-,\{3\},-,-)\,, \qquad m^c = 3\\
&\lambda^g_\alpha = (0,1,0,0,1)\,, \quad \mu^g_{\alpha x} = (-,\{1\},-,-,\{1\})\,, \qquad m^g = 1\\
&\lambda^b_\alpha = (1,1,0,1,0)\,, \quad \mu^b_{\alpha x} = (\{1\},\{1\},-,\{1\},-)\,, \qquad m^b = 1\,.
\end{aligned} \tag{6.115}$$

Clearly, all the summands in (6.114) are irreducible and obey the s-rule minimally (up to multiplicity). A choice of color sub-division is given by



, (6.116)

so that the areas of the parallelograms are

$$A^{cg} = 3\,, \quad A^{cb} = 3\,, \quad A^{gb} = 1\,. \tag{6.117}$$

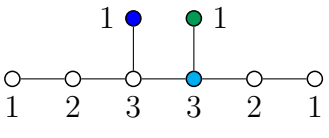
From (6.115) and (6.117) we can compute the intersections between the color nodes using (6.81) to be

$$k^{cg} = 1\,, \quad k^{cb} = 0\,, \quad k^{gb} = 0\,. \tag{6.118}$$

Now, let's turn to the additional nodes, which appear at edges E_1 and E_3. The node labels and mutual edges can be read off from the $\mu_{\alpha,x}$ and $\mu^c_{\alpha,x}$ in (6.112) and (6.115):

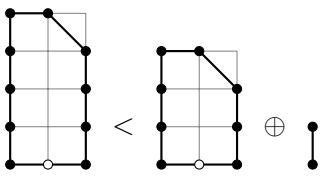
$$\begin{aligned}
&m_{1,x} = (3,2,1)\,, \qquad k^c_{1,1} = 1\,, \quad k^b_{1,1} = 1\\
&m_{3,x} = (2,1)\,, \qquad\quad k^c_{3,1} = 1\,,
\end{aligned} \tag{6.119}$$

and all others vanishing. Putting all this together the magnetic quiver is given by



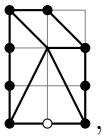
. (6.120)

Now, let us look at the Hasse diagram of this theory. We can check that P can be written as a refined Minkowski sum



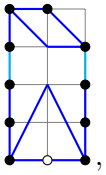
$$P \quad < \quad \Delta \quad \oplus \; S\,, \tag{6.121}$$

We can now check that this decomposition induces a transition in the Hasse diagram. It is straightforward to see that the magnetic quiver of Δ is the affine Dynkin diagram of $\mathfrak{d}_5$. Furthermore, there is an extension of Δ with internal lines such that the s-rule is minimally obeyed on each external edge, namely



(6.122)

which is Δ_ν. Thus, we can deduce Q, and its unique coloring, to be



(6.123)

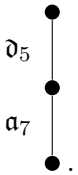
where we denote the color c^* by blue and the other color in the coloring of Q in cyan. We can read off the data of the external lines

$$\begin{aligned} &\lambda^c_\alpha = (1,0,1,0,0)\,, \quad \mu^c_{\alpha,x} = (\{1\},-,\{1\},-,-)\,, && m^c = 1 \\ &\lambda^b_\alpha = (3,2,2,1,1)\,, \quad \mu^b_{\alpha,x} = \left(\{1^3\},\{2\},\{1^2\},\{1\},\{1\}\right)\,, && m^b = 1\,. \end{aligned} \tag{6.124}$$

Together with $A^{cb} = 2$ we can deduce

$$\begin{aligned} &k^{cb} = 0 \\ &m_{1,x} = (1,1,1)\,, \qquad k^c_{1,1} = 1\,, \quad k^b_{1,3} = 1 \\ &m_{3,x} = (1,1)\,, \qquad k^c_{3,1} = 1\,, \quad k^b_{3,2} = 1\,, \end{aligned} \tag{6.125}$$

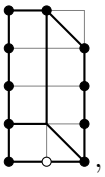
with all others vanishing. Altogether, we arrive at the affine Dynkin diagram of a_7. Since the magnetic quiver of Q itself is a symplectic singularity, there is a trivial transition with $\Delta = Q$. Thus, the Hasse diagram of the strongly coupled $SU(3)_1 + 6\boldsymbol{F}$ is



(6.126)

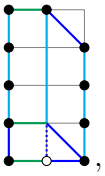
6.5.2 $SU(3)_1 + 6\mathbf{F}$ IR Theory

Now, we turn to the weakly coupled version of the theory, i.e. the gauge theory $SU(3)_1 + 6\boldsymbol{F}$, which has a description as a GTP P, where we have a ruling



(6.127)

There is one valid coloring, which is given by (with color sub-division)



(6.128)

i.e. the coloring data for the external lines is

$$\begin{aligned}
&\lambda^c_\alpha = (3,0,0,3,0,0)\,, \quad \mu^c_{\alpha,x} = (\{3\},-,-,\{3\},-,-)\,, && m^c = 3\\
&\lambda^g_\alpha = (0,0,1,0,0,1)\,, \quad \mu^g_{\alpha,x} = (-,-,\{1\},-,-,\{1\})\,, && m^g = 1\\
&\lambda^b_\alpha = (0,1,1,0,1,0)\,, \quad \mu^b_{\alpha,x} = (-,\{1\},\{1\},-,\{1\},-)\,, && m^b = 1\,.
\end{aligned} \tag{6.129}$$

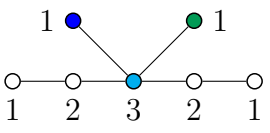
Note, that now we have an additional edge, since the edge on the left is subdivided by an internal line. The intersections between the color nodes are

$$A^{cg} = A^{cb} = 3\,, \quad A^{gb} = 1\,, \qquad k^{cg} = k^{cb} = 1\,, \quad k^{gb} = 0\,. \tag{6.130}$$

The additional nodes appear at edges E_1 and E_4 with

$$\begin{aligned}
m_{1,x} &= (2,1)\,, \qquad k^c_{1,1} = 1\\
m_{4,x} &= (2,1)\,, \qquad k^c_{4,1} = 1\,,
\end{aligned} \tag{6.131}$$

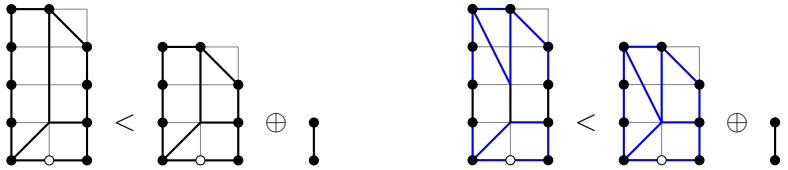
with all others vanishing. Putting all together the magnetic quiver of the weakly coupled theory is



(6.132)

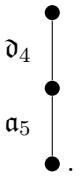
Again, we can look at the Hasse diagram. We can show that the following Minkowski

sum decomposition induces a transition in the Hasse diagram



$$P \quad < \quad \Delta \quad \oplus S\,, \qquad\qquad Q \quad < \quad \Delta_\nu \quad \oplus S\,, \tag{6.133}$$

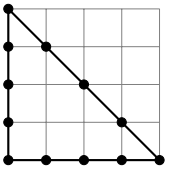
where the partitions of Q and P agree. We can again compute the magnetic quivers of Δ_ν and Q and find the affine Dynkin diagrams of $\mathfrak{d}_4$ and $\mathfrak{a}_5$ respectively. Thus, the Higgs branch of the weakly coupled $SU(3)_1 + 6\boldsymbol{F}$ is



. (6.134)

6.5.3 T_4

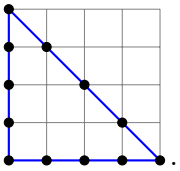
The trinions T_N with extremal vertices $(0,0)$, $(N,0)$, $(0,N)$ were studied in the context of 5d SCFTs in [116]. Their (and their descendants') magnetic quivers and Hasse diagrams were derived in [183]. We will derive these from the colored polygon method for T_4. The toric polygon for T_4 is

$P =$  (6.135)

The data characterizing P is

$$\begin{aligned} L_\alpha &= ((0,-1),(1,0),(-1,1)) \\ \lambda_\alpha &= (4,4,4)\,, \qquad \mu_{\alpha,x} = (\{1^4\},\{1^4\},\{1^4\})\,. \end{aligned} \tag{6.136}$$

We first compute the magnetic quiver. The only coloring that is consistent is by a single color $n_c = 1$:



. (6.137)

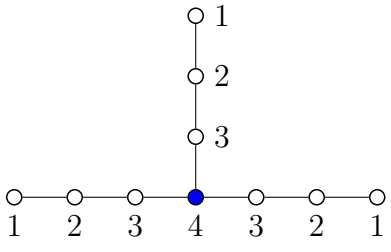
The coloring is specified by the partition data

$$\lambda^b_\alpha = (4,4,4)\,, \qquad \mu^b_\alpha = (\{4\},\{4\},\{4\})\,, \qquad m^b = 4\,. \tag{6.138}$$

We find that there is one vertex in the magnetic quiver from the single color with label 4. All three edges give rise to additional tail nodes in the magnetic quiver. Their labels and intersections with the blue node are

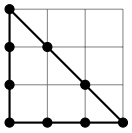
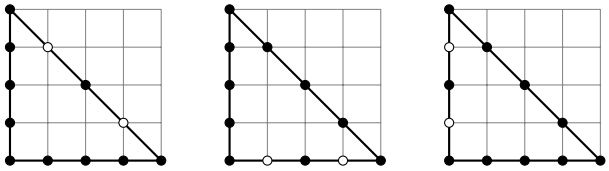
$$m_{\alpha,x} = (3,2,1)\,, \qquad k^b_{\alpha,1} = 1\,, \tag{6.139}$$

with all other vanishing. The complete magnetic quiver is

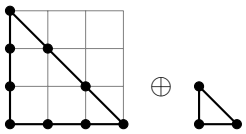
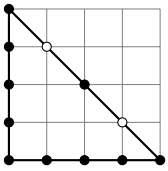
$\mathrm{MQ}(T_4) =$ 

. (6.140)

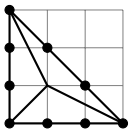
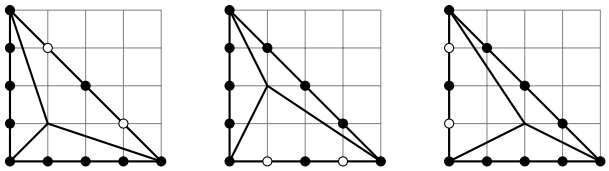
To determine the Hasse diagram, we determine all the subdiagrams that correspond to rank 1 theories: There is one $\mathfrak{e}_6$ theory and three ways to embed the $\mathfrak{e}_7$:

$\mathfrak{e}_6$:  $\mathfrak{e}_7$:  (6.141)

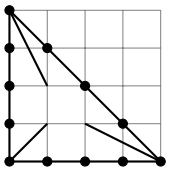
These are the first four transverse slices of the Hasse diagram. The magnetic quiver of the above diagrams can readily be checked to give the affine Dynkin diagrams of the corresponding groups. Clearly, the refined Minkowski sum $P \leq \Delta \oplus S$ can be realised as

$P <$  $P <$  (6.142)

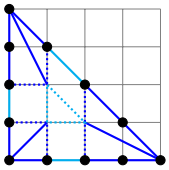
and likewise for the other two representations of $\mathfrak{e}_7$. Note that in the second case S is empty. There is an extension of each of the Δ with internal lines such that the s-rule is minimally obeyed on each external edge (Δ_ν):

$\mathfrak{e}_6$:  $\mathfrak{e}_7$:  (6.143)

The $\mathfrak{e}_6$ induces a transition in the Hasse diagram with Q given by

$T_4 - \mathfrak{e}_6 =$  (6.144)

To compute the magnetic quiver for this diagram we find the unique color sub-division

 (6.145)

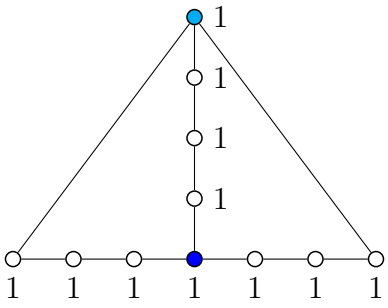
The data are

$$\begin{aligned} &\lambda^b_\alpha = (3,3,3) \qquad \mu^b_\alpha = (\{1^3\},\{1^3\},\{1^3\}) \qquad m^b = 1 \\ &\lambda^c_\alpha = (1,1,1) \qquad \mu^c_\alpha = (\{1\},\{1\},\{1\}) \qquad m^c = 1 \end{aligned} \tag{6.146}$$

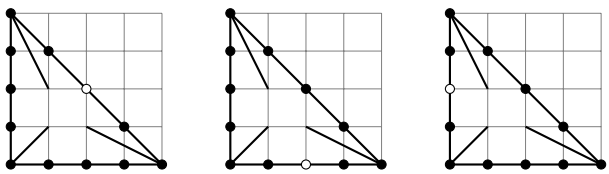
from which we deduce

$$\begin{aligned} &A^{cb} = 3 \qquad\qquad k^{cb} = 0 \\ &m_{\alpha,x} = (1,1,1) \qquad k^b_{\alpha,1} = 1 \qquad k^c_{\alpha,3} = 1 \qquad \forall \alpha \end{aligned} \tag{6.147}$$

with all others vanishing. Each of the three edges therefore contributes a chain three of $U(1)$ nodes. The magnetic quiver is thus

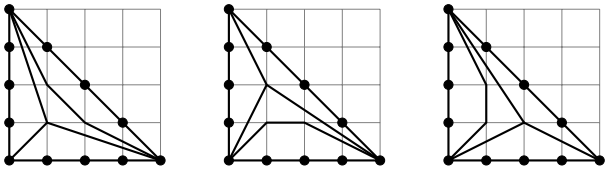
$\mathrm{MQ}(T_4 - \mathfrak{e}_6) =$  . (6.148)

Next we note that there are three embeddings of $\mathfrak{a}_7$ singularities into the partially resolved diagram $T_4 - \mathfrak{e}_6$:

$\mathfrak{a}_7$:  (6.149)

It can again be checked that the magnetic quiver of all these three diagrams is an affine Dynkin diagram for $\mathfrak{a}_7$. As before, there exists an extension of these diagrams (Δ_ν) by

internal lines such that the s-rule is minimally obeyed on each external edge. The embedding of these extended diagrams in $T_4 - \mathfrak{e}_6$ is

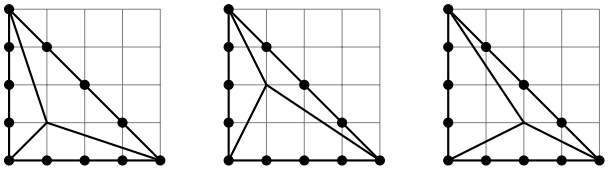
$T_4 - \mathfrak{e}_6 - \mathfrak{a}_7 =$  (6.150)

The magnetic quiver of each of these diagrams is

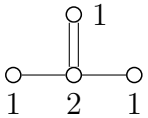
$$MQ(T_4 - \mathfrak{e}_6 - \mathfrak{a}_7) = \mathfrak{a}_3\,, \tag{6.151}$$

which is the final symplectic leave in the $\mathfrak{e}_6$ branch of the Hasse diagram.

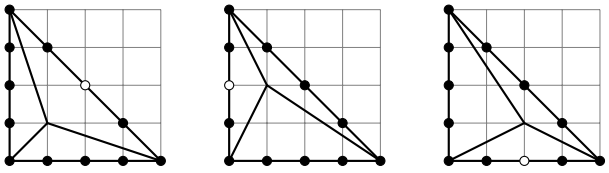
Likewise along the $\mathfrak{e}_7$ branches, the first step (the subtraction of the $\mathfrak{e}_7$ slice) is obtained by the following partial triangulation of the T_4 diagram

$T_4 - \mathfrak{e}_7 =$  (6.152)

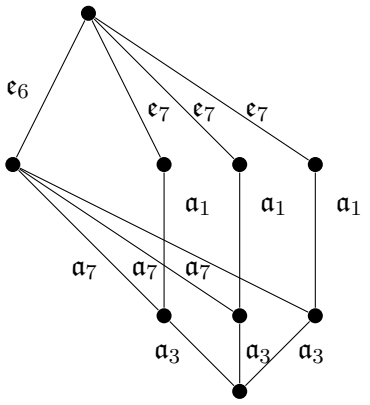
The magnetic quiver of this theory is readily obtained to be

$\mathrm{MQ}(T_4 - \mathfrak{e}_7) =$  . (6.153)

Finally, we note that there are $\mathfrak{a}_1$ singularities realizable as

$\mathfrak{a}_1 =$  (6.154)

These are precisely subtracted by partially triangulating further as in (6.150), which is where the branches meet. This completes the Hasse diagram of T_4, in agreement with [183]:



. (6.155)

6.6 Derivation from the Tropics

We now give details of the connection with brane-webs, from which the rules that we propose in section 6.3 derive. In the case where the GTP is toric, there is a precise relation to tropical geometry, and generalizing this to non-toric GTPs would be very interesting indeed.

6.6.1 Sub-web Decomposition to Colored Polygon

Recall that a (p, q) 5-brane-web is made up of connecting (p, q) 5-branes, where we distinguish between external branes (which end on corresponding (p, q) 7-branes) and internal branes (which only connect to other (p, q) 5-branes). Given a web, the corresponding GTP is its dual graph. As such, a set of n_5 (p, q) 5-branes maps to a line in the GTP, that is perpendicular to the branes, i.e. to an edge E_α with the properties

$$L_\alpha = (-q, p)\,, \qquad \lambda_\alpha = n_5\,. \tag{6.156}$$

This holds both for internal and external branes. Note that charge conservation in the web ensures closedness of the GTP. A stack of n_5 external 5-branes, which end on n_7 7-branes gives rise to an external edge in the GTP with

$$b_\alpha = n_7 - 1\,. \tag{6.157}$$

Such a web configuration naturally defines a partition of n_5 into the number of 5-branes ending on each 7-brane, which is exactly given by the $\mu_{\alpha,x}$.

To extract the magnetic quiver, the brane-web is divided into sub-webs that are themselves consistent brane-webs. There can be multiple (maximal) divisions into sub-webs, which are identified with different cones of the Higgs branch. Here, we will only consider a single

division. We distinguish between two kinds of sub-webs, which are those that are associated to colors in the GTP, and those that are not but which give rise to tails in the tropical quiver.

For now we will focus on the first class of sub-webs W^c, which are characterized by the fact that they end on two or more $[p,q]$ 7-branes of distinct $[p,q]$ charges. Each W^c is mapped to a colored sub-polygon S^c, as specified in definition 1. An edge segment is part of S^c if the corresponding 5-brane is contained in W^c, defining the partition of λ_α into λ_α^c for each edge. The refined Minkowski sum of two sub-polygons $S^{c_1} \oplus S^{c_2}$ is understood as combining two sub-webs W^{c_1} and W^{c_2}, where we identify the 7-branes involved in the W^c.

Definition 1 contains certain conditions for a coloring of a GTP to be valid, which have their origin in the brane-web:

1. Each sub-web W^c gives rise to a sub-polygon S^c because charge conservation in the brane-web ensures closed-ness in the GTP.

2. A sub-web W^c has a multiplicity, i.e. it consists of m^c identical minimal webs W^c_{min}.

3. **s-rule.** The s-rule states that the number of D5-branes that may connect a single D7-brane and a stack of NS5-branes is less or equal to the number of NS5-branes in the stack. An $SL(2,\mathbb{Z})$-invariant formulation was discussed in [206]. Consistent with this, we find that the intersection of three types of branes (p_i, q_i) obeys the s-rule, if

$$\left|\det \begin{pmatrix} p_i & q_i \\ p_j & q_j \end{pmatrix}\right| \geq \gcd(p_k, q_k)^2 \,, \tag{6.158}$$

   for every permutation (i,j,k) of $(1,2,3)$. This can be derived by considering an $SL(2,\mathbb{Z})$ transformation of a D5-NS5 junction [2]. Let us consider a minimal web W^c_{min}. It obeys the s-rule if there is a full resolution such that each intersection obeys the s-rule locally. This idea was advanced in [116] from which the introduction of tiles definition 5 obeying (6.37) follows.

4. The division into sub-webs is maximal, i.e. no sub-web can be further subdivided while still satisfying the s-rule. The same must be true for the partitions $\{\lambda_\alpha^c\}$.

Let us also comment on the case where a GTP has internal edges. This corresponds to a brane-web containing internal 5-branes, i.e. 5-branes that connect two 5-brane junctions (rather than ending on a 7-brane). Such a set of internal 5-branes necessarily pertains to a

collection of sub-webs $\{W^c\}$. There is no obstruction to sending the length of the internal 5-branes to infinity, i.e. the webs connected by the internal 5-branes are independent of each other, apart from a matching condition along the internal 5-branes, and must obey the s-rule locally. This is the reason the s-rule should be applied separately to each S^c_A, as detailed in section 6.4.1.

6.6.2 Magnetic Quivers

What we have seen so far is that a colored GTP contains the same data as the sub-web decomposition of the dual web. We will now argue for the derivation of the tropical quiver from GTP data, as explained in section 6.3.5, starting from the brane-web.

Each sub-web W^c corresponds to a node in the magnetic quiver, labeled by the multiplicity m^c of the sub-web. The sub-webs are mapped to colorings, or colored sub-polygons S^c, in the GTP. To each color we thus associate a node in the tropical quiver with label $m^c = \gcd_\alpha(\lambda^c_\alpha)$.

The intersections between the color nodes are computed as follows: consider the color sub-division of the GTP. The area $A^{c_1c_2}$ corresponds to the stable intersection (SI) between the sub-webs W^{c_1} and W^{c_2} in tropical geometry [120]. Recall, that the SI is defined by infinitesimally displacing the two minimal sub-webs and computing the intersection

$$\text{SI} = \sum \left| \det \begin{pmatrix} p^{c_1} & q^{c_1} \\ p^{c_2} & q^{c_2} \end{pmatrix} \right| , \tag{6.159}$$

where the sum goes over all intersections and the (p^c, q^c) are normalized by a factor of m^c. Now consider the parallelograms $G^{c_1c_2}$ in the color sub-divided polygon, with the two sides characterized by $\lambda^{c_1}_\alpha L_\alpha$ and $\lambda^{c_2}_\beta L_\beta$. The Euclidean area of $G^{c_1c_2}$ is then given by

$$\text{Area}(G^{c_1c_2}) = \lambda^{c_1}_\alpha \lambda^{c_2}_\beta \left|\det\left(L_\alpha, L_\beta\right)\right| = \lambda^{c_1}_\alpha \lambda^{c_2}_\beta \left| \det \begin{pmatrix} q^{c_1} & -p^{c_1} \\ q^{c_2} & -p^{c_2} \end{pmatrix} \right| , \tag{6.160}$$

because of (6.156). However, here the (p^c, q^c) are normalized to be coprime, so, by the inclusion of the λ^c, this agrees with the SI in (6.159).

There is an additional contribution to the intersection between two sub-webs, W^{c_1} and W^{c_2}, which is the effective number of 7-branes on which they both end. To see this contribution in the GTP consider a single edge E_α, corresponding to a tail of (p, q) 5- and 7-branes, all of the same charges p and q, in the brane-web. Recall that the number of 7-branes that an edge E_α gives rise to is $n_7 = b_\alpha + 1$, and the intermediate segments (which are stacks of

5-branes in the web) are labeled by x. Consider the 7-brane between segments $x-1$ and x. The number of 5-branes in color c on either side differ by $\mu^c_{\alpha,x}$, by definition. The sum over all 7-branes yields the second contribution to the intersection between W^{c_1} and W^{c_2}. However, we need to divide by the product of the multiplicities of the two sub-webs to obtain the effective intersection in the magnetic quiver, given by

$$-\frac{1}{m^{c_1}m^{c_2}}\sum_{x=1}^{b_\alpha}\mu^{c_1}_{\alpha,x}\mu^{c_2}_{\alpha,x}\,. \tag{6.161}$$

Together with the SI contribution (6.160) this gives the number of edges (6.81) between nodes in the tropical quiver associated to the two colors c_1 and c_2.

Furthermore, we can determine the number of 5-branes in a tail, which do not belong to any of the W^c. These sub-webs $W_{\alpha,x}$, spanning the segment x between 7-branes in a tail labeled by α, do not appear as sub-polygons in the GTP. Nonetheless, they do give rise to additional nodes in the magnetic quiver, and their presence can be detected in the GTP. Their multiplicities $m_{\alpha,x}$ are given by the total number of 5-branes along a segment x in the tail α, minus the number of 5-branes in that segment that belong to a W^c. The former is the total number of 5-branes protruding from the internal web in this direction, λ_α, minus the number of 5-branes that have ended on a 7-brane further up the tail, $\sum_{y=1}^{x}\mu_{\alpha,y}$. The computation of the latter is the same but restricted to a coloring c. Hence, the multiplicities of the sub-webs $W_{\alpha,x}$, in terms of GTP data, are

$$m_{\alpha,x}=\sum_{y=1}^{x}\left(-\mu_{\alpha,y}+\sum_{c=1}^{n_c}\mu^c_{\alpha,y}\right)\,, \tag{6.162}$$

which is (6.84). These sub-webs give rise to the additional tail nodes in the magnetic quiver with labels $m_{\alpha,x}$. They are connected to their nearest neighbors by a single edge, since the only contribution to the intersection between $W_{\alpha,x}$ and $W_{\alpha,x+1}$ comes from ending on opposite sides of the same 7-brane.

Finally, we determine the number of edges between color nodes and tail nodes in the tropical quiver. Consider a tail segment x made up of $m_{\alpha,x}$ 5-branes between two 7-branes. The number of 5-branes in color c ending on these two 7-branes is given by $\mu^c_{\alpha,x}$ and $\mu^c_{\alpha,x+1}$ respectively. Each time the number of c-colored 5-branes ending on the 7-branes on either side of a segment differs, the corresponding tail node is connected to the c-color node. Thus,

the intersection, after accounting for multiplicity, is

$$\frac{1}{m^c}\left(\mu^c_{\alpha,x}-\mu^c_{\alpha,x+1}\right)\,, \tag{6.163}$$

equivalent to (6.86).

6.6.3 Hasse Diagram

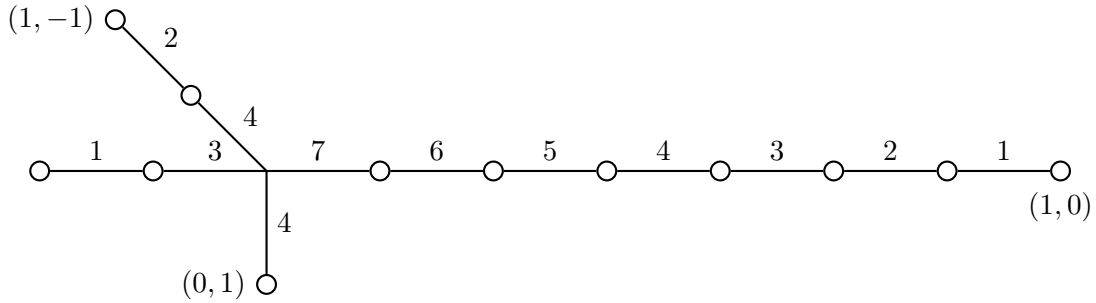
Now, let us turn to the computation of the Hasse diagrams in section 6.4.2. Recall that given a magnetic quiver of a theory, a transition in the Hasse diagram corresponds to the quiver subtraction of a symplectic leaf, i.e. either the affine Dynkin diagram of an ADE Lie algebra $\mathfrak{g}$ corresponding to the magnetic quiver of the closure of a minimal nilpotent orbit, or a Kleinian singularity – these are summarized in table 5.3. It was argued in [129,181] that this process can be translated into the language of brane-webs as follows. Consider a brane-web $\mathcal{W}_P$, corresponding to a theory with some original magnetic quiver. A quiver subtraction by a symplectic leaf [3] $\mathfrak{g}$ corresponds to turning on certain Coulomb branch parameters of the theory, i.e. the introduction of internal 5-branes in the brane-web, resulting in a new brane-web $\mathcal{W}_Q$. The Coulomb branch parameters must be turned on in such a way that, in a maximal sub-division of $\mathcal{W}_Q$, all the newly introduced 5-branes belong to the same sub-web W_{Δ_ν}. At the origin of its Coulomb branch (we could call this brane-web $\mathcal{W}_\Delta$ in parallel with the notation in section 6.4.1), the magnetic quiver of this sub-web is the affine Dynkin diagram of $\mathfrak{g}$. By going into the Coulomb branch of this sub-theory, the associated Higgs branch reduces to $\mathfrak{g}\to\mathfrak{u}(1)$. In the magnetic quiver this corresponds to a quiver subtraction with subsequent rebalancing with a $\mathfrak{u}(1)$ node.

Now, we can further translate this into the language of GTPs. Turning on Coulomb branch parameters corresponds to a partial resolution of the GTP P, i.e. the introduction of internal edges E_β of length ν_β, dual to the newly introduced internal 5-branes in the web, which results in a new GTP Q. The internal 5-branes belong to a sub-web W_{Δ_ν}, corresponding to a color sub-polygon Δ_ν in Q, which includes the internal edges. To describe the Higgs branch at a generic point on the Coulomb branch, the magnetic quiver of Δ_ν should be a single $U(1)$ node. However, at the origin of the Coulomb branch, i.e. in the absence of the E_β where the GTP is Δ, the magnetic quiver correspond to $\mathfrak{g}$.

[3] We assume for notational simplicity that the singularity is of ADE type, the logic holds in the Kleinian case.

6.6.4 Example

As an instructive example let us consider $SU(4)_{\frac{3}{2}} + 1\boldsymbol{AS} + 7\boldsymbol{F}$ at strong coupling, which was discussed in detail in [2] from the GTP point of view. The brane-web for this theory was discussed in [117] and is given by



(6.164)

where we state the number of 5-branes and the type of 7-branes explicitly. There are no internal 5-branes, so the dual GTP does not have internal edges. From (6.156) we can read off that the GTP has edges

$$L_\alpha = ((-1,-1),(0,-1),(1,0),(0,1))\,, \qquad \lambda_\alpha = (4,3,4,7)\,, \tag{6.165}$$

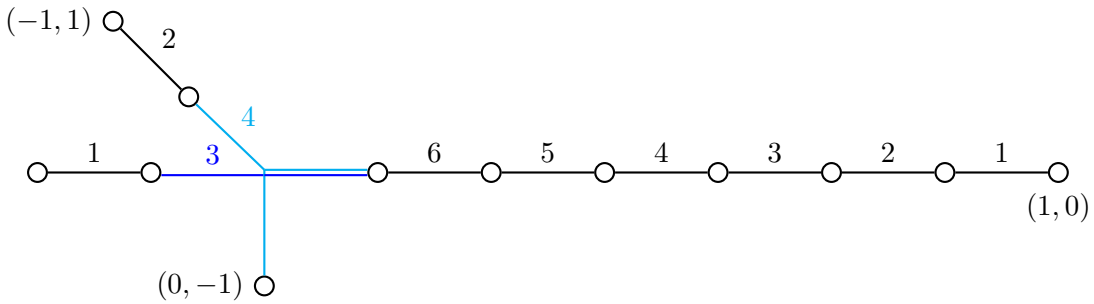
where λ_α is the number of 5-branes protruding from the central junction. From the number of 7-branes in each tail we find

$$b_\alpha = (1,1,0,6)\,. \tag{6.166}$$

Furthermore, we can read off the $\mu_{\alpha,x}$ as the number of 5-branes ending on each of the 7-branes. For example, for the first edge (with the $(1-,1)$-branes), two of the four 5-branes end on each of the two 7-branes, i.e. $\mu_{1,x} = \{2,2\}$. Conversely, for the second edge, of the three 5-branes two and one end on the two 7-branes respectively, so $\mu_{2,x} = \{2,1\}$. Using this we can easily determine the GTP.

Now, let us determine the division of the brane-web into sub-webs. This is a simple

exercise and we arrive at



(6.167)

where we colored the sub-webs in blue W_b, and cyan W_c. The number of 5-branes coming out of the central junction are

$$\lambda^b_\alpha = (0,3,0,3)\,, \qquad \lambda^c_\alpha = (4,0,4,4)\,. \tag{6.168}$$

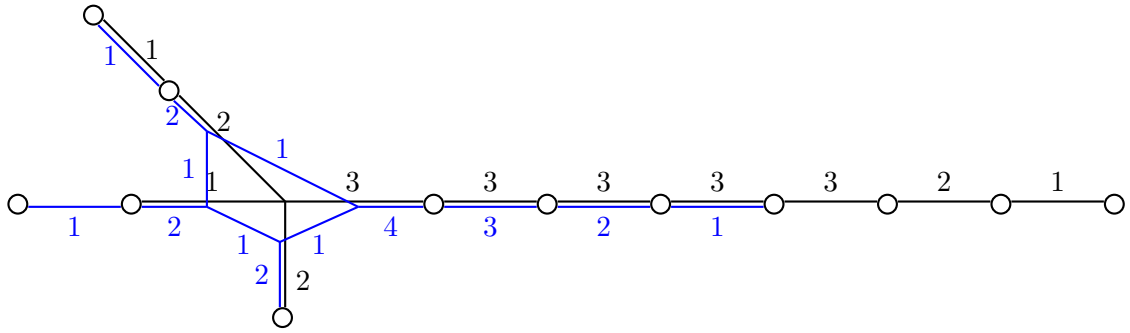
In this case the application of the s-rule is very simple, since the sub-webs are just (stacks of) a fundamental D5-NS5-brane junction and a D5-brane, so both sub-webs end on the first 7-branes they encounter. For example, we have $\mu^b_{4,x} = \{3\}$ and $\mu^c_{4,x} = \{4\}$, which contributes exactly

$$-\frac{1}{m^b m^c}\sum_{x=1}^{6}\mu^b_{4,x}\mu^c_{4,x} = -\frac{1}{3\cdot 4}\left(3\cdot 4 + 0\cdots + 0\right) = -1 \tag{6.169}$$

to the intersection of W^b, W^c. We can easily see that the stable intersection between the two colored sub-webs is one, after accounting for multiplicity, so they actually do not intersect in the magnetic quiver. Since W^b and W^c both end on the first 7-branes they encounter, the multiplicities $m_{\alpha,x}$ of the $W_{\alpha,x}$ sub-webs, coming from the 5-branes suspended between two identical kinds of 7-branes, are not reduced, e.g. we have $m_{4,x} = \{6,5,4,3,2,1\}$. Finally, the colored sub-webs intersect $W_{\alpha,x}$ if a different number of colored branes end on the 7-branes on either side of $W_{\alpha,x}$. This is true e.g. for W^c and $W_{4,1}$, since four cyan branes end on the 7-brane to the left of $W_{4,1}$ and none end on the 7-brane to the right. Following the usual rules we can quickly check that the magnetic quiver of this web agrees with the one derived from the GTP in [2].

Let us now consider the first transition in the Hasse diagram $P \xrightarrow{\Delta} Q$. From the magnetic quiver it is clear that we can subtract an $\mathfrak{e}_6$ singularity. The corresponding Coulomb branch

deformation in the web is given by



(6.170)

where the $\mathfrak{e}_6$ sub-web (W_{Δ_ν}) is shown in blue. We can read off the GTP after the transition Q, which is the dual diagram of (6.170). It is obtained from P by adding the internal edges dual to the internal 5-branes in (6.170). Similarly, the GTP Δ, indicating the subtracted symplectic leave is dual to the blue $\mathfrak{e}_6$ sub-web at the origin of the Coulomb branch.

Chapter 7

5d RG-flow Trees

Starting from a 5d SCFT, by turning on mass parameters to decouple hypermultiplets, one can flow to a different SCFT, giving rise to a tree of descendants. In this chapter we will apply the framework developed in chapter 6 to characterize the Higgs branch of a large set of 5d SCFTs, extending this analysis to the fixed points they flow to under RG.

To this end, we develop the concept of *edge-moves* in a generalized toric polygon, dual to Hanany-Witten brane creation (HW moves) [13] in the web, which allow us to pass between a non-convex polygon representing a 5d gauge theory, a so-called pre-GTP (pGTP), and the GTP realizing the associated SCFT. Moreover, we show how the geometric implementation of decoupling hypermultiplets by performing flop transitions [147] is realized as a flop of the corresponding matter curve in the pGTP, directly generalizing the application for toric models in [183]. Together, these operations allow us to reach any pGTP (i.e. 5d gauge theory) in a given descendant tree and take the strong-coupling limit to obtain the corresponding GTP (SCFT). We then apply the method presented in chapter 6 to each GTP to produce the associated magnetic quiver and Hasse diagram. From the magnetic quivers/Hasse diagrams we can furthermore read off the UV flavor symmetry algebra. In the magnetic quivers, the non-abelian part of the flavor algebra is given by the set of balanced nodes. In section 7.5, we discuss various new aspects of the flavor symmetries beyond the simple balanced nodes. In particular we will give rules how to identify certain non-simply laced flavor symmetries as well, like $\mathfrak{g}_2$.

The purely combinatorial nature of a GTP, and the algorithmic derivation of the magnetic quiver, makes the framework well-suited for implementation as a code – which was written and submitted with the pre-print of [2]. For the purpose of computing magnetic quivers

this is a major technical gain, which puts the goal of obtaining magnetic quivers for entire descendant trees within reach, at least from a practical point of view.

Here we will study a class of 5d SCFTs that can flow to single gauge node theories with anti-symmetric (**AS**) and fundamental (**F**) matter [140], as well as $SU(2)^m$ quiver gauge theories, in the IR. In [3] we gave a detailed description of the descendant trees obtained by decoupling matter multiplets in these theories, and provided *all* the associated magnetic quivers. In this thesis, however, we will be content to demonstrate the methodology, and provide the main results in a summarized form, referring the reader to [3] for additional details on computations and a plethora of magnetic quivers.

7.1 Overview of Results

We now give a summary of the theories and the main results of [3], namely the magnetic quivers for all decoupling trees. The rest of this chapter will be devoted to presenting the new developments that underlie these results, as well as illustrating the derivation in a selection of theories.

5d SCFTs that have a low-energy description as a gauge theory with a simple gauge group were classified in [140, 156]. They distinguish two types of theories, called *standard* and *exceptional*. In table 7.1 we list the standard gauge theories, whose UV magnetic quivers are shown as well. The exceptional theories are limited to rank of the gauge group ≤ 8. Using the strategy outlined above, we derive the magnetic quivers and flavor symmetry for the sub-marginal theories (obtained by a mass deformation from the 5d marginal theories), i.e. "tree tops". We consider 5d single gauge node theories with anti-symmetric ($N_{AS} = 0, 1, 2$) and fundamental matter shown in table 7.1.

1. Magnetic Quivers for all Rank 2 Theories:

   In appendix A of [3], in particular in tables 8, 9, 10, 11 we determine the complete set of magnetic quivers for all rank 2 5d SCFTs. The set of all rank 2 theories were determined from the geometries and flavor symmetries discussed in [141, 147, 148] and the brane-webs in [172][1] We provide the full rank 2 tree in terms of the Higgs branch data, i.e. magnetic quivers, and thereby resulting flavor algebras, which are in agreement with

[1] There are additional rank 2 theories obtained by twisted compactifications, which do not have a known web/GTP realization [149, 150]. It would be interesting to extend the results to these theories.

those found in [147], in particular we are able to extend the realm of magnetic quivers to non-simply laced symmetry algebras.

2. (D_{N+2}, D_{N+2}) Conformal Matter Trees:

   The (D_{N+2}, D_{N+2})-conformal matter theory gives rise to 5d SCFTs that are UV completions of an SQCD theory. We determine a representation of the sub-marginal theory in terms of a GTP, and identify the magnetic quiver and flavor symmetry, finding agreement with [120]. The tree of descendants can be determined for all, with the most interesting features appearing near the top, so we tabulate the magnetic quivers for a substantial part of the tree tops in table 12.

3. Rank $(N-1)$ E-string Trees:

   We then turn to the higher rank E-string, which has both an $SU(N)_{\frac{N+1}{2}} + 1\mathbf{AS} + 7\mathbf{F}$ and $Sp(N-1) + 1\mathbf{AS} + 7\mathbf{F}$ gauge theory realization. The 5d descendant tree of the higher rank E-string joins that of the (D_{N+2}, D_{N+2})-conformal matter theory by decoupling of the anti-symmetric matter. We identify the magnetic quiver for the sub-marginal rank $(N-1)$ E_8-theory, as well as those for all its 5d descendants with $N_F \geq 4$ in tables 13 and 14.

4. $SU(N)_{\frac{1}{2}} + 1\mathbf{AS} + (N+5)\mathbf{F}$ Trees:

   We subsequently study the 5d SCFT with an $SU(N)_{\frac{1}{2}} + 1\mathbf{AS} + (N+5)\mathbf{F}$ gauge theory realization, determining the GTP and magnetic quiver for the tree top. The decoupling tree of this class of theories can be determined for all ranks. We provide the magnetic quivers for a significant portion of the tree tops in tables 15 and 16.

5. $2\mathbf{AS}$ Trees:

   The last single gauge node theories that we discuss are the SCFTs whose tree tops flow to $SU(N)_{\frac{1}{2}} + 2\mathbf{AS} + 7\mathbf{F}$ and $SU(N)_2 + 2\mathbf{AS} + 6\mathbf{F}$ in the weak coupling regime. We give the magnetic quivers and manifest flavor symmetries for the complete descendant trees of these theories in tables 17 and 18. For $N = 4, 5$ the flavor symmetry exhibits a non-simply laced enhancement. We discuss this phenomenon for the magnetic quivers and tabulate them, along with the enhanced flavor symmetries, in tables 19 and 20.

6. Quiver Trees:

   Finally, we also consider the class of 5d SCFTs that have IR descriptions as $[n_1] - SU(2)^m - [n_2]$ 5d quiver gauge theories in the IR. These theories connect to the decoupling trees of (D_{m+3}, D_{m+3})-conformal matter as well as that of the rank 2 E-string. The majority of the quiver theories are UV dual to an SQCD theory (i.e. they share the same strong coupling fixed point). However, for quiver gauge theories with no fundamental matter associated to (at least) one of the $SU(2)$ factors and theta angle $\theta = 0$ this is not the case. We supply the GTPs and magnetic quivers for the latter theories in table 21.

7.2 Construction of GTPs and Edge-moves

In this chapter we will construct the GTPs for a large class of 5d SCFTs. The general strategy is to compute the (p)GTP for the sub-marginal theory from the dual web (and to then determine the descendants using polygon-only operations). Generically, the resulting diagram is not convex, which in the web-picture means that in order to take the strong-coupling limit, one has to first apply a sequence of Hanany-Witten moves. As the brane-practitioner will know, this can be a rather cumbersome enterprise. By mapping the problem to the dual graphs, these moves are realized in terms of monodromy-preserving edge-moves, the purely combinatorial information of which can easily be implemented in a code, see appendix B of [2]. We will now explain how to determine these.

7.2.1 Generalized Toric Polygons and Webs

In this section we present the pGTPs of $SU(N)$ gauge theories with fundamental and anti-symmetric matter that admit a UV completion. Our strategy is to start with the weakly coupled (p, q) 5-brane webs. From this, we can easily determine the pGTP of the gauge theory. These pGTPs, specified uniquely by the set of black vertices V_b, are summarised in table 7.2. However, if the polygon is non-convex, it is not possible to remove the internal edge representing the gauge coupling. To be able to pass to strong coupling, we need to perform the GTP equivalent of the Hanany-Witten moves, i.e. monodromy- and charge-preserving edge-moves.

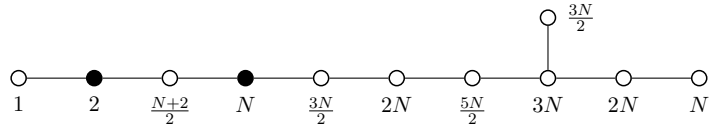
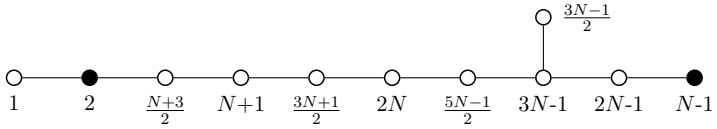
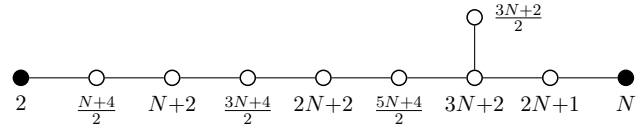
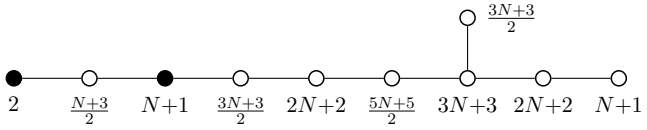
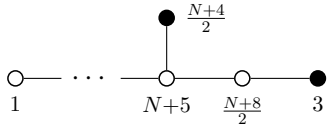
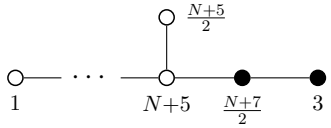
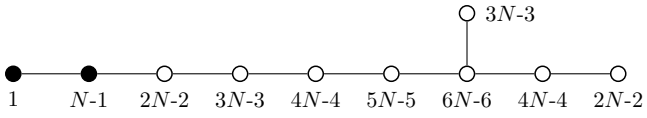
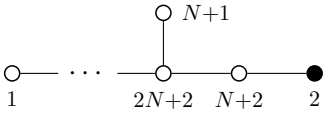
Gauge	Matter	Magnetic Quiver for sub-marginal theory
$SU(N)_0$	$2\boldsymbol{AS}+8\boldsymbol{F}$	N even:  N odd: 
$SU(N)_{3/2}$	$2\boldsymbol{AS}+7\boldsymbol{F}$	N even:  N odd: 
$SU(N)_0$	$1\boldsymbol{AS}+(N+6)\boldsymbol{F}$	N even:  N odd: 
$SU(N)_{N/2}$	$1\boldsymbol{AS}+8\boldsymbol{F}$	
$SU(N)_0$	$(2N+4)\boldsymbol{F}$	

Table 7.1: Marginal or KK-theories with single gauge group, which we will discuss. The magnetic quiver is shown for the theory obtained after decoupling one of the fundamental matter fields. These theories will be referred to as sub-marginal. The white nodes in the quivers are the balanced nodes which encode the flavor symmetry algebra.

Theory	pGTP
$SU(N)_k + N_F\boldsymbol{F}$	$\Big\{(0,0);(1,i)_{a\leq i\leq N_R+a};(0,N);$ $(-1,i)_{N-k-\frac{N_L-N_R}{2}-a\geq i\geq N-k-\frac{N_L+N_R}{2}-a}\Big\}$
$SU(2n)_k + 1\boldsymbol{AS} + N_F\boldsymbol{F}$	$\Big\{(0,-n);(1,i)_{k-\frac{N_F+2}{2}\leq i\leq k+\frac{N_F-2}{2}};$ $(0,n);(-1,n-1);(-n,0)\Big\}$
$SU(2n+1)_k + 1\boldsymbol{AS} + N_F\boldsymbol{F}$	$\Big\{(0,-n-1);(1,i)_{k-\frac{N_F+5}{2}\leq i\leq k+\frac{N_F-5}{2}};$ $(0,n);(-1,n);(-n-1,0)\Big\}$
$SU(2n)_k + 2\boldsymbol{AS} + N_F\boldsymbol{F}$	$\Big\{(0,-n);(1,-n);(n,n\ i)_{-1\leq i\leq N_R-1};$ $(0,n);(-1,n+k+\frac{N_L-N_R}{2});$ $(-n,n\ i)_{k+\frac{N_L-N_R}{2}+1\geq i\geq k-\frac{N_L+N_R}{2}+1}\Big\}$
$SU(2n+1)_k + 2\boldsymbol{AS} + N_F\boldsymbol{F}$	$\Big\{(0,-n-1);(n,-n-1);(n,n\ i)_{-1\leq i\leq N_R-1};$ $(0,n);(-n,n\ i)_{k+\frac{N_L-N_R}{2}+1\geq i\geq k-\frac{N_L+N_R}{2}+1};$ $(-n,n(k-\frac{N_L+N_R}{2}+1)-1)\Big\}$

Table 7.2: Construction of toric polygons (not necessarily convex) for the theories studied in this paper. For each theory, we give a list of pairs of integers which should be interpreted as the list of coordinates of the black dots defining the polygons in counter clockwise order; the white dots can then be added on the points of the interior of the edges with integer coefficients. The free parameter a can take any integer value, parametrising the $SL(2,\mathbb{Z})$-frame. The polygons presented here can be deduced from the brane webs constructed in [208].

Let us first fix the notation. We let P be a pre-GTP (pGTP), i.e. a GTP where we relax the convexity requirement. For simplicity we ignore interior edges, such as rulings, for now but will return to this issue later. The pGTP is characterised by the list of its black vertices $\boldsymbol{v}_i$ with $i \in \mathbb{Z}_{n_V}$, labelling them in counter clockwise order. Equivalently, P can be characterised by the list of vectors $[\boldsymbol{u}_i]_{i\in\mathbb{Z}_{n_V}}$ defined by

$$\boldsymbol{u}_i = \boldsymbol{v}_i - \boldsymbol{v}_{i-1}\,. \tag{7.1}$$

Note that such a list of vectors of $\mathbb{Z}^2$ defines a polygon only if they add up to zero. The polygon is convex if and only if two consecutive edges have direction vectors $\boldsymbol{u}_i$ and $\boldsymbol{u}_{i+1}$ forming a positively oriented basis of the plane. It is useful to introduce shorthand for the determinants and greatest common divisors

$$D_{i,j} = \det\left(\boldsymbol{u}_i, \boldsymbol{u}_j\right)\,, \qquad D_i = D_{i,i+1}\,, \qquad \mu_i = \gcd(\boldsymbol{u}_i)\,. \tag{7.2}$$

In other words,

$$P \text{ convex} \iff D_i \geq 0 \quad \forall i \in \mathbb{Z}_{n_V}\,. \tag{7.3}$$

Let

$$\mathfrak{C} := \{i \mid D_i < 0\} \tag{7.4}$$

be the set of labels, which indicate the non-convexities of P. Clearly, the polygon is convex if and only if $\mathfrak{C} = \emptyset$.

7.2.2 From Non-convex to Convex Polygons: Edge-moves

We now assume $\mathfrak{C} \neq \emptyset$, and our goal is to find a GTP, which is convex and physically equivalent to P. Inspired by the brane-web, we exhibit two basic, related operations which, upon being iterated in an appropriate way, can result in such a GTP:

1. Monodromies:

   Let $i \in \mathfrak{C}$. We define two operations on the polygon P, which affect the two vectors $\boldsymbol{u}_i$ and $\boldsymbol{u}_{i+1}$ in the following way, leaving the other vectors unchanged:

$$\begin{aligned}\mathfrak{M}_i^+ \;:\; & [\ldots, \boldsymbol{u}_{i-1}, \boldsymbol{u}_i, \boldsymbol{u}_{i+1}, \boldsymbol{u}_{i+2}, \ldots] \mapsto \\ & \left[\ldots, \boldsymbol{u}_{i-1}, \boldsymbol{u}_{i+1}\left(1 - \frac{D_i}{\mu_{i+1}^2}\right), \boldsymbol{u}_i + \boldsymbol{u}_{i+1}\left(\frac{D_i}{\mu_{i+1}^2}\right), \boldsymbol{u}_{i+2}, \ldots\right]\end{aligned} \tag{7.5}$$

$$\begin{aligned}\mathfrak{M}_i^- \;:\; & [\ldots, \boldsymbol{u}_{i-1}, \boldsymbol{u}_i, \boldsymbol{u}_{i+1}, \boldsymbol{u}_{i+2}, \ldots] \mapsto \\ & \left[\ldots, \boldsymbol{u}_{i-1}, \boldsymbol{u}_{i+1} + \boldsymbol{u}_i\left(\frac{D_i}{\mu_i^2}\right), \boldsymbol{u}_i\left(1 - \frac{D_i}{\mu_i^2}\right), \boldsymbol{u}_{i+2}, \ldots\right]\end{aligned} \tag{7.6}$$

One can check that after having applied $\mathfrak{M}_i^{\pm}$, the polygon is convex at i, as

$$\det\left[\boldsymbol{u}_{i+1}\left(1-\frac{D_i}{\mu_{i+1}^2}\right),\boldsymbol{u}_i+\boldsymbol{u}_{i+1}\left(\frac{D_i}{\mu_{i+1}^2}\right)\right]=-D_i\left(1-\frac{D_i}{\mu_{i+1}^2}\right)>0\,, \tag{7.7}$$

and similarly for $\mathfrak{M}_i^-$. However, it is now possible that $i\pm 1\in\mathfrak{C}$.

2. Pruning:

   Let $i\in\mathfrak{C}$. Let $k_\pm$ be the smallest positive integers such that

$$\begin{aligned} &D_{i+1,i+k_++1}>0 \quad\wedge\quad D_{i+1,i+k_++2}\leq 0 \quad\wedge\quad i+1,...,i+k_+\notin\mathfrak{C}\\ &D_{i-k_-,i}>0 \quad\wedge\quad D_{i-k_--1,i}\leq 0 \quad\wedge\quad i-1,...,i-k_-\notin\mathfrak{C}\,. \end{aligned} \tag{7.8}$$

   If the respective integer $k_\pm$ exists we define the operations

$$\begin{aligned} \mathfrak{P}_i^+ \;:\; &[\ldots,\boldsymbol{u}_i,\boldsymbol{u}_{i+1},\boldsymbol{u}_{i+2},\ldots,\boldsymbol{u}_{i+k_++1},\boldsymbol{u}_{i+k_++2},\ldots]\mapsto \\ &\left[\ldots,\boldsymbol{u}_i,\boldsymbol{u}_{i+2}+\frac{D_{i+1,i+2}}{\mu_{i+1}^2}\boldsymbol{u}_{i+1},\ldots,\boldsymbol{u}_{i+k_++1}+\frac{|D_{i+1,i+k_++1}|}{\mu_{i+1}^2}\boldsymbol{u}_{i+1},\right. \\ &\left.\boldsymbol{u}_{i+1}\left(1-\sum_{j=1}^{k_+}\frac{D_{i+1,i+j+1}}{\mu_{i+1}^2}\right),\boldsymbol{u}_{i+k_++2}\ldots\right] \end{aligned} \tag{7.9}$$

$$\begin{aligned} \mathfrak{P}_i^- \;:\; &[\ldots,\boldsymbol{u}_{i-k_--1},\boldsymbol{u}_{i-k_-},\ldots,\boldsymbol{u}_{i-1},\boldsymbol{u}_i,\boldsymbol{u}_{i+1},\ldots]\mapsto \\ &\left[\ldots,\boldsymbol{u}_{i-k_--1},\boldsymbol{u}_i\left(1-\sum_{j=1}^{k_-}\frac{D_{i,i-j}}{\mu_i^2}\right),\boldsymbol{u}_{i-k_-}+\frac{D_{i,i-k_-}}{\mu_i^2}\boldsymbol{u}_i,\ldots,\right. \\ &\left.\boldsymbol{u}_{i-1}+\frac{D_{i,i-1}}{\mu_i^2}\boldsymbol{u}_i,\boldsymbol{u}_{i+1}\ldots\right]\,. \end{aligned} \tag{7.10}$$

   This does not necessarily remove the non-convexity at i, but may increase D_i.

We can represent any monodromy- and charge-preserving transformation on P as a (finite) word using these operations as letters. We will present detailed examples in section 7.4.

Let us now consider internal edges, which in our context represent finite parameters along the extended Coulomb branch, i.e, gauge couplings m_0 or hypermultiplet masses m_f. Under an edge-move $\boldsymbol{u}\mapsto\mathfrak{M}_i^{\pm}\boldsymbol{u}$, the original internal edges are unchanged and $\boldsymbol{u}_i$ and $\boldsymbol{u}_{i+1}$ become internal lines in the transformed polygon. We can also prune a polygon with internal edges, however, the transformation is very impractical to implement, and will therefore not be used in the following.

7.3 Decoupling

5d SCFTs can be related by decoupling matter hypermultiplets. In the context of geometric models realized as singular Calabi-Yau spaces, this is achieved by flop transitions, which take matter curves of normal bundle degree $(-1,-1)$ and flop them out of the compact surfaces, that realize the Cartan subgroups of the gauge group. In this way in 5d, one can construct decoupling trees, which start with a marginal theory, which itself UV completes in 6d, and apply decoupling limits [147]. Applied in the context of toric models, these flops have a simple realization: the $(-1,-1)$ curves are particular curves, which are connections of an internal vertex (compact divisors) to an external one – subject to the normal bundle condition. This decoupling was applied in [183] to toric models and the construction of decoupling trees and relation to so-called CFDs was discussed. Here we will extend this to pGTPs and GTPs.

The first important point to note is that the decoupling in the pGTP is straight forward, as we will explain in this section. We can trace the decoupling process through the monodromy transformations, which map the pGTP to a convex GTP. However, we do not find a simple decoupling rule on GTPs: the main complication is that applying the decoupling to a GTP usually results in a pGTP, i.e. convexity is not retained in this process. We will therefore construct our decoupling trees before applying the edge-moves, and then map them to GTPs afterwards.

There are two cases of interest to consider: those that are purely made of black dots, convex or not, and those that do not have such a representation, e.g. the situation with **AS** matter. We now discuss decoupling in all these instances for the SCFTs, and also the decoupling for IR magnetic quivers, which has a much more straight forward realization in terms of quiver subtractions.

7.3.1 Decoupling Fundamental Matter

Let us first recall briefly the toric situation. In this case a hypermultiplet curve is decoupled by a flop, which contracts the curve and flops it outside of the compact surfaces – in practice this means that one of the external vertices (corresponding to non-compact divisors) is no longer connected to an internal vertex. An example is shown in figure 7.1.

Similarly for the case of pGTPs a fundamental matter multiplet will correspond locally to a curve connecting an internal to an external corner vertex. Decoupling this we follow the

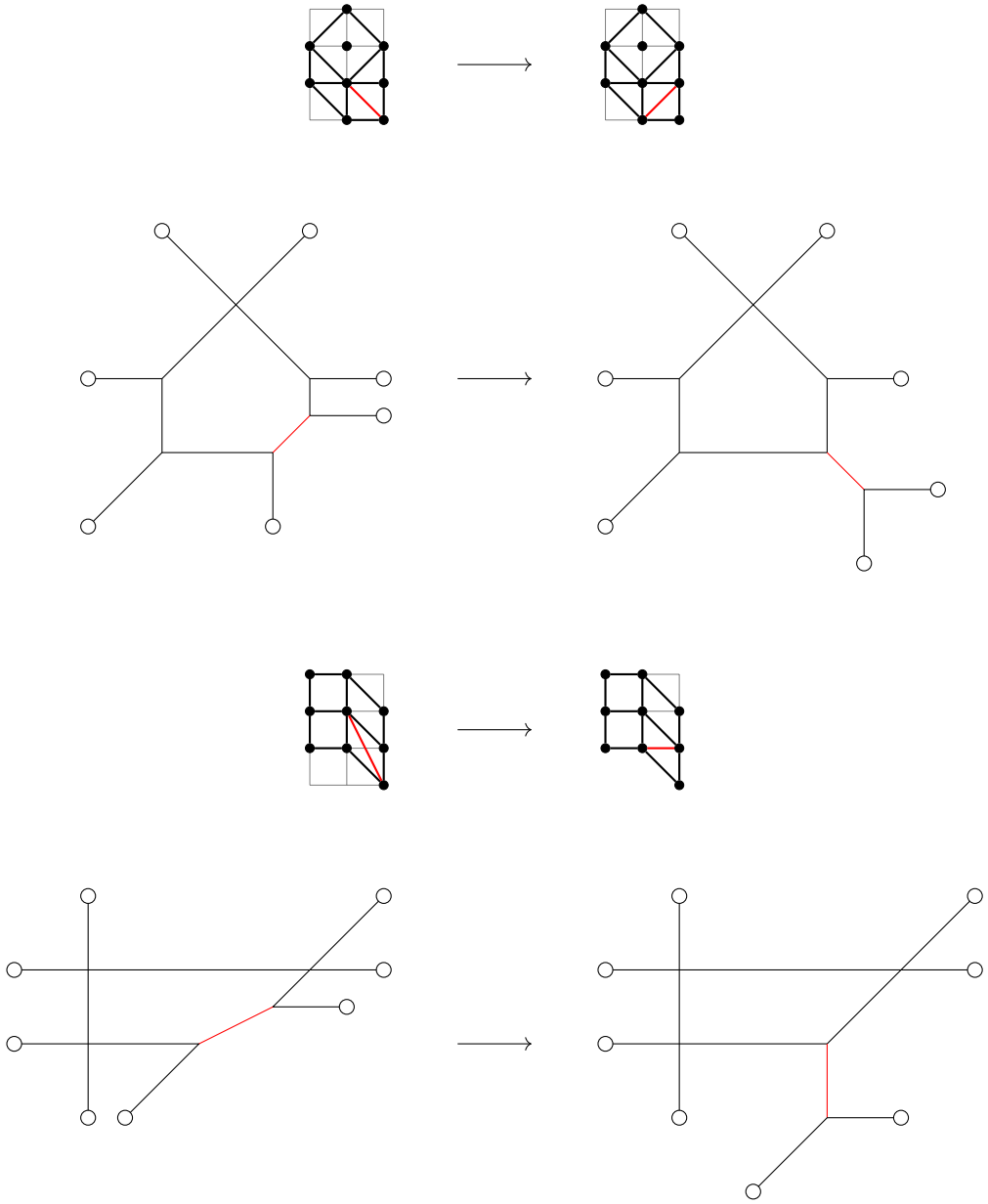


Figure 7.1: Decoupling in a toric (top) and pGTP (bottom), as well as their counterparts in the brane-web. In each of the figures the left hand side shows the configuration before the flop, with the matter hypermultiplet "curve" shown in red, and the right hand side shows the configuration, after the decoupling/flop.

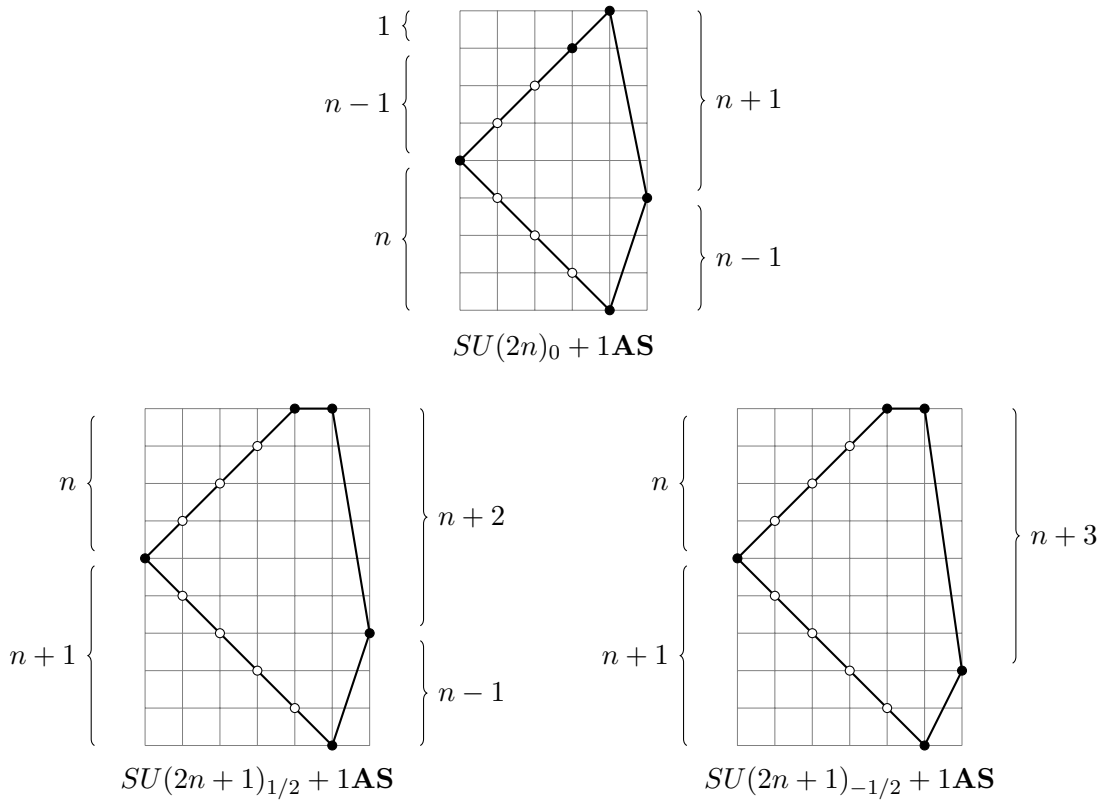


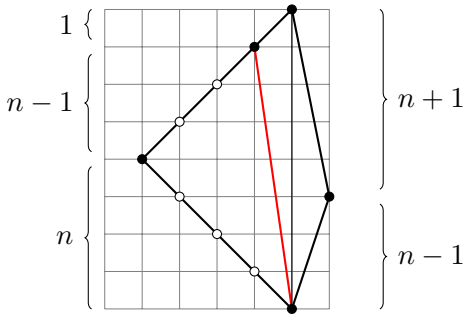
Figure 7.2: Toric polygons for $SU(N)_k + 1\mathbf{AS}$ for the lowest possible values of the Chern-Simons level, $|k| < 1$. We have to distinguish between the cases where $N = 2n$ is even and $N = 2n + 1$ is odd. The polygons presented here can be deduced from the brane webs constructed in [208]. The integers next to the braces indicate the vertical length of the corresponding segment; for the drawings we picked $n = 4$. The Chern-Simons level can be increased / decreased by one unit by moving the rightmost dot upwards / downwards by one unit of distance.

same procedure as in the toric diagram (even though of course the geometric analogy does not exist here). Figure 7.1 shows an example.

7.3.2 Decoupling Anti-symmetric Matter

The decoupling of anti-symmetric hypermultiplets proceeds in a similar way. The theories which we consider have one or two **AS** of an $SU(N)$ gauge theory. First in the (p)GTP we identify the ruling, which are internal black dots, corresponding to the Cartan subgroups of the gauge group. To decouple an **AS**, a sub-division of the (p)GTP needs to be achieved, such that there is no connection between the vertices of the ruling and the external node corresponding to the **AS** matter. In addition this decoupling needs to satisfy all the rules of GTPs (the r-rule in particular, see definition 7).

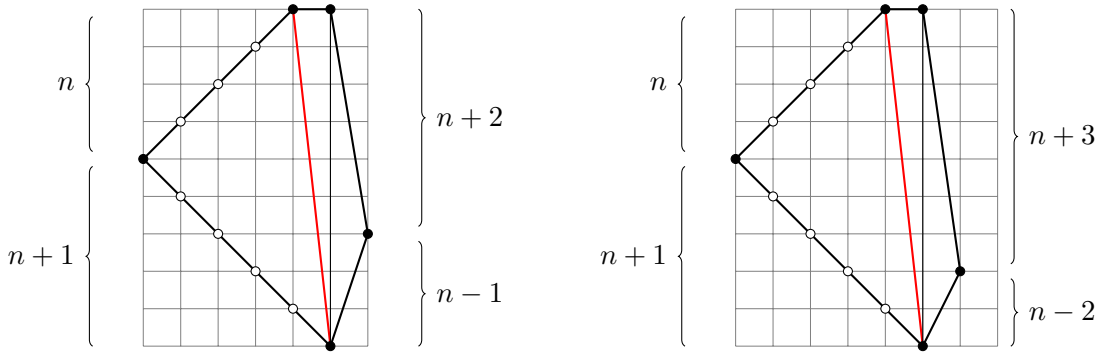
Let us illustrate the decoupling of an anti-symmetric hypermultiplet. It is particularly interesting to keep track of the Chern-Simons level in the process. Starting from the first polygon in figure 7.2, which is $SU(2n)_0 + 1\mathbf{AS}$, the decoupling of the **AS** hyper is given by



(7.11)

The sub-division is shown in terms of the red line, and the ruling is indicated in black. After decoupling, we obtain a polygon which corresponds to the pure theory $SU(2n)_{n-2}$. Therefore the **AS** hyper contributes to $n-2$ units of Chern-Simons level in $SU(2n)$ theories. This is in perfect agreement with the expectation (5.13), according to which the Chern-Simons level is shifted by $\frac{1}{2}A(\boldsymbol{AS}) = n-2$ upon decoupling of the antisymmetric hyper.

We can do the same for the other two polygons of figure 7.2, and obtain



$SU(2n+1)_{1/2} + 1\mathbf{AS}$ $\qquad$ $SU(2n+1)_{-1/2} + 1\mathbf{AS}$

(7.12)

In the first case, the level after decoupling is $n-1$ while in the second case it is $n-2$. This means that the **AS** hyper contributes $\frac{1}{2} - (n-1) = -\frac{1}{2} - (n-2) = \frac{3}{2} - n$ units of Chern-Simons level in $SU(2n+1)$ theories. Again this is in perfect agreement with (5.13), according to which the Chern-Simons level is shifted by $\frac{1}{2}A(\boldsymbol{AS}) = n - \frac{3}{2}$ upon decoupling of the antisymmetric hyper.

In all cases, we see that the **AS** hyper as constructed in these polygons contribute $\frac{N-4}{2}$ units of Chern-Simons level in $SU(N)$ theories, in accordance with (5.13) and table 5.2. Note that for $SU(3)$ theories, this is indeed $-\frac{1}{2}$, as expected from the fact that $\mathbf{AS} \equiv \bar{\mathbf{F}}$ in that case. In particular, we see that

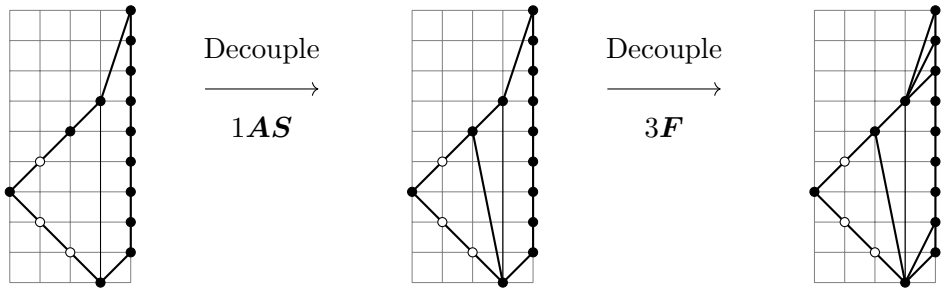


Figure 7.3: Example of decoupling matter. We start from $SU(2n)_n + 1\boldsymbol{AS} + 8\boldsymbol{F}$ and after decoupling an anti-symmetric we obtain $SU(2n)_{2n-2} + 8\boldsymbol{F}$. We then decouple three fundamentals (one with positive and two with negative mass) to reach $SU(2n)_{2n-\frac{5}{2}} + 5\boldsymbol{F}$.

- The marginal theory $SU(N)_{N/2} + 1\mathbf{AS} + 8\mathbf{F}$ gives after decoupling the **AS** the non-marginal theory $SU(N)_{N-2} + 8\mathbf{F}$, which can also be seen as the marginal theory $SU(N)_0 + (2N+4)\mathbf{F}$ where we have decoupled $N-4$ fundamentals with level $\frac{1}{2}$.
- The marginal theory $SU(N)_0 + 1\mathbf{AS} + (N+6)\mathbf{F}$ gives after decoupling the **AS** the non-marginal theory $SU(N)_{\frac{N}{2}-2} + (N+6)\mathbf{F}$, which can also be seen as the marginal theory $SU(N)_0 + (2N+4)\mathbf{F}$ where we have decoupled $N-3$ fundamentals with level $\frac{1}{2}$ and one fundamental with level $-\frac{1}{2}$.

The toric diagram interpretation guarantees that these statements are valid at the SCFT (strong coupling) point. One can also decouple several hypers at the same time using the same procedure. This is illustrated in figure 7.3.

7.3.3 Decoupling for IR Magnetic Quivers

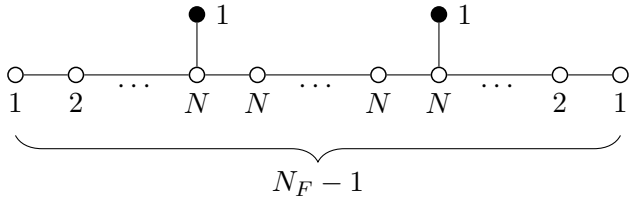
So far we discussed the decoupling for a generic pGTP, having in mind GTPs that correspond to strongly-coupled UV fixed points. In this section we implement decoupling directly in the IR magnetic quivers. A word of caution is in place here: the IR magnetic quivers are blind to several important characteristics of a theory, e.g. the CS-couplings. This means that one cannot, at least not without additional information, infer the UV from the IR magnetic quiver. To understand in general how the MQ – of a UV or IR theory – responds to motion along the extended Coulomb branch, a more flexible technology is needed. This question is precisely the topic of chapter 8 where we develop the necessary framework by taking the perspective of the 3d $\mathcal{N}=4$ theory. Nevertheless, the decoupling is a relevant concept also in the IR, and we will see here that it reduces in may cases simply to a quiver subtraction.

We consider the cases

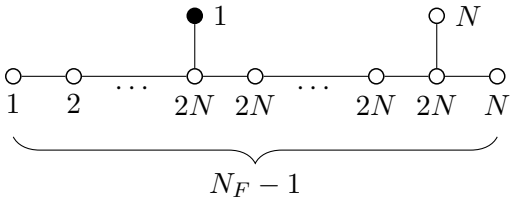
$$SU(N)_k + N_F\mathbf{F}\,, \qquad Sp(N) + N_F\mathbf{F}\,. \tag{7.13}$$

Decoupling essentially corresponds to subtracting a hypermultiplet from the magnetic quiver. The magnetic quivers for these theories are given by

$SU(N) + N_F\mathbf{F}$:



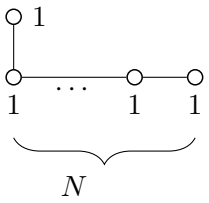
$Sp(N) + N_F\mathbf{F}$:



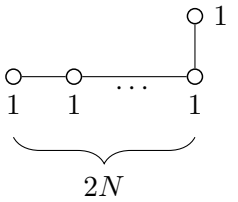
(7.14)

To pass from these magnetic quivers to the ones with one fundamental decoupled is equivalent to the quiver subtraction by

Quiver subtraction for $SU(N) + N_F\mathbf{F}$:



Quiver subtraction for $Sp(N) + N_F\mathbf{F}$:



(7.15)

The interpretation of each of these diagrams is of course that they correspond to a free hyper in the fundamental. Subtracting these using the rules in [128], gives rise to the magnetic quiver of the theory with one less flavor.

This approach generalizes readily, e.g. to the 5d quiver theories $SU(2) - SU(2)$, where decoupling in the IR-MQ is just subtracting an $\mathfrak{su}(4)$.

7.4 UV Magnetic Quivers for $SU(N)$ with AS and F via GTPs

For general $SU(N)$ with fundamental and anti-symmetric matter there are five marginal theories introduced in [141]. In [3] we considered the submarginal theory, obtained by decoupling a single fundamental hypermultiplet, for each of them as well as for $SU(2)$ quiver gauge theories. In this thesis, we illustrate the methodology for two theories, namely $SU(N)_{\frac{1}{2}} + (2N+3)\boldsymbol{F}$ and $SU(N)_{\frac{1}{2}} + 1\boldsymbol{AS} + (N+5)\boldsymbol{F}$, and refer the reader to the paper for analogous computations for

Section 5.2 $SU(N)_{\frac{N+1}{2}} + 1\boldsymbol{AS} + 7\boldsymbol{F}$

Section 5.4 $SU(N)_{\frac{1}{2}} + 2\boldsymbol{AS} + 7\boldsymbol{F}$

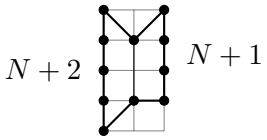
Section 5.5 $SU(N)_2 + 2\boldsymbol{AS} + 6\boldsymbol{F}$

Section 5.6 5d Quivers

We will give the (p)GTP before and after edge-moves and compute the magnetic quiver for the SCFT. Decoupling further matter was discussed in section 7.3 and the magnetic quivers of the descendant trees are given in appendix B of [3].

7.4.1 $SU(N)_{\frac{1}{2}} + (2N+3)\boldsymbol{F}$

GTP for Tree Tops. First, we study the submarginal theory associated to the circle reduction of (D_{N+2}, D_{N+2})-conformal matter. This theory is the parent of all 5d SCFTs with an SQCD description in the IR. The polygon for $SU(N)_{\frac{1}{2}} + (2N+3)\boldsymbol{F}$ is given by



(7.16)

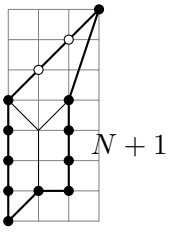
We draw the pGTP for $N = 3$, but the generalization to any N is obtained by increasing the number of vertical edges as shown. The ruling indicating the $SU(N)$ gauge theory description is given by the thin internal line. The edge-moves necessary to make this polygon convex were discussed in [120] in the web description. However, let us exemplify them on the polygon

and in our language. Fix $\boldsymbol{v}_0$ to be the lower left corner. Then, the polygon is given by the vectors

$$\boldsymbol{u} = \begin{bmatrix} (1,1), (1,0), \underbrace{(0,1)}_{N+1}, (-1,-1), (-1,1), \underbrace{(0,-1)}_{N+2} \end{bmatrix} . \tag{7.17}$$

The non-convex edges are $\mathfrak{C} = \{1, N+4\}$. First, let us perform an edge-move $\mathfrak{M}^-_{N+4}$. Using the rules laid out in (7.5), the polygon becomes

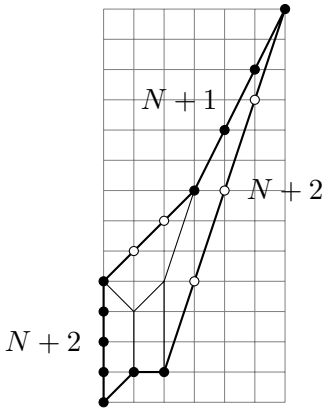
$$\boldsymbol{u} \mapsto \mathfrak{M}^-_{N+4}\boldsymbol{u} = \begin{bmatrix} (1,1), (1,0), \underbrace{(0,1)}_{N+1}, (1,3), (-3,-3), \underbrace{(0,-1)}_{N+2} \end{bmatrix} , \qquad \tag{7.18}$$



As we can see there are now white vertices, because in the resulting polygon $\mathfrak{M}^-_{N+4}\boldsymbol{u}$ we have $\mu_{N+5} = \{3\}$. Next, we move the $(1,3)$ edge through all the $(0,1)$ edges by applying $\mathfrak{M}^+_3 \cdots \mathfrak{M}^+_{N+3}$. Then, the vectors are given by

$$\mathfrak{M}^+_3 \cdots \mathfrak{M}^+_{N+3}\mathfrak{M}^-_{N+4}\boldsymbol{u} = \begin{bmatrix} (1,1), (1,0), (N+2, 3N+6), \underbrace{(-1,-2)}_{N+1}, (-3,-3), \underbrace{(0,-1)}_{N+2} \end{bmatrix} , \tag{7.19}$$

and the polygon is

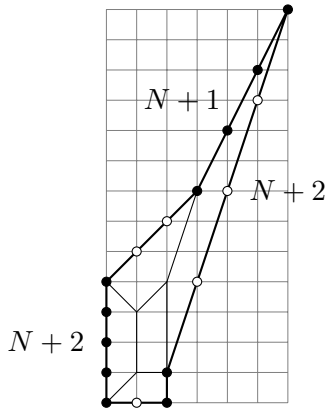


(7.20)

Now, we remove the non-convexity at $i = 1$. We apply the edge-move $\mathfrak{M}^+_1$ which yields the vectors

$$\mathfrak{M}^+_1\mathfrak{M}^+_3 \cdots \mathfrak{M}^+_{N+3}\mathfrak{M}^-_{N+4}\boldsymbol{u} = \begin{bmatrix} (2,0), (0,1), (N+2, 3N+6), \underbrace{(-1,-2)}_{N+1}, (-3,-3), \underbrace{(0,-1)}_{N+2} \end{bmatrix} , \tag{7.21}$$

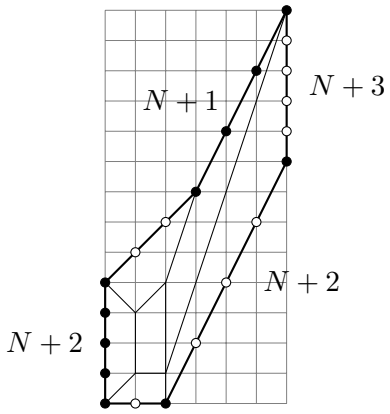
and polygon



(7.22)

We apply the operation $\mathfrak{M}_2^-$ to arrive at

$$\mathfrak{M}_2^-\mathfrak{M}_1^+\mathfrak{M}_3^+\cdots\mathfrak{M}_{N+3}^+\mathfrak{M}_{N+4}^-\boldsymbol{u} = \left[(2,0),(N+2,2N+4),(0,N+3),\underbrace{(-1,-2)}_{N+1},(-3,-3),\underbrace{(0,-1)}_{N+2}\right], \tag{7.23}$$



(7.24)

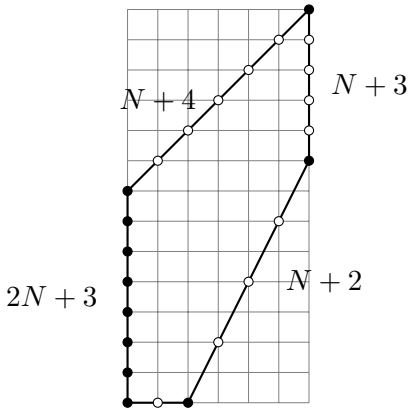
Finally, we move the $(-3,-3)$ edge through the $(-1,-2)$ edges, and obtain the vectors

$$\mathfrak{T}\boldsymbol{u} = \left[(2,0),(N+2,2N+4),(0,N+3),(-N-4,-N-4),\underbrace{(0,-1)}_{2N+3}\right], \tag{7.25}$$

where we have written the entire sequence of transformations in a compact form as

$$\mathfrak{T} = \mathfrak{M}_4^+\cdots\mathfrak{M}_{N+4}^+\mathfrak{M}_2^-\mathfrak{M}_1^+\mathfrak{M}_3^+\cdots\mathfrak{M}_{N+3}^+\mathfrak{M}_{N+4}^-\,. \tag{7.26}$$

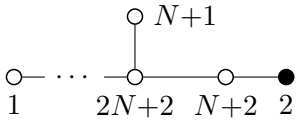
The convex polygon is



(7.27)

We have removed the interior edges, since we are interested in the SCFT corresponding to this polygon. It is easy to check that $\mathfrak{C} = \emptyset$ for $\mathfrak{T}\boldsymbol{u}$.

Magnetic Quivers and Decoupling In chapter 6 it was discussed how to compute the magnetic quiver from such a GTP. In this case there is a single coloring of (7.27), i.e. a single magnetic quiver. As is well-known, this is given by

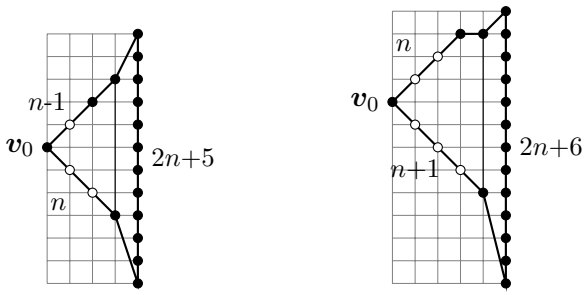


(7.28)

from which one can read off the $\mathfrak{so}(4N+8)$ flavor symmetry.

7.4.2 $SU(N)_{\frac{1}{2}} + 1AS + (N+5)F$

GTP for Tree Tops. In this case the pGTP depends on whether N is even or odd, so we will discuss them in turn. The polygons before edge-moves are (drawn for $n = 3$)



(7.29)

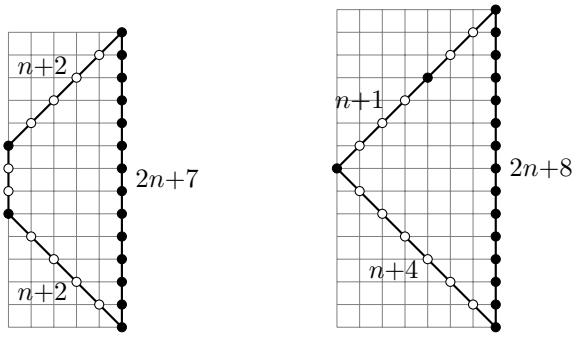
where $N = 2n$ and $N = 2n+1$, respectively. The vectors of the pGTPs are

$$\begin{aligned} N = 2n: \qquad & \boldsymbol{u} = \left[(n,-n),(1,-3),\underbrace{(0,1)}_{2n+5},(-1,-2),(-1,-1),(-n+1,-n+1)\right] \\ N = 2n+1: \qquad & \boldsymbol{u} = \left[(n+1,-n-1),(1,-4),\underbrace{(0,1)}_{2n+6},(-1,-1),(-1,0),(-n,-n)\right] \end{aligned} \tag{7.30}$$

The sequences of edge-moves that make the polygons convex are given by

$$\begin{aligned} N = 2n: \qquad & \mathfrak{T} = \mathfrak{M}^-_{-1}\mathfrak{M}^-_{0}\mathfrak{M}^-_{1}\mathfrak{M}^+_{-1}\mathfrak{M}^-_{-2} \\ N = 2n+1: \qquad & \mathfrak{T} = \mathfrak{M}^-_{-2}\mathfrak{M}^-_{-3}\mathfrak{M}^-_{0}\mathfrak{M}^-_{1} \end{aligned} \tag{7.31}$$

The resulting GTPs are (drawn for $n = 3$)



(7.32)

given by the vectors

$$\begin{aligned} N = 2n: \qquad & \mathfrak{T}\boldsymbol{u} = \left[(n+2,-n-2),\underbrace{(0,1)}_{2n+7},(-n-2,-n-2),(0,-3)\right] \\ N = 2n+1: \qquad & \mathfrak{T}\boldsymbol{u} = \left[(n+4,-n-4),\underbrace{(0,1)}_{2n+8},(-3,-3),(-n-1,-n-1)\right] \end{aligned} \tag{7.33}$$

Magnetic Quivers and Decoupling. From this we can compute the magnetic quivers for general N



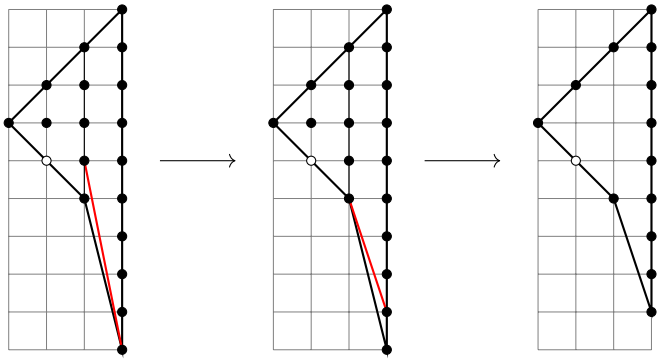
(7.34)

for $N = 2n$ and $N = 2n+1$ respectively. From the balanced nodes we see that generally the theory has flavor group $\mathfrak{su}(N+7) \oplus \mathfrak{u}(1)$, which is enhanced for small N. Concretely, the symmetry enhances to $\mathfrak{su}(12) \oplus \mathfrak{su}(2)$ for $N = 5$ and $\mathfrak{su}(12)$ for $N = 4$. For $N = 3$ the theory is

$SU(3)_{\frac{1}{2}}+9\boldsymbol{F}$ with $\mathfrak{so}(20)$ flavor symmetry, whereas the $N=2$ case is the rank one E_8 theory.

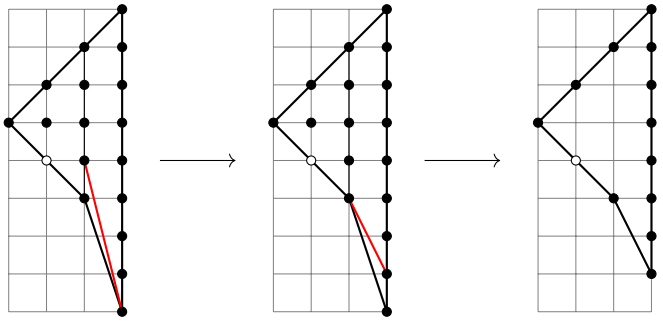
Example. $SU(4)_k+1\mathbf{AS}+N_F\mathbf{F}$

Let us illustrate the decoupling of matter in the polygons associated to $SU(4)_k+1\mathbf{AS}+N_F\mathbf{F}$ theories. We consider the theories with $0\leq N_F\leq 9$ with $k=0$ or $k=\frac{1}{2}$ depending on the parity of N_F. We first identify the ruling associated to the gauge theory phase. The decoupling of fundamental matter is then implemented by flopping a curve connecting an internal vertex on the ruling to a corner vertex. The relevant fundamental matter curves will be indicated in red in the following. For $N_F=9$, the pGTP before and after the flop of the matter curve is



(7.35)

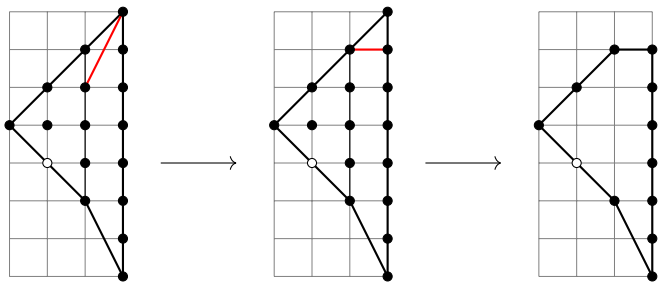
After the flop, the corner vertex is no longer connected to the internal gauge vertices, so this theory is represented by the right-most polygon, which is exactly the pGTP of $SU(4)_0+1\mathbf{AS}+8\mathbf{F}$. This pGTP also has a fundamental matter curve connecting its bottom right vertex to an internal gauge node, which we can again flop to obtain the pGTP of $SU(4)_{1/2}+1\mathbf{AS}+7\mathbf{F}$:



(7.36)

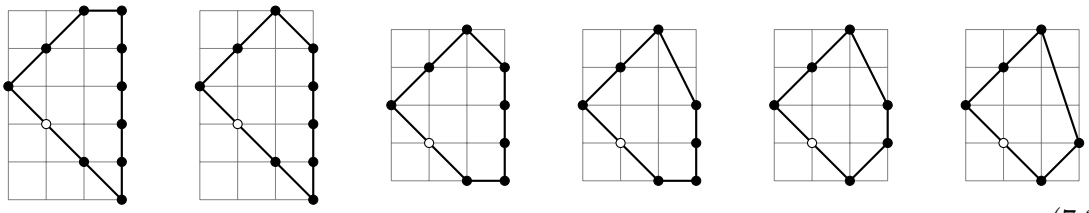
Strictly speaking, the two previous flops correspond to decoupling fundamental matter multiplets by giving them a mass with the same sign. For this reason, the change in CS level is actually $k=\frac{1}{2}\to 0\to -\frac{1}{2}$. However, since the Higgs branch only depends on the absolute value of the CS level, the previous flops are indeed equivalent to the sequence $k=\frac{1}{2}\to 0\to\frac{1}{2}$.

To stay in the $k = 0, \frac{1}{2}$ regime, we now flop a matter curve connecting to the top right corner vertex, which corresponds to giving a fundamental a mass with the opposite sign of the previous two decoupled matter multiplets. Flopping this curve, we thus arrive at the polygon for $SU(4)_0 + 1\mathbf{AS} + 6\mathbf{F}$:



(7.37)

We can continue in this way until all fundamental matter is decoupled. For $N_F = 5, \ldots, 1, 0$, one finds

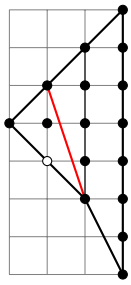


(7.38)

Clearly the last polygon has no more fundamental matter curves that can be flopped. These pGTPs are convex so the magnetic quiver for the corresponding SCFT can be obtained directly from these polygons, using the method developed in chapter 6. On the contrary for $N_F = 6, 7, 8, 9$ the pGTPs are not convex, and edge-moves have to be performed. The resulting GTPs as well as their UV magnetic quivers are shown in table 7.3. Note that the edge-moves can be done in different ways, giving distinct GTPs. However, all resolutions lead to the same UV magnetic quivers.

One can also at any point choose to decouple the anti-symmetric matter, thereby making contact with the $SU(4)$ SQDC theories. If we take the left-most vertex as the origin, the relevant matter curve connects the vertex at $(1, 1)$ to the bottom vertex of the ruling at $(2, -2)$. Clearly this curve exists in all the above polygons. E.g. for $SU(4)_{1/2} + 1\mathbf{AS} + 7\mathbf{F}$

the relevant curve is



(7.39)

7.5 Enhanced Non-simply-laced Flavor Symmetry

In the previous section, we have computed a set of simply-laced unitary magnetic quivers. Furthermore, the tables in appendix B of [3] include almost entirely simply-laced magnetic quivers. However, it is known that the flavor symmetry of some lower rank SCFTs, more precisely $SU(4)$ and $SU(5)$ with two antisymmetric and various fundamental matter multiplets, have a non-simply laced flavor symmetry. This section is devoted to the analysis of this apparent problem.

We begin by recalling that certain simply laced quivers can have a Coulomb branch with a non-simply-laced isometry algebra. The quivers which we will use are summarized in table 7.4. These quivers were studied in [189, 209–212] in which the computation of their Hilbert series and heighest weight generating functions (HWGs) are performed, thus identifying the corresponding nilpotent orbits and Hasse diagrams. The simplest occurrence of this phenomenon can be traced back to a the observation by Kostant and Brylinski [213] that a $\mathbb{Z}_2$ quotient of the closure of the minimal nilpotent orbit of $\mathfrak{d}_{n+1}$ yields the closure of the next-to-minimal nilpotent orbit of $\mathfrak{b}_n$, combined with the fact that this quotient can be implemented on the quiver using the *bouquet* construction [214] or *wreathing* [189]. Note that magnetic quivers for the closures of the non-extremal leaves in the diagrams of table 7.4 are non-simply-laced, possibly with additional identifications (see section 5.2.4 in [189] for a detailed discussion of this subtle point). In the following, we do not represent these non-simply-laced quivers, and we apply the quiver subtraction algorithm using directly the non-elementary slices of table 7.4.

We now illustrate on examples how these quivers intervene in the process of the quiver subtraction algorithm [129, 130] and allow to identify non-simply-laced symmetries in the

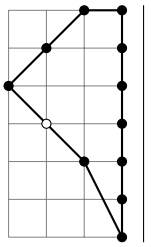
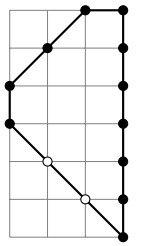
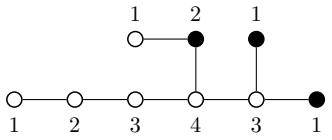
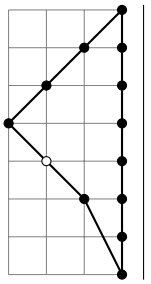
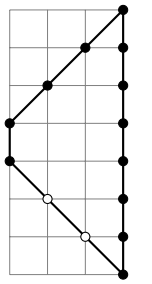
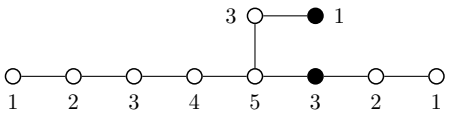
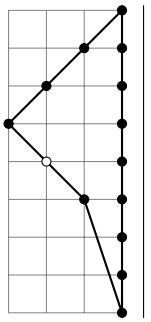
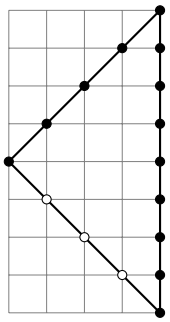
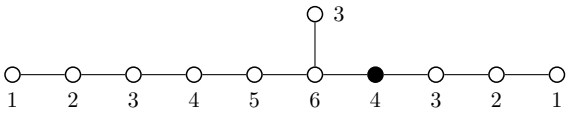
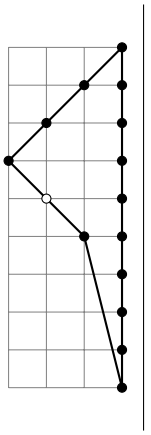
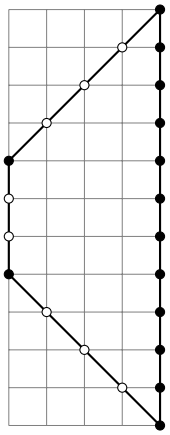
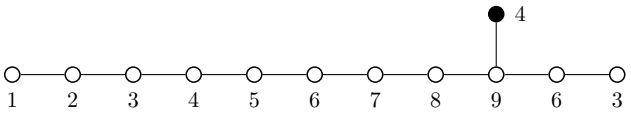
N_F	pGTP	GTP	Magnetic quiver and Flavor Symmetry
6			 $\mathfrak{su}(6) \oplus \mathfrak{su}(2) \oplus \mathfrak{u}(1) \oplus \mathfrak{u}(1)$
7			 $\mathfrak{su}(7) \oplus \mathfrak{su}(3) \oplus \mathfrak{u}(1)$
8			 $\mathfrak{su}(8) \oplus \mathfrak{su}(4)$
9			 $\mathfrak{su}(12)$

Table 7.3: pGTPs, GTPs, MQs and flavor symmetries for $SU(4)_k + 1\mathbf{AS} + N_F\mathbf{F}$ for $N_F = 6, 7, 8, 9$ and $k = 0$ or $k = \frac{1}{2}$.

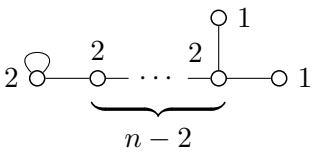
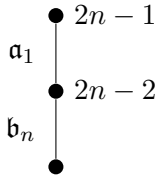
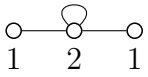
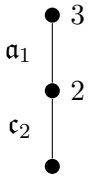
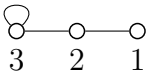
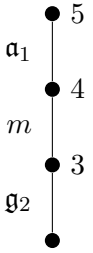
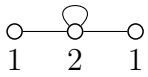
Algebra	Singularity	Magnetic quiver	Hasse diagram
$\mathfrak{b}_n$	$\overline{\mathcal{O}}_{\text{nmin}}(\mathfrak{so}(2n+1,\mathbb{C}))$		
$\mathfrak{c}_2$	$\overline{\mathcal{O}}_{\text{nmin}}(\mathfrak{sp}(2,\mathbb{C}))$		
$\mathfrak{g}_2$	$\overline{\mathcal{O}}_{\text{subreg}}(\mathfrak{g}_2)$		

Table 7.4: Summary of non-simply laced symplectic leaves and their magnetic quivers. The quivers for the closure of the next-to-minimal orbit of $\mathfrak{b}_n$ is obtained from the quiver for the closure of the minimal nilpotent orbit of $\mathfrak{d}_{n+1}$ after S_2 wreathing acting on the two spinor nodes, which can be depicted equivalently by an adjoint hyper. The $\mathfrak{c}_2$ quiver is obtained by identification with the $\mathfrak{b}_2$ quiver. Finally the $\mathfrak{g}_2$ quiver is obtained from S_3 wreathing of the $\mathfrak{d}_4$ closure of the minimal nilpotent orbit quiver. Note that the closures of next-to-minimal nilpotent orbits of the other non-simply laced algebras $\mathfrak{c}_n$ and $\mathfrak{f}_4$ are also available in terms of wreathed quivers, but the wreathing acts on more than $\mathfrak{u}(1)$ nodes, so they can not be rephrased as quivers with adjoint matter.

Coulomb branch of simply laced quivers, even with no adjoint matter. The results agree with the conclusions of [211].

7.5.1 $\mathfrak{c}_2$ Quiver

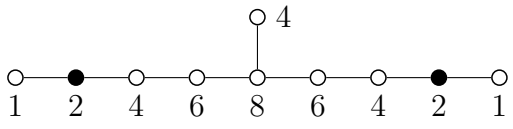
Let us start with a particularly simple theory, $SU(4)_1 + 2\boldsymbol{AS}$. The flavor symmetry is known not to enhance at strong coupling and is given by $\mathfrak{sp}(2) \oplus \mathfrak{u}(1)$, where the $\mathfrak{sp}(2)$ appears as the antisymmetric representation of $\mathfrak{su}(4)$ is real. The magnetic quiver at the SCFT point is conjectured to be



(7.40)

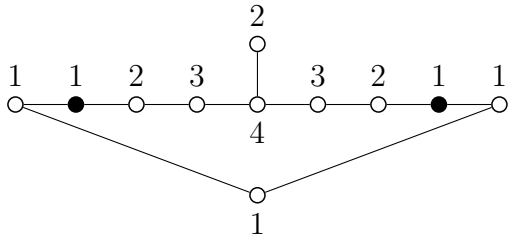
see table 19 of [3] entry $(0,1)$. This quiver appears in table 7.4 and provides the $\mathfrak{sp}(2)$ symmetry. Note that the $\mathfrak{u}(1)$ factor of the flavor symmetry is invisible, a feature that is common to most low N_F theories.

Let us turn to a more involved theory. Consider the strongly coupled $SU(4)_0 + 2\boldsymbol{AS} + 6\boldsymbol{F}$ with magnetic quiver



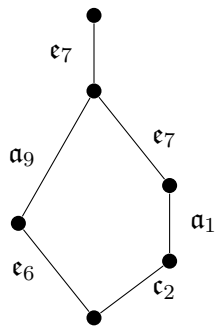
. (7.41)

The only possible quiver subtraction is with an $\mathfrak{e}_7$ diagram to obtain



. (7.42)

From here, there are two possibilities. Either we can subtract an $\mathfrak{a}_9$ diagram, leading to the affine $\mathfrak{e}_6$ diagram. Alternatively, we can subtract another $\mathfrak{e}_7$ diagram. It was discussed in [130] that subtracting two equivalent quivers leads to the two rebalancing nodes to be identified, together with the coupling to an adjoint. Thus, this subtraction leads precisely to the quiver in (7.40) and we deduce that the Hasse diagram is conjectured to be

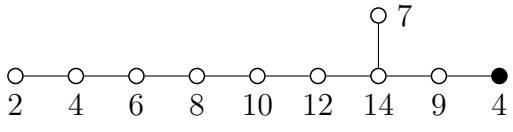


(7.43)

The flavor symmetry is $\mathfrak{e}_6 \oplus \mathfrak{sp}(2) \oplus \mathfrak{u}(1)$, as expected.

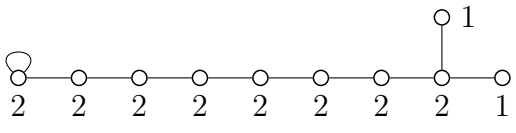
7.5.2 $\mathfrak{b}_9$ Quiver

We now check two other interesting theories, the strongly coupled $SU(N)_2 + 2\boldsymbol{AS} + 6\boldsymbol{F}$, i.e. the submarginal theory discussed in section 5.5 of [3], for $N = 4$ and $N = 5$. They have enhanced flavor symmetries $\mathfrak{so}(19)$ and $\mathfrak{e}_7 \oplus \mathfrak{g}_2$ respectively. The magnetic quiver of the former is given by



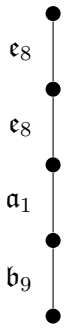
. (7.44)

We see that we can subtract two equivalent $\mathfrak{e}_8$ diagrams, leading to



(7.45)

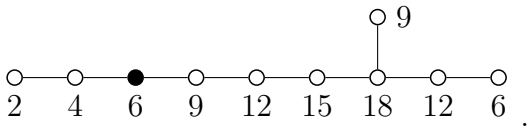
The Hasse diagram of the $SU(4)_2 + 2\boldsymbol{AS} + 6\boldsymbol{F}$ is then conjectured to be



(7.46)

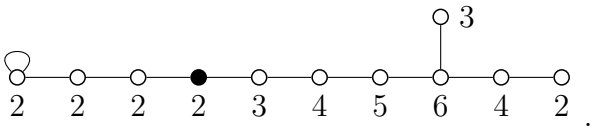
7.5.3 $\mathfrak{g}_2$ Quiver

Finally, consider the magnetic quiver



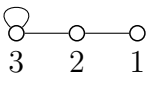
(7.47)

After subtracting two $\mathfrak{e}_8$ diagrams this becomes



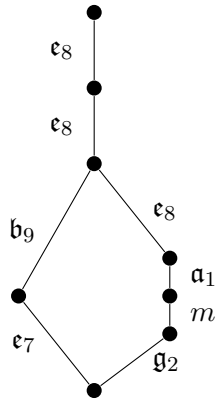
(7.48)

Comparing with (7.45) this quiver allows for the subtraction of a $\mathfrak{b}_9$ leaf, leading to the affine $\mathfrak{e}_7$ Dynkin diagram. Alternatively, we can subtract a third equivalent copy of the $\mathfrak{e}_8$ leaf, which gives



(7.49)

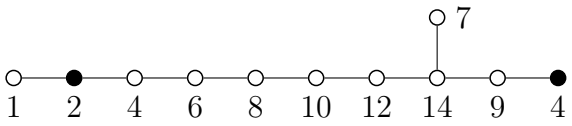
which we therefore identify with the $\mathfrak{g}_2$ leaf. To summarise, the Hasse diagram of the $SU(5)_2+2\boldsymbol{AS}+6\boldsymbol{F}$ is conjectured to be



(7.50)

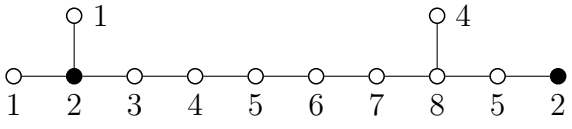
7.5.4 Hidden $\mathfrak{su}(2)$ Symmetries

As a final example let us look at the submarginal $SU(5)_{\frac{1}{2}}+2\boldsymbol{AS}+7\boldsymbol{F}$. This theory has a $\mathfrak{so}(16)\oplus\mathfrak{su}(2)^2$ flavor symmetry, although one of the $\mathfrak{su}(2)$s can not immediately be seen from the magnetic quiver



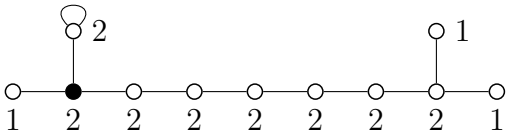
(7.51)

Note that this enhancement occurs for all theories in tables 17 and 18 of [3], but we consider the case at hand which is the simplest. First, we need to subtract an $\mathfrak{e}_8$ diagram, leading to



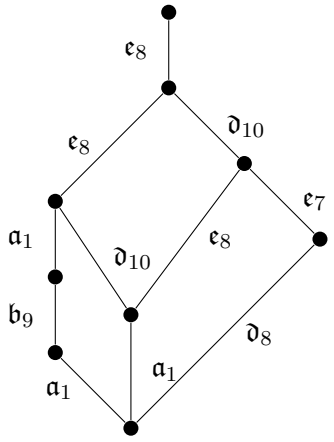
(7.52)

Subtracting the $\mathfrak{d}_{10}$ diagram leads us to a simply-laced diagram, from which an $\mathfrak{so}(16)\oplus\mathfrak{su}(2)$ flavor symmetry can be read off. The more interesting route is subtracting a second equivalent $\mathfrak{e}_8$ diagram



(7.53)

We can now subtract either the $\mathfrak{b}_9$ diagram of table 7.4 or a $\mathfrak{d}_{10}$ diagram, each leading to an $\mathfrak{su}(2)$. Thus, the full Hasse diagram is conjectured to be



(7.54)

unveiling the full $\mathfrak{so}(16) \oplus \mathfrak{su}(2) \oplus \mathfrak{su}(2)$ flavor symmetry.

Chapter 8

Connecting 5d Higgs branches via 3d Fayet-Iliopoulos Deformations

8.1 Introduction

The principal motivation for the work presented in this chapter is to understand how the geometry of the 5d Higgs branch is transformed, as we move around the extended Coulomb branch. The most literal way to answer this question is to work directly with the magnetic quiver, and understand, for instance, how to decouple matter or take a weak coupling limit directly in the magnetic quiver. We show that this is achieved by Fayet-Iliopoulos (FI) deformations, and argue that, for any extended Coulomb branch deformation of the 5d SCFT, implemented as partial resolutions of the GTP, there is an FI deformation that enacts the corresponding change in the magnetic quiver, thus extrapolating between the Higgs branches emanating from the two points in the extended Coulomb branch.

Remarkably, although we always start from a star-shaped magnetic quiver describing the Higgs branch of the 6d SCFT [211], FI deformations allow us to generate all the ingredients observed in magnetic quivers of 5d theories, namely edges with nontrivial multiplicity, quivers with loops, adjoint matter and free hypermultiplets. As is well known, many SCFTs are described by a collection of quivers since their Higgs branch is made of multiple components. For such models the mirror map is not well-defined, but we find in several nontrivial cases that each quiver describes the mirror dual of the low-energy effective theory at a singular point in the Coulomb branch of the SCFT dimensionally reduced to 3d. We therefore have in these cases an interpretation in terms of a local mirror symmetry, in which different singular points in the Coulomb branch lead to different quivers.

In section 8.2 we explain how to turn on FI parameters in a generic unitary quiver and propagate the non-zero vevs in a consistent (but highly non-unique) way. The strategy we implement in section 8.3 for matching 5d mass deformations and FI deformations in the magnetic quiver makes use of the GTP realization of the 5d SCFT. A partial resolution of a GTP P moves us onto the extended Coulomb branch, described by a new polygon P'. In any such phase of the 5d theory, we can use the map in [2] to determine the associated magnetic quiver, and identify the FI deformation that connects the two points. The method can be represented diagrammatically as

$$\begin{array}{ccc} P & \xrightarrow{\text{resolution}} & P' \\ \downarrow & & \downarrow \\ MQ_P & \xrightarrow{\text{FI deformation}} & MQ_{P'} \end{array} \tag{8.1}$$

We discuss the concept of local mirror symmetry in the context of SQCD with special unitary gauge group in Section 8.3.5. Section 8.4 illustrates the method in the case of (D_{N+2}, D_{N+2}) conformal matter, and in section 8.5 we analyze the T_N theory. Moreover, in many cases, one can use symmetry considerations to constrain the possible FI deformations, allowing us to bypass the construction of P'. The method then provides a useful tool for obtaining new quivers, e.g. of descendant SCFTs, or finding new weakly coupled 5d gauge theory descriptions, as we do in section 8.5.3.

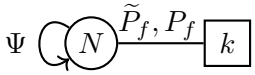
8.2 FI Deformations

In this paper we are concerned with 5d SCFTs originating from orbi-instanton theories of type A, i.e. the 6d theories on the world-volume of M5-branes probing an M9 wall which wraps a $\mathbb{C}^2/\mathbb{Z}_k$ singularity (transverse to the M5 world-volume) in M-theory. The Higgs branch of all these theories is described by a unitary magnetic quiver, or a collection of them whenever the moduli space of the theory exhibits multiple branches. Upon dimensional reduction of the 6d theory we get a 5d SCFT whose Higgs branch is a single cone described by a star-shaped unitary quiver, which can be identified with the mirror dual of the theory dimensionally reduced to 3d, called $\mathbb{EQ}_{3d}$. By activating mass deformations of the 5d SCFT we can move along the decoupling tree of the theory, and, for the first few decouplings, we can exploit the

mirror map dictionary. In particular, we are guaranteed that turning on a mass deformation in the 5d SCFT (which may correspond to a decoupling or to turning on a gauge coupling) results in a mass deformation of the 3d theory, which in turn corresponds to a Fayet-Iliopoulos deformation in the mirror dual quiver. The duality between the magnetic quiver and $\mathbb{EQ}_{3d}$ breaks down typically as soon as we reach theories whose Higgs branch consists of multiple cones. Remarkably, we find that the correspondence between mass deformations of the 5d SCFT and FI deformations of the magnetic quiver remains true even when the magnetic quiver cannot be identified with the mirror dual of $\mathbb{EQ}_{3d}$.

8.2.1 FI Deformations of Unitary Quivers

We would now like to understand FI deformations in a unitary quiver. Let us start by reviewing how FI deformations affect the equations of motion at a given gauge node in the quiver. We turn on a (say complex) FI parameter λ in a $U(N)$ gauge theory with k fundamental hypermultiplets $\widetilde{P}_f$ and P_f (in four supercharges notation) and we denote with Ψ the adjoint chiral in the $\mathcal{N}=4$ vector multiplet.



After the FI deformation the superpotential reads

$$\mathcal{W} = \widetilde{P}_f \Psi P^f + \lambda \operatorname{Tr} \Psi \,, \tag{8.2}$$

and consequently we have to solve the following F-term and D-term equations:

$$\begin{aligned} &P^f \widetilde{P}_f = \lambda I_N \,, \\ &P^f P_f^\dagger - \widetilde{P}^{\dagger f} \widetilde{P}_f = 0 \,, \end{aligned} \tag{8.3}$$

where the summation over flavor indices implies a summation over all the bifundamental hypermultiplets charged under the $U(N)$ gauge group, when this is embedded as a node inside a bigger quiver. From F-terms we can deduce that

$$\operatorname{Tr}(P^f \widetilde{P}_f) = N\lambda \,. \tag{8.4}$$

Considering each node in the larger quiver in turn, and combining this with the identity $\operatorname{Tr}(P^f \widetilde{P}_f) = \operatorname{Tr}(\widetilde{P}_f P^f)$, we conclude that for any quiver with unitary gauge groups and bifundamental hypermultiplets the FI parameters should obey the relation

$$\sum_i N_i \lambda^i = 0 \,, \tag{8.5}$$

where N_i denotes the rank of the i'th node. We therefore see that we always need to turn on FI parameters at multiple nodes. We will mainly focus on the minimal option with only two FI parameters, although sometimes it is convenient to turn on more than two. We will see examples of this below.

Consider the case of FI parameters turned on at two abelian nodes. Because of (8.5), the two FI parameters are λ and $-\lambda$. The deformation induces a nontrivial expectation value for a chain of bifundamentals connecting the two nodes. This follows from the constraint on the trace of bifundamental bilinears in (8.4). Finding an explicit solution to the F- and D-term equations in this case is simple. First, we choose a subquiver beginning and ending at the nodes at which we have turned on the FI parameter. All the bifundamentals along the subquiver, which we denote B_i and $\widetilde{B}_i$, acquire a nontrivial vev and modulo gauge transformations we can set

$$\langle B_i \rangle = \sqrt{\lambda}(v_1, 0, \dots, 0); \quad \langle \widetilde{B}_i \rangle = \langle B_i \rangle^T \,, \tag{8.6}$$

where v_1 is the unit vector whose entries are all trivial except for the first. Of course the size of the matrix $\langle B_i \rangle$ is dictated by the rank of the gauge groups under which the bifundamental is charged. If two nodes are connected by $j > 1$ bifundamental hypermultiplets, modulo a flavor rotation, we can turn on the vev (8.6) for one of them, and set the vev of all the others to zero. All the unitary gauge groups along the subquiver are spontaneously broken as $U(n_i) \to U(n_i - 1)$, whereas the other nodes in the quiver are unaffected. Among all the broken $U(1)$ factors, the diagonal combination survives and gives rise to a new $U(1)$ node, which is coupled to all the nodes of the quiver connected to those of the subquiver. Overall, this is equivalent to subtracting [128] an abelian quiver, isomorphic to the subquiver described above, and the new $U(1)$ is identified with the rebalancing node. Notice that if one of the bifundamentals has multiplicity j we should also include $j - 1$ adjoints for the rebalancing node. These become $j - 1$ free hypermultiplets which are identified with the Goldstone multiplets arising from the global symmetry breaking. Notice that this deformation reduces the dimension of the Higgs branch of (the interacting part of) the quiver.

Generalizing to the case of FI parameters turned on at two nodes of the same rank $k \geq 1$ is straightforward. The vev for the bifundamentals is obtained from (8.6) by picking the tensor product with the $k \times k$ identity matrix I_k. All the groups along the subquiver are broken

as $U(n_i) \to U(n_i - k)$ and finally we need to add a $U(k)$ node associated with the surviving gauge symmetry. This operation corresponds to a modified quiver subtraction, where we subtract a quiver with $U(k)$ nodes only and rebalance with a $U(k)$ node. Again, if one of the bifundamentals has multiplicity j the rebalancing node has $j-1$ adjoint hypermultiplets.

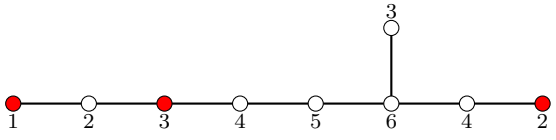
We can also write down a more elaborate variant of the above deformation which involves three nodes. Say we turn on FI parameters at the nodes $U(n)$, $U(m)$ and $U(n+m)$. The FI parameters satisfy the relation (8.5) and we further impose the constraint $\lambda_m = \lambda_n$, so that we still have only one independent parameter. The equations of motion can be solved as follows: We set the vev of all the bifundamentals in the subquiver connecting the nodes $U(m)$ and $U(n+m)$ to be

$$\langle B_i \rangle = \sqrt{\lambda_m}(I_m, 0, \ldots, 0); \quad \langle \widetilde{B}_i \rangle = \langle B_i \rangle^T , \tag{8.7}$$

and the vev of the bifundamentals in the subquiver connecting the nodes $U(n+m)$ and $U(n)$ to be

$$\langle B_i \rangle = \sqrt{\lambda_m}(I_n, 0, \ldots, 0); \quad \langle \widetilde{B}_i \rangle = \langle B_i \rangle^T . \tag{8.8}$$

Here we are assuming that the two subquivers meet at the $U(n+m)$ node only[1]. Overall, the higgsing of the theory can be described in terms of a sequence of two modified quiver subtractions: We first subtract a quiver of $U(n)$ nodes going from $U(n)$ to $U(n+m)$ and, as in the previous case, we rebalance with a $U(n)$ node. Then we subtract from the resulting quiver a quiver of $U(m)$ nodes going from $U(m)$ to $U(n+m)$ and rebalance with a $U(m)$ node. A careful analysis of the higgsing reveals that the $U(n)$ node we introduced at the first step should not be rebalanced when we perform the second subtraction. Let us illustrate the procedure for $m=1$ and $n=2$ in the case of the E_8 quiver:

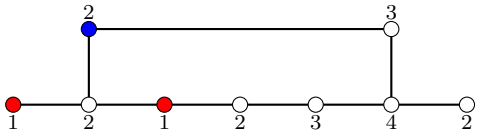


(8.9)

We turn on FI parameters at the nodes in red. We first subtract an A_6 quiver with $U(2)$

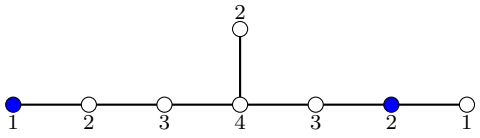
[1]This assumption can actually be relaxed without any major changes, provided that all the nodes in the intersection have rank at least $n+m$. We will shortly see an example of this in Figure 8.1.

nodes, getting



(8.10)

The node in blue is used to rebalance. Then we subtract an A_3 abelian quiver, obtaining



(8.11)

The $U(1)$ node in blue is introduced to rebalance in the second subtraction, and, as we have explained before, is not connected to the blue $U(2)$ node. Overall, this FI deformation describes the transition from the E_8 to the E_7 theory.

Finally, let us consider the example of the UV completion of $SU(3)$ SQCD with 6 flavors and Chern-Simons (CS) level 2. The corresponding magnetic quiver is depicted on the left in Figure 8.1. We want to turn on a finite gauge coupling in 5d and therefore keep a balanced A_5 subquiver. This can be done by turning on an FI parameter at the top $U(2)$ node. We then also have to turn on FI parameters at the abelian nodes on the right. The simplest choice is to turn on the same FI parameter $-\lambda$ at both abelian nodes. Because of (8.5), we then conclude that the $U(2)$ FI parameter is λ. If we denote the $U(1) \times U(3)$ bifundamentals

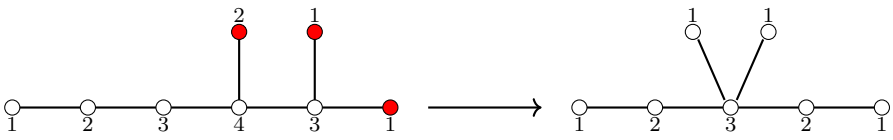


Figure 8.1: One FI deformation leading from the $SO(12) \times U(1)$ SCFT to its low-energy gauge description, namely $SU(3)$ SQCD with 6 flavors.

as $\widetilde{P}_{1,2}$ and $P_{1,2}$, all F-terms are solved by setting

$$\langle \widetilde{P}_1 \rangle = (\sqrt{\lambda}, 0, 0); \ \langle P_1 \rangle = \langle \widetilde{P}_1 \rangle^T; \quad \langle \widetilde{P}_2 \rangle = (0, \sqrt{\lambda}, 0); \ \langle P_2 \rangle = \langle \widetilde{P}_2 \rangle^T . \tag{8.12}$$

The $U(3) \times U(4)$ and $U(4) \times U(2)$ bifundamentals have instead a nonvanishing 2×2 block equal to $\sqrt{\lambda} I_2$. The result of the higgsing is the quiver on the right of Figure 8.1. Notice that the same RG flow can be implemented by turning on an FI deformation at the two $U(2)$ nodes. We clearly see here that generically there are multiple choices of FI deformation which implement a given mass deformation.

8.2.2 More General FI Deformations

So far we have discussed only a particular set of FI deformations. Most mass deformations in 5d can be understood using the methods described above, however, it is also interesting to identify more general possibilities not considered in [130]. When the quiver contains a tail of the form $U(1)-U(2)-\cdots$ we can turn on FI parameters at these $U(1)$ and $U(2)$ nodes only. As before, the generalization to the case $U(k)-U(2k)-\cdots$ is straightforward. Because of (8.5), we set $\lambda_1 = -2\lambda_2 \equiv 2\lambda$. If we denote the $U(1)\times U(2)$ bifundamentals as $\widetilde{Q}$, Q and the other $U(2)$ fundamentals as $\widetilde{P}_f$, P^f, the relevant F-terms are

$$\langle \widetilde{Q} Q\rangle = 2\lambda; \quad \langle \widetilde{P}_f P^f\rangle - \langle Q\widetilde{Q}\rangle = \lambda I_2\,, \tag{8.13}$$

where we are summing over flavor indices. These equations are solved by

$$\langle \widetilde{Q}\rangle = \sqrt{\lambda}(1,1);\ \langle Q\rangle = \langle \widetilde{Q}\rangle^T;\ \langle \widetilde{P}\rangle = \sqrt{\lambda}\begin{pmatrix} 1 & 0 & 0 & \dots \\ 0 & 1 & 0 & \dots \end{pmatrix};\ \langle P\rangle^T = \sqrt{\lambda}\begin{pmatrix} 0 & 1 & 0 & \dots \\ 1 & 0 & 0 & \dots \end{pmatrix}, \tag{8.14}$$

This vev spontaneously breaks $U(1)\times U(2)$ to a diagonal $U(1)$ subgroup. It is easy to check that D-terms are satisfied as well. The vev for the $U(2)$ fundamentals is

$$\langle \widetilde{P}_f P^f\rangle = \begin{pmatrix} 0 & \lambda \\ \lambda & 0 \end{pmatrix} = \begin{pmatrix} 0 & \lambda \\ 0 & 0 \end{pmatrix} + \begin{pmatrix} 0 & 0 \\ \lambda & 0 \end{pmatrix}. \tag{8.15}$$

This propagates along the quiver, breaking all the groups as $U(n)\to U(n-2)$, until we find a junction where we can "decompose" the vev as above. The two nodes connected to the junction are higgsed as $U(n)\to U(n-1)$ and the vev does not propagate any further. All the nodes connected to the subquiver of nodes which are (partially) higgsed are now coupled to a new $U(1)$ node, which is left unbroken by the vev. We give an example of this process in Figure 8.2, which constitutes an alternative way to understand the flow from the E_7 theory to $SU(2)$ SQCD with 6 flavors at the level of the 3d mirror theory.

Let us now consider a more complicated example, namely the UV completion of $SU(3)$ SQCD with 8 flavors and CS level 1. The SCFT has global symmetry $SO(16)\times SU(2)$. We wish to turn on a mass deformation which breaks the symmetry to $SU(8)\times SU(2)$, leading to another SCFT whose gauge theory phase is given by $SU(3)$ SQCD with 7 flavors and CS level 1/2. In other words, we are decoupling by sending a hypermultiplet mass to $-\infty$. In order to preserve an $A_7\times A_1$ balanced subquiver we turn on FI parameters at a $U(2)$ and

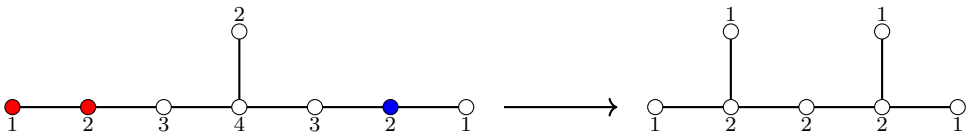


Figure 8.2: The $SO(12)$-preserving FI deformation of the rank 1 E_7 theory. This corresponds to turning on the gauge coupling in 5d. We turn on FI parameters at the red nodes, and we indicate in blue the node of the E_7 quiver which is not higgsed but is connected to a higgsed node. The extra $U(1)$ node is coupled to the blue node only.

$U(4)$ node as shown in Figure 8.3. The F-terms are solved as explained above. The only difference is that we have to tensor all the matrices in (8.14) by the 2×2 identity matrix. The central node is higgsed to $U(2)$ and the neighbouring nodes are higgsed as $U(n) \to U(n-2)$. We further need to add a $U(2)$ node attached to the unhiggsed $U(1)$ and $U(4)$ nodes.

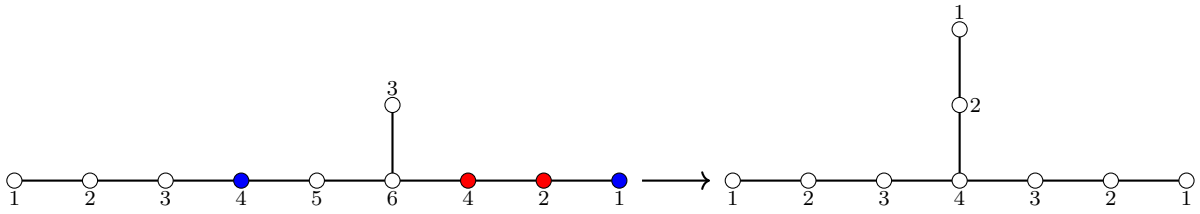
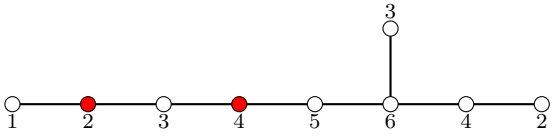


Figure 8.3: The $SU(8) \times SU(2)$ preserving mass deformation of the rank 2 $SO(16) \times SU(2)$ theory. We turn on FI parameters at red nodes. As a result of the higgsing a new $U(2)$ node appears, coupled to the blue nodes.

Finally, let us consider a variant of the above construction involving nodes which are not next to one another. We illustrate this with an example based on the E_8 quiver:



(8.16)

If we turn on FI parameters at the $U(2)$ and $U(4)$ nodes, we can solve the equations of motion by setting the expectation value for the $U(2) \times U(3)$ bifundamental to[2]

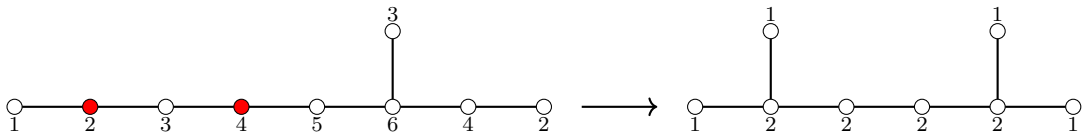
$$\langle B_{23} \rangle = \begin{pmatrix} \sqrt{2} & 0 & 0 \\ 0 & \sqrt{2} & 0 \end{pmatrix}; \quad \langle \widetilde{B}_{32} \rangle = \begin{pmatrix} \sqrt{2} & 0 \\ 0 & \sqrt{2} \\ 0 & 0 \end{pmatrix}. \tag{8.17}$$

[2]Here we have normalized the FI parameter to one at the $U(4)$ node for simplicity.

and the vev of the $U(3) \times U(4)$ bifundamental to

$$\langle B_{34} \rangle = \begin{pmatrix} 1 & 0 & 1 & 0 \\ 0 & 1 & 0 & 1 \\ 0 & 0 & 0 & 0 \end{pmatrix}; \quad \langle \widetilde{B}_{43} \rangle = \begin{pmatrix} 1 & 0 & 0 \\ 0 & 1 & 0 \\ 1 & 0 & 0 \\ 0 & 1 & 0 \end{pmatrix}. \tag{8.18}$$

The $U(2) \times U(4)$ gauge symmetry is spontaneously broken to a diagonal $U(2)$ and the $U(3)$ in between is broken to $U(1)$. The vev propagates in the rest of the quiver as in the case of a $U(2)$ node followed by a $U(4)$ node; all the groups along the tail are higgsed as $U(n) \to U(n-4)$. It turns out that this deformation is equivalent to a weak coupling limit of the 5d theory:



(8.19)

8.2.3 FI Deformations of the Higher Rank E-string Theory

As an application of the above discussion, we will now see that using the set of rules we have explained, we can identify the FI deformations which implement decouplings and weak coupling limits of all rank 1 SCFTs, namely the E-string theory and its descendants. The analysis can be easily extended to higher rank E-string theories and therefore we directly discuss this case. The general answer is given in Figure 8.4.

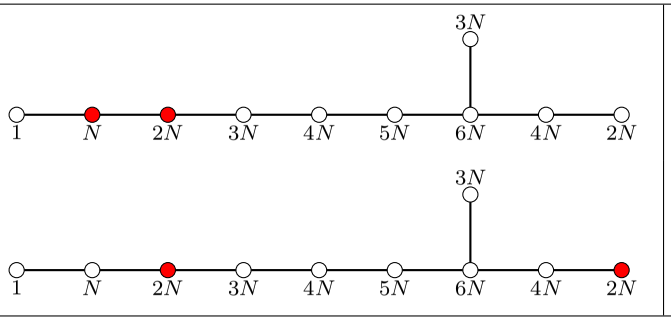
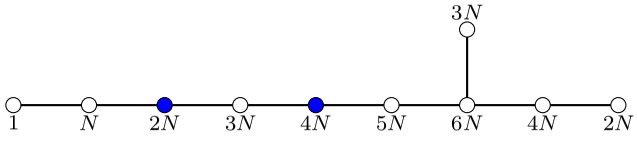
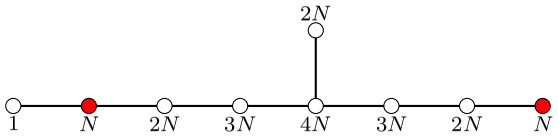
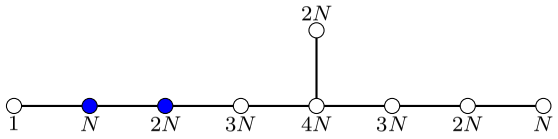
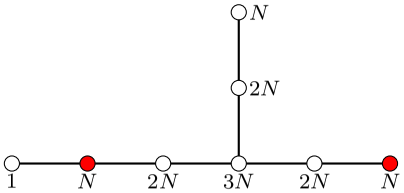
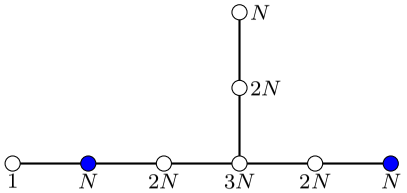
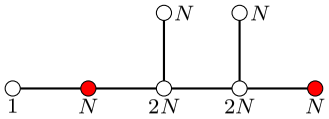
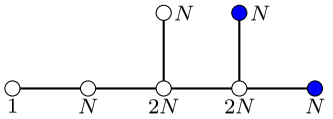
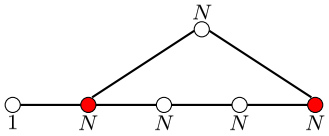
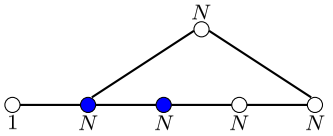
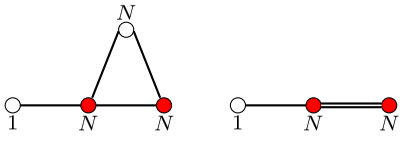
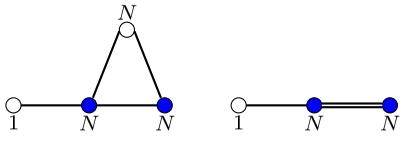
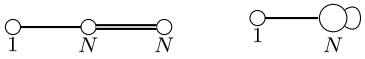
Rank N E_n	MQ with FI for rank N E_n to rank N E_{n-1}	MQ with FI to get $Sp(N-1)+1\boldsymbol{AS}+(n-1)\boldsymbol{F}$
E_8		
E_7		
E_6		
E_5		
E_4		
E_3		
E_2		

Figure 8.4: Magnetic quivers for the rank N E-strings. The red colored nodes correspond to the FI parameters that need to be turned on to decouple and flow from the rank N E_n to the rank N E_{n-1} theory. The blue nodes denote those at which we have to turn on FI parameters to find the weakly coupled description in terms of $USp(2N)$.

8.3 Mass Deformations in 5d via 3d FI Deformations

Our aim is to describe, using the map between GTP and magnetic quiver, how the Higgs branch emanating from one point in the extended Coulomb branch is changed as we move to a different point. We focus first on describing transitions in the magnetic quiver associated to decoupling matter, and then discuss gauge theory phases. Finally, we open up general extended Coulomb branch directions that include turning on vevs for the 5d vector-multiplet scalars.

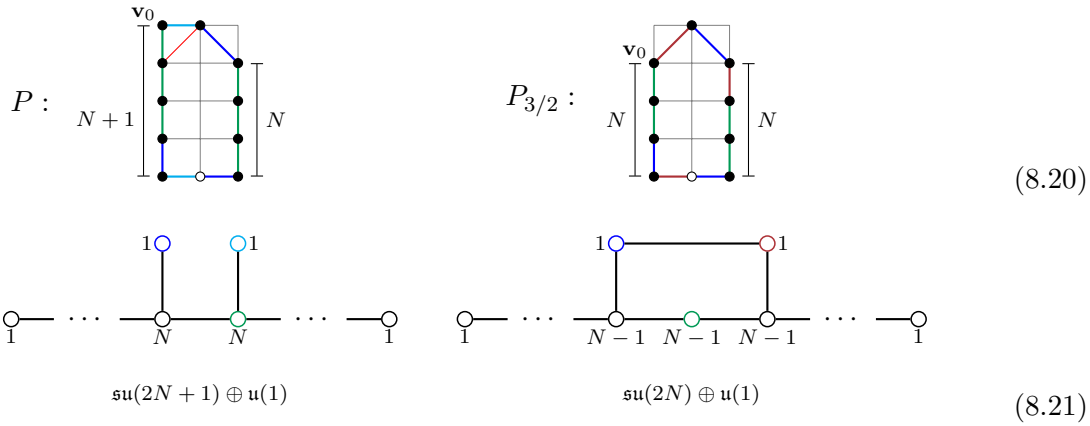
Because any significant change in the structure of the GTP, i.e. to its shape or distribution of vertices, will result in a major change to the combinatorial data contained in the magnetic quiver, a unified treatment of all 5d SCFTs is not feasible at this point and thus, a case by case analysis is necessary. Therefore, rather than aiming for generality, we demonstrate the correspondence with FI deformations focusing on a representative example. On the other hand, the mechanisms of the correspondence are themselves general, meaning that they carry over from our example to any other 5d SCFT, whose magnetic quivers have only unitary nodes, without any conceptual changes to the analysis. In sections 8.4 and 8.5 we give more examples, including the UV fixed points of higher CS level SQCD theories, the T_N theory and its parent SCFTs P_N and G_N, and new lagrangian descriptions of P_N given by quiver gauge theories with fundamental and anti-symmetric matter.

8.3.1 Decoupling

5d $\mathcal{N} = 1$ SCFTs can be deformed away from the fixed point either by turning on a gauge coupling or a mass parameter. The latter decouples a matter multiplet from the theory, which will then flow to a new SCFT. In this way, the 5d SCFTs fall into trees of descendants related by mass deformations. In the M-theory realization, decoupling is implemented geometrically by performing flop transitions on curves in the geometry [147]. In chapter 7 we showed that the application for toric models in [183] can be directly generalized: decoupling can be achieved in the pre-GTP by flopping a curve, which connects an internal vertex along the ruling to an external vertex. Sending the mass to infinity corresponds to removing the section of the polygon that the matter curve separates from the gauge nodes along the ruling after the flop. As we perform the edge-moves necessary to arrive at the SCFT point, we can keep track of the matter curve, identify the corresponding curve in the GTP, and decouple

the associated sector. We discuss how a decoupling curve in the GTP is associated to a (non-unique) FI deformation in the magnetic quiver, so that the deformation extrapolates between the Higgs branches before and after decoupling.

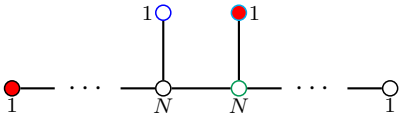
We study the UV completion of $SU(N)$ with CS level 1 and $2N$ fundamentals, with GTP P, and consider the theories resulting from sending a hypermultiplet mass to $m \to \pm\infty$, namely $SU(N)$ with $2N-1$ fundamentals and CS level $1/2$ or $3/2$. We label the GTPs of the descendants by their CS levels. Let us first consider the transition to $SU(N)_{3/2} + (2N-1)\mathbf{F}$. The decoupling curve is indicated in P in red, and the descendant and magnetic quivers are



(8.20)

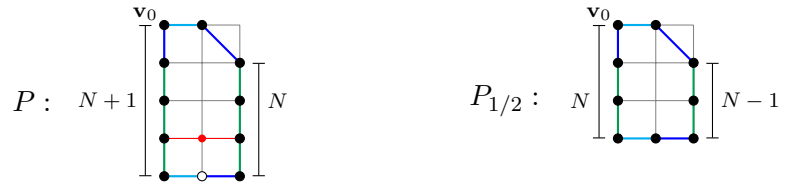
(8.21)

The effect of the decoupling on the map to the magnetic quiver can be described as follows. Shortening E_1 (the left-hand vertical edge) by 1 segment reduces the rank of the tail nodes associated to E_1 by 1 along the entire tail. The intersections of the blue and green nodes with one another and the tail nodes are preserved by the internal edge, but the rank of the green node is reduced by 1. The turquoise sub-polygon does not appear in the Minkowski sum decomposition of $P_{3/2}$. Instead the decomposition of $P_{3/2}$ contains the new triangle shown in maroon in (8.20). The appearance of the maroon triangle gives an new $U(1)$ node, which intersects with the blue triangle and the first tail node from E_3 (right-hand vertical edge). The FI deformation that accomplishes these changes in the magnetic quiver is

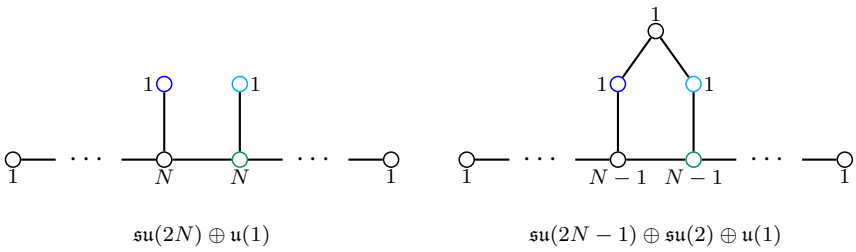


(8.22)

We reach the other descendant SCFT by partially resolving and decoupling as

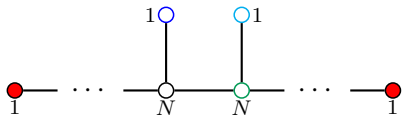


(8.23)



(8.24)

Decoupling the sector below the matter curve has the effect of shortening both tails by 1, and decreasing the rank of the green sub-polygon by 1. Furthermore, the vertex at the bottom of the polygon is filled in, producing an additional length 1 tail, connected to the blue and turqoise nodes. This is precisely the effect of the FI deformation



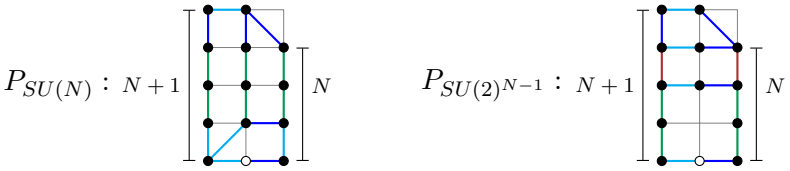
(8.25)

8.3.2 Weak Coupling

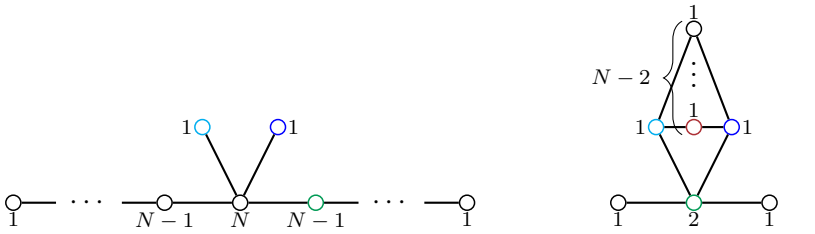
The SCFTs that we consider admit a weakly coupled gauge theory description. This is reached from the UV by turning on a Super Yang-Mills term for a gauge group, which is a relevant operator and thus triggers an RG-flow. In the GTP we go to the gauge theory phase by identifying the ruling, whose vertices correspond to the Cartan subgroup of the gauge group. A UV fixed point often admits of multiple gauge theory descriptions. When a set of 5d gauge theories have the same SCFT fixed point we say that they are UV dual to each other.

Let us consider the gauge theory descriptions of the example SCFT with GTP P. It admits a ruling associated with the $SU(N)_1 + 2N\mathbf{F}$ gauge theory, as well as another ruling giving rise to $[1] - SU(2)^{N-1} - [3]$. We denote the GTPs of the two gauge theory phases by $P_{SU(N)}$ and $P_{SU(2)^{N-1}}$, respectively. For the latter the ruling consists of $N-1$ internal edges, corresponding to consecutively turning on a SYM coupling for the $N-1$ gauge groups. The

GTPs and magnetic quivers are given by

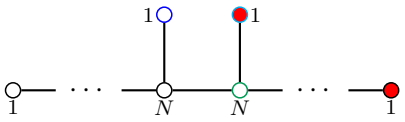


(8.26)



(8.27)

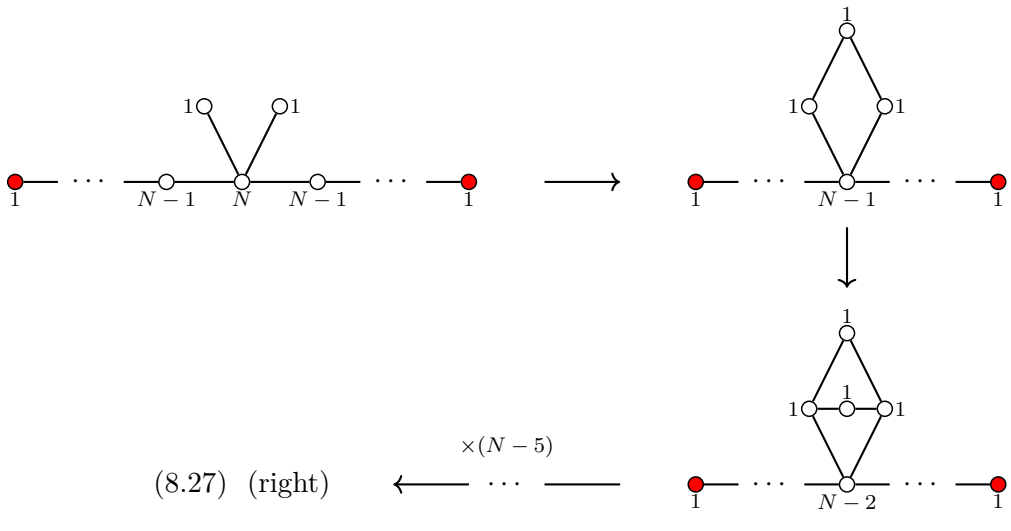
The FI deformation that gives rise to the magnetic quiver of the weakly coupled $SU(N)$ gauge theory should reduce the length of the short tail and the rank of the green node by 1, and redistribute the intersections of the turqoise node. This is accomplished by



(8.28)

To arrive at the $SU(2)$ quiver gauge theory from the UV, we deform the SCFT by turning on $N-1$ independent gauge couplings, each of which corresponds to an FI deformation in the magnetic quiver. The $N-1$ transitions can be implemented as follows. The top ruling in (8.26) (right) induces a deformation in the magnetic quiver which is equivalent to (8.28). (Indeed this implies that the Higgs branches of the two theories coincide.) The remaining $N-2$ $SU(2)$ rulings will then simply correspond to successively turning on FI parameters at

the $U(1)$ nodes in the tails:



(8.27) (right) (8.29)

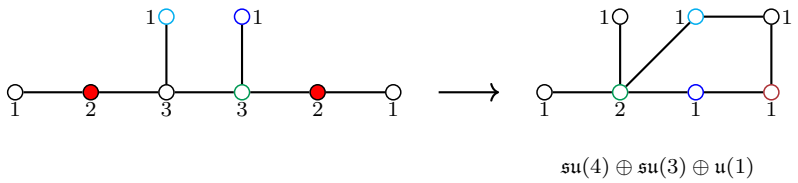
8.3.3 General Movement on the Extended Coulomb Branch

We have seen that the Higgs branches, described by magnetic quivers, of theories that are related by decoupling hypermultiplets or turning on a gauge coupling have a direct connection in terms of an FI deformation. For any given magnetic quiver there are, however, many more ways to consistently turn on FI parameters than is captured by decoupling or going to weak coupling in 5d. FI deformations in the magnetic quiver can in general be interpreted in 5d as moving along a sub-manifold of the extended Coulomb branch, adjusting the mass matrix in such a way that a non-trivial Higgs branch emanates there.

Distinct FI deformations may give rise to the same magnetic quiver. In particular, it is common that the more involved FI deformations may equivalently be implemented by composing a set of simpler deformations by applying them successively. It is therefore convenient to introduce an organizing principle that allows us to weed out some of this intrinsic degeneracy. We conjecture that an FI deformation which decreases the rank of the flavor symmetry group of the 5d theory by more than 1 is decomposable into several FI deformations. We call FI deformations which are not decomposable *simple*. In the following, we will focus on these simple FI deformations. However, even within this smaller set of deformations we encounter degeneracies, where inequivalent FI deformations produce the same magnetic quiver.

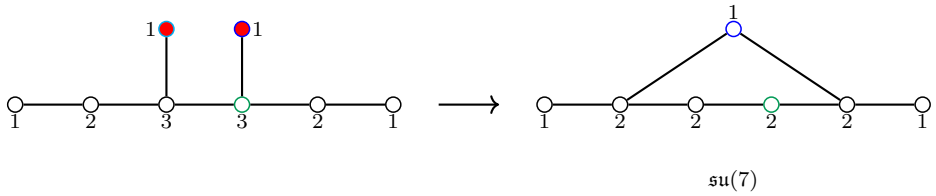
We now specialize our example further to $SU(3)_1$+6**F**, so we can give a complete treatment of the simple FI deformations of its magnetic quiver, without the exposition becoming too tedious. We consider all the FI deformations of the type presented in section 8.2, which lower

the rank of the flavor symmetry group of the 5d theory by at most 1, and show that they correspond to partial resolutions of the GTP. We have the following choices for turning on FI parameters at two nodes of the same rank: the two $U(3)$ nodes, the $U(2)$ nodes, and four distinct pairs of $U(1)$ nodes of which we have already considered (8.22), (8.25) and (8.28), leaving the two abelian color nodes. The $U(3)$ deformation gives rise to the magnetic quiver of the weakly coupled $SU(3)_1 + 6\mathbf{F}$ gauge theory in (8.27) (left). Turning on FI parameters at the $U(2)$ nodes we find the magnetic quiver



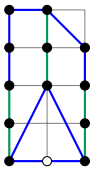
(8.30)

which corresponds to inserting only the bottom ruling in $P_{SU(2)^2}$ in (8.26) (right). The color $U(1)$ nodes give rise to



(8.31)

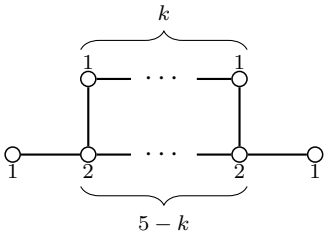
which corresponds to opening the Coulomb branch as



(8.32)

There is furthermore a number of ways to turn on FI parameters at a $U(n)$, $U(m)$ and $U(n+m)$ node, as shown in section 8.2. However, no new magnetic quivers are produced in addition to the ones we have already encountered. The same is true of the $U(1) - U(2)-$ deformation which implements a decoupling and subsequent weak coupling limit. We note that the set of magnetic quivers we obtain from simple FI deformations of the magnetic quiver of strongly coupled $SU(3)_1 + 6\mathbf{F}$ can be summarized as comprising the weakly coupled

description and



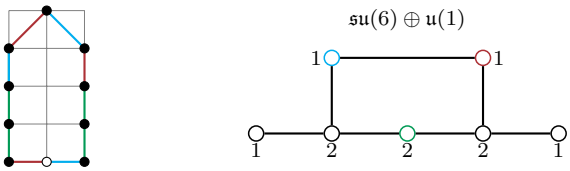
(8.33)

for $k = 1, 2, 3, 4$.

8.3.4 Magnetic Quivers with Loops

Magnetic quivers with loops are typically associated with low-flavor 5d SCFTs. The presence of a loop implies that to turn on FI parameters at a generic set of nodes, we must specify a path for the propagation of non-zero vevs. In the context of decoupling, the path ambiguity is associated to the existence of multiple cones in the 5d Higgs branch of the descendant SCFT. Furthermore, we observe that choosing a longer path, i.e. one that implicates more gauge nodes, usually decreases the rank of the flavor symmetry group by more than 1. We also encounter affine Dynkin diagrams, which correspond to a movement onto the extended Coulomb branch where we turn on a mass m and a vev $\langle\phi\rangle$ such that $m - \langle\phi\rangle = 0$.

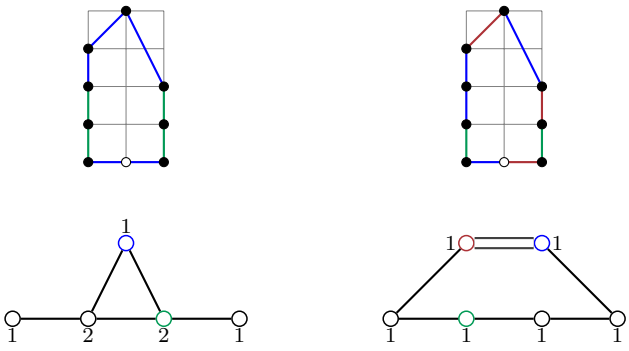
Let us consider the UV fixed point of $SU(3)_{3/2} + 5\mathbf{F}$ found in (8.20). We repeat it here for convenience:



(8.34)

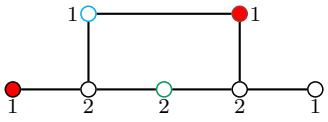
Decoupling a hypermultiplet generates a theory whose Higgs branch is described by two cones. In the GTP the two cones arise as two inequivalent edge colorings, whereas in the magnetic quiver the two cones appear as we turn on FI parameters at the associated set of gauge nodes and propagate the non-zero vevs around the loop along the two possible paths. In other words, a single matter curve can still be associated with turning on FI parameters at a single set of nodes, and the multiple cones arise from the ambiguity in connecting these nodes. Sending a hypermultiplet mass to $+\infty$ we obtain the UV fixed point of $SU(3)_2 + 4\mathbf{F}$,

whose Higgs branch is described by



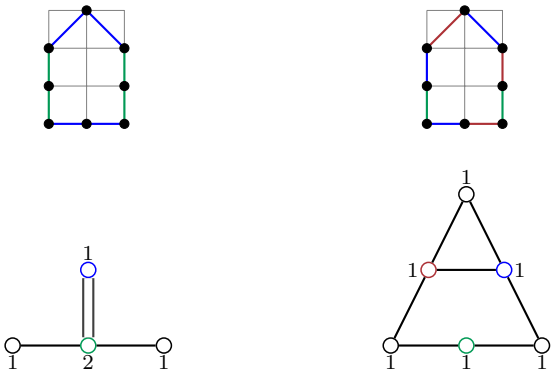
$\mathfrak{su}(5)$ $\mathfrak{su}(5) \oplus \mathfrak{u}(1)$ (8.36)

If the flavor symmetry is not simple, it is possible that only certain simple components act on each cone of the Higgs branch. Here we see that the $\mathfrak{u}(1)$ only acts on the cone described by the righthand magnetic quiver, whereas the lefthand magnetic quiver does not see it. The corresponding FI deformation is given by moving along the top, respectively the bottom, of the loop in



(8.37)

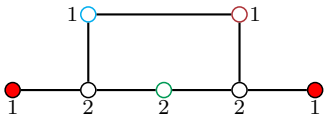
We note that, in correspondence with our conjecture, the lefthand magnetic quiver can also be obtained from two separate FI deformations, e.g. by identifying two adjacent $U(2)$ nodes in (8.34) (right) and subsequently identifying the two adjacent $U(1)$ nodes at the top. Sending a hypermultiplet mass to $-\infty$ we obtain strongly coupled $SU(3)_1 + 4\mathbf{F}$, whose Higgs branch is described by



$\mathfrak{su}(4)$ $\mathfrak{su}(4) \oplus \mathfrak{su}(2) \oplus \mathfrak{u}(1)$ (8.39)

For this descendant, only the cone characterized by the righthand quiver sees the full flavor symmetry, whereas the lefthand quiver only knows about the $\mathfrak{su}(4)$ subalgebra. The FI

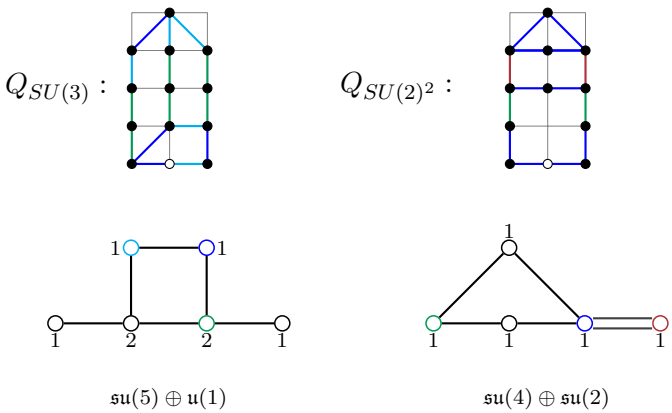
deformation that implements this decoupling in the magnetic quiver is given by turning on FI parameters at



(8.40)

and propagating the non-zero vevs along the top/bottom of the loop. The lefthand quiver in (8.39) can also be obtained by composing three FI deformations, e.g. by merging the $U(2)$ nodes in (8.36) (left).

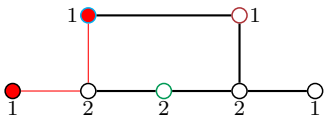
Like its parent, the 5d SCFT given by (8.34) admits two weakly coupled gauge theory descriptions, namely $SU(3)_{3/2} + 5\mathbf{F}$ and $SU(2)_\pi - SU(2) - [3]$. We denote the GTPs of the two gauge theory phases by $Q_{SU(3)}$ and $Q_{SU(2)^2}$, respectively. The GTPs and associated magnetic quivers are



(8.41)

(8.42)

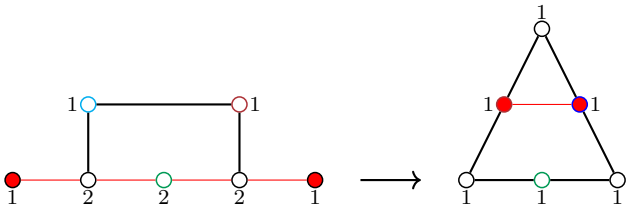
To reach the magnetic quiver of the weakly coupled $SU(3)$ gauge theory, we turn on FI parameters at



(8.43)

taking the shortest path around the loop. The long path gives $\widetilde{A}_4$, which does not correspond to a decoupling or gauge theory description. The latter transition can be decomposed into two separate FI deformations e.g. identify the $U(1)$ nodes connected by a double edge in (8.36) (right). The magnetic quiver of the $SU(2)$ quiver gauge theory is obtained by composing the

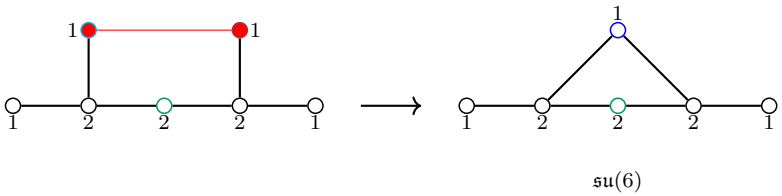
two steps



(8.44)

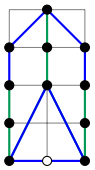
corresponding to first inserting the bottom ruling and then the top in $Q_{SU(2)^2}$ of (8.41).

Which other FI deformations can we perform on the magnetic quiver of (8.34) such that the rank of the flavor group is lowered by at most 1? There are four distinct ways of turning on FI deformations at two $U(1)$ nodes, and two ways for the $U(2)$ nodes. We have already studied three of the deformations using $U(1)$ pairs, namely $m \to \pm\infty$ in (8.37) and (8.40), and the weak coupling limit in (8.43). The remaning set of $U(1)$s gives



(8.45)

The long way around the loop gives $\widetilde{A}_5$. The above transition corresponds to going onto the Coulomb branch as

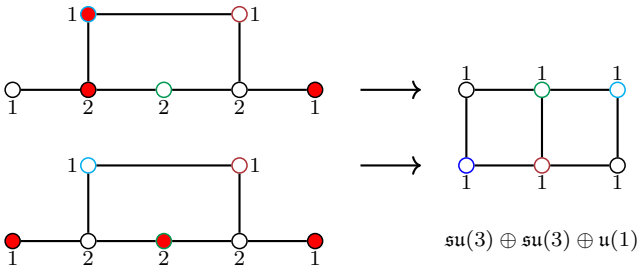


(8.46)

For the $U(2)$ nodes we can turn on FI parameters at two adjacent nodes or at the two tail nodes. This time it is only possible to propagate through the bottom of the loop, since a vev for the bifundamental of $U(2) \times U(1)$ does not contain enough degrees of freedom to solve the equations of motion. Turning on FI parameters at adjacent $U(2)$ nodes is another way to obtain the magnetic quiver of weakly coupled $SU(3)_{3/2} + 5\mathbf{F}$. The FI deformation of the other set of $U(2)$ nodes is decomposable into two applications of the former transition.

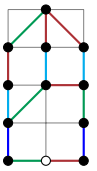
Finally, we can also turn on FI parameters at two $U(1)$ nodes and a $U(2)$ node. There are ten distinct ways of choosing this set of nodes, and three of them allow for multiple paths. A

single new magnetic quiver is obtained, which can be generated in two ways



(8.47)

Note that there is no choice of path in either of these deformations. The resulting magnetic quiver characterizes the Higgs branch emanating from the point on the Coulomb branch described by

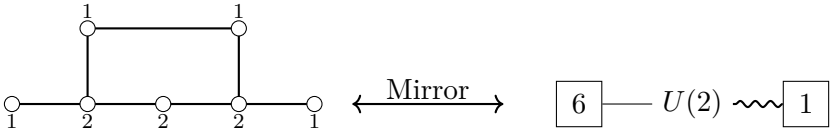


(8.48)

8.3.5 Mirror Symmetry and FI Deformations

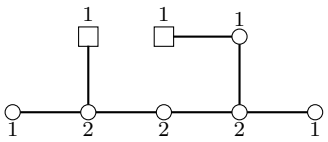
Let us now discuss the 3d interpretation of the mass deformations we have just studied. We focus for simplicity on the rank 2 example discussed above, although all we do in this section can be generalized to higher rank models.

We consider again the magnetic quiver for the SCFT UV completing $SU(3)_{3/2}$ with $5\mathbf{F}$, whose mirror dual is a $U(2)$ gauge theory with six fundamentals and one hypermultiplet with charge 2 under the central $U(1)$ subgroup. This latter theory can therefore be interpreted as the dimensional reduction to 3d of the SCFT in five dimensions.



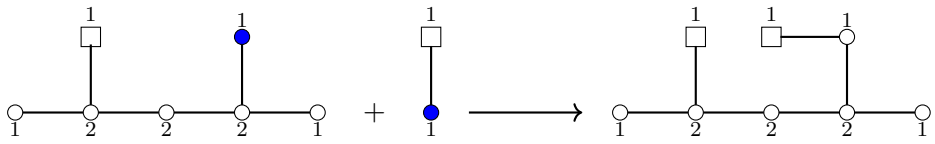
(8.49)

The statement (8.49) can be explained as follows: We first notice that by ungauging one abelian node, the magnetic quiver can be equivalently described as



(8.50)

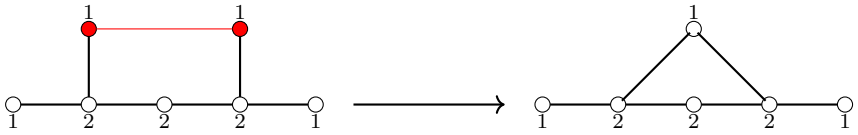
Next we notice that this quiver can be obtained by "fusing" two smaller quivers,



(8.51)

where fusing means gauging the diagonal combination of the topological symmetries associated with the nodes colored in blue. On the left-hand side of (8.51) one can now recognize the mirror duals of $SU(2)$ SQCD with $6\mathbf{F}$ and a free hypermultiplet and the topological symmetries associated with the nodes in blue are mapped to the baryonic symmetry of SQCD and the $U(1)$ acting on the hypermultiplet respectively. We therefore conclude that by gauging the diagonal combination of these symmetries we find the model on the right-hand side of (8.49).

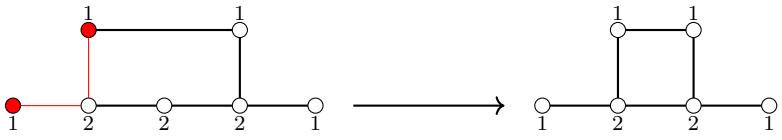
Let us now discuss all the transitions which decrease the rank of the flavor symmetry by 1. The easiest to describe involves FI parameters at the two abelian nodes on top, which reduces the magnetic quiver to the mirror dual of $U(2)$ SQCD with $6\mathbf{F}$.



(8.52)

In the dual $U(2)$ theory this simply corresponds to turning on a mass for the hypermultiplet charged under the central $U(1)$ only.

It is also easy to describe the deformation to the weakly-coupled theory:



(8.53)

where on the right of (8.53) we recognize the mirror dual of $SU(3)$ SQCD with $5\mathbf{F}$ (see e.g. [181]). In the dual $U(2)$ theory of (8.49) this deformation corresponds to turning on a mass for one of the fundamentals. This reduces the theory to the dual of $SU(3)$ SQCD with $5\mathbf{F}$ recently discussed in [215]. This represents a nice consistency check of our claim (8.49).

Let us now turn our attention to the decouplings. As we have reviewed before, the Higgs branch of the UV completion of $SU(3)_2$ with $4\mathbf{F}$ is described by two quivers. One of them is

the mirror dual of $U(2)$ SQCD with $5\mathbf{F}$. Let us now analyze in detail this deformation from the perspective of the $U(2)$ theory: We should turn on an $SU(5)$-preserving mass for the six fundamentals, i.e. five of them are given the same mass, which we denote as m, and $-5m$ for the sixth. We can make the first five fields massless again by tuning the vev for the scalar in the central $U(1)$ vector multiplet. This also has the effect of making the hypermultiplet charged under the central $U(1)$ massive. At low-energy we are therefore left with a $U(2)$ theory with $5\mathbf{F}$. Here we see that we should combine a mass deformation with a motion in the Coulomb branch. Said differently, the FI deformation describes a motion in the extended Coulomb branch.

The magnetic quiver describing the second cone of the Higgs branch of the UV completion of $SU(3)_2$ with $4\mathbf{F}$ arises by deforming the $U(2)$ theory to the model

$$\boxed{5} - U(1) - U(1) - \boxed{1} \tag{8.54}$$

which is achieved by activating a vev for the $SU(2)$ scalar as well. This can of course be diagonalized thus breaking the gauge symmetry to the Cartan subgroup. For ease of presentation we collect the charges of the various matter fields in Table 8.1.

Matter Fields	I_3	$U(1)$	Mass
B_1	$\frac{1}{2}$	-1	$M_{su(6)} + \phi - \varphi$
B_2	$-\frac{1}{2}$	-1	$M_{su(6)} - \phi - \varphi$
q	0	2	$2\varphi - M_{u(1)}$

Table 8.1: Masses and charges of matter fields. $B_{1,2}$ denote the $SU(2)$ color components of the fundamentals and q the $U(1)$ flavor. I_3 stands for the charge under the Cartan of $SU(2)$. We also denote with ϕ the eigenvalue of the $SU(2)$ scalar and with φ the vev of the $U(1)$ field.

Choosing again the mass matrix for the flavors of the form

$$M_{su(6)} = \text{diag}(m, m, m, m, m, -5m)\,, \quad \phi = -3m\,, \quad \varphi = M_{u(1)}/2 = -2m\,, \tag{8.55}$$

the theory reduces precisely to (8.54), where the two abelian gauge groups correspond to the sum and difference of I_3 and $U(1)/2$ in the table.

From the above discussion we clearly see that in 3d the two cones of the Higgs branch of the 5d theory arise by deforming (8.49) with the $SU(6)$ mass matrix $M_{su(6)} = \text{diag}(m, m, m, m, m, -5m)$ and then restricting to different singular loci of the Coulomb branch of the resulting theory.

The corresponding magnetic quivers are simply the mirror duals of the low-energy effective theories at the singular loci. In particular the Higgs branch of the magnetic quiver describes the local structure of the Coulomb branch of the theory (dimensionally reduced to 3d) in a neighbourhood of the singular loci.

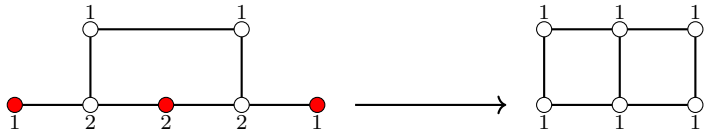
With the choice

$$M_{su(6)} = \text{diag}(m, m, m, -m, -m, -m)\,, \quad \phi = -m\,, \quad \varphi = M_{U(1)} = 0\,, \tag{8.56}$$

we can similarly obtain the theory

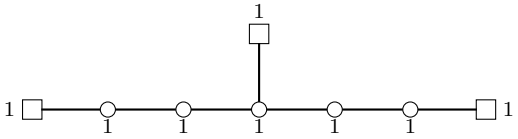
$$\boxed{3} - U(1) - U(1) - \boxed{3} \tag{8.57}$$

This corresponds to the transition we have discussed before (see (8.47))



(8.58)

If we ungauge one of the nodes at the center of the second quiver we get equivalently



(8.59)

which is indeed the mirror dual of (8.57).

Similarly we can discuss the decoupling to the SCFT which UV completes $SU(3)_1$ with $4\mathbf{F}$. The corresponding magnetic quivers are given in (8.39). This process involves an $SU(6)$ mass deformation of the form

$$M_{su(6)} = (m, m, m, m, -2m, -2m)\,. \tag{8.60}$$

Again we find the two cones by zooming in around different loci in the Coulomb branch. If we set

$$\phi = M_{U(1)} = 0\,, \quad \varphi = m\,, \tag{8.61}$$

the $U(2)$ theory reduces to $U(2)$ SQCD with $4\mathbf{F}$, whose mirror dual is the quiver on the left of (8.39). The other quiver is obtained by choosing the locus

$$\phi = -3m/2\,, \quad \varphi = -m/2\,, \quad M_{U(1)} = -m\,, \tag{8.62}$$

which reduces the $U(2)$ theory to

$$\boxed{4} - U(1) - U(1) - \boxed{2} \tag{8.63}$$

Again we see that the magnetic quivers of the 5d theory can be interpreted as the mirror duals of the low-energy theories at special loci in the Coulomb branch.

Finally, let us briefly revisit the case of trivial $M_{su(6)}$. We have already seen that choosing one path around the closed loop of the magnetic quiver (8.34) we find the mirror dual of $U(2)$ SQCD with $6\mathbf{F}$. Choosing the other path leads instead to the $\widetilde{A}_5$ quiver plus one free hypermultiplet, which is the mirror dual of SQED with $6\mathbf{F}$ plus one twisted free hyper. This is the low-energy theory on the locus $\phi = \varphi = a$ with a arbitrary. The twisted free hyper is identified with the variation of the modulus a. We therefore see that we have a flat direction in the Coulomb branch and this explains why the magnetic quiver has a one dimensional Higgs branch although the theory we are discussing has rank two.

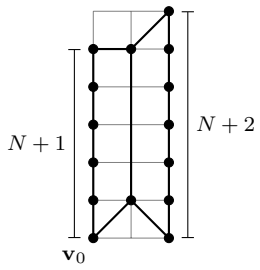
In conclusion, this analysis illustrates that the magnetic quivers describe the structure of the theory at the singular points in the moduli space of the SCFT, dimensionally reduced to 3d. When the Coulomb branch is a cone we have a single magnetic quiver which is the mirror dual of the SCFT. When instead there are multiple singular loci in the Coulomb branch, we have for each one of them a quiver which is the mirror dual of the low-energy theory at the corresponding singular locus. When the singular locus is not a single point but rather a submanifold the dimension of the Higgs branch of the magnetic quiver is lower than the rank of the SCFT and is accompanied by free hypermultiplets, reflecting the presence in the low-energy theory of free twisted hypermultiplets whose moduli parametrize the motion along the singular locus.

8.4 (D_{N+2}, D_{N+2}) Conformal Matter Descendant Tree

In this section we study the descendants of the (D_{N+2}, D_{N+2}) conformal matter theory (for the definition of six-dimensional conformal matter see [216]). In the polygon description, we can successively decouple fundamental matter multiplets by flopping out the corresponding curves. These curves are easily identified in the pre-GTP, which describes the gauge theory phase, and can be traced through the edge-moves to the corresponding curves in the GTP. A matter curve in the pre-GTP connects a vertex bounding the ruling to a vertex along an

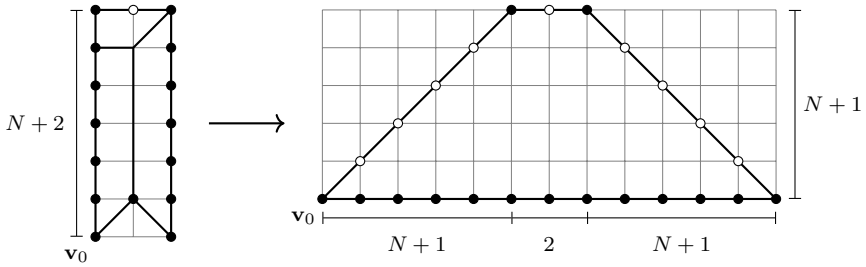
external edge. Sending a fundamental mass to $+\infty$ or $-\infty$ corresponds to a matter curve emanating from either end of the ruling, and respectively increases or decreases the CS by $\frac{1}{2}$ in the decoupling.

The pre-GTP representing the gauge theory phase of the first descendant $SU(N)_{\frac{1}{2}} + (2N+3)\mathbf{F}$ is (drawn for $N=4$)



(8.64)

To reach the SCFT point, we must remove the non-convexities by applying edge-moves. This can be achieved by first exchanging the $(-1,-1)$- and $(-1,0)$-edge at the top, and subsequently pruning the $(1,1)$- and $(1,-1)$-edges at the bottom of the polygon:

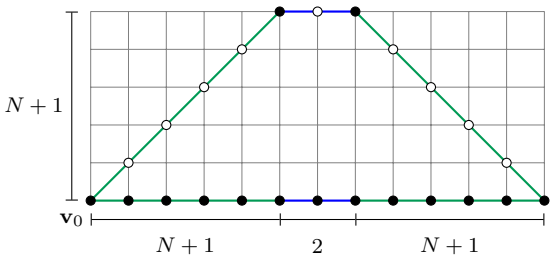


(8.65)

Taking the bottom left vertex as the origin and using the definitions in (7.5) and (7.9) the transformations are summarised as

$$\mathfrak{T} = \mathfrak{M}^{+}_{N+5}\mathfrak{P}^{+}_{1}\mathfrak{P}^{-}_{1}\,. \tag{8.66}$$

For the UV completion of $SU(N)_{\frac{1}{2}} + (2N+3)\mathbf{F}$ the unique edge coloring is



(8.67)

The data of the decomposition is

$$\begin{aligned}
\lambda_\alpha &= (2N+4, N+1, 2, N+1)\,, & \mu_\alpha &= (\{1^{2N+4}\}, \{N+1\}, \{2\}, \{N+1\})\,, \\
\lambda^b_\alpha &= (2, 0, 2, 0)\,, & \mu^b_\alpha &= (\{2\}, -, \{2\}, -)\,, \\
\lambda^g_\alpha &= (2N+2, N+1, 0, N+1)\,, & \mu^g_\alpha &= (\{N+1, N+1\}, \{N+1\}, -, \{N+1\})\,,
\end{aligned} \tag{8.68}$$

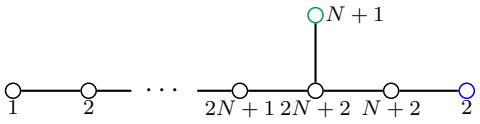
which results in the nodes

$$m^b = 2\,, \qquad m^g = N+1\,, \qquad m_{1,x} = (N+2, 2N+2, 2N+1, \ldots, 1)\,, \tag{8.69}$$

and non-zero intersections

$$k^g_{1,2} = 1\,, \qquad k^b_{1,1} = 1\,, \tag{8.70}$$

as well as nearest neighbours intersecting once in the tail. Thus, the magnetic quiver is



$\mathfrak{su}(4N+8)$ (8.71)

Using this theory as a starting point and with a decoupling we get either $SU(N)_1$ or $SU(N)_0$ with $2N+2$ flavors. By further decoupling (always with positive sign) we get the two sequences $SU(N)_{\frac{k+1}{2}}$ with $2N+3-k$ flavors or $SU(N)_{\frac{k-1}{2}}$ with $2N+3-k$ flavors. These two sequences are described by the FI deformations in Figure 8.5. We note that the magnetic quivers of the descendants of (D_{N+2}, D_{N+2}) conformal matter are star shaped for $N_f > 2N-1$. At $N_f = 2N-1$ a loop appears, which results in multiple cones for $N_f < 2N-1$. The corresponding descendant tree of GTPs is given in Figure 8.6.

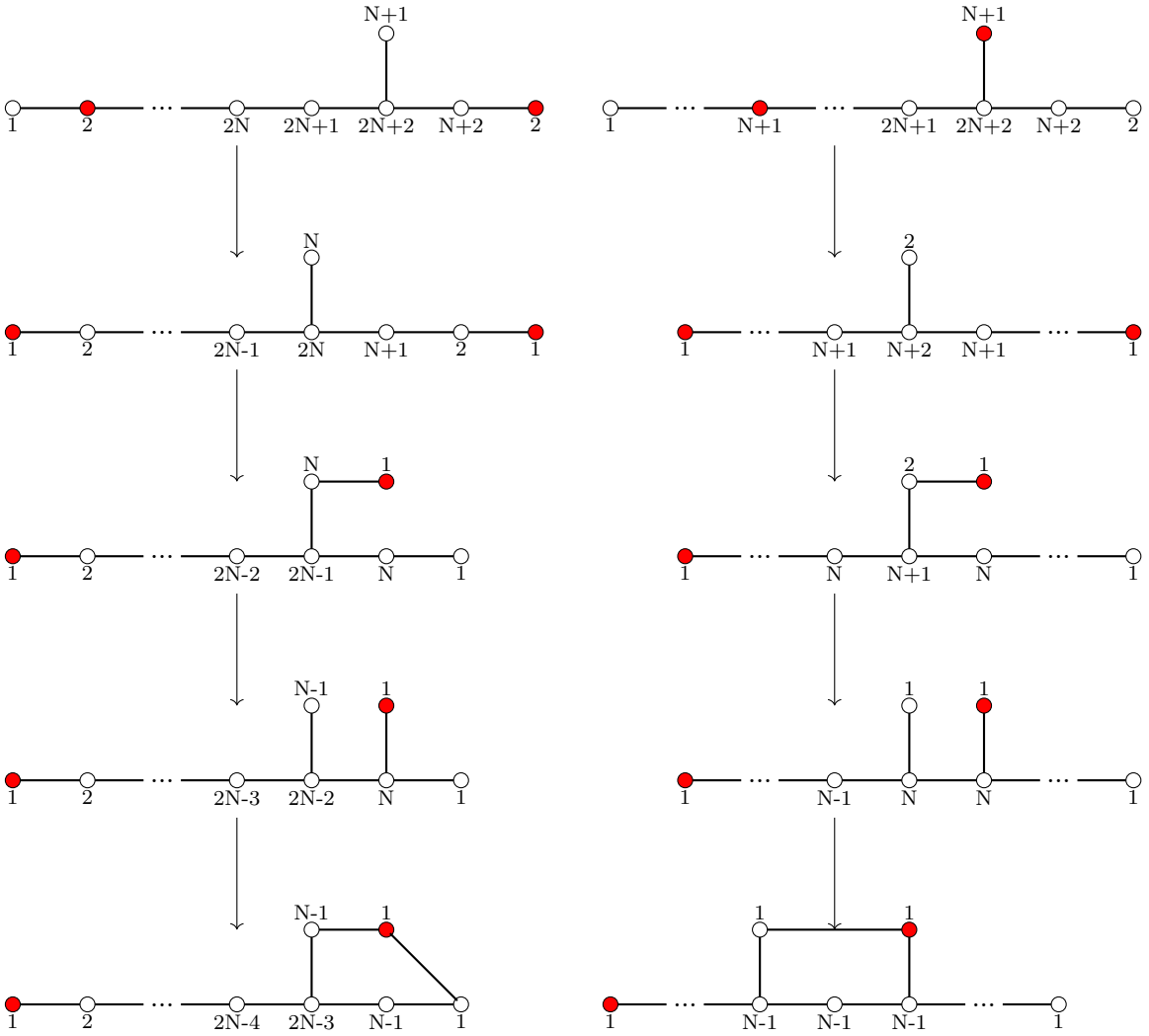


Figure 8.5: The decoupling trees for $SU(N)_{\frac{k+1}{2}}$ with $2N+3-k$ flavors (on the left) and $SU(N)_{\frac{k-1}{2}}$ with $2N+3-k$ flavors (on the right). We exhibit explicitly all the deformations from $k=0$ to $k=4$. Notice that apart from the first decoupling we always turn on FI parameters at two abelian nodes and in this case the deformation is equivalent to a standard quiver subtraction. If we proceed further with the decoupling the Higgs branch becomes the union of multiple cones, each described by a quiver. With our procedure this arises because the magnetic quivers for $k=4$ contain closed loops and therefore we have multiple choices for the set of bifundamentals for which we turn on a vev. The FI deformation leading to the $k=5$ magnetic quivers is given explicitly.

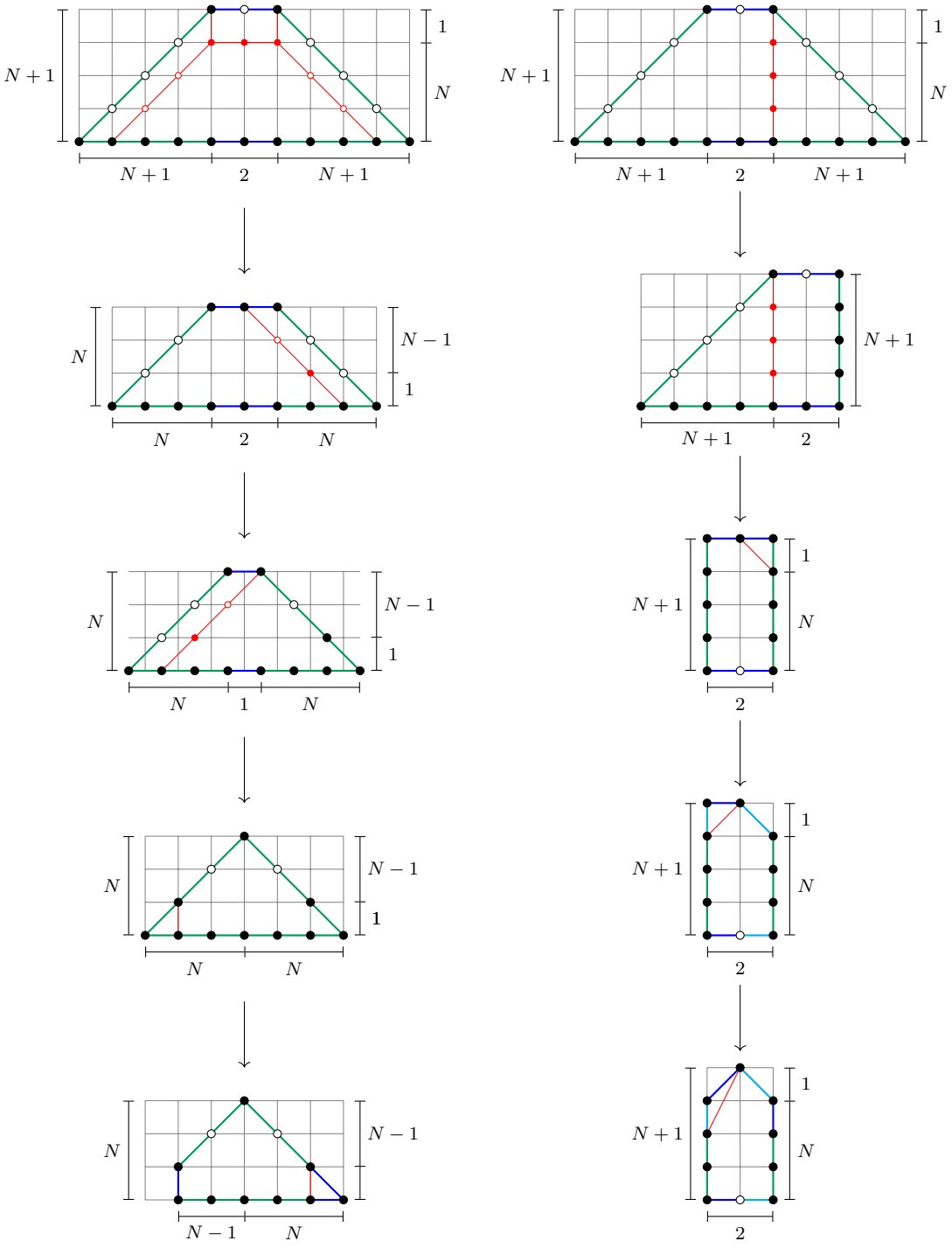
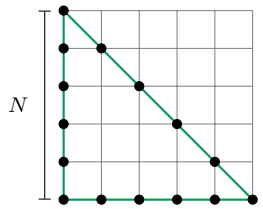


Figure 8.6: The GTP decoupling trees for $SU(N)_{\frac{k+1}{2}}$ with $2N+3-k$ flavors (on the left) and $SU(N)_{\frac{k-1}{2}}$ with $2N+3-k$ flavors (on the right), drawn for $N=3$, corresponding to the FI deformations shown in Figure 8.5.

8.5 T_N Theory

We will now study the T_N theory, its parent SCFTs and its Lagrangian descriptions. In particular we are interested in relating the magnetic quivers describing the Higgs branches of these 5d theories through FI deformations. The GTP of T_N is (drawn for $N = 5$)



(8.72)

where we have also given the unique edge coloring with

$$\begin{aligned} \lambda_\alpha &= (N, N, N)\,, \qquad & \mu_\alpha &= (\{1^N\}, \{1^N\}, \{1^N\})\,, \\ \lambda^g_\alpha &= (N, N, N)\,, \qquad & \mu^g_\alpha &= (\{N\}, \{N\}, \{N\})\,, \end{aligned} \tag{8.73}$$

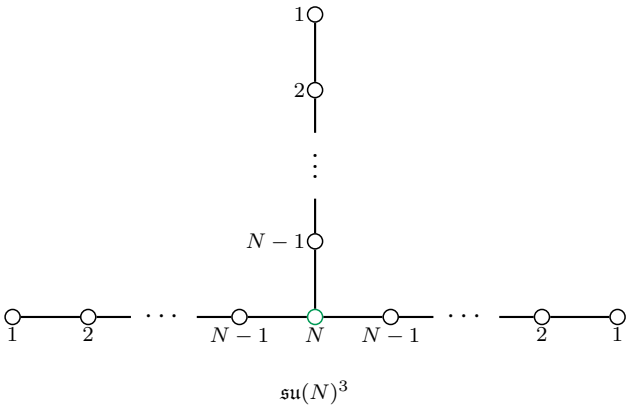
which results in the nodes

$$m^g = N\,, \qquad m_{\alpha,x} = (N-1, N-2, \ldots, 1)\ \forall \alpha \tag{8.74}$$

and non-zero intersections

$$k^g_{\alpha,1} = 1\ \forall \alpha \tag{8.75}$$

along with nearest neighbours intersecting once in the tails. Hence, the magnetic quiver is



(8.76)

8.5.1 Parent SCFTs

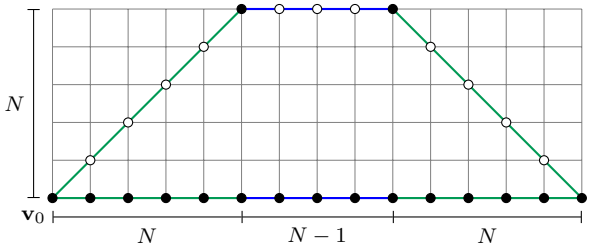
The respective parent and "grandparent" SCFTs of T_N are the so-called P_N and G_N theories. The GTPs of these theories can be obtained by constructing the pre-GTP representing their

low energy Lagrangian descriptions

$$\begin{aligned} G_N &: [N+1] - SU(N-1)_{\frac{1}{2}} - \cdots - SU(2) - [3] \\ &\quad [N+2] - SU(N-1)_0 - \cdots - SU(2) - [2] \end{aligned} \tag{8.77}$$

$$\begin{aligned} P_N &: [N] - SU(N-1)_0 - \cdots - SU(2) - [3] \\ &\quad [N+1] - SU(N-1)_{\frac{1}{2}} - \cdots - SU(2) - [2] \end{aligned}$$

and performing edge-moves to reach the SCFT point. For G_N we find



(8.78)

with

$$\begin{aligned} \lambda_\alpha &= (3N-1, N, N-1, N)\,, & \mu_\alpha &= (\{1^{3N-1}\}, \{N\}, \{N-1\}, \{N\})\,, \\ \lambda^b_\alpha &= (N-1, 0, N-1, 0)\,, & \mu^b_\alpha &= (\{N-1\}, -, \{N-1\}, -)\,, \\ \lambda^g_\alpha &= (2N, N, 0, N)\,, & \mu^g_\alpha &= (\{N, N\}, \{N\}, -, \{N\})\,, \end{aligned} \tag{8.79}$$

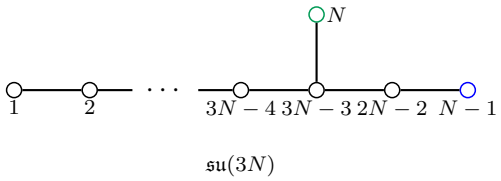
which results in the nodes

$$m^b = N-1\,, \qquad m^g = N\,, \qquad m_{1x} = (2N-2, 3N-3, 3N-4, \ldots, 1)\,, \tag{8.80}$$

and intersections

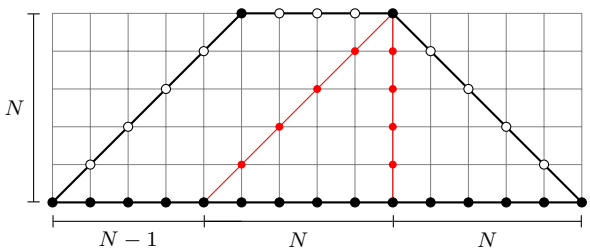
$$k^g_{1,2} = 1\,, \qquad k^b_{1,1} = 1\,, \tag{8.81}$$

as well as nearest neighbours intersecting once in the tail. Thus, the magnetic quiver is



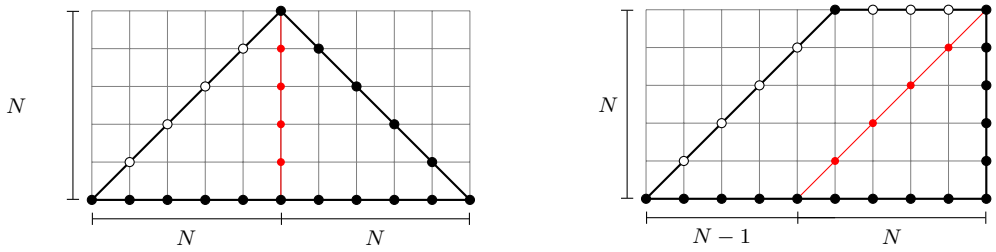
(8.82)

The matter curves which give P_N and T_N are



(8.83)

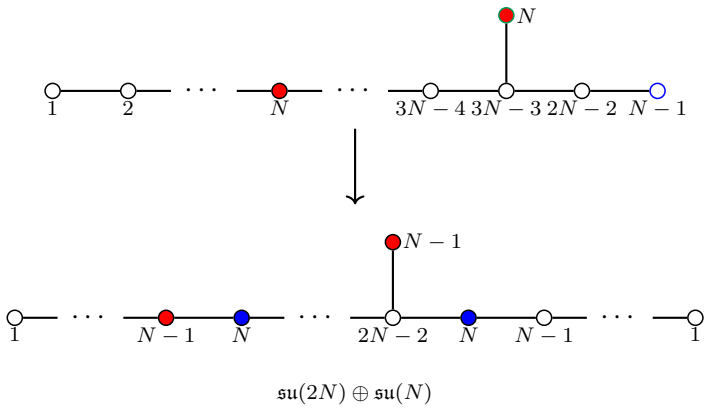
Resolving by either curve on its own and decoupling gives a representation of P_N:



(8.84)

The two representations are related by pruning the horizontal edge, i.e. in the left polygon we move a single segment from the bottom edge anti-clockwise through the polygon to give the top horizontal edge in the right polygon. Three edges are created in the process, realizing Hanany-Witten brane creation. Further decoupling using the other curve gives T_N.

The magnetic quiver of P_N can be obtained from that of G_N by turning on FI deformations at the $U(N)$ node in the tail and the green node of the same rank (equivalently, we could use the $U(2N-1)$ node in the tail and the two color nodes). Subsequently, the magnetic quiver of T_N may be obtained by turning on an FI parameter either at the $U(N-1)$ node in the long tail and the central $U(N-1)$ node (red), or at the two $U(N)$ nodes (blue):



(8.85)

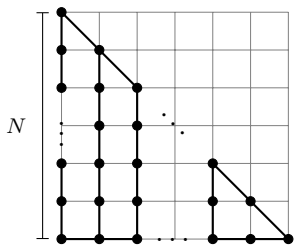
From either of these transitions we recover the magnetic quiver of T_N.

8.5.2 IR Descriptions

T_N has a Lagrangian description as

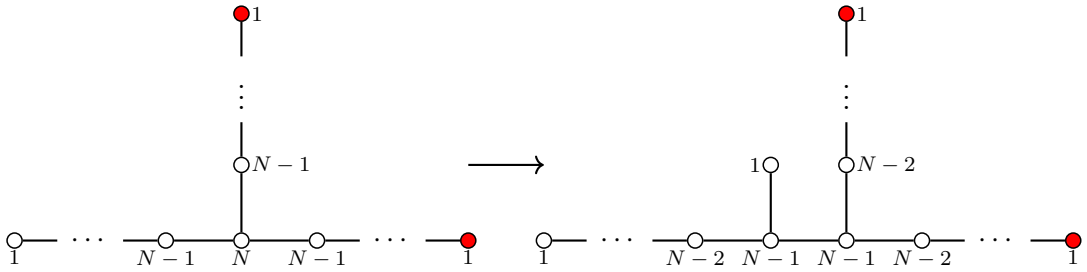
$$[N] - SU(N-1)_0 - SU(N-2) - \cdots - SU(2) - [2]\,. \tag{8.86}$$

In the toric polygon, we can go to this weak coupling description by successively introducing a set of $N-2$ internal edges as follows



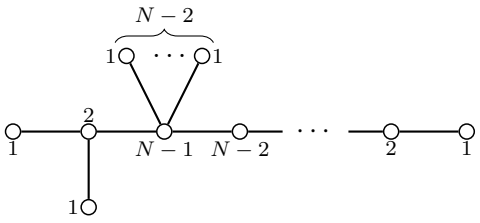
(8.87)

The left-most ruling corresponds to turning on a SYM term for the $SU(N-1)$ gauge group. The magnetic quiver of this theory is obtained from that of T_N by an FI deformation at two $U(1)$ nodes



(8.88)

The second ruling from left in (8.87) is associated to the $SU(N-2)$ gauge group. The magnetic quiver of this theory is obtained from the FI deformation indicated in the right-hand magnetic quiver of (8.88). By iterating this procedure of turning on FI parameters at the $U(1)$ nodes in the symmetric tails, after $N-2$ times, we arrive at the following magnetic quiver for the IR Lagrangian theory (8.86):

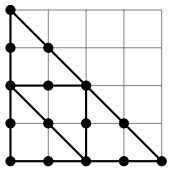


(8.89)

with flavor symmetry algebra $\mathfrak{su}(N) \oplus \mathfrak{su}(2)^2$ for $N \neq 3$ and, for $N = 3$, the balanced nodes form $\widetilde{D}_5$.

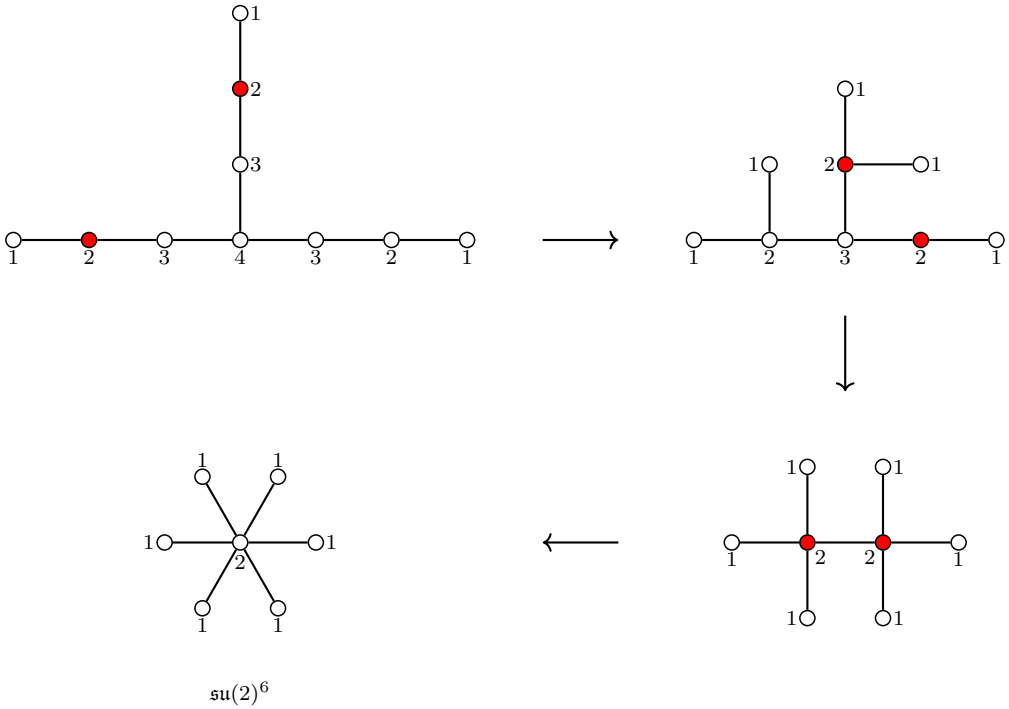
In [183] a new weakly coupled gauge theory description for T_4 was found, with three $SU(2)$ gauge groups with a trifundamental half-hypermultiplet in the representation $\frac{1}{2}(\mathbf{2},\mathbf{2},\mathbf{2})$

among them, as well as 2 fundamentals associated to each gauge group. The corresponding partial resolution is



(8.90)

This ruling structure is associated to three transitions in the magnetic quiver, namely

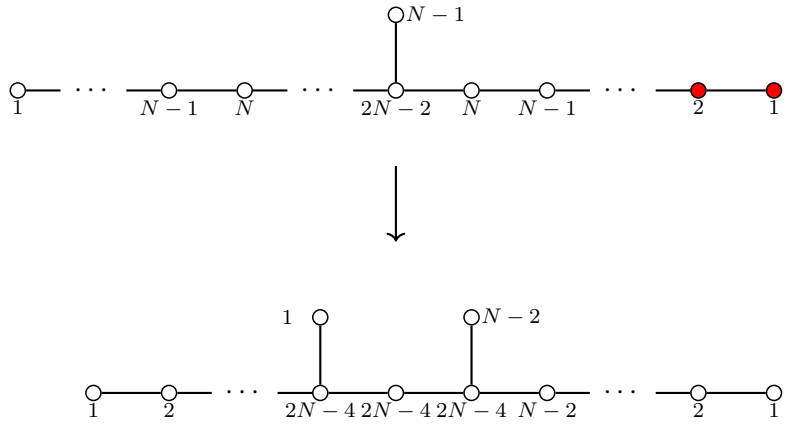


(8.91)

8.5.3 New Lagrangians from FI Deformations

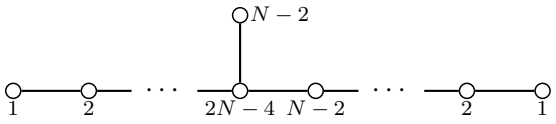
In this section we will see how the analysis of FI deformations can be helpful to guess new low-energy lagrangian descriptions for 5d SCFTs. We will focus on the case of P_N theory, for which we find a new linear unitary quiver. The basic idea is to turn on FI deformations (in one-to-one correspondence with the number of simple factors in the gauge group) until we find the 3d mirror of a gauge theory. Notice that this argument alone does not allow us to determine the value of the CS levels or θ angles.

We proceed inductively, starting from the magnetic quiver of P_N theory given in (8.85). We first activate FI parameters at the $U(1)$ and $U(2)$ nodes on the right.



(8.92)

The resulting quiver describes (i.e. is the 3d mirror of) an $SU(2N-4)$ vector multiplet coupled to $2N-2$ flavors and to an SCFT whose 3d mirror is given by the quiver



(8.93)

Notice that the central node is underbalanced and we can use the Seiberg-like duality of [127]:

$$U(n) \text{ w/ } 2n-1 \text{ flavors} \quad \simeq \quad U(n-1) \text{ w/ } 2n-1 \text{ flavors} + 1 \text{ free hyper}. \tag{8.94}$$

With this modification both the $U(N-2)$ above and the $U(2N-3)$ on the left become underbalanced and we can apply the duality again. Once we get rid of all the underbalanced nodes with this procedure, we find $4N-8$ decoupled hypermultiplets, organized into 2 flavors of $SU(2N-4)$, and an interacting SCFT which can be identified with P_{N-2}. We therefore end up with the theory

$$P_{N-2} - SU(2N-4) - \boxed{2N}. \tag{8.95}$$

By iterating the above argument, we conclude that for N odd ($N = 2k+1$) after k FI deformations we end up with the quiver

$$P_3 - SU(6) - \cdots - SU(2N-4) - \boxed{2N}. \tag{8.96}$$

Setting $N = 3$ in (8.92) we recognize the magnetic quiver of the rank-1 E_7 theory, which flows to $SU(2)$ with 6 flavors and therefore the final answer is

$$SU(2) - SU(6) - \cdots - SU(2N-4) - \boxed{2N}. \tag{8.97}$$

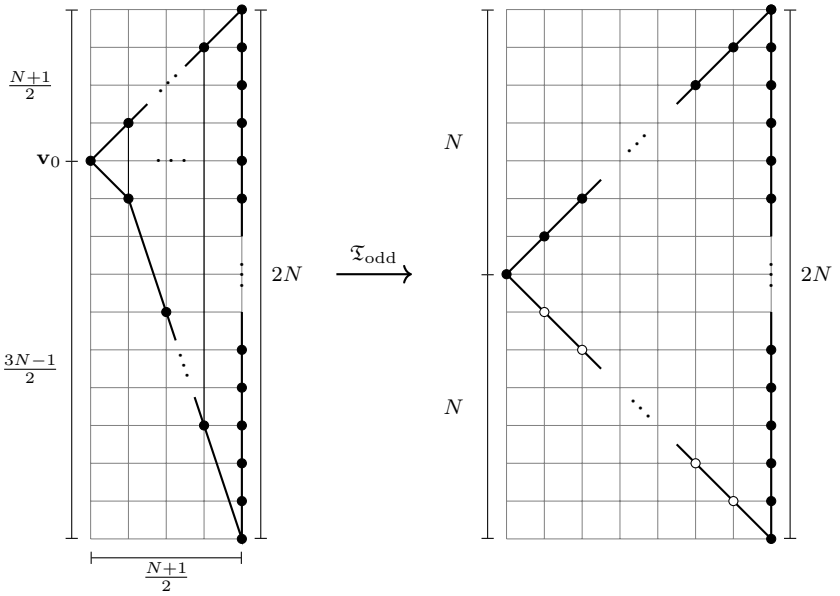
For N even ($N = 2k$) instead, after $k-1$ FI deformations we get

$$P_4 - SU(8) - \cdots - SU(2N-4) - \boxed{2N}. \tag{8.98}$$

Let us now focus on the FI deformation of P_4. For $N = 4$ we recognize the second quiver in (8.92) as the 3d mirror of $SU(4)$ with 8 fundamentals and 1 anti-symmetric hypermultiplet. Overall, the theory after k FI deformations becomes

$$\boxed{1\ AS} - SU(4) - SU(8) - \cdots - SU(2N-4) - \boxed{2N}. \tag{8.99}$$

We can substantiate that the new Lagrangians in (8.97) and (8.99) indeed UV complete to P_N by constructing pre-GTPs realizing the gauge theories, and showing that they can be put into the form (8.84). The pre-GTP of the quiver gauge theory in (8.97) with (CS levels 0) is shown to the left



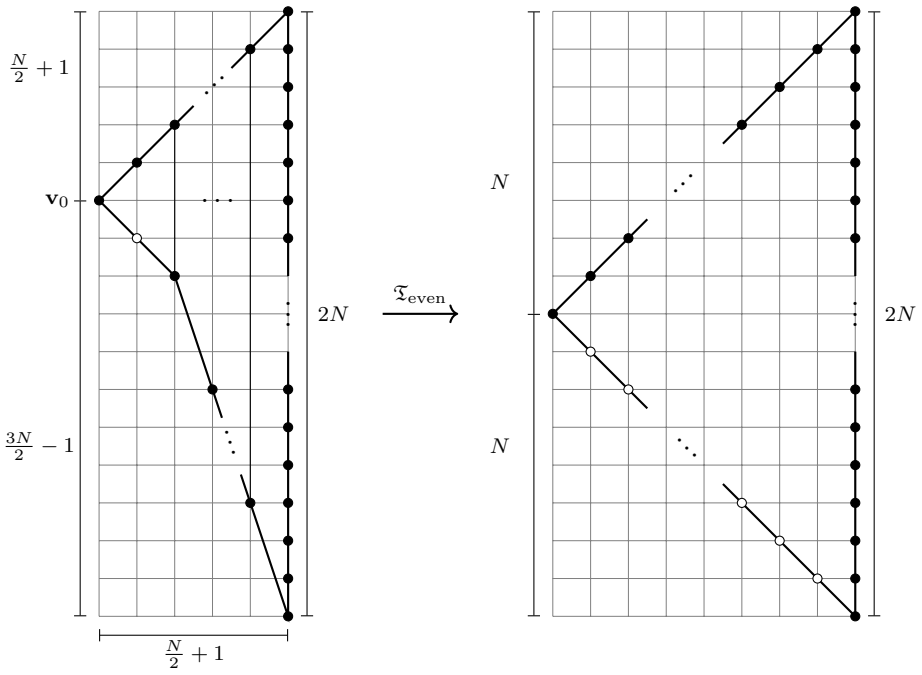
(8.100)

where the $SU(2)$ gauge node sits along the left-most ruling with no matter multiplets. The ranks of the gauge groups increase in steps of 4 to the right, until $SU(2N-4)$ with its $2N$ hypers sitting along the right-hand vertical edge. The $(1,1)$ and $(1,-3)$ edges furnish the bi-fundamental matter. In the notation of 7.5, applying the edge-moves given by

$$\mathfrak{T}_{\text{odd}} = \mathfrak{M}_1^- \mathfrak{M}_2^- \ldots \mathfrak{M}_{\frac{N-1}{2}}^- , \tag{8.101}$$

renders the polygon convex, giving exactly the GTP of P_N in (8.84) (left). The pre-GTP of

the gauge theory with anti-symmetric matter in (8.99) (and CS levels 0) is shown to the left



(8.102)

where the left-hand sector with the white vertex supplies the anti-symmetric matter, and the $SU(4)$ sits along the left-most ruling. Again, the ranks of the gauge groups increase in steps of 4 to the right until $SU(2N-4)$, which has $2N$ hypers sitting on the vertical edge. Applying the following edge-moves,

$$\mathfrak{T}_{\text{even}} = \mathfrak{M}_1^- \mathfrak{M}_2^- \dots \mathfrak{M}_{\frac{N}{2}-1}^- , \tag{8.103}$$

gives the GTP of P_N.

Bibliography

[1] M. van Beest, S. Cizel, S. Schafer-Nameki and J. Sparks, *$\mathcal{I}$/c-Extremization in M/F-Duality*, *SciPost Phys.* **9** (2020) 029, [2004.04020].

[2] M. van Beest, A. Bourget, J. Eckhard and S. Schafer-Nameki, *(Symplectic) Leaves and (5d Higgs) Branches in the Poly(go)nesian Tropical Rain Forest*, *JHEP* **11** (2020) 124, [2008.05577].

[3] M. Van Beest, A. Bourget, J. Eckhard and S. Schäfer-Nameki, *(5d RG-flow) Trees in the Tropical Rain Forest*, *JHEP* **03** (2021) 241, [2011.07033].

[4] F. Apruzzi, M. van Beest, D. S. W. Gould and S. Schäfer-Nameki, *Holography, 1-form symmetries, and confinement*, *Phys. Rev. D* **104** (2021) 066005, [2104.12764].

[5] M. van Beest and S. Giacomelli, *Connecting 5d Higgs branches via Fayet-Iliopoulos deformations*, *JHEP* **12** (2021) 202, [2110.02872].

[6] G. 't Hooft, *Dimensional reduction in quantum gravity*, *Conf. Proc. C* **930308** (1993) 284–296, [gr-qc/9310026].

[7] L. Susskind, *The World as a hologram*, *J. Math. Phys.* **36** (1995) 6377–6396, [hep-th/9409089].

[8] J. M. Maldacena, *The Large N limit of superconformal field theories and supergravity*, *Adv. Theor. Math. Phys.* **2** (1998) 231–252, [hep-th/9711200].

[9] O. Aharony, N. Seiberg and Y. Tachikawa, *Reading between the lines of four-dimensional gauge theories*, *JHEP* **08** (2013) 115, [1305.0318].

[10] D. Gaiotto, A. Kapustin, N. Seiberg and B. Willett, *Generalized Global Symmetries*, *JHEP* **02** (2015) 172, [1412.5148].

[11] S. H. Katz, A. Klemm and C. Vafa, *Geometric engineering of quantum field theories*, *Nucl. Phys. B* **497** (1997) 173–195, [hep-th/9609239].

[12] S. H. Katz and C. Vafa, *Geometric engineering of N=1 quantum field theories*, *Nucl. Phys. B* **497** (1997) 196–204, [hep-th/9611090].

[13] A. Hanany and E. Witten, *Type IIB superstrings, BPS monopoles, and three-dimensional gauge dynamics*, *Nucl. Phys. B* **492** (1997) 152–190, [hep-th/9611230].

[14] N. Seiberg, *Five-dimensional SUSY field theories, nontrivial fixed points and string dynamics*, *Phys. Lett.* **B388** (1996) 753–760, [hep-th/9608111].

[15] D. R. Morrison and N. Seiberg, *Extremal transitions and five-dimensional supersymmetric field theories*, *Nucl. Phys.* **B483** (1997) 229–247, [hep-th/9609070].

[16] K. A. Intriligator, D. R. Morrison and N. Seiberg, *Five-dimensional supersymmetric gauge theories and degenerations of Calabi-Yau spaces*, *Nucl. Phys.* **B497** (1997) 56–100, [hep-th/9702198].

[17] O. Aharony, A. Hanany and B. Kol, *Webs of (p,q) five-branes, five-dimensional field theories and grid diagrams*, *JHEP* **01** (1998) 002, [hep-th/9710116].

[18] C. Vafa, *Evidence for F theory*, *Nucl. Phys. B* **469** (1996) 403–418, [hep-th/9602022].

[19] D. R. Morrison and C. Vafa, *Compactifications of F theory on Calabi-Yau threefolds. 1*, *Nucl. Phys. B* **473** (1996) 74–92, [hep-th/9602114].

[20] D. R. Morrison and C. Vafa, *Compactifications of F theory on Calabi-Yau threefolds. 2.*, *Nucl. Phys. B* **476** (1996) 437–469, [hep-th/9603161].

[21] T. Weigand, *Lectures on F-theory compactifications and model building*, *Class. Quant. Grav.* **27** (2010) 214004, [1009.3497].

[22] F. Denef, *Les Houches Lectures on Constructing String Vacua*, *Les Houches* **87** (2008) 483–610, [0803.1194].

[23] B. R. Greene, A. D. Shapere, C. Vafa and S.-T. Yau, *Stringy Cosmic Strings and Noncompact Calabi-Yau Manifolds*, *Nucl. Phys.* **B337** (1990) 1–36.

[24] E. Sharpe, *Notes on generalized global symmetries in QFT*, *Fortsch. Phys.* **63** (2015) 659–682, [1508.04770].

[25] Y. Tachikawa, *On gauging finite subgroups*, *SciPost Phys.* **8** (2020) 015, [1712.09542].

[26] C. Córdova, T. T. Dumitrescu and K. Intriligator, *Exploring 2-Group Global Symmetries*, *JHEP* **02** (2019) 184, [1802.04790].

[27] F. Benini, C. Córdova and P.-S. Hsin, *On 2-Group Global Symmetries and their Anomalies*, *JHEP* **03** (2019) 118, [1803.09336].

[28] C. Cordova, T. T. Dumitrescu and K. Intriligator, *2-Group Global Symmetries and Anomalies in Six-Dimensional Quantum Field Theories*, 2009.00138.

[29] Y. Choi, C. Cordova, P.-S. Hsin, H. T. Lam and S.-H. Shao, *Non-Invertible Duality Defects in 3+1 Dimensions*, 2111.01139.

[30] J. Kaidi, K. Ohmori and Y. Zheng, *Kramers-Wannier-like Duality Defects in (3+1)D Gauge Theories*, *Phys. Rev. Lett.* **128** (2022) 111601, [2111.01141].

[31] B. Heidenreich, J. McNamara, M. Montero, M. Reece, T. Rudelius and I. Valenzuela, *Non-invertible global symmetries and completeness of the spectrum*, *JHEP* **09** (2021) 203, [2104.07036].

[32] C. Couzens, C. Lawrie, D. Martelli, S. Schafer-Nameki and J.-M. Wong, *F-theory and AdS_3/CFT_2*, *JHEP* **08** (2017) 043, [1705.04679].

[33] C. Couzens, D. Martelli and S. Schafer-Nameki, *F-theory and AdS_3/CFT_2 (2, 0)*, *JHEP* **06** (2018) 008, [1712.07631].

[34] J. P. Gauntlett, O. A. P. Mac Conamhna, T. Mateos and D. Waldram, *Supersymmetric AdS(3) solutions of type IIB supergravity*, *Phys. Rev. Lett.* **97** (2006) 171601, [hep-th/0606221].

[35] J. P. Gauntlett, O. A. P. Mac Conamhna, T. Mateos and D. Waldram, *New supersymmetric AdS(3) solutions*, *Phys. Rev.* **D74** (2006) 106007, [hep-th/0608055].

[36] N. Kim, *AdS(3) solutions of IIB supergravity from D3-branes*, *JHEP* **01** (2006) 094, [hep-th/0511029].

[37] J. P. Gauntlett, N. Kim and D. Waldram, *Supersymmetric AdS(3), AdS(2) and Bubble Solutions*, *JHEP* **04** (2007) 005, [hep-th/0612253].

[38] J. P. Gauntlett and N. Kim, *Geometries with Killing Spinors and Supersymmetric AdS Solutions*, *Commun. Math. Phys.* **284** (2008) 897–918, [0710.2590].

[39] A. Donos, J. P. Gauntlett and N. Kim, *AdS Solutions Through Transgression*, *JHEP* **09** (2008) 021, [0807.4375].

[40] N. Doroud, J. Gomis, B. Le Floch and S. Lee, *Exact Results in D=2 Supersymmetric Gauge Theories*, *JHEP* **05** (2013) 093, [1206.2606].

[41] F. Benini and S. Cremonesi, *Partition Functions of $\mathcal{N} = (2, 2)$ Gauge Theories on S^2 and Vortices*, *Commun. Math. Phys.* **334** (2015) 1483–1527, [1206.2356].

[42] S. Datta, L. Eberhardt and M. R. Gaberdiel, *Stringy $\mathcal{N} = (2, 2)$ holography for AdS_3*, *JHEP* **01** (2018) 146, [1709.06393].

[43] Y. Lozano, N. T. Macpherson, C. Nunez and A. Ramirez, *AdS_3 solutions in Massive IIA with small $\mathcal{N} = (4, 0)$ supersymmetry*, *JHEP* **01** (2020) 129, [1908.09851].

[44] L. Martucci, *Topological duality twist and brane instantons in F-theory*, *JHEP* **06** (2014) 180, [1403.2530].

[45] B. Haghighat, S. Murthy, C. Vafa and S. Vandoren, *F-Theory, Spinning Black Holes and Multi-string Branches*, *JHEP* **01** (2016) 009, [1509.00455].

[46] B. Assel and S. Schäfer-Nameki, *Six-dimensional origin of $\mathcal{N} = 4$ SYM with duality defects*, *JHEP* **12** (2016) 058, [1610.03663].

[47] C. Lawrie, S. Schafer-Nameki and T. Weigand, *Chiral 2d theories from N = 4 SYM with varying coupling*, *JHEP* **04** (2017) 111, [1612.05640].

[48] T. W. Grimm, H. het Lam, K. Mayer and S. Vandoren, *Four-dimensional black hole entropy from F-theory*, *JHEP* **01** (2019) 037, [1808.05228].

[49] A. Passias and D. Prins, *On AdS_3 solutions of Type IIB*, 1910.06326.

[50] C. Couzens, $\mathcal{N} = (0,2)$ *AdS_3 Solutions of Type IIB and F-theory with Generic Fluxes*, 1911.04439.

[51] C. Couzens, H. het Lam and K. Mayer, *Twisted $\mathcal{N} = 1$ SCFTs and their AdS_3 duals*, *JHEP* **03** (2020) 032, [1912.07605].

[52] C. Lawrie, D. Martelli and S. Schafer-Nameki, *Theories of Class F and Anomalies*, *JHEP* **10** (2018) 090, [1806.06066].

[53] I. Bah, F. Bonetti, R. Minasian and P. Weck, *Anomaly Inflow Methods for SCFT Constructions in Type IIB*, 2002.10466.

[54] J. M. Maldacena, A. Strominger and E. Witten, *Black hole entropy in M theory*, *JHEP* **12** (1997) 002, [hep-th/9711053].

[55] F. Benini and N. Bobev, *Exact two-dimensional superconformal R-symmetry and c-extremization*, *Phys. Rev. Lett.* **110** (2013) 061601, [1211.4030].

[56] F. Benini and N. Bobev, *Two-dimensional SCFTs from wrapped branes and c-extremization*, *JHEP* **06** (2013) 005, [1302.4451].

[57] F. Benini, N. Bobev and P. M. Crichigno, *Two-dimensional SCFTs from D3-branes*, *JHEP* **07** (2016) 020, [1511.09462].

[58] K. A. Intriligator and B. Wecht, *The Exact superconformal R symmetry maximizes a*, *Nucl. Phys.* **B667** (2003) 183–200, [hep-th/0304128].

[59] F. Benini, K. Hristov and A. Zaffaroni, *Black hole microstates in AdS_4 from supersymmetric localization*, *JHEP* **05** (2016) 054, [1511.04085].

[60] F. Benini and A. Zaffaroni, *A topologically twisted index for three-dimensional supersymmetric theories*, *JHEP* **07** (2015) 127, [1504.03698].

[61] F. Benini and A. Zaffaroni, *Supersymmetric partition functions on Riemann surfaces*, *Proc. Symp. Pure Math.* **96** (2017) 13–46, [1605.06120].

[62] C. Closset and H. Kim, *Comments on twisted indices in 3d supersymmetric gauge theories*, *JHEP* **08** (2016) 059, [1605.06531].

[63] C. Couzens, J. P. Gauntlett, D. Martelli and J. Sparks, *A geometric dual of c-extremization*, 1810.11026.

[64] J. P. Gauntlett, D. Martelli and J. Sparks, *Toric geometry and the dual of $\mathcal{I}$-extremization*, *JHEP* **06** (2019) 140, [1904.04282].

[65] D. Martelli, J. Sparks and S.-T. Yau, *The Geometric dual of a-maximisation for Toric Sasaki-Einstein manifolds*, *Commun. Math. Phys.* **268** (2006) 39–65, [hep-th/0503183].

[66] D. Martelli, J. Sparks and S.-T. Yau, *Sasaki-Einstein manifolds and volume minimisation*, *Commun. Math. Phys.* **280** (2008) 611–673, [hep-th/0603021].

[67] N. Kim and J.-D. Park, *Comments on AdS(2) solutions of D=11 supergravity*, *JHEP* **09** (2006) 041, [hep-th/0607093].

[68] S. M. Hosseini and A. Zaffaroni, *Proving the equivalence of c-extremization and its gravitational dual for all toric quivers*, *JHEP* **03** (2019) 108, [1901.05977].

[69] S. M. Hosseini and A. Zaffaroni, *Geometry of $\mathcal{I}$-extremization and black holes microstates*, *JHEP* **07** (2019) 174, [1904.04269].

[70] P. Karndumri and E. O Colgain, *Supergravity dual of c-extremization*, *Phys. Rev. D* **87** (2013) 101902, [1302.6532].

[71] P. Karndumri and E. O Colgain, *3D supergravity from wrapped M5-branes*, *JHEP* **03** (2016) 188, [1508.00963].

[72] T. Pantev and E. Sharpe, *Duality group actions on fermions*, *JHEP* **11** (2016) 171, [1609.00011].

[73] J. D. Brown and M. Henneaux, *Central Charges in the Canonical Realization of Asymptotic Symmetries: An Example from Three-Dimensional Gravity*, *Commun. Math. Phys.* **104** (1986) 207–226.

[74] A. Castro and W. Song, *Comments on AdS(2) Gravity*, 1411.1948.

[75] R. Wazir, *Arithmetic on elliptic threefolds*, *Compos. Math.* **140** (2004) 567–580.

[76] M. Cvetič and I. Papadimitriou, *AdS_2 holographic dictionary*, *JHEP* **12** (2016) 008, [1608.07018].

[77] N. Bobev, M. Bullimore and H.-C. Kim, *Supersymmetric Casimir Energy and the Anomaly Polynomial*, *JHEP* **09** (2015) 142, [1507.08553].

[78] J. P. Gauntlett, D. Martelli and J. Sparks, *Toric geometry and the dual of c-extremization*, 1812.05597.

[79] J. P. Gauntlett, D. Martelli and J. Sparks, *Fibred GK geometry and supersymmetric AdS solutions*, 1910.08078.

[80] J. P. Gauntlett, D. Martelli, J. Sparks and D. Waldram, *Sasaki-Einstein metrics on $S^2 \times S^3$*, *Adv. Theor. Math. Phys.* **8** (2004) 711–734, [hep-th/0403002].

[81] D. Martelli and J. Sparks, *Toric geometry, Sasaki-Einstein manifolds and a new infinite class of AdS/CFT duals*, *Commun. Math. Phys.* **262** (2006) 51–89, [hep-th/0411238].

[82] E. Witten, *Constraints on Supersymmetry Breaking*, *Nucl. Phys. B* **202** (1982) 253.

[83] C. Córdova and T. T. Dumitrescu, *Candidate Phases for SU(2) Adjoint QCD_4 with Two Flavors from $\mathcal{N} = 2$ Supersymmetric Yang-Mills Theory*, 1806.09592.

[84] C. Cordova and K. Ohmori, *Anomaly Obstructions to Symmetry Preserving Gapped Phases*, 1910.04962.

[85] E. Witten, *AdS / CFT correspondence and topological field theory*, *JHEP* **12** (1998) 012, [hep-th/9812012].

[86] O. Aharony and E. Witten, *Anti-de Sitter space and the center of the gauge group*, *JHEP* **11** (1998) 018, [hep-th/9807205].

[87] D. J. Gross and H. Ooguri, *Aspects of large N gauge theory dynamics as seen by string theory*, *Phys. Rev. D* **58** (1998) 106002, [hep-th/9805129].

[88] D. M. Hofman and N. Iqbal, *Generalized global symmetries and holography*, *SciPost Phys.* **4** (2018) 005, [1707.08577].

[89] O. Bergman, Y. Tachikawa and G. Zafrir, *Generalized symmetries and holography in ABJM-type theories*, *JHEP* **07** (2020) 077, [2004.05350].

[90] I. Bah, F. Bonetti and R. Minasian, *Discrete and higher-form symmetries in SCFTs from wrapped M5-branes*, *JHEP* **03** (2021) 196, [2007.15003].

[91] N. Seiberg and E. Witten, *Electric - magnetic duality, monopole condensation, and confinement in N=2 supersymmetric Yang-Mills theory*, *Nucl. Phys. B* **426** (1994) 19–52, [hep-th/9407087].

[92] N. Seiberg and E. Witten, *Monopoles, duality and chiral symmetry breaking in N=2 supersymmetric QCD*, *Nucl. Phys.* **B431** (1994) 484–550, [hep-th/9408099].

[93] A. Klemm, W. Lerche, S. Yankielowicz and S. Theisen, *Simple singularities and N=2 supersymmetric Yang-Mills theory*, *Phys. Lett. B* **344** (1995) 169–175, [hep-th/9411048].

[94] P. C. Argyres and A. E. Faraggi, *The vacuum structure and spectrum of N=2 supersymmetric SU(n) gauge theory*, *Phys. Rev. Lett.* **74** (1995) 3931–3934, [hep-th/9411057].

[95] I. R. Klebanov and N. A. Nekrasov, *Gravity duals of fractional branes and logarithmic RG flow*, *Nucl. Phys. B* **574** (2000) 263–274, [hep-th/9911096].

[96] I. R. Klebanov and M. J. Strassler, *Supergravity and a confining gauge theory: Duality cascades and chi SB resolution of naked singularities*, *JHEP* **08** (2000) 052, [hep-th/0007191].

[97] I. R. Klebanov and A. A. Tseytlin, *Gravity duals of supersymmetric SU(N) x SU(N+M) gauge theories*, *Nucl. Phys. B* **578** (2000) 123–138, [hep-th/0002159].

[98] C. P. Herzog, I. R. Klebanov and P. Ouyang, *Remarks on the warped deformed conifold*, in *Modern Trends in String Theory: 2nd Lisbon School on g Theory Superstrings*, 8, 2001. hep-th/0108101.

[99] I. R. Klebanov, P. Ouyang and E. Witten, *A Gravity dual of the chiral anomaly*, *Phys. Rev. D* **65** (2002) 105007, [hep-th/0202056].

[100] M. J. Strassler, *The Duality cascade*, in *Theoretical Advanced Study Institute in Elementary Particle Physics (TASI 2003): Recent Trends in String Theory*, 5, 2005. hep-th/0505153. DOI.

[101] D. Cassani and A. F. Faedo, *A Supersymmetric consistent truncation for conifold solutions*, *Nucl. Phys. B* **843** (2011) 455–484, [1008.0883].

[102] I. Bena, G. Giecold, M. Grana, N. Halmagyi and F. Orsi, *Supersymmetric Consistent Truncations of IIB on $T^{1,1}$*, *JHEP* **04** (2011) 021, [1008.0983].

[103] J. Schon and M. Weidner, *Gauged N=4 supergravities*, *JHEP* **05** (2006) 034, [hep-th/0602024].

[104] N. Seiberg, *Electric - magnetic duality in supersymmetric nonAbelian gauge theories*, *Nucl. Phys.* **B435** (1995) 129–146, [hep-th/9411149].

[105] A. Dymarsky, I. R. Klebanov and N. Seiberg, *On the moduli space of the cascading SU(M+p) x SU(p) gauge theory*, *JHEP* **01** (2006) 155, [hep-th/0511254].

[106] E. Witten, *Baryons and branes in anti-de Sitter space*, *JHEP* **07** (1998) 006, [hep-th/9805112].

[107] R. Minasian and D. Tsimpis, *On the geometry of nontrivially embedded branes*, *Nucl. Phys. B* **572** (2000) 499–513, [hep-th/9911042].

[108] I. R. Klebanov and E. Witten, *Superconformal field theory on three-branes at a Calabi-Yau singularity*, *Nucl. Phys. B* **536** (1998) 199–218, [hep-th/9807080].

[109] D. Gaiotto, Z. Komargodski and N. Seiberg, *Time-reversal breaking in QCD_4, walls, and dualities in 2 + 1 dimensions*, *JHEP* **01** (2018) 110, [1708.06806].

[110] M. Berg, M. Haack and W. Mueck, *Bulk dynamics in confining gauge theories*, *Nucl. Phys. B* **736** (2006) 82–132, [hep-th/0507285].

[111] G. Papadopoulos and A. A. Tseytlin, *Complex geometry of conifolds and five-brane wrapped on two sphere*, *Class. Quant. Grav.* **18** (2001) 1333–1354, [hep-th/0012034].

[112] N. Seiberg, Y. Tachikawa and K. Yonekura, *Anomalies of Duality Groups and Extended Conformal Manifolds*, *PTEP* **2018** (2018) 073B04, [1803.07366].

[113] J. M. Maldacena and C. Nunez, *Towards the large N limit of pure N=1 superYang-Mills*, *Phys. Rev. Lett.* **86** (2001) 588–591, [hep-th/0008001].

[114] C. Córdova, D. S. Freed, H. T. Lam and N. Seiberg, *Anomalies in the Space of Coupling Constants and Their Dynamical Applications II*, *SciPost Phys.* **8** (2020) 002, [1905.13361].

[115] O. Aharony and A. Hanany, *Branes, superpotentials and superconformal fixed points*, *Nucl. Phys.* **B504** (1997) 239–271, [hep-th/9704170].

[116] F. Benini, S. Benvenuti and Y. Tachikawa, *Webs of five-branes and N=2 superconformal field theories*, *JHEP* **09** (2009) 052, [0906.0359].

[117] O. Bergman and G. Zafrir, *5d fixed points from brane webs and O7-planes*, *JHEP* **12** (2015) 163, [1507.03860].

[118] G. Zafrir, *Brane webs and O5-planes*, *JHEP* **03** (2016) 109, [1512.08114].

[119] H. Hayashi, S.-S. Kim, K. Lee, M. Taki and F. Yagi, *More on 5d descriptions of 6d SCFTs*, *JHEP* **10** (2016) 126, [1512.08239].

[120] S. Cabrera, A. Hanany and F. Yagi, *Tropical Geometry and Five Dimensional Higgs Branches at Infinite Coupling*, *JHEP* **01** (2019) 068, [1810.01379].

[121] S. Cremonesi, A. Hanany and A. Zaffaroni, *Monopole operators and Hilbert series of Coulomb branches of* $3d$ $\mathcal{N} = 4$ *gauge theories*, *JHEP* **01** (2014) 005, [1309.2657].

[122] M. Bullimore, T. Dimofte and D. Gaiotto, *The Coulomb Branch of 3d* $\mathcal{N} = 4$ *Theories*, *Commun. Math. Phys.* **354** (2017) 671–751, [1503.04817].

[123] H. Nakajima, *Towards a mathematical definition of Coulomb branches of* 3*-dimensional* $\mathcal{N} = 4$ *gauge theories, I*, *Adv. Theor. Math. Phys.* **20** (2016) 595–669, [1503.03676].

[124] A. Braverman, M. Finkelberg and H. Nakajima, *Coulomb branches of* $3d$ $\mathcal{N} = 4$ *quiver gauge theories and slices in the affine Grassmannian*, *Adv. Theor. Math. Phys.* **23** (2019) 75–166, [1604.03625].

[125] H. Nakajima, *Introduction to a provisional mathematical definition of Coulomb branches of* 3*-dimensional* $\mathcal{N} = 4$ *gauge theories*, 1706.05154.

[126] C. Closset, S. Schafer-Nameki and Y.-N. Wang, *Coulomb and Higgs Branches from Canonical Singularities: Part 0*, 2007.15600.

[127] D. Gaiotto and E. Witten, *S-Duality of Boundary Conditions In N=4 Super Yang-Mills Theory*, *Adv. Theor. Math. Phys.* **13** (2009) 721–896, [0807.3720].

[128] S. Cabrera and A. Hanany, *Quiver Subtractions*, *JHEP* **09** (2018) 008, [1803.11205].

[129] A. Bourget, S. Cabrera, J. F. Grimminger, A. Hanany, M. Sperling, A. Zajac et al., *The Higgs mechanism — Hasse diagrams for symplectic singularities*, *JHEP* **01** (2020) 157, [1908.04245].

[130] A. Bourget, S. Giacomelli, J. F. Grimminger, A. Hanany, M. Sperling and Z. Zhong, *S-fold magnetic quivers*, 2010.05889.

[131] K. Altmann, *Infinitesimal deformations and obstructions for toric singularities*, *arXiv preprint alg-geom/9405008* (1994) .

[132] K. Altmann, *The versal deformation of an isolated toric Gorenstein singularity*, *Invent. Math.* **128** (1997) 443–479.

[133] C. Closset, S. Giacomelli, S. Schafer-Nameki and Y.-N. Wang, *5d and 4d SCFTs: Canonical Singularities, Trinions and S-Dualities*, *JHEP* **05** (2021) 274, [2012.12827].

[134] C. Closset, S. Schäfer-Nameki and Y.-N. Wang, *Coulomb and Higgs branches from canonical singularities. Part I. Hypersurfaces with smooth Calabi-Yau resolutions*, *JHEP* **04** (2022) 061, [2111.13564].

[135] D.-E. Diaconescu and R. Entin, *Calabi-Yau spaces and five-dimensional field theories with exceptional gauge symmetry*, *Nucl. Phys. B* **538** (1999) 451–484, [hep-th/9807170].

[136] H. Hayashi, C. Lawrie and S. Schafer-Nameki, *Phases, Flops and F-theory: SU(5) Gauge Theories*, *JHEP* **10** (2013) 046, [1304.1678].

[137] H. Hayashi, C. Lawrie, D. R. Morrison and S. Schafer-Nameki, *Box Graphs and Singular Fibers*, *JHEP* **05** (2014) 048, [1402.2653].

[138] M. Del Zotto, J. J. Heckman and D. R. Morrison, *6D SCFTs and Phases of 5D Theories*, *JHEP* **09** (2017) 147, [1703.02981].

[139] D. Xie and S.-T. Yau, *Three dimensional canonical singularity and five dimensional $\mathcal{N} = 1$ SCFT*, *JHEP* **06** (2017) 134, [1704.00799].

[140] P. Jefferson, H.-C. Kim, C. Vafa and G. Zafrir, *Towards Classification of 5d SCFTs: Single Gauge Node*, 1705.05836.

[141] P. Jefferson, S. Katz, H.-C. Kim and C. Vafa, *On Geometric Classification of 5d SCFTs*, *JHEP* **04** (2018) 103, [1801.04036].

[142] L. Bhardwaj and P. Jefferson, *Classifying 5d SCFTs via 6d SCFTs: Rank one*, *JHEP* **07** (2019) 178, [1809.01650].

[143] L. Bhardwaj and P. Jefferson, *Classifying 5d SCFTs via 6d SCFTs: Arbitrary rank*, *JHEP* **10** (2019) 282, [1811.10616].

[144] F. Apruzzi, L. Lin and C. Mayrhofer, *Phases of 5d SCFTs from M-/F-theory on Non-Flat Fibrations*, *JHEP* **05** (2019) 187, [1811.12400].

[145] C. Closset, M. Del Zotto and V. Saxena, *Five-dimensional SCFTs and gauge theory phases: an M-theory/type IIA perspective*, *SciPost Phys.* **6** (2019) 052, [1812.10451].

[146] F. Apruzzi, C. Lawrie, L. Lin, S. Schafer-Nameki and Y.-N. Wang, *5d Superconformal Field Theories and Graphs*, *Phys. Lett. B* **800** (2020) 135077, [1906.11820].

[147] F. Apruzzi, C. Lawrie, L. Lin, S. Schäfer-Nameki and Y.-N. Wang, *Fibers add Flavor, Part I: Classification of 5d SCFTs, Flavor Symmetries and BPS States*, *JHEP* **11** (2019) 068, [1907.05404].

[148] F. Apruzzi, C. Lawrie, L. Lin, S. Schafer-Nameki and Y.-N. Wang, *Fibers add Flavor, Part II: 5d SCFTs, Gauge Theories, and Dualities*, *JHEP* **03** (2020) 052, [1909.09128].

[149] L. Bhardwaj, *On the classification of 5d SCFTs*, *JHEP* **09** (2020) 007, [1909.09635].

[150] L. Bhardwaj, P. Jefferson, H.-C. Kim, H.-C. Tarazi and C. Vafa, *Twisted Circle Compactifications of 6d SCFTs*, *JHEP* **12** (2020) 151, [1909.11666].

[151] L. Bhardwaj, *Dualities of 5d gauge theories from S-duality*, *JHEP* **07** (2020) 012, [1909.05250].

[152] V. Saxena, *Rank-two 5d SCFTs from M-theory at isolated toric singularities: a systematic study*, *JHEP* **04** (2020) 198, [1911.09574].

[153] F. Apruzzi, S. Schafer-Nameki and Y.-N. Wang, *5d SCFTs from Decoupling and Gluing*, *JHEP* **08** (2020) 153, [1912.04264].

[154] C. Closset and M. Del Zotto, *On 5d SCFTs and their BPS quivers. Part I: B-branes and brane tilings*, 1912.13502.

[155] L. Bhardwaj, *Do all 5d SCFTs descend from 6d SCFTs?*, *JHEP* **04** (2021) 085, [1912.00025].

[156] L. Bhardwaj and G. Zafrir, *Classification of 5d $\mathcal{N} = 1$ gauge theories*, *JHEP* **12** (2020) 099, [2003.04333].

[157] L. Bhardwaj, *More 5d KK theories*, 2005.01722.

[158] M. Hubner, *5d SCFTs from (E_n, E_m) conformal matter*, *JHEP* **12** (2020) 014, [2006.01694].

[159] L. Bhardwaj, *Flavor Symmetry of 5d SCFTs, Part 1: General Setup*, 2010.13230.

[160] L. Bhardwaj, *Flavor symmetry of 5d SCFTs. Part II. Applications*, *JHEP* **04** (2021) 221, [2010.13235].

[161] L. Bhardwaj and S. Schäfer-Nameki, *Higher-form symmetries of 6d and 5d theories*, *JHEP* **02** (2021) 159, [2008.09600].

[162] A. P. Braun, J. Chen, B. Haghighat, M. Sperling and S. Yang, *Fibre-base duality of 5d KK theories*, *JHEP* **05** (2021) 200, [2103.06066].

[163] F. Apruzzi, L. Bhardwaj, J. Oh and S. Schafer-Nameki, *The Global Form of Flavor Symmetries and 2-Group Symmetries in 5d SCFTs*, 2105.08724.

[164] C. Closset and H. Magureanu, *The U-plane of rank-one 4d $\mathcal{N} = 2$ KK theories*, 2107.03509.

[165] A. Collinucci, A. Sangiovanni and R. Valandro, *Genus zero Gopakumar-Vafa invariants from open strings*, 2104.14493.

[166] A. Collinucci, M. De Marco, A. Sangiovanni and R. Valandro, *Higgs branches of 5d rank-zero theories from geometry*, 2105.12177.

[167] O. DeWolfe, A. Hanany, A. Iqbal and E. Katz, *Five-branes, seven-branes and five-dimensional E(n) field theories*, *JHEP* **03** (1999) 006, [hep-th/9902179].

[168] O. Bergman, D. Rodríguez-Gómez and G. Zafrir, *5-Brane Webs, Symmetry Enhancement, and Duality in 5d Supersymmetric Gauge Theory*, *JHEP* **03** (2014) 112, [1311.4199].

[169] G. Zafrir, *Duality and enhancement of symmetry in 5d gauge theories*, *JHEP* **12** (2014) 116, [1408.4040].

[170] H. Hayashi, S.-S. Kim, K. Lee and F. Yagi, *6d SCFTs, 5d Dualities and Tao Web Diagrams*, *JHEP* **05** (2019) 203, [1509.03300].

[171] H. Hayashi, S.-S. Kim, K. Lee, M. Taki and F. Yagi, *A new 5d description of 6d D-type minimal conformal matter*, *JHEP* **08** (2015) 097, [1505.04439].

[172] H. Hayashi, S.-S. Kim, K. Lee and F. Yagi, *Dualities and 5-brane webs for 5d rank 2 SCFTs*, *JHEP* **12** (2018) 016, [1806.10569].

[173] H. Hayashi, S.-S. Kim, K. Lee and F. Yagi, *5-brane webs for 5d $\mathcal{N} = 1$ G_2 gauge theories*, *JHEP* **03** (2018) 125, [1801.03916].

[174] H. Hayashi, S.-S. Kim, K. Lee and F. Yagi, *Rank-3 antisymmetric matter on 5-brane webs*, *JHEP* **05** (2019) 133, [1902.04754].

[175] O. Bergman and D. Rodríguez-Gómez, *The Cat's Cradle: deforming the higher rank E_1 and $\tilde{E}_1$ theories*, *JHEP* **02** (2021) 122, [2011.05125].

[176] M. Martone and G. Zafrir, *On the compactification of 5d theories to 4d*, *JHEP* **08** (2021) 017, [2106.00686].

[177] M. Bertolini and F. Mignosa, *Supersymmetry breaking deformations and phase transitions in five dimensions*, 2109.02662.

[178] G. Ferlito and A. Hanany, *A tale of two cones: the Higgs Branch of Sp(n) theories with 2n flavours*, 1609.06724.

[179] G. Ferlito, A. Hanany, N. Mekareeya and G. Zafrir, *3d Coulomb branch and 5d Higgs branch at infinite coupling*, *JHEP* **07** (2018) 061, [1712.06604].

[180] S. Cabrera, A. Hanany and M. Sperling, *Magnetic quivers, Higgs branches, and 6d N=(1,0) theories*, *JHEP* **06** (2019) 071, [1904.12293].

[181] A. Bourget, S. Cabrera, J. F. Grimminger, A. Hanany and Z. Zhong, *Brane Webs and Magnetic Quivers for SQCD*, *JHEP* **03** (2020) 176, [1909.00667].

[182] S. Cabrera, A. Hanany and M. Sperling, *Magnetic quivers, Higgs branches, and 6d $\mathcal{N}$ = (1, 0) theories — orthogonal and symplectic gauge groups*, *JHEP* **02** (2020) 184, [1912.02773].

[183] J. Eckhard, S. Schäfer-Nameki and Y.-N. Wang, *Trifectas for T_N in 5d*, *JHEP* **07** (2020) 199, [2004.15007].

[184] J. F. Grimminger and A. Hanany, *Hasse Diagrams for* **3d** $\mathcal{N} = 4$ *Quiver Gauge Theories – Inversion and the full Moduli Space*, 2004.01675.

[185] A. Bourget, J. F. Grimminger, A. Hanany, M. Sperling and Z. Zhong, *Magnetic Quivers from Brane Webs with O5 Planes*, *JHEP* **07** (2020) 204, [2004.04082].

[186] A. Bourget, J. F. Grimminger, A. Hanany, M. Sperling, G. Zafrir and Z. Zhong, *Magnetic quivers for rank 1 theories*, 2006.16994.

[187] M. Akhond, F. Carta, S. Dwivedi, H. Hayashi, S.-S. Kim and F. Yagi, *Five-brane webs, Higgs branches and unitary/orthosymplectic magnetic quivers*, 2008.01027.

[188] A. Dancer, A. Hanany and F. Kirwan, *Symplectic duality and implosions*, 2004.09620.

[189] A. Bourget, A. Hanany and D. Miketa, *Quiver origami: discrete gauging and folding*, 2005.05273.

[190] A. Bourget, J. F. Grimminger, A. Hanany, R. Kalveks, M. Sperling and Z. Zhong, *Magnetic Lattices for Orthosymplectic Quivers*, *JHEP* **12** (2020) 092, [2007.04667].

[191] M. Akhond, F. Carta, S. Dwivedi, H. Hayashi, S.-S. Kim and F. Yagi, *Factorised 3d $\mathcal{N} = 4$ orthosymplectic quivers*, *JHEP* **05** (2021) 269, [2101.12235].

[192] A. Bourget, J. F. Grimminger, A. Hanany, M. Sperling and Z. Zhong, *Branes, Quivers, and the Affine Grassmannian*, 2102.06190.

[193] A. Bourget, A. Dancer, J. F. Grimminger, A. Hanany, F. Kirwan and Z. Zhong, *Orthosymplectic implosions*, *JHEP* **08** (2021) 012, [2103.05458].

[194] M. Akhond and F. Carta, *Magnetic quivers from brane webs with $O7^+$-planes*, 2107.09077.

[195] J. Bao, A. Hanany, Y.-H. He and E. Hirst, *Some Open Questions in Quiver Gauge Theory*, 2108.05167.

[196] K. Gledhill and A. Hanany, *Coulomb Branch Global Symmetry and Quiver Addition*, 2109.07237.

[197] A. Hanany and R. Kalveks, *Highest Weight Generating Functions for Hilbert Series*, *JHEP* **10** (2014) 152, [1408.4690].

[198] S. Cremonesi, G. Ferlito, A. Hanany and N. Mekareeya, *Instanton Operators and the Higgs Branch at Infinite Coupling*, *JHEP* **04** (2017) 042, [1505.06302].

[199] L. Bao, E. Pomoni, M. Taki and F. Yagi, *M5-Branes, Toric Diagrams and Gauge Theory Duality*, *JHEP* **04** (2012) 105, [1112.5228].

[200] M. Taki, *Seiberg Duality, 5d SCFTs and Nekrasov Partition Functions*, 1401.7200.

[201] D. Maclagan and B. Sturmfels, *Introduction to Tropical Geometry*, vol. 161 of *Graduate Studies in Mathematics*. American Mathematical Society, Providence, RI, 2015.

[202] H. Kraft and C. Procesi, *Minimal singularities in gl n*, *Inventiones mathematicae* **62** (1980) 503–515.

[203] H. Kraft and C. Procesi, *On the geometry of conjugacy classes in classical groups*, *Commentarii Mathematici Helvetici* **57** (1982) 539–602.

[204] A. Malkin, V. Ostrik, M. Vybornov et al., *The minimal degeneration singularities in the affine grassmannians*, *Duke Mathematical Journal* **126** (2005) 233–249.

[205] B. Fu, D. Juteau, P. Levy and E. Sommers, *Generic singularities of nilpotent orbit closures*, *Advances in Mathematics* **305** (2017) 1–77.

[206] O. Bergman and A. Fayyazuddin, *String junction transitions in the moduli space of N=2 SYM*, *Nucl. Phys. B* **535** (1998) 139–151, [hep-th/9806011].

[207] G. Pick, "Geometrisches zur Zahlenlehre." Sonderabdr. Naturw.-medizin. Verein f. Böhmen "Lotos" Nr. 8, 9 S. 8° (1899)., 1899.

[208] G. Zafrir, *Brane webs, 5d gauge theories and 6d $\mathcal{N}=(1,0)$ SCFT's*, *JHEP* **12** (2015) 157, [1509.02016].

[209] D. Gaiotto and S. S. Razamat, *Exceptional Indices*, *JHEP* **05** (2012) 145, [1203.5517].

[210] S. Cremonesi, A. Hanany, N. Mekareeya and A. Zaffaroni, *Coulomb branch Hilbert series and Three Dimensional Sicilian Theories*, *JHEP* **09** (2014) 185, [1403.2384].

[211] N. Mekareeya, K. Ohmori, Y. Tachikawa and G. Zafrir, *E_8 instantons on type-A ALE spaces and supersymmetric field theories*, *JHEP* **09** (2017) 144, [1707.04370].

[212] A. Hanany and G. Zafrir, *Discrete Gauging in Six Dimensions*, *JHEP* **07** (2018) 168, [1804.08857].

[213] R. Brylinski and B. Kostant, *Nilpotent orbits, normality, and hamiltonian group actions*, *Journal of the American Mathematical Society* **7** (1994) 269–298.

[214] A. Hanany and A. Zajac, *Discrete Gauging in Coulomb branches of Three Dimensional $\mathcal{N}=4$ Supersymmetric Gauge Theories*, *JHEP* **08** (2018) 158, [1807.03221].

[215] A. Dey, *Higgs Branches of Argyres-Douglas theories as Quiver Varieties*, 2109.07493.

[216] M. Del Zotto, J. J. Heckman, A. Tomasiello and C. Vafa, *6d Conformal Matter*, *JHEP* **02** (2015) 054, [1407.6359].